Microwave Spectroscopic and Atoms in Molecules Theoretical Investigations on Weakly Bound Complexes: From Hydrogen Bond to 'Carbon Bond'.

A Thesis

Submitted for the Degree of

Doctor of Philosophy

in the Faculty of Science

by

Devendra Mani

Department of Inorganic and Physical Chemistry

INDIAN INSTITUTE OF SCIENCE

BANGALORE- 560012, INDIA

December, 2013

Dedicated to Amma, Papa

and All My Teachers.

Declaration

I hereby declare that the work presented in this thesis entitled ***Microwave Spectroscopic and Atoms in Molecules Theoretical Investigations on Weakly Bound Complexes: From Hydrogen Bond to 'Carbon Bond'*** has been carried out by me at the Department of Inorganic and Physical Chemistry, Indian Institute of Science, Bangalore, India, under the supervision of Professor E. Arunan.

Date Devendra Mani

Certificate

I hereby certify that the work presented in this thesis entitled ***Microwave Spectroscopic and Atoms in Molecules Theoretical Investigations on Weakly Bound Complexes: From Hydrogen Bond to 'Carbon Bond'*** has been carried out by Mr. Devendra Mani at the Department of Inorganic and Physical Chemistry, Indian Institute of Science, Bangalore, India, under my supervision.

Date

Prof. E. Arunan

(Research Supervisor)

ACKNOWLEDGMENTS

I take this opportunity to express my sincere gratitude to my thesis supervisor Prof. E. Arunan for giving me an opportunity to work with him. I consider myself fortunate for having completed graduation under his guidance. I could not have imagined a better guide than him. His dedication and enthusiasm towards science has been a constant source of inspiration for me. His constant support, encouragement and enthusiasm in my research work have helped me keep going. I specially thank him for encouraging me to take part in different conferences and for his helps at various levels to ensure the participation. The discussions with him about different aspects of life have left me feel enriched. He has been a father figure in my life and my gratitude and respect towards him cannot be expressed in these few words.

I thank Prof. K.J. Vinoy for allowing me to work in his laboratory for the chirped pulse measurements.

I owe thanks to Prof. P.C. Mathias for his kind helps towards maintaining the spectrometer. He has taken us out from very difficult situations on many occasions.

I wish to thank all the members of the Chemical Dynamics Group. It was a pleasure to be a part of this group. The wonderful talks during the group meetings have helped me immensely to grow as a researcher. My special thanks to Prof. E. Arunan, Prof. P.K. Das, Prof. K.L. Sebastian, Dr. A. Bhattacharya, Dr. U. Harbola and Dr. Sai G. Ramesh for their enthusiastic involvements and invaluable inputs during the talks.

I am grateful to Prof. P.K. Das and Prof. K.L. Sebastian for their encouragement throughout my thesis work. I would like to thank them for many valuable lessons I have learnt from them, during the chemical dynamics group meetings. My special thanks to Prof. K.L. Sebastian for selecting me to work with him as a teaching assistant. I also thank him for giving me a wonderful course on Statistical

Mechanics. He has been a wonderful teacher and his lucid way of teaching has helped me grasp the subject better.

I express my sincere thanks to Prof. S. Umapathy for giving me a chance to participate in the ICORS-2012 conference. It was a good learning experience.

I wish to thank Prof. S. Ramakrishnan for all his encouraging words towards me and for his valuable comments during the manuscript preparation on the carbon bond.

I would like to thank present and past chairmen of our department for their constant support and providing me a wonderful infrastructure to carry out my research. I wish to thank all the faculty members of our department for their helpful and encouraging attitude. I specially thank Dr. Sai G. Ramesh for maintaining a wonderful computational facility in the department and for his always approachable presence.

I thank all the staff members of our department for taking care of all the official matters.

I gratefully acknowledge financial supports from CSIR and IISc during my Ph.D. tenure. I also acknowledge the financial grants from DST and IISc for attending the Ohio State Conference in 2012.

I sincerely acknowledge the SERC department, IISc for providing excellent computational facilities.

I would like to take this opportunity to thank Mrs. Arunan for being so nice and affectionate, and for inviting us on different festivals and making us feel at home with all those delicious meals.

I thank Dr. Santosh Mishra and Bhawana Bhabhi for their loving company and advices.

I express my sincere thanks to my seniors Dr. Mausumi, Dr. Aiswaryalakshmi and Dr. Harish for their valuable advices. Special thanks to Mausumi di and Aiswarya di

for making me familiar with the instrument. It has been a wonderful experience to work with my dear colleagues Abhishek, Sharath, Kiran, Kunal, Sharon and Emmanuel. I cherish the time spent with them. I wish to thank all the summer students and visiting faculties of our lab.

I take this opportunity to thank Abhishek for being such a wonderful friend and for being with me in all the ups and downs of my life.

I feel privileged for being surrounded with some wonderful people. It gives me immense pleasure to mention the constant support of my friends during my research work. My special thanks to Abhishek, Debarati, Chandrabhushan, Deepika and Manisha for giving me some of the most wonderful moments of my life. I thank them for adding extra spice to all the special occasions of my Ph.D. life. Things would have not been so easy and smooth without these people in IISc. I rely so much on them that I would deeply miss their joyous presence after leaving IISc. My Special thanks to my junior Sharon for remembering my favorite things and for all those chocolates and *Kaju barfis*. Abhishek, Sharon and Debarati deserve special thanks for all their care during the course of writing the thesis.

I am thankful to my friends, Bhabatosh, Koushambi, Sthita, Pallavi, Rati, Shubhadip and Soumi for all the wonderful times we spent together. I would also like to thank Deepika J., Rekha, Rohit, Himangshu, Saheli, Puja, Barun, Koushik, Sujoy, Sourav, Deepmala, Uttara, Raja Mitra, Neha, Bijayalaxmi, Aninadita, Yogesh, Balaji, Ravi, Joydeb, Ruchi, Yashpal, Rishi bhaiya and Bhawana di for making my tenure in IISc a wonderful experience. My special thanks to Vijayashree for her helps during the course of chirped-pulse generation experiments and for being a wonderful friend.

I would like to thank all the members of '2011' Al(l)chemists' club. It was fun working with them for arranging different programs of the department.

I thank my friends Awanish and Raju from depth of my heart for their evergreen friendship and all their encouragements in my life.

I would like to thank all the members of the IPC cricket team for their refreshing company. I will really miss those wonderful days and practice sessions. The 2013 tournament win was a special moment which I will always cherish.

I owe my thanks to all my teachers who have helped me reach here.

I would like to extend my sincere thanks to my cousin Dr. Satyendra Kumar Pandey for his valuable advices at every crucial junctures of my academic life.

I thank my bhaiya, bhabhi and didi for all their love and affection.

Finally, I would like to thank the divine figures of my life, my parents, Mr. Yogendra Mani and Mrs. Manju Lata Mani, for all their efforts and sacrifices for making me what I am today. Thanks to both of them for giving me strength and freedom to achieve my goals. However much I try to say it would still be the least and with this I dedicate my thesis to them.

Devendra Mani

Contents

Preface

Weak intermolecular interactions have very strong impact on the structures and properties of life giving molecules like H_2O, DNA, RNA etc. These interactions are responsible for many biological phenomena. The directional preference of some of these interactions is used for designing different synthetic approaches in the supramolecular chemistry. The work reported in this Thesis comprises of investigations of weak intermolecular interactions in gas phase using home-built Pulsed Nozzle Fourier Transform Microwave (PN-FTMW) spectrometer as an experimental tool and ab-initio and Atoms in Molecules (AIM) theory as theoretical tools. The spectrometer which is coupled with a pulsed nozzle is used to record pure rotational spectra of the molecular clusters in a jet cooled molecular beam. In the molecular beam molecules/complexes are free from interactions with other molecules/complexes and thus, spectroscopy in the molecular beams provides information about the 'isolated' molecule/complex under investigation. The rotational spectra of the molecules/complexes in the molecular beam provide their geometry in the ground vibrational states. These experimental geometries can be used to test the performance and accuracy of theoretical models like ab-initio theory, when applied to the weakly bound complexes. Further the AIM theory can be used to gain insights into the nature and strength of the intermolecular interactions present in the system under investigation.

Chapter I of this Thesis gives a brief introduction of intermolecular interactions. Other than hydrogen bonding, which is considered as the most important intermolecular interaction, many other intermolecular interactions involving different atoms have been observed in past few decades. The chapter summarizes all these interactions. The chapter also gives a brief introduction to the experimental and theoretical methods used to probe these interactions.

In Chapter II, the experimental and theoretical methods used in this work are summarized. Details of our home-built PN-FTMW spectrometer are given in this chapter. The chapter also discusses briefly the theoretical methods like ab-initio, AIM and Natural bond orbital (NBO) analysis. We have made few changes in the mode of control of one of our delay generators which have also been described.

Chapter III and Chapter V of this Thesis are dedicated to the propargyl alcohol complexes. Propargyl alcohol (PA) is a molecule of astrophysical interest. It is also important in combustion chemistry since propargyl radical is considered as the precursor in soot formation. Moreover, PA is a multifunctional molecule, having a hydroxyl (-OH) and an acetylenic (-C≡C-H) group. Both of the groups can individually act as hydrogen bond acceptor as well as donor and thus PA provides an exciting possibility of studying many different types of weak interactions. Due to internal motion of -OH group, PA monomer can exist in gauche as well as trans form. However, rotational spectra of PA-monomer show the presence of only gauche conformer.

In Chapter III, rotational spectra of Ar•••PA complex are discussed. The pure rotational spectra of the parent Ar•••PA complex and its two deuterated isotopologues, Ar•••PA-D (OD species) and Ar•••PA-D (CD species), could be observed and fitted within experimental uncertainty. The structural fitting confirmed a structure in which PA is present as gauche conformer and argon interacts with both the O-H group and the acetylenic group leading to Ar•••H-O and Ar•••π interactions respectively. Presence of these interactions was further confirmed by AIM theoretical analysis. In all the three isotopologues c-type rotational transitions showed significant splitting. Splitting patterns in the three isotopologues suggest that it originates mainly due to the large amplitude motion of the hydroxyl group and the motion is weakly coupled with the carbon chain bending motion. No evidence for the complex with trans conformer of PA was found. Although, we could not observe Ar•••trans-PA complex experimentally, we decided to perform ab-initio and AIM theoretical calculations on this complex as well. AIM calculations suggested the presence of Ar•••H-O and a unique Ar•••C interaction in this complex which was later found to be present in the Ar•••methanol complex as well. This prompted us to explore different possible interactions in methanol, other than the well known O-H•••O hydrogen bonding interactions, and eventually led us to an interesting interaction which we termed as carbon bond.

Chapter IV discusses carbon bonding interaction in different complexes. Electrostatic potential (ESP) calculations show that tetrahedral face of methane is electron-rich and thus can act as hydrogen/halogen bond acceptor. This has already been observed in

many complexes, e.g. CH_4●●●H_2O/HF/HCl/ClF etc., both experimentally and theoretically. However, substitution of one of the hydrogens of methane with -OH leads to complete reversal of the properties of the CH_3 tetrahedral face and this face in methanol is electron-deficient. We found that CH_3 face in methanol interacts with electron rich sites of H_nY molecules and leads to the formation of complexes stabilized by Y●●●C-X interactions. This interaction was also found to be present in the complexes of many different CH_3X (X=OH/F/Cl/Br/NO_2/NF_2 etc.) molecules. AIM, NBO and C-X frequency shift analyses suggest that this interaction could be termed as "carbon bond". The carbon bonding interactions could be important in understanding hydrophobic interactions and thus could play an important role in biological phenomena like protein folding. The carbon bonding interaction could also play a significant role in the stabilization of the transition state in S_N2 reactions.

In Chapter V of this Thesis rotational spectra of propargyl alcohol dimer are discussed. Rotational spectra of the parent dimer and its three deuterated (O-D) isotopologues (two mono-substituted and one bi-substituted) could be recorded and fitted within experimental uncertainty. The fitted rotational constants are close to one of the ab-initio predicted structure. In the dimer also propargyl alcohol exists in the gauche form. Atoms in molecules analysis suggests that the experimentally observed dimer is bound by O-H●●●O, O-H●●●π and C-H●●●π interactions.

Chapter VI of the thesis explores the 'electrophore concept'. To observe the rotational spectra of any species and determine its rotational constant by microwave spectroscopy, the species should have a permanent dipole moment. Can we obtain rotational constants of a species having no dipole moment via microwave spectroscopy? Electrophore concept can be used for this purpose. An electrophore is an atom or molecule which could combine with another molecule having no dipole moment thereby forming a complex with a dipole moment, e.g. Argon atom is an electrophore in Ar●●●C_6H_6 complex. The microwave spectra of Ar●●●$^{13}CC_5H_6$ and Ar●●●C_6H_5D complexes were recorded and fitted. The A rotational constant of these complexes was found to be equal to the C rotational constant of $^{13}CC_5H_6$ and C_6H_5D molecules respectively and thus we could determine the C rotational constant of microwave 'inactive' $^{13}CC_5H_6$. This concept could be used to obtain the rotational spectra of parallel displaced benzene-dimer if it exists.

We recently showed that the square pyramidal $Fe(CO)_5$ can act as hydrogen bond acceptor. Appendix I summarizes the extension of this work and discusses interactions of trigonal bipyramidal $Fe(CO)_5$ with HF, HCl, HBr and ClF. Our initial attempts on generating a chirped pulse to be used in a new broadband spectrometer are summarized in Appendix II. Preliminary investigations on the propargyl•••water complex are summarized in Appendix III.

List of Abbreviations

FID	Free Induction Decay
ZPE	Zero point (vibrational) Energy
ZPC	Zero point (vibrational energy) Correction
BSSE	Basis Set Super Position Error
AIM	Atoms in Molecules
NBO	Natural Bond Orbital
PN-FTMW	Pulsed Nozzle Fourier Transform Microwave Spectrometer
RF	Radio Frequency
MW	Microwave
SPDT	Single Pole Double Throw
SSBM	Single Side Band Mixer
BCP	Bond Critical Point
RCP	Ring Critical Point
PA	Propargyl Alcohol

List of Tables

List of Figures

Chapter I.

Introduction.

I.1. Intermolecular interactions

Importance of intermolecular interactions can be highlighted by the fact that the structures and properties of almost all vital molecules of life like DNA, RNA and proteins are governed by them.[1,2] Life as we know it, would not be the same without intermolecular interactions. The liquid state of water is due to the intermolecular hydrogen bonding present between the water molecules.[3] The double stranded structure of DNA exists because of π-stacking and hydrogen bonding interactions between the nitrogenous base pairs. The secondary structure of proteins is mainly due to the hydrogen bonding between the backbone amino and carbonyl groups. The tertiary structure of proteins is also strongly influenced by the intermolecular interactions. Hydrogen bonding and other van der Waals interactions are responsible for many biological phenomena like protein folding, and also play important role in various biological reactions. Intermolecular interactions are important in synthetic chemistry also and often decide the outcome of chemical reactions. The orientational preference of more specific intermolecular interactions like hydrogen bonding, and halogen bonding, is often utilized in supramolecular chemistry and crystal engineering to design macromolecules.[4-8] The intermolecular interactions are also important in medicinal chemistry and site-specific drug delivery is often governed by these forces.[6,9,10]

Ideal gas law was proposed by E. Clapeyron in 1834.[11] The law assumes that the gas molecules are point masses and no interaction exists between them. J.D. van der Waals modified the ideal gas law by taking the definite size of molecules and the intermolecular forces into account and introduced his equation of state in 1873.[12] The van der Waals equation of state is

$$\left(P + \frac{an^2}{V^2}\right)(V - nb) = nRT$$

P, V, T and n are pressure, volume, temperature and number of moles of the gas. Factors *a* and *b* are called van der Waals coefficients and their values differ for different gases. The coefficient 'a' depends on intermolecular forces present between the gaseous molecules and the coefficient 'b' depends on the size of the molecules. As the values of 'a' and 'b' approach zero the equation tends to the ideal gas law.

In practice, none of the gases are ideal. The intermolecular forces become more and more important as the temperature of the gas is lowered. Liquefaction of helium (^{4}He)

by H.K. Onnes, in 1908, provided the final validation of the van der Waals equation. However, the van der Waals equation does not give any information about the nature of interactions present between the molecules. For many years all the intermolecular interactions were called van der Waals interactions. However, many observed facts like the difference between the physical states of bulk H_2O and H_2S could not be explained on the basis of the 'same van der Waals interactions'. This highlighted the need of understanding the nature of the interactions involved between these molecules. In the early 20th century, Moore and Winmill,[13] Huggins,[14] Latimer and Rodebush[15] and later Pauling[3] introduced a new classification called "hydrogen bonding" which could be considered a subset of van der Waals interactions. Using the concept of hydrogen bonding the bulk properties of H_2O and H_2S could be explained.

Interaction energy for a molecular complex can be decomposed into five terms: electrostatic ΔE_{elec}, exchange repulsion ΔE_{ex}, induction ΔE_{ind}, dispersion ΔE_{disp}, and charge transfer ΔE_{ct}.

$$\Delta E_{total} = \Delta E_{elec} + \Delta E_{ex} + \Delta E_{ind} + \Delta E_{disp} + \Delta E_{ct}$$

The ΔE_{elec} term arises due to electrostatic interactions between permanent multipoles. The electrostatic forces dominate in the complexes of polar molecules e.g. in the HF•••HF and ClF•••ClF dimers. The exchange repulsion term ΔE_{ex} is due to repulsion between electrons and is a result of Pauli's exclusion principle which prevents the electrons from two monomer units from occupying the same region of space, the term is always repulsive. A non-polar molecule can be polarized by interaction with an ion or multipole. When an ion polarizes a molecule and induces a dipole moment, it is called ion-induced dipole. Similarly if the polarizing entity is a dipole, it is called dipole-induced dipole and so on. The induction term ΔE_{ind} appears due to these interactions. Induction is the prominent force behind the formation of complexes of rare gases with polar molecules like hydrogen halides (HX). The complexes like Ne•••HF, Ar•••HF, Kr•••HF, Ar_n•••HF/HCl, Ar_n•••H_2O etc. are known experimentally.[16-22] The ΔE_{disp} term is due to dispersion interactions between the interacting molecules. Dispersion is the dominant force between two non-polar units and can be thought as induced-dipole-induced-dipole interaction. Due to fluctuation in the electron density all the molecules/atoms possess instantaneous dipole moments. The instantaneous dipole moment of one molecule/atom interacts with other molecule/atom and creates an instantaneous dipole in the other unit as well.

The instantaneous dipoles in the two units are correlated and follow the direction of each other i.e. the electron density of one molecule/atom changes with the electron density of the other molecule/atom. The dispersion interactions stabilize complexes between rare gas atoms like Ar•••Ar, Ne•••Ar and Ar•••Kr etc. The mixed rare gas dimers have a net dipole moment and have been observed by microwave spectroscopy.[23,24] The charge transfer interaction term ΔE_{ct} accounts for the covalent character and becomes more important at close distances. All these interactions contribute towards the stability of the intermolecular complexes. However, the proportion of the contribution differs from system to system.

Quantum chemical calculations have helped immensely in expanding our knowledge about the nature of the intermolecular interactions. In the last few decades, computing power has increased multifold and now quantum chemical calculations on many body systems can be performed rapidly. The improvement in the computing power also paralleled the development of new quantum chemical methods. Consequently, several new specific interactions involving other groups have been reported in the recent past and the realm of intermolecular interactions is widening with much improved understanding.[25-35]

I.1.a. Hydrogen bonding

Hydrogen bonding is the most celebrated intermolecular interaction. The ubiquitous presence of this interaction in nature attracts researchers from diverse fields towards it. The hydrogen bonding is studied by chemists, biologists and physicists with equal interest. The literature on hydrogen bonding is extensive and many monographs exist on this topic.[1,2,36-39] It is not surprising that every hour roughly one paper gets cited on SciFinder with the topic hydrogen bond.

Hydrogen bonded systems are usually represented as X-H•••Y where hydrogen atom acts as a bridge between two electronegative atoms X and Y and is closer to one of them (X). The X-H unit is known as hydrogen bond donor or electron acceptor and Y as hydrogen bond acceptor or electron donor. Classically X and Y atoms were limited to F, N and O atoms and it was considered that only these atoms can act as hydrogen bond acceptor/donor. However, now many different donors and acceptors are known in literature. Weak donors like C-H & S-H and weak acceptor like C & S can also participate in the hydrogen bond formation.[1,40,41] Systems in which π-electron density,

radicals and sigma electrons act as hydrogen bond acceptors are known in literature.[40,42-45] Formation of hydrogen bond is generally followed by an increase in the X-H bond length and a red-shift in the X-H stretching frequency.[38] However, unusual blue shifting hydrogen bonds are also known in the literature.[46] Possibility of many different donors and acceptors and ambiguity in nomenclature of these different systems prompted IUPAC to come up with a new broader definition of hydrogen bonds.[47,48] According to the new IUPAC definition the X can be any atom which is more electronegative than hydrogen i.e. the hydrogen atom should have a partial positive charge, and Y can be any electron rich region. Thus, the new definition does not put any restriction on the acceptor unit. Depending on the participating donor and acceptor units, energy of the hydrogen bond lies in the range 2-170 kJ/mol.[1] Thus, the strongest hydrogen bonds approach the lower limit for the covalent bonds and the weakest hydrogen bonds approach the upper limit for the van der Waals interactions. Forces acting in the van der Waals interactions and hydrogen bonding are similar. However, what makes hydrogen bonding different from van der Waals interactions is its directional preference. A dynamic criteria for the hydrogen bonding has also been proposed recently.[49] Recently, the hydrogen bond has been 'visualized' for the first time by *Atomic Force Microscopy (AFM)*. The AFM images of 8-hydroxyquinoline assembled on Cu (111) surface, showed widely accepted O-H•••O hydrogen bonds as well as weaker C-H•••O and N-H•••O hydrogen bonds.[50]

Microwave spectroscopy in molecular beams provides an ideal opportunity of probing isolated hydrogen bonded clusters in gas phase. In *Chapter III and V* of this *Thesis*, hydrogen bonding properties of propargyl alcohol molecules have been studied using microwave spectroscopy and Atoms in Molecules (AIM) theory. The propargyl alcohol dimer, discussed in *Chapter V*, has been found to be bound with three different types of hydrogen bonds namely O-H•••O, O-H•••π and C-H•••π hydrogen bonds. The van der Waals complexes of propargyl alcohol with Ar and benzene with Ar have also been studied and are discussed in *Chapter III and Chapter VI* respectively.

I.1.b. Halogen bonding

Similar to hydrogen bonding, halogen bonding can be represented as X-Hal•••Y, where Hal is the halogen atom. There is no restriction on the nature of X and it can be any atom or group and Y should be having electron rich regions like lone-pairs of

electrons, π-electron density etc. Since the halogen bonds involve direct interaction between an electronegative atom (halogen) and another electron rich centre Y, these interactions were initially confusing. However, sigma-hole concept proposed by Politzer et al. explained that the interaction is indeed between the electropositive pole of the halogen atom (sigma-hole) and electron rich centres.[26,28,51] Chlorine, bromine and iodine frequently form halogen bonded complexes, however, few cases of fluorine acting as halogen bond donor have also been reported.[52] The halogen bond strength typically increases in the order F<Cl<Br<I which is also the order of increasing polarizablity for these elements. Strength of the halogen bonds increases with increase in the electron withdrawing power of the X moiety e.g. halogen bonds formed with CF_3Cl are much stronger than those formed with CH_3Cl.[28] Halogen bonds have been found to be even more directional than the hydrogen bonds and the X-Hal•••Y angle approaches to linearity in most of the cases. Halogen bonding has found important applications in crystal engineering, molecular recognition, and medicinal chemistry.[6,7,27] Its importance in biological systems has also been identified.[6,53]

I.1.c. Lithium bonding

Lithium is a congener of hydrogen and so is lithium bonding of hydrogen bonding. Li-bonded systems can be represented as X-Li•••Y where X is a more electronegative atom than Li or is an electron withdrawing moiety, Y can be an atom with lone pairs of electrons or it can be an electron rich region. Pioneering work on Lithium bonding was done by Kollman et al.[54] They performed Hartree-Fock level calculations on the Li-bonded F-Li•••H-F complex and concluded that the interaction is analogous to hydrogen bonding. The work was followed by experimental work by Pimentel et al. who studied a number of Li-bonded complexes by matrix isolated infrared spectroscopy.[55] Since then there have been many studies on Li-bonding.[43,56-61] Alkali halide dimers, like $(LiF)_2$ and $(NaF)_2$ prefer cyclic structure over the linear one and are more electrostatic in nature than the linear hydrogen bonded dimers.[62] The Li-bonding is not as popular as hydrogen or halogen bonding due to its rare presence in the chemical systems.

I.1.d. Other non-covalent interactions

Our understanding of non-covalent interactions is still evolving. As mentioned earlier, theoretical calculations have helped immensely in understanding these interactions in a better way. In the past two to three decades many new unique interactions have been reported and classified. Interactions like beryllium bond,[35] chalcogen bond, pnicogen bond, have been reported in literature. Beryllium bond was analyzed by Yanez et al. in 2009. They studied complexes of BeX_2 (X=H, F, Cl, OH) with different bases (NH_3, H_2O, HF, HCl, HBr, H_2S and PH_3) using *ab initio* and Atoms in Molecules (*AIM*) theoretical methods.[35] Structural changes, frequency shifts and *AIM* parameters confirmed the presence of beryllium bonds in these systems. Pnicogen bond was first analyzed by Scheiner.[31,32] It is an interaction between pnicogen elements (N, P, As, Sb, Bi). These interactions were analyzed in the PH_3•••NH_3 complex and it was found that the structure in which two units are bound with P•••N interaction, is the global minimum for the complex. For the homodimer $(PH_3)_2$, also the structure bound with P•••P interaction was found to be the global minimum.[31] Chalcogen bond is an interaction of a chalcogen atom (O, S, Se, Te and Po) with an electron rich centre Y.[29,30] It can be represented as either X-Chal•••Y or X=Chal•••Y depending on whether the chalcogen atom is bound by a single bond or double bond with the X moiety. The origin of this interaction could be explained on the basis of sigma hole concept used for halogen bonds.

Recently, we proposed another interesting interaction termed as carbon bond.[34] Carbon bond can be represented as X-C•••Y where X and Y are electronegative atoms. The carbon bond could be important in understanding hydrophobic effects which are responsible for many biological phenomena like protein folding.[63,64] The carbon bond could also play a role in stabilization of transition states in the S_N2 reactions. More recently, Guru Row et al. have provided the first experimental proof of carbon bond.[33] It is clear that research in the field of non-covalent interactions has made an impressive progress and different dimensions of these interactions are being explored now. The carbon bonding interactions are discussed in detail in *Chapter IV* of this *Thesis*.

I.2. Introduction to the theoretical and experimental methods used to study the intermolecular interactions

I.2.a. Theoretical methods

Quantum chemistry methods, like *ab initio* and *Density function Theory* (DFT) are used for the structure optimization of molecules and intermolecular complexes.[65,66] Harmonic frequency calculations are performed to confirm if the optimized structures are minima at the potential energy hypersurface by confirming the presence of all real frequencies for the normal modes of vibration. *Ab initio*-Hartree-Fock calculations are computationally cheaper and can be performed quickly. However, these calculations do not take care of correlation effects and therefore, are not advised for the complexes bound with weak intermolecular interactions. Møller-Plesset perturbation theory, which is an improvement of Hartree-Fock methods, inherently takes care of correlation interactions and is often considered to be one of the best methods available for weakly bound complexes. The theory is used for small molecular clusters since accessing bigger systems with this theory is difficult due to its high computation cost. The DFT methods are computationally cheaper and can be used to perform calculations on bigger molecules. There are many DFT hybrid functionals available and many new functionals are being reported in the literature. One of the most popular DFT-functional is the B3LYP functional. However, it is known to perform poorly for correlation effects. Recently, many dispersion corrected DFT methods (DFT-d) have been reported and have been tested to perform better for the correlation effects as compared to the earlier functionals like B3LYP.[67-69]

For microwave spectroscopy, these methods are used to obtain an approximate initial geometry of the complex or molecule under study. The rotational constants of this initial geometry are then used to predict the rotational spectra and search for the rotational transitions are made on the basis of these predictions. These quantum chemical calculations are improving consistently with time. High level calculations like MP2 theory augmented with a proper basis set, often predict a geometry which is found to be close to the eventual experimental geometry. These methods have been very useful for microwave spectroscopists and the predictions often accelerate the recording of the microwave spectra. More about these methods is discussed in *Chapter II*.

The wave-functions of the optimized geometries can further be analysed to gain more insights into many different properties of the molecules and complexes. Electrostatic potential calculations have been used to locate the possible interactions sites in a molecule.[70,71] Atoms in molecules (AIM) analysis[72,73] can be performed to gain more insights into the nature of bonding in a weakly bound complex. The AIM calculations give many types of electron density critical points, bond critical point (BCP) being one of them. Bonding interactions between two atoms can be confirmed by analysing these BCPs. The Laplacian of electron density at the BCP gives information about the nature of bonding. These methods are discussed in details in *Chapter II*.

I.2.b. Experimental methods

Structure and dynamics of the weakly bound molecular clusters can be known by performing spectroscopy in molecular beams. Supersonic expansion of the gases from a region of high pressure (~0.1-10 atm) to a region of very low pressure (~10^{-9} atm) results in cooling of the molecules and leads to the formation of weakly bound 'isolated' molecular clusters which can be probed by a suitable technique.

Rotational spectroscopy is used to determine the structure of molecules and molecular clusters. Fourier transform microwave (FTMW) spectrometers were very sensitive. However, it could be used to study only stable molecules in gas phase. Weakly bound complexes could be studied using *Molecular Beam Electric Resonance (MBER)* spectrometers but these spectrometers were much less sensitive. Balle and Flygare combined Fourier transform microwave spectroscopy with molecular beam technique for the first time.[74] These spectrometers have very high sensitivity and weakly bound complexes could be produced in the molecular beam. In the molecular beam most of the molecules cool down to their ground vibrational state and the spectra becomes much less congested. Since its inception, many weakly bound complexes have been studied using this technique.[75] In our lab, *Pulsed Nozzle Fourier Transform Microwave (PN-FTMW)* spectrometer has been fabricated.[76-78] The PN-FTMW spectrometer is based on the Balle-Flygare design. The spectrometer was used for recording the rotational spectra of complexes reported in this *Thesis*. More details about the PN-FTMW spectrometer are given in *Chapter II* of this *Thesis*. New chirped-pulse based microwave spectrometers[79-81] are becoming popular now. These spectrometers have revolutionized the field of microwave spectroscopy and many

limitations of the cavity based microwave spectrometers have been overcome. We are also planning to build a chirped-pulse based broadband spectrometer in our lab. Details of our initial attempts towards building the broadband spectrometer can be found in *Appendix II* of this *Thesis*.

Vibrational (IR) spectroscopy has been used to study the hydrogen bonded structures in solution phase as well as in the gas phase. Shift in the vibrational frequency of a particular mode on cluster formation provide information about the weak interactions. However, studying the gas-phase molecular structures by IR-spectroscopy requires very high sensitivity. Double resonance techniques like IR-UV double resonance, have been used to obtain the IR-spectra in molecular beams.[82-84] The UV laser is fixed at a known electronic transition of the complex and the IR-laser is scanned. The IR-spectra are obtained by noticing the dip in the fluorescence or ion intensity signal while scanning the IR-laser. The most common method used for the ionization is *Resonance Two Photon Ionization (R2PI)*. The generated ions using R2PI can be detected by a Time-of-Flight Mass-spectrometer (ToF-MS). Thus, the combination of these techniques provides spectral as well as the mass resolution. Clusters of the same mass but having different conformations can be distinguished using hole-burning spectroscopy, in which population of a particular conformer is burned out using an IR or a UV laser.[85,86]

Spectroscopy in the far-IR region, 20-150 cm^{-1}, allows probing transitions between vibrational-rotational-tunneling states. Saykally and coworkers have pioneered the vibrational-rotational-tunneling spectroscopy[87] and have used it extensively to perform investigations on the water-clusters.[88-90]

Dynamics of the molecules/clusters in cationic states can be investigated using *Zero Kinetic Energy (ZEKE)*[91,92] and *Mass Analyzed Threshold Ionization (MATI)*[93] techniques. These techniques are variants of the photo electron spectroscopy. These techniques have sufficiently high resolution to resolve the rotational transitions which was not possible by the conventional photo electron spectroscopy. These techniques can also be used to probe the low frequency inter molecular vibrational modes.

I.3. Microwave spectroscopy

Microwave spectroscopy has a reputation of being the most accurate method to determine structures of molecules in the gas phase. Transition frequency between two rotational levels of a molecule depends on its moment of inertia. Thus, by measuring the rotational spectra one can obtain the moment of inertia and eventually rotational constants, which are inversely proportional to the moment of inertia, of a molecule.

On the basis of the symmetry of the moment of inertia ellipsoid, the molecules are divided into four main categories: (i) Asymmetric top ($I_a < I_b < I_c$), (ii) Symmetric top ($I_a < I_b = I_c$ (prolate) or $I_a = I_b < I_c$ (oblate)), (iii) Linear top (I_a=0, I_b=I_c) and (iv) Spherical top ($I_a = I_b = I_c$), here I_a, I_b and I_c are the moment of inertia of the molecule along principal axis *a, b and c*. The spherical top molecules are microwave inactive since they do not possess a permanent dipole moment which is essential for the detection of pure rotational spectra. Spectra for the symmetric top molecules are quite simple and are easy to observe and assign. However, the simplicity in the spectra comes with a cost and for these molecules only one rotational constant (B) can be determined experimentally. Asymmetric top molecules have complex spectra which are difficult to assign. The complexity in the spectra increases with the asymmetry in the molecule. However, once the spectra is assigned and fitted, all three *A, B and C* rotational constants can be determined which helps in extracting much more structural information for these molecules. Theoretical details about the spectra of these different categories are not discussed here and can be found elsewhere.[94,95] The main focus of this section is to provide a glimpse about microwave spectroscopy and the information which could be extracted from the rotational spectra.

In addition to accurate structural determination, microwave spectroscopy can also provide other valuable information about the molecules/complexes. The centrifugal distortion constants can be obtained by fitting of the rotational spectra. These distortion constants depend on the various vibrational frequencies of the molecules. For a simple diatomic molecule, the centrifugal distortion constant D_J is related to both the rotational constant and vibrational frequency and hence from the rotational spectra one could determine the vibrational frequency. For a simple diatomic molecule having vibrational frequency in the infrared region, it may appear like a more difficult and circuitous way of getting the vibrational frequency. However, the same method can be successfully used for weakly bound complexes such as

Ar•••Ne,[23] where the stretching frequency is usually in the terahertz (THz) region and microwave spectroscopy offers a cheaper and easier method for determining the stretching frequency and bond strength. More about the use of distortion constants in extracting information about the low frequency intermolecular vibrational modes is discussed in *Chapter VI* of this *Thesis*.

Quadrupole moment of nuclei can interact with molecular field gradient of molecules to give rise to nuclear hyperfine splitting in the rotational spectra. Only those nuclei for which nuclear spin (*I)* is ≥ 1, have non-zero quadrupole moment and can lead to such splitting. Nuclei with nuclear spin 0 or ½ do not affect the rotational spectra in this way as such nuclei are spherical and hence have no quadrupole moment. Nuclear quadrupole coupling constants for the coupling nuclei can be obtained by fitting the nuclear hyperfine spectra with a suitable Hamiltonian. These coupling constants, which are directly related to the electric field gradient around the coupling nuclei, give information about the electronic structure and chemical bonds of the molecule. For example, for HCl, large value of the Cl coupling constant (-67.819 MHz) indicates non-spherical electronic charge distribution around Cl due to covalent bonding whereas the small value for the same in KCl (<0.04 MHz) implies Cl in KCl is in Cl^- form and has a spherical charge distribution similar to Ar.[95]

The (2J+1) degeneracy of rotational levels associated with M_J values (M_J=-J to +J including zero) can partially be lifted by the application of an electric field. Here J denotes rotational quantum number corresponding to a rotational state having angular momentum $[J(J+1)]^{1/2}$ and M_J is the projection of angular momentum on a space fixed reference axis, Z, both in units of $h/2\pi$. This is known as the Stark effect. Perturbation theory can be used to calculate the energies of the split levels. Linear molecules (K=0) have no first order Stark effect and same is true for the K=0 levels of the symmetric top molecules, K is the projection of angular momentum on the body fixed z-axis which is the symmetry axis in case of symmetric top molecules. However, second order Stark effect is non-zero for these molecules. Asymmetric top molecules have non-zero first order as well as non-zero second order Stark effect. The first order Stark energy is directly proportional to the dipole moment of the molecule whereas second-order Stark energy depends on the square of the dipole moment. Thus, by measuring the extent of splitting in the rotational spectra, permanent dipole moment for the molecule in the ground state can be obtained. The splitting due to the Stark effect also depends on the rotational quantum number J and thus the Stark effect can

also be used to assign the rotational transitions of the molecules having complex rotational spectra, e.g. asymmetric top molecules.

Internal rotation within a molecule (like relative rotation of two methyl fragments in ethane molecule) can couple with the overall rotation of the molecule leading to splitting of the rotational transitions. The observed splitting depends on both the symmetry of the potential as well the barrier height for the internal rotation. Thus, by measuring the value of splitting due to internal motions the nature of the potential and the barrier height can be determined for several molecules.

Microwave spectroscopy has recently been used in detecting chirality in the molecules as well.[96]

I.4. Present investigations

In this *Thesis*, investigations on weakly bound complexes using rotational spectroscopy and various theoretical methods have been reported. In *Chapter II* experimental techniques and theoretical methods are discussed. Rotational spectra and *AIM* analysis of the Ar•••propargyl alcohol complex are discussed in *Chapter III*. Rotational spectra of the parent complex and its two deuterated isotopologues have been observed and assigned. The structure of the complex has been confirmed. *AIM* analysis confirms the presence of Ar•••H-O and Ar•••π interactions in the experimentally observed structure. In *Chapter IV*, the X-C•••Y carbon bond interactions have been discussed. These interactions were analysed using *ab initio* and *AIM* theoretical methods. *Chapter V* reports the rotational spectra of propargyl alcohol-dimer. Spectra for the parent dimer and its three deuterated isotopologues were observed and fitted within experimental uncertainty. In *Chapter VI*, rotational spectra of deuterium and C-13 isotopologues of the Ar•••benzene complex have been reported and the concept of electrophore is discussed.

Hydrogen bonding and halogen bonding interactions of trigonal bypyramidal $Fe(CO)_5$ with HF/HCl/HBr/ClF are discussed in *Appendix I*. Our initial attempts towards a new broadband spectrometer have been summarized in *Appendix II*. Preliminary investigations on PA•••H_2O complexes are given in *Appendix III*.

I.5. References

1. Desiraju, G. R., Steiner, T. *The weak hydrogen bond in structural chemistry and biology* Oxford University Press: Oxford, **1999**.

2. Jeffrey, G. A.; Saenger, W. *Hydrogen bonding in biological structures*; Berlin ; New York : Springer-Verlag, **1994**.

3. Pauling, L. *The Nature of Chemical Bonding*; Cornell University Press: Ithaka, **1960**.

4. Desiraju, G. R. *Chem. Commun.* **1997**, 1475-1482.

5. Desiraju, G. R.; Vittal, J. J.; Ramanan, A. *Crystal engineering : a textbook*; Hackensack, NJ : World Scientific : IISc Press, c2011.

6. Metrangolo, P.; Neukirch, H.; Pilati, T.; Resnati, G. *Acc. Chem. Res.* **2005**, *38*, 386-395.

7. Metrangolo, P.; Resnati, G. *Chemistry – A European Journal* **2001**, *7*, 2511-2519.

8. Desiraju, G. R.; Vittal, J. J.; Ramanan, A. *Crystal Engineering: A Textbook*; World Scientific, **2011**.

9. Wilcken, R.; Zimmermann, M. O.; Lange, A.; Joerger, A. C.; Boeckler, F. M. *J. Med. Chem.* **2012**, *56*, 1363-1388.

10. Davies, D. R.; Cohen, G. H. *Proceedings of the National Academy of Sciences* **1996**, *93*, 7-12.

11. Clapeyron, E. *Journal de l'École Polytechnique* **1834**, 153-190.

12. van der Waals, J. D. *Ph.D. dissertation*, *Univ. Leiden*, *1873*.

13. Moore, T. S.; Winmill, T. F. *Journal of the Chemical Society, Transactions* **1912**, *101*, 1635-1676.

14. Huggins, M. L. *Phys. Rev.* **1921**, *18*, 333.

15. Latimer, W. M.; Rodebush, W. H. *J. Am. Chem. Soc.* **1920**, *42*, 1419-1433.

16. Nauta, K.; Miller, R. E. *J.Chem.Phys.* **2001**, *115*, 4508-4514.

17. Farrell, J. T.; Sneh, O.; McIlroy, A.; Knight, A. E. W.; Nesbitt, D. J. *J.Chem.Phys.* **1992**, *97*, 7967-7978.

18. Lovejoy, C. M.; Schuder, M. D.; Nesbitt, D. J. *J.Chem.Phys.* **1986**, *85*, 4890-4902.

19. Gutowsky, H. S.; Emilsson, T.; Arunan, E. *J. Chem. Phys.* **1997**, *106*, 5309-5315.

20. Gutowsky, H. S.; Klots, T. D.; Chuang, C.; Keen, J. D.; Schmuttenmaer, C. A.; Emilsson, T. *J. Am. Chem. Soc.* **1985**, *107*, 7174-7175.

21. Chuang, C.-C.; Tsang, S. N.; Hanson, J. G.; Klemperer, W.; Chang, H.-C. *J.Chem.Phys.* **1997**, *107*, 7041-7056.

22. Farrell, J. T.; Nesbitt, D. J. *J.Chem.Phys.* **1996**, *105*, 9421-9440.

23. Grabow, J. U.; Pine, A. S.; Fraser, G. T.; Lovas, F. J.; Suenram, R. D.; Emilsson, T.; Arunan, E.; Gutowsky, H. S. *J.Chem.Phys.* **1995**, *102*, 1181-1187.

24. Xu, Y.; Jäger, W.; Djauhari, J.; Gerry, M. C. L. *J.Chem.Phys.* **1995**, *103*, 2827-2833.

25. Politzer, P.; Murray, J. S. *ChemPhysChem* **2013**, *14*, 278-294.

26. Politzer, P.; Murray, J. S.; Clark, T. *Phys. Chem. Chem. Phys.* **2013**.

27. Legon, A. C. *Phys. Chem. Chem. Phys.* **2010**, *12*, 7736-7747.

28. Politzer, P.; Lane, P.; Concha, M.; Ma, Y.; Murray, J. *J. Mol. Model.* **2007**, *13*, 305-311.

29. Manna, D.; Mugesh, G. *J. Am. Chem. Soc.* **2012**, *134*, 4269-4279.

30. Wang, W.; Ji, B.; Zhang, Y. *J. Phys. Chem. A* **2009**, *113*, 8132-8135.

31. Scheiner, S. *J. Chem. Phys.* **2011**, *134*, 094315-094319.

32. Scheiner, S. *J. Phys. Chem. A* **2011**, *115*, 11202-11209.

33. Thomas, S. P.; Pavan, M. S.; Guru Row, T. N. *Chem. Commun.* **2013**.

34. Mani, D.; Arunan, E. *Phys. Chem. Chem. Phys.* **2013**, *15*, 14377-14383.

35. Yáñez, M.; Sanz, P.; Mó, O.; Alkorta, I.; Elguero, J. *Journal of Chemical Theory and Computation* **2009**, *5*, 2763-2771.

36. Grabowski, S. J. *Hydrogen Bonding: New Insights*; Springer: Dordrecht, **2006**.

37. Jeffrey, G. A. *An Introduction to Hydrogen Bonding*; Oxford University Press: Oxford, **1997**.

38. Scheiner, S. *Hydrogen Bonding: A Theoretical Perspective*; Oxford University Press: Oxford, **1997**.

39. Gilli, P.; Gilli, G. *The Nature of the Hydrogen Bond*; Oxford University Press: Oxford, **2009**.

40. Raghavendra, B.; Arunan, E. *Chem. Phys. Lett.* **2008**, *467*, 37-40.

41. Allen, F. H.; Bird, C. M.; Rowland, R. S.; Raithby, P. R. *Acta Crystallographica Section B* **1997**, *53*, 696-701.

42. Wessel, J.; Lee, J. C.; Peris, E.; Yap, G. P. A.; Fortin, J. B.; Ricci, J. S.; Sini, G.; Albinati, A.; Koetzle, T. F.; Eisenstein, O.; Rheingold, A. L.; Crabtree, R. H. *Angewandte Chemie International Edition in English* **1995**, *34*, 2507-2509.

43. Raghavendra, B.; Arunan, E. *The Journal of Physical Chemistry A* **2007**, *111*, 9699-9706.

44. Alkorta, I.; Elguero, J. *Chem. Soc. Rev.* **1998**, *27*, 163-170.

45. Szymczak, J. J.; Grabowski, S. J.; Roszak, S.; Leszczynski, J. *Chem. Phys. Lett.* **2004**, *393*, 81-86.

46. Hobza, P.; Havlas, Z. *Chem. Rev.* **2000**, *100*, 4253-4264.

47. Arunan, E.; Desiraju, G. R.; Klein, R. A.; Sadlej, J.; Scheiner, S.; Alkorta, I.; Clary, D. C.; Crabtree, R. H.; Dannenberg, J. J.; Hobza, P.; Kjaergaard, H. G.; Legon, A. C.; Mennucci, B.; Nesbitt, D. J. *Pure Appl. Chem.* **2011**, *83*, 1637-1641.

48. Arunan, E.; Desiraju, G. R.; Klein, R. A.; Sadlej, J.; Scheiner, S.; Alkorta, I.; Clary, D. C.; Crabtree, R. H.; Dannenberg, J. J.; Hobza, P.; Kjaergaard, H. G.; Legon, A. C.; Mennucci, B.; Nesbitt, D. J. *Pure Appl. Chem.*, *83*, 1619-1636.

49. Goswami, M.; Arunan, E. *Phys. Chem. Chem. Phys.* **2009**, *11*, 8974-8983.

50. Zhang, J.; Chen, P.; Yuan, B.; Ji, W.; Cheng, Z.; Qiu, X. *Science* **2013**, *342*, 611-614.

51. Murray, J.; Lane, P.; Politzer, P. *J. Mol. Model.* **2009**, *15*, 723-729.

52. Metrangolo, P.; Murray, J. S.; Pilati, T.; Politzer, P.; Resnati, G.; Terraneo, G. *CrystEngComm* **2011**, *13*, 6593-6596.

53. Auffinger, P.; Hays, F. A.; Westhof, E.; Ho, P. S. *Proceedings of the National Academy of Sciences of the United States of America* **2004**, *101*, 16789-16794.

54. Kollman, P. A.; Liebman, J. F.; Allen, L. C. *J. Am. Chem. Soc.* **1970**, *92*, 1142-1150.

55. Ault, B. S.; Pimentel, G. C. *The Journal of Physical Chemistry* **1975**, *79*, 621-626.

56. Esrafili, M. D.; Juyban, P.; Solimannejad, M. *Computational and Theoretical Chemistry* **2014**, *1027*, 84-90.

57. Solimannejad, M.; Rezaei, Z.; Esrafili, M. D. *Mol. Phys.* **2013**, 1-19.

58. Li, Q.; Wang, H.; Liu, Z.; Li, W.; Cheng, J.; Gong, B.; Sun, J. *The Journal of Physical Chemistry A* **2009**, *113*, 14156-14160.

59. Li, Y.; Wu, D.; Li, Z.-R.; Chen, W.; Sun, C.-C. *J.Chem.Phys.* **2006**, *125*, -.

60. Ammal, S. S. C.; Venuvanalingam, P. *J.Chem.Phys.* **1998**, *109*, 9820-9830.

61. Sannigrahi, A. B.; Kar, T.; Niyogi, B. G.; Hobza, P.; Schleyer, P. v. R. *Chem. Rev.* **1990**, *90*, 1061-1076.

62. Parajuli, R.; Arunan, E. *Chem. Phys. Lett.* **2013**, *568–569*, 63-69.

63. Tanford, C. *The Hydrophobic Effect: Formation of Micelles and Biological Membranes 2d Ed*; John Wiley & Sons, **1980**.

64. Ben-Naim, A. *Hydrophobic interactions*; Plenum Press: New York and London, **1980**.

65. Szabo, A.; Ostlund, N. S. *Modern Quantum Chemistry: Introduction to Advanced Electronic Structure Theory*; Dover Publications Inc. : Mineola, **1996**.

66. Jensen, F. *Introduction to Computational Chemistry* John Wiley & Sons: New York, **1999**.

67. Grimme, S.; Antony, J.; Ehrlich, S.; Krieg, H. *J.Chem.Phys.* **2010**, *132*, 154104.

68. Chai, J.-D.; Head-Gordon, M. *Phys. Chem. Chem. Phys.* **2008**, *10*, 6615-6620.

69. Grimme, S. *J. Comput. Chem.* **2006**, *27*, 1787-1799.

70. Gadre, S. R.; Shirsat, R. N. *Electrostatics of Atoms and Molecules*; Universities Press: Hyderabad,, **2000**.

71. Sjoberg, P.; Politzer, P. *J. Phys. Chem.* **1990**, *94*, 3959-3961.

72. Bader, R. F. W. *Chem. Rev.* **1991**, *91*, 893-928.

73. Bader, R. F. W. *Atoms in Molecules: A Quantum Theory* Clarendon Press: Oxford, **1990**.

74. Balle, T. J.; Flygare, W. H. *Rev. Sci. Instrum.* **1981**, *52*, 33-45.

75. Novick, S. E. *Bibliography of Rotational Spectra of Weakly Bound Complexes* **2013**.

76. Arunan, E.; Dev, S.; Mandal, P. K. *Applied Spectroscopy Reviews* **2007**, *39*, 131-181.

77. Arunan, E.; Tiwari, A. P.; Mandal, P. K.; Mathias, P. C. *Curr. Sci.* **2002**, *82*, 533-540.

78. Mandal, P. K. *Ph.D. Dissertation*, *Indian Institute of Science*, *2005*.

79. Brown, G. G.; Dian, B. C.; Douglass, K. O.; Geyer, S. M.; Shipman, S. T.; Pate, B. H. *Rev. Sci. Instrum.* **2008**, *79*, -.

80. Brown, G. G.; Dian, B. C.; Douglass, K. O.; Geyer, S. M.; Pate, B. H. *J. Mol. Spectrosc.* **2006**, *238*, 200-212.

81. Grubbs, G. S.; Dewberry, C. T.; Etchison, K. C.; Kerr, K. E.; Cooke, S. A. *Rev. Sci. Instrum.* **2007**, *78*, -.

82. Zwier, T. S. *Annu. Rev. Phys. Chem.* **1996**, *47*, 205-241.

83. Pribble, R. N.; Zwier, T. S. *Science* **1994**, *265*, 75-79.

84. de Vries, M. S.; Hobza, P. *Annu. Rev. Phys. Chem.* **2007**, *58*, 585-612.

85. Dian, B. C.; Longarte, A.; Zwier, T. S. *Science* **2002**, *296*, 2369-2373.

86. Dian, B. C.; Longarte, A.; Mercier, S.; Evans, D. A.; Wales, D. J.; Zwier, T. S. *J.Chem.Phys.* **2002**, *117*, 10688.

87. Saykally, R. J. *Acc. Chem. Res.* **1989**, *22*, 295-300.

88. Liu, K.; Loeser, J. G.; Elrod, M. J.; Host, B. C.; Rzepiela, J. A.; Pugliano, N.; Saykally, R. J. *J. Am. Chem. Soc.* **1994**, *116*, 3507-3512.

89. Richardson, J. O.; Wales, D. J.; Althorpe, S. C.; McLaughlin, R. P.; Viant, M. R.; Shih, O.; Saykally, R. J. *The Journal of Physical Chemistry A* **2013**.

90. Saykally, R. J.; Wales, D. J. *Science* **2012**, *336*, 814-815.

91. Müller-Dethlefs, K. *J. Electron. Spectrosc. Relat. Phenom.* **1995**, *75*, 35-46.

92. Mueller-Dethlefs, K.; Dopfer, O.; Wright, T. G. *Chem. Rev.* **1994**, *94*, 1845-1871.

93. Zhu, L.; Johnson, P. *J.Chem.Phys.* **1991**, *94*, 5769-5771.

94. Schawlow, A.; Townes, C. H. *Microwave spectroscopy*; Dover, **1975**.

95. Gordy, W.; Cook, R. L. *Microwave Molecular Spectra*; Wiley: New York, **1984**.

96. Patterson, D.; Schnell, M.; Doyle, J. M. *Nature* **2013**, *497*, 475-477.

Chapter II. Experimental and Theoretical Methods.

II.1. Introduction

Microwave spectroscopy has traditionally been used to determine structures of molecules and weakly bound complexes. Initially absorption cell spectrometers were used to record the rotational spectra of molecules. However, sensitivity of these spectrometers was rather low and therefore, spectra of only stable molecules could be recorded. Balle and Flygare introduced cavity based microwave spectrometers which were coupled with molecular beam technique, for the first time.[1] These spectrometers are very sensitive and could be used to study the rotational spectra of several weakly bound complexes. Sensitivity of these spectrometers can be gauged by the fact that complexes as weak as between two rare-gas atoms have been studied using these techniques.[2,3] There have been several modifications in the design of these spectrometers since its first inception.[4-10] The employment of broadband chirped pulse sources for the polarization of molecules has given a new flip to microwave spectroscopy.[5] New methods of sample preparation have widened the scope of microwave spectroscopy. Using techniques like laser ablation, solid samples can also be brought into the gas phase and thus, can be studied by microwave spectroscopy.[10]
In our lab a *Pulsed Nozzle Fourier Transform (PN-FTMW)* spectrometer has been fabricated. The spectrometer is based on the Balle-Flygare design. Details of the spectrometer can be found elsewhere.[11-13] In the next few sections main components of the spectrometer have been described in brief.

II.2. PN-FTMW spectrometer

Design of the PN-FTMW spectrometer can be divided mainly into two parts (i) Mechanical design and (ii) Electrical design.

II.2.a. Mechanical design

Mechanical design of the spectrometer is shown in *Figure II.1*. The spectrometer consists of a cylindrical vacuum sealed chamber which is made of stainless steel (SS-304). Length and diameter of the chamber are 1000 mm and 850 mm respectively. The chamber houses two identical aluminium mirrors which are mounted coaxially on three stainless steel rods. The overall arrangement is called Fabry-Perot cavity or resonator. The mirrors are highly polished and the surface roughness and radius are

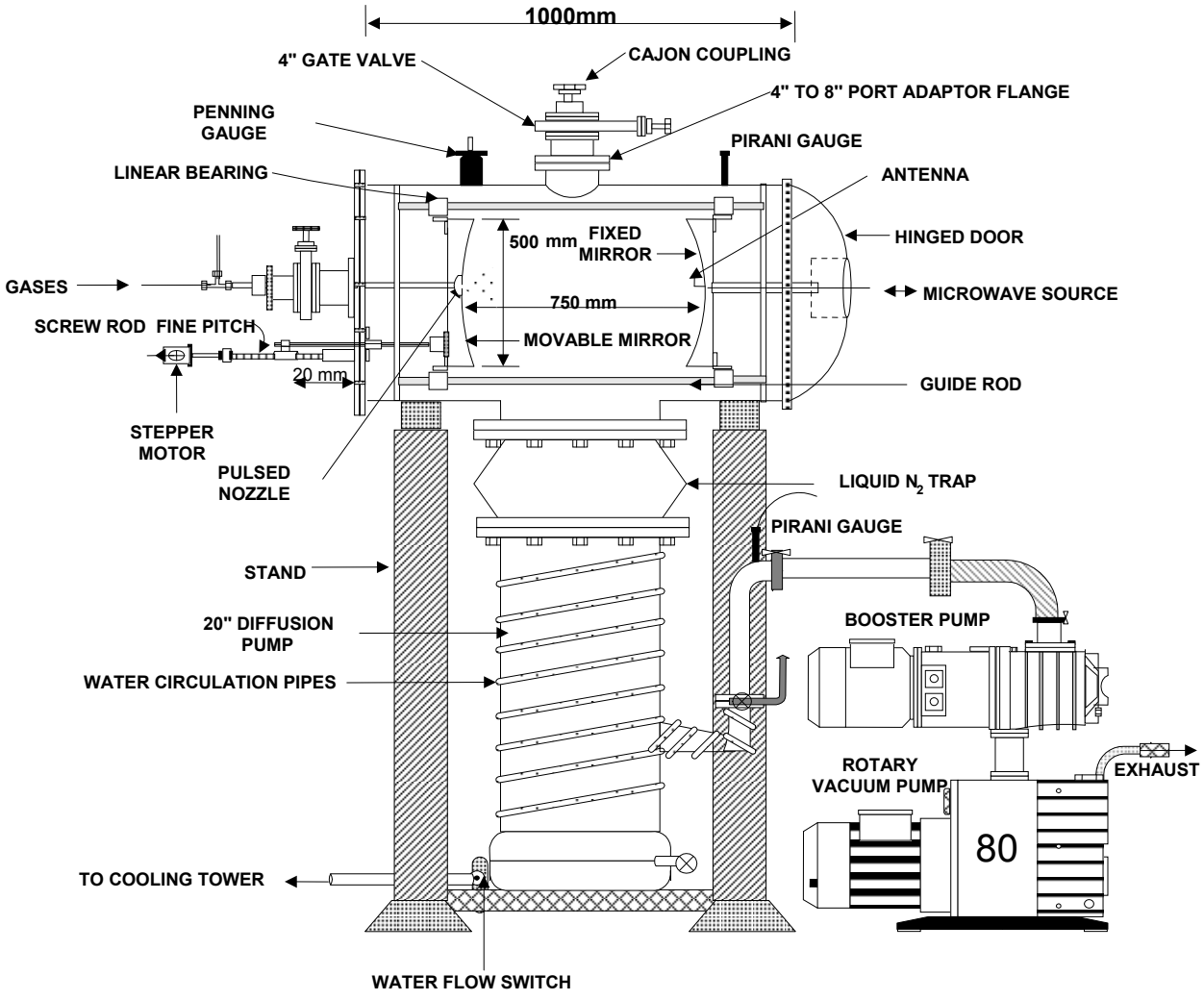

Figure II.1. Mechanical design of the PN-FTMW spectrometer

good to 1 micron. Diameter of the mirrors is 500 mm and radius of curvature is 800 mm. The Fresnel's condition determines the lower frequency cut-off for the spectrometer. The condition says

$$\frac{a^2}{R\lambda} \geq 1 \qquad \text{(II.a)}$$

where *a* is radius and R is radius of curvature of the mirror. This condition puts a low frequency cut-off of 3.8 GHz for our spectrometer. However, signal as low as 2447.8427 MHz for Ar•••H_2S complex has been observed from this spectrometer.[11] Operating range of the spectrometer is 2 to 26GHz.

The chamber is seated on a 20" diffusion pump (Vacuum Techniques, Bangalore, India) which has a pumping speed of 10,000 $l.s^{-1}$. The diffusion pump is backed by a roots blower (Boc Edward, EH 250) and a belt less rotary pump (Boc Edward, E2M80). These backing pumps have a combined pumping speed of ~4000 $l.s^{-1}$. The pumps can evacuate the chamber to 10^{-6} *torr*. Operation of diffusion pump generates enormous amount of heat. To keep the diffusion pump at room temperature, it is water-cooled using water circulation facility.

One of the mirrors is movable and the distance between the mirrors can be varied between 630 *nm* to 730 *nm*. The movable mirror is fixed with a micrometer controlled fine pitch linear screw rod and is driven by a stepper motor (103H8221-5041, Sanyo Denki, Japan). The linear screw rod has a pitch of 5 mm i.e. in a full 360^0 rotation the motor covers a linear distance of 5 mm. In high resolution mode the stepper motor takes 4000 steps to cover this distance, i.e. in each step mirror moves by 1.25 micron. Thus, the mirror movement can be controlled very precisely.

The movable mirror has a 10 mm diameter hole in the centre. A pulse nozzle (General Valve, USA, Service 9) of 0.8 mm diameter is placed at this hole. The valve is connected with a stainless steel tube of 0.25 inch outer diameter through which the sample is sent. The sample is pulsed into the cavity by opening the valve for typically 1ms. The trigger to open and close the valve is fed through a pin connector which is sealed with an O-ring and a clamp. The stationary mirror also has a small hole at its centre. A female SMA connector, which is at the end of a coaxial cable, is placed at the mirror hole centre. An L-shaped antenna is connected to the SMA pin. The microwave power can be transmitted to and received back from the cavity through this arrangement. The same antenna works as both the transmitter and the receiver. The working frequency range of the antenna depends on its length (L) and

$$L \approx \lambda/4 \qquad \text{(II.b)}$$

Using this approximation antenna can be designed for a particular frequency range. Entire frequency range of the spectrometer can be covered using 3 to 4 different antennae.

II.2.b. Electrical design

Electrical design of the spectrometer is shown in *Figure II.2*. It is used to generate the microwave pulse which is sent to the cavity and also to detect back the microwave signal. The microwave source is a Signal generator (#1 in *Figure II.2*, Agilent, MXG signal generator, N5183A) which can generate frequency from 100kHz to 32GHz with a resolution of 0.01 Hz. The RF output (frequency ν, power 13dBm) of the signal generator is directed to a single-pole-double-throw (SPDT) switch (#7, Sierra Microwave, 0.5-26.5 SFD0526-00, isolation 60dB). Output of this switch is either sent to a single side band mixer (SSBM, #5, Miteq, SMO-226LC1A) or to an image rejection mixer (IRM, #11, Miteq, IRO-0226LC1A). During the polarization cycle (top half of the electric design) the output is sent to the SSBM where it is mixed with the output [ν_1 (=30 MHz), power 13-16dBm] of a function generator (#23, SRS, DS345). The SSBM gives the upper band $\nu + \nu_1$ as an output. This output is amplified by a medium power amplifier (#6, Miteq, JS3-02002600-5-7A) with a gain of 24 dB. The amplified signal then goes to another identical switch (#7'). This switch works synchronously with the other SPDT switch. These SPDT switches are controlled by a delay generator (BNC-555). The delay generator sends two pulses of same time duration (typically 0.2-3.0 μs) but of opposite polarity to these switches. Due to the time duration, the $\nu + \nu_1$ signal has a certain width (~1 MHz for 1 μs time duration). The output of the switch (#7') is sent to a direction coupler (#8, Narda, 1.7-26.5–4227–16) which directs the signal to the antenna through a diode detector. The antenna couples the signal to the cavity. The molecules are polarized by this microwave signal. If the molecules absorb within the width of the signal a transition occurs and molecules coherently emit microwave radiation of frequency $\nu + \nu_1 \pm \Delta$, where Δ is the offset from $\nu + \nu_1$. This signal is detected back by the same antenna and goes to the direction coupler via the diode detector. During the polarization the cavity should be tuned i.e. the distance between the two mirrors should be a half integral multiple of the wavelength of the microwave radiation. This ensures the formation of

a standing wave between the mirrors. The distance is adjusted by moving the movable mirror by the stepper motor which is controlled by a stepper motor driver (Micrologix, embedded systems Ltd, MSB-403). The stepper motor driver is triggered by a PC. If the cavity is not tuned almost all the microwave power is reflected. During the detection cycle, the direction coupler sends 2.5% of this reflected power to a digital storage oscilloscope (DSO, #27 Tektronix TDS 2022). This power is monitored while tuning the cavity. As the cavity is tuned there is a huge dip in the reflected power. DSO outputs are shown in the *Figure II.3* for both the conditions (i) when cavity is not tuned and (ii) when the cavity is tuned. Rest of the microwave signal goes to a low noise amplifier (#10, Miteq JS4-02002600-3-5P, noise 2.8dB, gain 28 dB) via the SPDT switch (#7'). The amplified signal is mixed with the signal generator's output (ν) in an image rejection mixer (#11, Miteq, IRO-0226LC1A). The IRM gives $\nu_1 \pm \Delta$ signal as the output which is directed to a band pass filter (#12, Mini Circuits, BBP-30) and a low noise RF amplifier (#13, Mini Circuits, ZFL-500LN). This signal is down converted to Δ by mixing it with the output of the function generator (ν_1) in an RF mixer (#14, Mini Circuits, ZAD-1). The Δ signal is sent to a low pass filter (#15, Mini Circuits, BLP-5) and then it is further amplified by another an RF amplifier (#16, HD communication corp., HD 17153BB). This amplified signal is digitized by an NI-scope card (National Instrument, PCI 5112) which has a maximum sampling speed of 100MHz. However, the signal (Δ) which we amplify is typically <1 MHz and therefore, we generally use sampling speed of 5MHz.

The digitized signal is sent to a computer for further analysis. The time domain signal is Fourier transformed to obtain signal in the frequency domain. The time domain and the frequency domain signals are shown in *Figure II.4*. As shown in the figure the signal always appears as a doublet. This is because of the coaxial arrangement of the antenna and the pulsed nozzle. The standing wave in the cavity is a super-position of two waves travelling in opposite directions which leads to Doppler doubling.

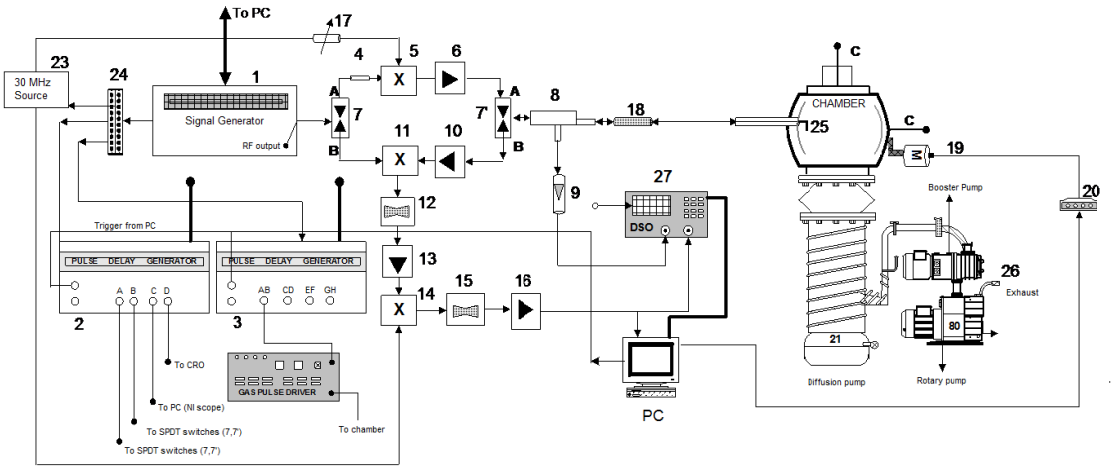

Figure II.2. Electrical design of the PN-FTMW spectrometer. 1, Signal generator (Agilent, MXG signal generator, N5183A); 2, Delay generator (BNC-555); 3, Delay generator (SRS DG645); 4, Microwave attenuator (HP, 8493C, 3dB); 5, SSB mixer (Miteq,SMO-226LC1A); 6, Medium power amplifier (Miteq, JS3-02002600-5-7A); 7, MW SPDT switch (Sierra Microwave, 0.5-26.5 SFD0526-000); 8, Direction coupler (Narda, 1.7-26.5–4227–16); 9, Diode detector (Narda, 0.01-26.5–4507); 10, Low noise amplifier (Miteq, JS4-02002600-3-5P); 11, Image rejection mixer (Miteq, IRO-0226LC1A); 12, Band pass filter (Mini Circuits, BBP-30); 13, RF amplifier (Mini Circuits, ZFL-500LN); 14, RF mixer (Mini Circuits, ZAD-1); 15, Low pass filter (Mini Circuits, BLP-5); 16, RF amplifier (HD communication corp., HD 17153BB); 17, Attenuator (Mini Circuits, ZAFT-51020); 18, Blocking capacitor (HP, 11742A); 19, Stepper motor; 20, Motor driver; 21, Diffusion pump and 22,Rrotary pump; 23, 30MHz function generator (Stanford Research System, DS345); 24, Distribution amplifier (Stanford Research System, FS710); 25, Antenna; 26, Exhaust; 27, Digital storage oscilloscope (Tektronix TDS 2022).

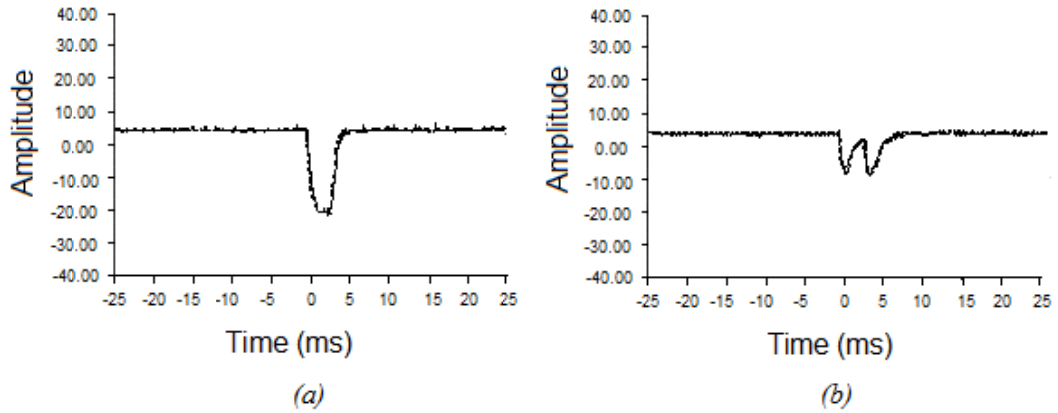

Figure II.3. Reflected signal on the oscilloscope, (a) when cavity is not tuned and (b) when cavity is tuned.

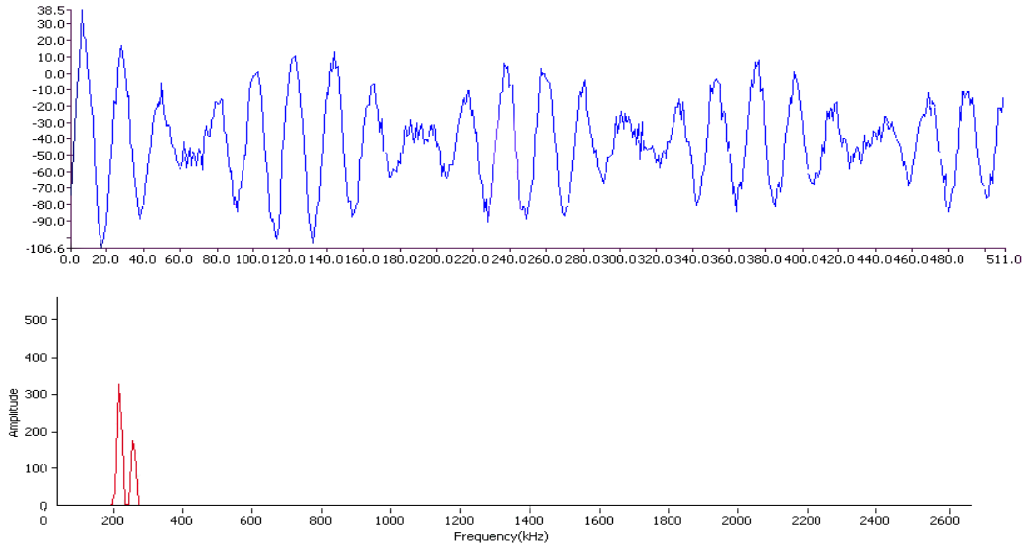

Figure II.4. Time domain and frequency domain signals collected from PN-FTMW spectrometer.

II.2.c. Time sequence of the pulses

The microwave and gas pulses are controlled by two different delay generators: BNC-555 and DG-645 respectively. First a microwave pulse of time duration (0.2-3.0 μs) is sent inside the cavity. Time duration of the microwave pulse depends on the molecule/complex under study. The microwave pulse forms a standing wave inside the tuned cavity and the decay time for this pulse is typically <40 μs. The decay time varies from one frequency range to the other. Usually in the low frequency range the decay time is longer. The peak to peak amplitude of the standing wave formed by microwave pulse is 6-8 V and it is very difficult to detect the molecular signal of millivolt strength in presence of such a high background. Therefore, digitization is not started until this high background signal (also called ringing) decays. This is done by creating a delay between the digitising pulse and the first microwave pulse. This delay is set according to the decay time of the ringing. After the digitization, the data is stored as noise. A gas pulse of 1 ms time duration is then sent into the cavity. The gas pulse which contains the sample molecules and clusters is then polarized by another microwave pulse (0.2-3.0 μs). Usually, there is a delay of few tens of microseconds between the gas pulse and the microwave pulse. This delay is called 'Start delay'. The delay is not created by the delay generators as it is taken care of by the processing time of the programme. The gas pulse takes nearly 2 ms to hit the other mirror whereas the typical data acquisition time is 100 μs. Thus, multiple microwave pulses can be sent for a single gas pulse. Signal is obtained by subtracting the record collected before sending the gas pulse from the corresponding record after sending the

gas pulse. This whole process starting from the first microwave pulse and ending with the polarization of the molecules by multiple microwave pulses is called one shot. The experiment can be performed for *n* number of shots to improve the signal to noise ratio. Strong signals appear within few shots. The pulse sequence is given in the *Figure II.5*.

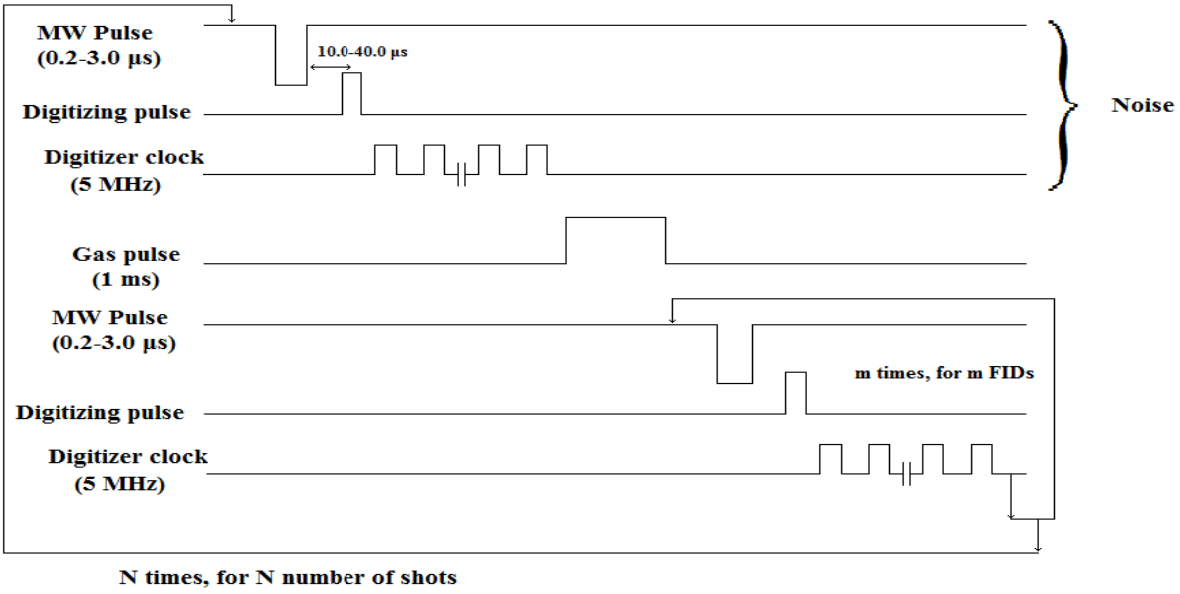

Figure II.5. Pulse sequence for the PN-FTMW spectrometer.

II.2.d. Software for the PN-FTMW spectrometer

Software code for the spectrometer is based on LabView 7.1. LabView is a graphical development programme and provides a very user friendly interface. The Labview codes are called virtual instruments (VIs). These VIs have two main parts, (i) Front panel and (ii) Block diagram. The front panel is the user interface and has components like controllers and indicators. Inputs are given using controllers and outputs are displayed using indicators. Many different types of controllers and indicators are available in the software. The block diagram provides an interface for the programming. Many built-in VIs are available in the software. Using these VIs different codes can be written for different needs.

For the PN-FTMW spectrometer, different VIs have been created for controlling different instruments like, signal generator, function generator pulse driver, delay generators and the stepper motor driver. All the instruments except the stepper motor driver use GPIB interface to communicate with PC. The stepper motor driver is interfaced using parallel-port connection. In addition to the codes written for the instrument controls, codes for the data acquisition have also been written in Labview.

All these VIs together constitute the main programme for the PN-FTMW spectrometer. Details of the software code can be found in the *Reference 12*.

Of late, we have been controlling one of the delay generators (BNC-555) using RS-232 connections. Hyperterminal software is used to communicate with this delay generator. Inputs to set the microwave pulse lengths and to create delays can be given using SCPI commands. For Channel 1 of the delay generator following commands can be used to set different parameters:

(i) :PULSe1:STATE ON

(ii) :PULSe1:WIDth 0.000002

(ii) :PULSe1:POLarity NORMal

The first command turns on the first channel. The second command sets the width of the pulse to 2 μs and the third command sets normal polarity for the pulse.

The commands are shown as a mixture of upper and lower case letters. The upper case letters indicate the abbreviated spelling for the command. Either the abbreviated version or the entire keyword can be used to send the command. Moreover, upper and/or lower case characters are acceptable. e.g. POL, POLARITY, POLarity and polarity all are valid commands. Whole set of commands can be found in the manual for the delay generator.

II.3. Sample preparation

In the experiments, a molecular beam is produced using a pulse nozzle. Typically, argon or helium is used as carrier gas which carries the sample molecules into the cavity. A fraction of the carrier gas (usually 1-5%) is bubbled through a bubbler containing the liquid sample. In case of systems involving two or more liquid samples, the carrier gas is bubbled through each of the samples separately and then the mixing is done in a four-way junction. Flow of the gases is controlled by four different mass flow controllers (MKS, 1179). Mass flow meter unit is used to set the flow limit of these mass flow controllers. After the mixing, the gas seeded with the sample molecules is expanded from a back pressure of 0.1-1.5 bar into the evacuated cavity through a pulse nozzle of 0.8 mm diameter. Due to the back pressure, the mean free path of the molecules decreases and becomes much less than the nozzle diameter. Expansion takes place when the nozzle opens and within very close distance (few nozzle diameters) from the nozzle, many molecular collisions occur. Due to these collisions molecules lose energy and molecular complexes like dimer, trimers are

formed. After a few diameters, the flow is collision free and hence it is called a free jet. The supersonic expansion is a very high directional mass flow resulting in the formation of a molecular beam. In the beam the translation degree of freedom relaxes very fast and the translational temperature achieved in the beam is 0.02-0.03K. However, rotational and vibrational energy relaxations are much slower and the rotational and vibrational temperatures achieved in the beam are 2-3K and 50-100K respectively. The beams are called supersonic beams because velocity of the molecules in the beam is much more than the velocity of sound at the local density.

II.4. Quantum chemical methods

To optimize the structure of the molecules and complexes, various quantum chemical methods like *ab initio* and density functional theory (DFT),[14,15] have been used in this *Thesis* work. In most of the cases MP2 level calculations have been performed. DFT methods have also been used in some studies. In some cases, single point calculations at CCSD level have also been performed. Main motive behind performing these calculations was to obtain an initial 'guess' geometry for the complex of interest. These guess geometries were used as a lead for further experimental investigations. Harmonic frequency calculations were performed to confirm that the optimized structures are minima at the potential energy hypersurface. In some cases, vibrational-rotational coupling was also computed using Freq=VibRot keyword. Distortion constants for the complexes can be extracted from these calculations. All these calculations were performed using Gaussian 09 software suite.[16]

Interaction energies for the complexes were calculated using supermolecular approach. According to this approach

$$\Delta E\ (Complex) = E\ (Complex) - \Sigma\ E\ (Monomer) \qquad (II.c)$$

Where, ΔE (Complex) is the interaction energy for the complex. E (complex) and E (monomer) are the energies of the complex and the monomer respectively. Using this approach interaction energies can be calculated for the structures optimized using small basis sets. However, for large basis sets such as those used in this *Thesis* work, these energies must be corrected for the *Basis Set Superposition error (BSSE)*.[17-19] The correction was made using counterpoise method developed by Boys and

Bernardi.[20] Gaussian software has a built-in command 'counterpoise=n' for these calculations, where n is the number of monomer units constituting the complexes i.e. for dimer n will be 2, for trimer n will be 3 and so on. BSSE corrected energy for the complex can be extracted from the counterpoise calculations.

BSSE corrected interaction energy of the complex can be calculated as

$$\Delta E_{BSSE}\,(Complex) = E_{BSSE}\,(Complex) - \Sigma\, E\,(Monomers) \qquad (II.d)$$

Where, ΔE_{BSSE} (Complex) is the BSSE corrected interaction energy and E_{BSSE} (Complex) is the BSSE corrected energy for the complex,

BSSE corrected interaction energies were further corrected for the zero-point vibrational motion and the BSSE+Zero-point corrected interaction energies were obtained in the following way,

$$\Delta E_{BSSE+ZPC}\,(Complex) = E_{BSSE+ZPC}\,(Complex) - \Sigma\, E_{ZPC}\,(Monomers) \qquad (II.e)$$

Where, $\Delta E_{BSSE+ZPC}$ is the BSSE and zero-point corrected interaction energy.

E_{ZPC} is zero point corrected energy and $E_{BSSE+ZPC}$ is the BSSE+zero point corrected energy. These are defined as follows.

$E_{BSSE+ZPC}$ *(Complex) =* E_{BSSE} *(Complex) + Zero-point energy correction for the complex*

E_{ZPC} *(Monomer) =* E_{BSSE} *(Monomer) + Zero-point energy correction for the monomer.*

II.5. Atoms in Molecules analysis

Microwave spectroscopy determines structure of the complexes under study. However, it does not quantify the strength and nature of the intermolecular interactions present in the complex. Atoms in Molecules (AIM) theory,[21,22] developed by Bader, can be used for this purpose. The theory is based on electron density (ρ) topology analysis of the molecules and complexes. Critical points resulting from this analysis can be used to quantify the intermolecular interactions. A critical point is a point in space at which gradient of the electron density (∇ρ) vanishes, i.e. critical point is an extremum point at the electron density topology. Nature of the critical point is decided by the second derivative of the electron density. If critical point is a maximum the second derivative will be negative and if it is a minimum the second

derivative will be positive. Critical points have been classified as nuclear/non-nuclear attractor, bond critical point (BCP), ring critical point (RCP) and cage critical point (CCP). The classification is based on the Eigen values of the Hessian matrix of electron density. Koch and Popelier have proposed a set of criteria for hydrogen bonding on the basis of AIM analysis.[23]

Different types of critical points

Critical points are classified on the basis of the Hessian matrix of electron density. The critical points are denoted as (r, s) where r is the rank (number of non zero eigenvalues) and s is the signature (algebraic sum of the signs of non-zero eigenvalues) of the Hessian matrix. Different critical points are as follows:

(i) Nuclear attractor: Nuclear attractor is denoted as (3,-3) i.e. at this point electron density is maximum along each of the three directions. This critical point corresponds to the nucleus of atoms in molecules. However, in some cases non-nuclear attractor (3,-3) critical points have also been reported.

(ii) Bond critical point (BCP)

Bond critical point is denoted as (3,-1) and appears between two atoms. At this point, electron density is maximum along two directions and minimum along the direction of the two atoms. In most of the cases, bond paths appear which connect the BCP to each of the atoms.

(iii) Ring critical point: Ring critical point is denoted as (3, +1) and appears in case of cyclic structures. At this point the electron density is minimum along two directions and maximum along the third direction.

(iv) Cage critical point: Cage critical point is denoted as (3, +3). Electron density at this point is minimum along all three directions.

Laplacian of electron density ($\nabla^2\rho$) gives an idea about the nature of interaction. Positive value of $\nabla^2\rho$ suggests a closed shell interaction and its negative value suggests an open shell interaction.

Positive value of mutual penetration between two interacting atoms is considered as

the necessary and sufficient criteria for hydrogen bonding interactions.[23] Mutual penetration is defined as sum of the difference between bonded and non-bonded radii of the interacting atoms i.e. for two atoms A and B; the mutual penetration is defined as

$$Mutual\ penetration\ (AB) = \Delta r_A + \Delta r_B \qquad (II.f)$$

$\Delta r_{A/B}$ is the difference between bonded and non-bonded radii of A/B.

Bonded radius is the distance between the atom and the bond critical point corresponding to the interaction. Non bonded radius is defined as the distance between the atom and 0.001 *a.u.* electron density surface. The non-bonded radius should always be calculated along the direction of the bond critical point.

II.6. Natural bond orbitals (NBO) analysis

NBO analysis[24] has been performed on the complexes to understand the donor-acceptor interactions. Atomic charges resulting from this analysis are used to estimate charge transfer from the electron donor molecule to the electron acceptor molecule. Second order perturbation analysis resulting from the NBO calculations gives information about the orbitals involved in the charge transfer. The calculations were performed using NBO 6.0 software.[24]

II.7. References

1. Balle, T. J.; Flygare, W. H. *Rev. Sci. Instrum.* **1981**, *52*, 33-45.

2. Grabow, J. U.; Pine, A. S.; Fraser, G. T.; Lovas, F. J.; Suenram, R. D.; Emilsson, T.; Arunan, E.; Gutowsky, H. S. *J.Chem.Phys.* **1995**, *102*, 1181-1187.

3. Xu, Y.; Jäger, W.; Djauhari, J.; Gerry, M. C. L. *J.Chem.Phys.* **1995**, *103*, 2827-2833.

4. Kolbe, W. F.; Leskovar, B. *Rev. Sci. Instrum.* **1985**, *56*, 97-102.

5. Brown, G. G.; Dian, B. C.; Douglass, K. O.; Geyer, S. M.; Shipman, S. T.; Pate, B. H. *Rev. Sci. Instrum.* **2008**, *79*, -.

6. Storm, V.; Dreizler, H.; Consalvo, D.; Grabow, J. U.; Merke, I. *Rev. Sci. Instrum.* **1996**, *67*, 2714-2719.

7. Harmony, M. D.; Beran, K. A.; Angst, D. M.; Ratzlaff, K. L. *Rev. Sci. Instrum.* **1995**, *66*, 5196-5202.

8. Etchison, K. C.; Dewberry, C. T.; Kerr, K. E.; Shoup, D. W.; Cooke, S. A. *J. Mol. Spectrosc.* **2007**, *242*, 39-45.

9. Arunan, E.; Dev, S.; Mandal, P. K. *Applied Spectroscopy Reviews* **2007**, *39*, 131-181.

10. Grubbs, G. S.; Dewberry, C. T.; Etchison, K. C.; Kerr, K. E.; Cooke, S. A. *Rev. Sci. Instrum.* **2007**, *78*, -.

11. Mandal, P. K. *Ph.D. Dissertation*, *Indian Institute of Science*, *2005*.

12. Arunan, E.; Tiwari, A. P.; Mandal, P. K.; Mathias, P. C. *Curr. Sci.* **2002**, *82*, 533-540.

13. Goswami, M. *Ph.D. Dissertation*, *Indian Institute of Science*, *2009*.

14. Szabo, A.; Ostlund, N. S. *Modern Quantum Chemistry: Introduction to Advanced Electronic Structure Theory*; Dover Publications Inc. : Mineola, **1996**.

15. Jensen, F. *Introduction to Computational Chemistry* John Wiley & Sons: New York, **1999**.

16. Frisch, M. J.; Trucks, G. W.; Schlegel, H. B.; Scuseria, G. E.; Robb, M. A.; Cheeseman, J. R.; Scalmani, G.; Barone, V.; Mennucci, B.; Petersson, G. A.; Nakatsuji, H.; Caricato, M.; Li, X.; Hratchian, H. P.; Izmaylov, A. F.; Bloino, J.; Zheng, G.; Sonnenberg, J. L.; Hada, M.; Ehara, M.; Toyota, K.; Fukuda, R.; Hasegawa, J.; Ishida, M.; Nakajima, T.; Honda, Y.; Kitao, O.; Nakai, H.; Vreven, T.; Montgomery, J. A.; Peralta, J. E.; Ogliaro, F.; Bearpark, M.; Heyd, J. J.; Brothers, E.; Kudin, K. N.; Staroverov, V. N.; Kobayashi, R.; Normand, J.; Raghavachari, K.; Rendell, A.; Burant, J. C.; Iyengar, S. S.; Tomasi, J.; Cossi, M.; Rega, N.; Millam, J. M.; Klene, M.; Knox, J. E.; Cross, J. B.; Bakken, V.; Adamo, C.; Jaramillo, J.; Gomperts, R.; Stratmann, R. E.; Yazyev, O.; Austin, A. J.; Cammi, R.; Pomelli, C.; Ochterski, J. W.; Martin, R. L.; Morokuma, K.; Zakrzewski, V. G.; Voth, G. A.;

Salvador, P.; Dannenberg, J. J.; Dapprich, S.; Daniels, A. D.; Farkas; Foresman, J. B.; Ortiz, J. V.; Cioslowski, J.; Fox, D. J. Wallingford CT, 2009.

17. Liu, B.; McLean, A. D. *J.Chem.Phys.* **1973**, *59*, 4557-4558.

18. Szczęśniak, M. M.; Scheiner, S. *J.Chem.Phys.* **1986**, *84*, 6328-6335.

19. Gutowski, M.; Chal/asiński, G. *J.Chem.Phys.* **1993**, *98*, 5540-5554.

20. Boys, S. F.; Bernardi, F. *Mol. Phys.* **1970**, *19*, 553.

21. Bader, R. F. W. *Chem. Rev.* **1991**, *91*, 893-928.

22. Bader, R. F. W. *Atoms in Molecules: A Quantum Theory* Clarendon Press: Oxford, **1990**.

23. Koch, U.; Popelier, P. L. A. *J. Phys. Chem.* **1995**, *99*, 9747-9754.

24. Glendening, E.; Badenhoop, J.; Reed, A.; Carpenter, J.; Bohmann, J.; Morales, C.; Landis, C.; Weinhold, F. In *(Theoretical Chemistry Institute, University of Wisconsin, Madison, WI, 2013); http://nbo6.chem.wisc.edu/*.

Chapter III.

Rotational Spectra of Ar●●●Propargyl Alcohol Complex: Ar●●●H-O, Ar●●●π and Ar●●●C Interactions.

(This work has been published as an article in ChemPhysChem 2013, 14, 754-763.)

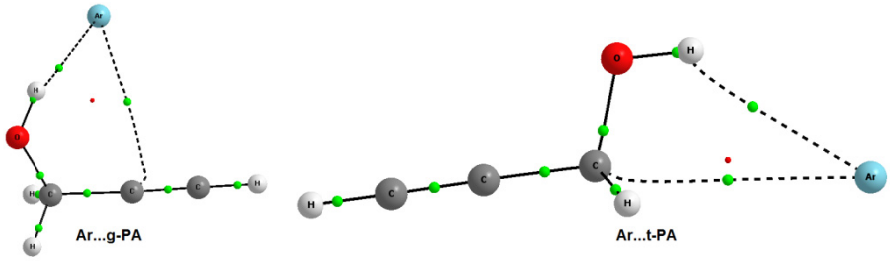

III.1. Introduction

Propargyl alcohol (C_3H_4O), hereafter noted as PA, is a molecule of interest in astrophysics as well as in combustion chemistry. Propenal, (C_3H_4O), which is a structural isomer of PA, has been detected in interstellar medium[1] and there is a strong possibility of finding PA molecule also in the interstellar medium. Will its complexes be found anywhere? In combustion chemistry, combination of two propargyl radicals is considered to be an important channel for the formation of benzene, en route to polycyclic aromatic hydrocarbons (PAH) and soot formation.[2,3]

$C_3H_3 + C_3H_3 \rightarrow C_6H_6 \rightarrow PAH \rightarrow soot$

Kinetics of this reaction has recently been investigated by Tranter et al. in a shock tube study.[4] The intermolecular potentials control chemical reactions and the first step to the potential is the equilibrium structure of molecular complexes which can be determined by microwave spectroscopy of molecular complexes.

PA is a multifunctional molecule containing an acetylenic group (-C≡C-H) and a hydroxyl group (-OH). Due to internal rotation of C-OH group, this molecule can exist in two forms: gauche form and trans form with respect to carbon chain of the molecule (*Figure III.1a and III.1b*).

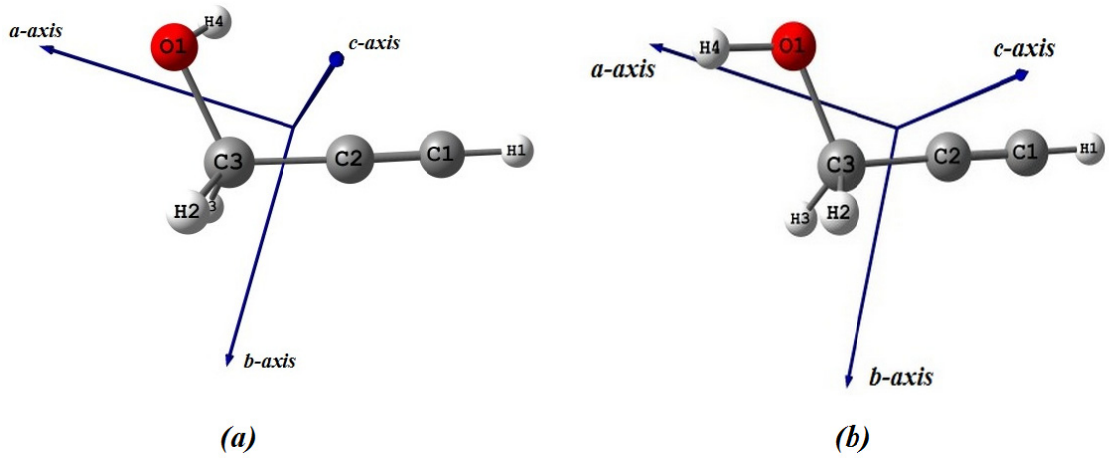

Figure III.1. (a) Propargyl alcohol in gauche form and (b) propargyl alcohol in trans form. The principal axes system is also shown for both the conformers.

Relaxed scan of the potential energy surface of PA as a function of dihedral angle ($C_2C_3O_1H_4$), is shown in *Figure III.2*. Two equivalent gauche forms are separated by a barrier of ~ 1.1 kcal mol^{-1}. Trans form with $C_2C_3O_1H_4$ dihedral angle exactly 180^0,

is a saddle point at this level of calculation and separates two equivalent minima having $C_2C_3O_1H_4$ dihedral angles 160^0 and 200^0. However, the energy barrier for inter-conversion of these two equivalent forms is a mere 0.04 kcal mol^{-1}. Rotational spectroscopic studies on this molecule have confirmed the presence of only the gauche form.[5-7] Similarly, only gauche form has been observed for the analogous molecules, propargyl thiol (C_3H_4S)[8-11] and propargyl selenol (C_3H_4Se).[12] also. Hirota suggested that the extra stabilization of gauche form may be due to intra-molecular interaction between the -OH group and π- electrons.[5] However, our AIM calculations have not shown a bond critical point between hydroxyl proton and the π- bond in agreement with an earlier result.[13]

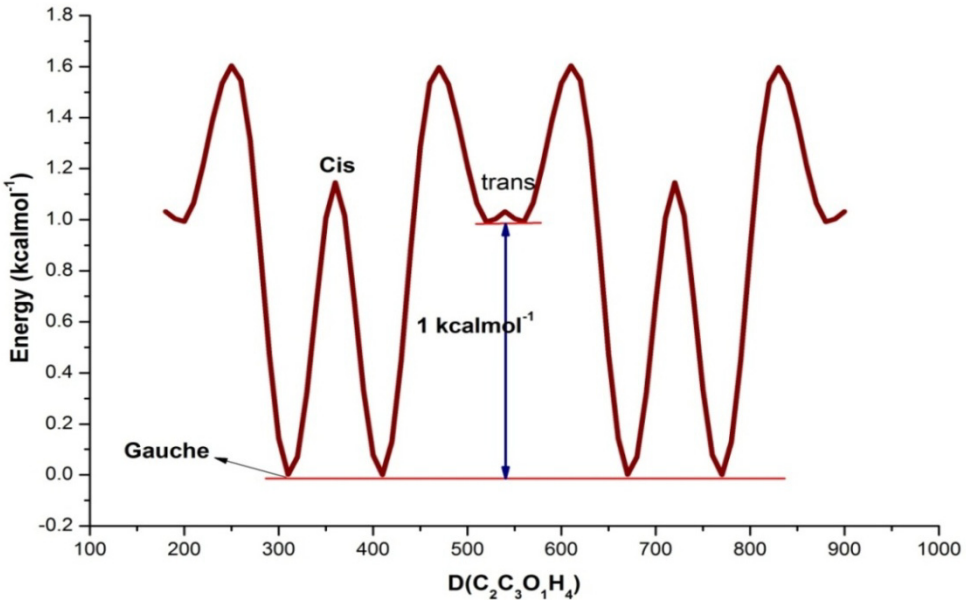

Figure III.2. Relaxed Potential energy scan for propargyl alcohol molecule as a function of dihedral angle (C2C3O1H4) at MP2/6-311+G(d,p) level of theory.

Recently, Patwari and co-workers have investigated many complexes of phenylacetylene (C_6H_5CCH), another multifunctional molecule, by infrared-optical double resonance spectroscopy and showed the diversity in the complexes' structures.[14] Goswami and Arunan reported the microwave spectrum of $C_6H_5CCH{\bullet\bullet\bullet}H_2O$,[15] providing positive confirmation for the structure proposed by Patwari's group. While the main objective of this study was to find whether H_2O acts as a hydrogen bond donor to the π electrons or as an acceptor to the acetylenic H, the results revealed that the complex had a cyclic structure in which H_2O played both roles. The $C_6H_5CCH{\bullet\bullet\bullet}H_2O$ complex is planar and has O from H_2O interacting with

the ortho C-H hydrogen of the phenyl ring and the OH interacting with acetylenic π-electrons. Goswami and Arunan investigated C_6H_5CCH•••H_2S complex[16] next and determined the structure to be very different having S-H•••π (phenyl ring) interaction, very similar to that of C_6H_6•••H_2S complex[17]. PA also offers many interesting possibilities of inter-molecular interactions with other atoms/molecules and in this chapter the results on the first complex chosen for investigation Ar•••PA, are discussed. While there have been numerous studies on this interesting molecule, it appears that there have been no prior experimental or theoretical studies on any of its complexes.

Complexes of rare gas atoms with molecules have been studied extensively both theoretically and experimentally.[18-26] These complexes are mainly stabilized due to induction and dispersion forces and offer a direct probe of these interactions. Experimental results on these clusters can be used to test the reliability of theoretical calculations. As PA contains a -C≡C-H group and an -OH group, comparisons with already studied Ar•••alcohol and Ar•••acetylene complexes would be worthwhile. Microwave spectra of Ar•••CH_3OH[25,26] and Ar•••butan-2-ol[21] complexes are known. In both complexes, Ar•••H-O interaction is the predominant one but the secondary interactions between Ar and the hydrocarbon chain of alcohol molecule also plays a significant role in the stabilization of these complexes. As a result of these secondary interactions, Ar•••H-O angle deviates largely from linearity in these complexes, being 151.6^0 and 134.4^0 for Ar•••CH_3OH and Ar•••butan-2-ol, respectively. On the other hand, in complexes like Ar•••acetylene[22,24] and Ar•••benzene,[18,23] Ar interacts with π-electrons and is located at the top of π- electron density. Our main objectives in this study are twofold: 1) Would the equilibrium structure of Ar•••PA resemble Ar•••alcohol or Ar•••acetylene or would it have both interactions in a cyclic structure resembling phenylacetylene•••H_2O? 2) Could the trans form of PA be stabilized by interactions with Ar or other molecules, like water, and observed experimentally? In addition to microwave spectroscopic measurements, we performed *ab initio* and Atoms in molecules (AIM) theoretical calculations also to address these questions and the details are discussed in the next sections.

III.2. Theoretical and Experimental details

III.2.a. Theoretical methods

All *ab initio* calculations were performed using Gaussian-09 suite of programs.[27] Structural optimization and frequency calculations were carried out at MP2 level with large basis set 6-311+G(3df,2p), to help in the search for rotational spectra. Atoms in Molecules (AIM) calculations were carried out using AIMALL package[28]. Electrostatic potential (ESP) calculations were performed using Multiwfn software developed by Lu and Chen[29] and GaussView software. Wave functions used in AIM and ESP calculations were extracted from Gaussian calculations.

III.2.b. Experimental Section

III.2.b.1. Sample preparation

Propargyl alcohol sample was purchased from Sigma-Aldrich and was used without further purification. The OD isotopologue HC≡C-CH_2OD, hereafter termed as PA-D(OD), was prepared by simple mixing of PA and D_2O in 9:4 ratio to get optimum intensity signals. The acetylenic proton of PA is also acidic in nature and could be replaced by deuterium in the PA and D_2O mixture. We could observe the known signals for the C-D isotopologue of PA-monomer (DC≡C-CH_2OH), hereafter termed as PA-D(CD), but the signal intensity was very low. Mixture ratio was varied and the best intensity signals for the PA-D(CD) monomer were observed with 1:1 mixture of PA and D_2O. However, PA-D(CD) concentration in even this mixture proved to be too low to observe the Ar●●●PA-D(C-D) complex signals. Hence, we decided to synthesise the PA-D(CD) isotopologue and followed the procedure reported by Bew et al.[30] Based on the intensities of the parent and PA-D(CD) signal, the isotopic conversion was estimated to be only 50% as opposed to 95% achieved by the authors. However, this was enough to observe the transitions from Ar●●●PA-D(CD) complex.

III.2.b.2. Rotational spectrum

Rotational spectra for the three isotopologues were recorded using already discussed Pulsed Nozzle Fourier Transform Microwave (PN-FTMW) Spectrometer[31]. A mixture of 3% PA (or isotopologue) in Ar carrier gas was expanded from a back pressure of

0.5 atm into an evacuated Fabry-Perot cavity. Multiple FIDs were collected per gas pulse. During the search 256 points were collected for each FID at 5 MHz sampling speed. Observed signals were recorded again with 512 or 1024 points to improve the resolution. Microwave pulse of 1 μs duration was found to be optimum for all *a*, *b* and *c*- dipole transitions and it was consistent with very similar dipole moments along the three principal axes as determined by the *ab initio* calculations.

III.3. Results: Search, assignments and fitting

Ab initio quantum chemical calculations were carried out to optimize the structure of Ar•••PA complex. Optimized structures for the complex, with both gauche *(Structure A)* and trans conformers of PA *(Structure B)* at the MP2/6-311+G(3df,2p) are shown in *Figure III.3*. Harmonic frequency calculations confirmed that both the structures correspond to minima on the intermolecular potential energy hypersurface. Complex with gauche-PA (Ar•••g-PA, *Structure* A) is slightly more stable (by ~0.6 kJ.mole^{-1}) than the complex in which Argon binds to the trans-PA (Ar•••t-PA, *Structure* B). In *Structure* A and *Structure* B, Ar•••H-O bond distance is 2.815 Å and 2.857 Å, respectively which are smaller than the sum of van der Waals radii of Ar and H atoms. The Ar•••H-O angle is 145.2^0 and 138.8^0 for *Structure* A and *Structure* B, respectively. The deviation of Ar•••H-O angle from linearity in both of the complexes has different origins: In *Structure* A, it is due to Ar•••π- interaction (Ar•••π-centre distance is 3.801 Å) while in *Structure* B, it is most probably due to some interaction between Ar and the CH_2O face of the t-PA (Ar•••C-3 carbon distance is 3.582 Å). More about the nature of interactions in these complexes is discussed in *Section III.4.b*. From rotational spectroscopic point of view, for *Structure* A, all three dipole moment components along principal axes are non-zero and have significant magnitude which indicates that *a*-, *b*- and *c*-type transitions could be measured while for *Structure* B, *c*-component of dipole moment is zero and only *a*- and *b*-type transitions are expected. The rotational constants for the two structures are very different and these can unambiguously be differentiated by microwave spectroscopy. Calculated rotational constants and dipole moment components for both the structures are given in *Table III.1*.

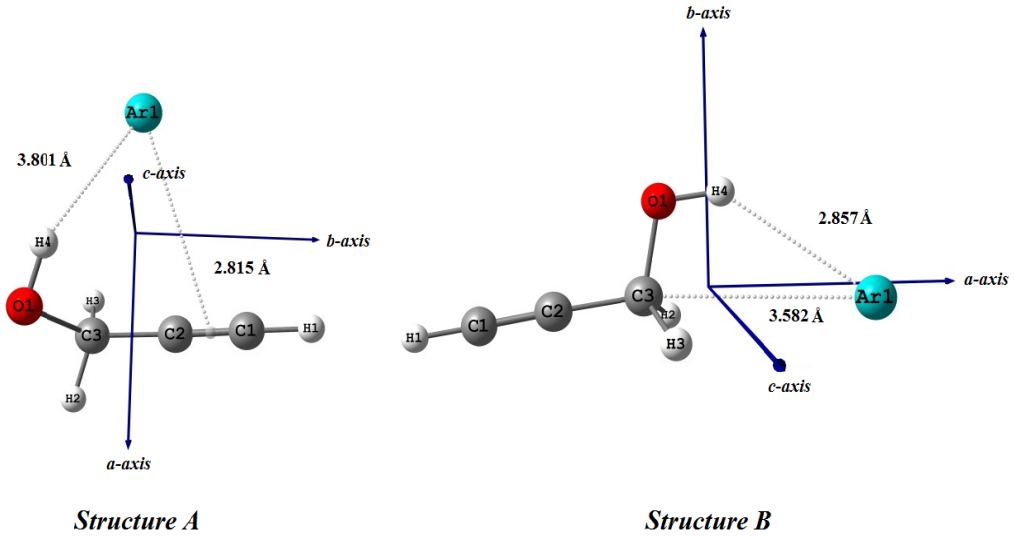

Figure III.3. Optimized geometries of (a) Ar●●●g-PA complex and (b)Ar●●●t-PA complex at MP2/6-311+G(3df,2p) level. Principal axes are also shown for both the structures.

Table III.1. Calculated rotational constants and components of dipole moment along principal axes for the Ar●●●PA complex at MP2/6-311+G(3df,2p) level.

	Structure A (PA in gauche form)	*Structure B (PA in trans form)*
A/MHz	4312	13563
B/MHz	1684	932
C/MHz	1281	863
μ_a/*D*	0.9	1.8
μ_b/*D*	1.1	1.3
μ_c/*D*	0.8	0.0

Search for the rotational transitions was started on the basis of the predicted spectra using *ab initio* constants. For the Ar●●●g-PA complex, $2_{1,2}$-$3_{1,3}$, $2_{0,2}$-$3_{0,3}$ and $2_{1,1}$-$3_{1,2}$ transitions were predicted around 8266, 8727 and 9471 MHz respectively while for the Ar●●●t-PA $4_{1,4}$-$5_{1,5}$, $4_{0,4}$-$5_{0,5}$ and $4_{1,3}$-$5_{1,4}$ transitions were predicted around 8907, 9042 and 9182 MHz respectively. We decided to start our search at 8150 MHz and almost immediately a signal was observed at 8188.180 MHz. Further search led to observation of more signals: one at 8222.2770 MHz and a doublet separated by 12.2 kHz and centred at 8447.2856 MHz and 8447.2978 MHz. All these signals depended on both the Ar concentration and the PA concentration, as confirmed by changing the carrier gas to He and also stopping the carrier gas flow through PA. Though these

lines were closer to the predictions for Ar•••g-PA, the spacing between these transitions was similar to that for Ar•••t-PA. Considering signal at ~8222.3 MHz as $4_{0,4}$-$5_{0,5}$ transition and ~8447.3 MHz as $4_{1,3}$-$5_{1,4}$ transition, we searched for the $4_{1,4}$-$5_{1,5}$ transition and almost immediately observed another doublet centred at 8008.007 and 8008.0168 MHz, separated by 9.8 kHz. On the basis of this initial assignment, other signals were predicted and a few of them could be observed. An initial coarse fitting of these transitions with semi-rigid asymmetric rotor Hamiltonian gave rotational constants close to that of *Structure* B having t-PA, which is yet to be experimentally observed. The excitement generated was short lived as further searches made on the basis of these fitted constants were largely unsuccessful. Fortunately, during this search, a very intense doublet centred at 11112.0188MHz and 11112.0286 MHz, separated by 9.8 kHz was observed, *Figure III.4*. This signal and the signal at ~8447.3 MHz were very similar in terms of intensity and splitting. Considering 8447.3MHz signal as $2_{0,2}$-$3_{0,3}$ transition and signal at ~11112MHz as $3_{0,3}$-$4_{0,4}$ transition for *Structure A*, $4_{0,4}$-$5_{0,5}$ transition could be predicted and observed as a doublet at 13681.0644MHz and 13681.0693MHz, again separated by 9.8 kHz. These assignments turned out to be correct and soon a total of 27 *a*-type transitions were measured, for J up to 6 and K_a up to 3. All these transitions appeared as doublets and the splitting ranged between 9.8 kHz to 56.1 kHz. After fitting the *a*-type transitions search was made for the *b*-type and *c*-type transitions. A total of 20 *b*-type and 5 *c*-type transitions could be observed and these appeared as doublets as well. The R-branch *b*-type transitions show a small splitting ranging between 9.8-29.3 kHz. Three Q-branch-*b*-type transitions were observed and the splitting for them was higher, ranging between 48.9-114.8 KHz. In case of *c*-type transitions the splitting was even higher, ranging between 2.5562-2.6125 MHz.

The observed spectrum for Ar•••PA complex was fitted with semi-rigid rotor Watson's S-reduced asymmetric Hamiltonian. Data could be fitted in two different ways: (i) fitting the lower and upper components of the *a*- and *b*- type transitions separately (not including the c-type transitions) and (ii) fitting the line centres of the observed doublets for all the three (*a*-, *b*- and *c*-) type of transitions. When the *a*- and *b*-type transitions were fitted in two different sets (lower and upper), rms deviation for the lower set's fitting was 10.6 kHz and for the upper set's fitting was 7.7 kHz. This

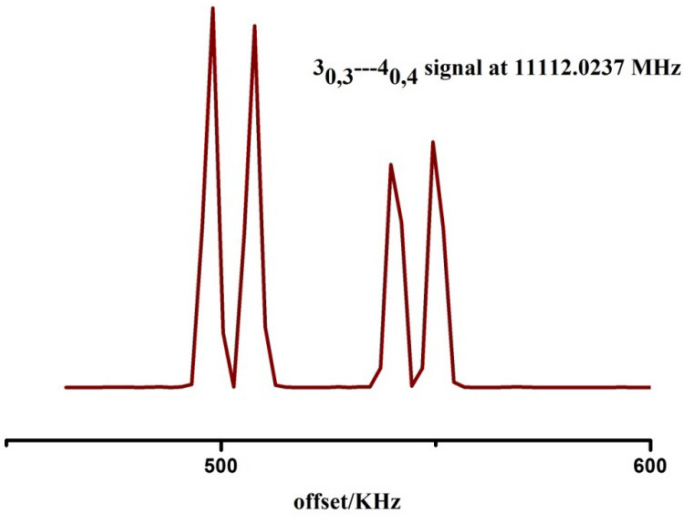

Figure III.4. $3_{0,3}$-$4_{0,4}$ transition of the Ar●●●g-PA complex. Smaller splitting is due to tunnelling and the larger splitting is due to Doppler doubling. Tunnelling splitting is 9.8 kHz. Line centre is given in the Figure.

is not surprising given the small splitting observed in these transitions. However, the two sets of *c*-type transitions could not be independently fitted and they differed from the predicted transitions by nearly a constant value ±Δ (+ for the upper set and – for the lower set), where Δ varies from 1.2585 to 1.3003 MHz for the upper set and 1.2562 to 1.2999 MHz for the lower set. For a given *c*-type transition the Δ value is nearly equal in the two sets. Clearly, the large amplitude vibrational/tunnelling motion that leads to the experimental splitting changes the sign of *c*-dipole and the allowed transitions connect the lower state to upper state and vice versa. Considering the small splitting observed in the *a*-and *b*-dipole transitions and the fact that either the line centres or the individual lines could be fitted within experimental deviations, it would not be possible to conclude whether *a*-and *b*-dipole moments change sign following the large amplitude motion. Fitting the line centres of all three dipole transitions reduces the rms deviation to 3.1 kHz. All the observed transitions and their residues from the different fits are given in *Table III.2* and the rotational constants obtained from these fits are given in *Table III.3*. The fitted rotational constants are very close to that for Ar●●●g-PA. For the PA monomer also, two sets of transitions were found and *a*- and *b*-dipole transitions could be fitted independently to a semi-rigid rotor. However, the *c*-dipole transitions needed tunnelling and coriolis terms.[4-6] As the principal axes systems for the monomer and complex are not identical, see *Figures. III.1 and III.3*, some caution must be exercised in comparing these splitting, *vide*

infra.

Spectra for Ar●●●g-PA-D(OD) and Ar●●●g-PA-D(CD) isotopologues could be predicted and readily observed confirming *Structure A*. For the Ar●●●g-PA-D(OD) complex, a total of 20 *a*-type, 19 *b*-type and 3 *c*-type transitions were observed. The small splitting observed in the *a*- and *b*-type transitions for the parent isotopologue could not be resolved for both the deuterated isotopologues. The deuterium quadrupole splitting could be resolved in some low J transitions for both but the data was not sufficient to extract the quadrupole coupling constant. The *c*-type transitions were present as doublets and the splitting was smaller and ranged between 900.7 - 919.7 kHz. The significant reduction in the splitting for the PA-D(OD) compared to PA, suggests that the large amplitude motion could have significant contribution from C-OH torsion. For the Ar●●●g-PA-D(CD) complex, a total of 8 *a*-type, 5 *b*-type and 2 *c*-type transitions were observed. For this isotopologue, the *c*-type transitions again appeared as doublets and the splitting was closer to 2.046 MHz for $1_{0,1}$-$2_{1,1}$ and 2.0121 MHz for the $2_{0,2}$-$3_{1,2}$ transition. Clearly the large amplitude motion leading to the splitting of *c*-dipole transitions is not localized in OH torsion (*vide infra*). These transitions were fitted using the same Hamiltonian used for the parent complex and for the *c*-dipole transitions line centres were used in the fit. In the case of CD isotopologue, the distortion constant D_K was not fitting well and the uncertainty in A rotational constant was also higher. This was most probably due to the absence of K_a=2 and other higher K_a transitions. To get an estimate of D_K value for this isotopologue, we decided to extract all quartic distortion constants from *ab initio* calculations. Freq=VibRot command was used for this purpose. Calculations were carried out for all the three isotopologues of the Ar●●●PA complex and the calculated distortion constants are given in Table *III.4*.

Table III.2. Observed transitions for the Ar•••g-PA complex and their residues from different fits.

Transition							lower set		Upper set		Line centre	
J	K_{-1}	K_{+1}	J	K_{-1}	K_{+1}	Type	Frequency (MHz)	obs-cal (MHz)	Frequency (MHz)	obs -cal (MHz)	Frequency (MHz)	obs -cal (MHz)
4	1	3	4	0	4	*b*	5182.1220	-0.0034	5182.1709	0.0006	5182.1465	-0.0013
2	1	2	1	1	1	*a*	5353.0058	0.0071	5353.0058	-0.0008	5353.0058	0.0017
1	1	1	0	0	0	*b*	5591.5059	0.0060	5591.5059	-0.0026	5591.5059	0.0003
2	0	2	1	0	1	*a*	5689.4687	0.0022	5689.4785	-0.0007	5689.4736	-0.0008
3	0	3	2	1	2	*b*	6054.7867	-0.0034	6054.8087	-0.0007	6054.7977	-0.0035
2	1	1	1	1	0	*a*	6096.3210	0.0012	6096.3370	-0.0019	6096.3290	-0.0017
5	1	4	5	0	5	*b*	6559.9265	-0.0021	6560.0046	0.0023	6559.9655	0.0007
3	2	1	3	1	2	*b*	7826.6709	-0.0065	7826.6904	0.0127	7826.6806	0.0037
3	1	3	2	1	2	*a*	8008.0070	-0.0008	8008.0168	-0.0014	8008.0119	-0.0030
2	1	2	1	0	1	*b*	8081.9631	0.0048	8081.9631	-0.0047	8081.9631	-0.0020
2	2	0	2	1	1	*b*	8222.2710	-0.0075	8222.2831	-0.0010	8222.2771	-0.0037
6	1	5	6	0	6	*b*	8320.9026	-0.0030	8321.0196	0.0021	8320.9600	0.0003
3	0	3	2	0	2	*a*	8447.2256	-0.0563	8447.2978	-0.0002	8447.2917	-0.0002
8	2	6	8	1	7	*b*	8529.9156	-0.0018	8529.9889	-0.0023	8529.9522	-0.0022
3	2	2	2	2	1	*a*	8585.5155	0.0034	8585.5303	-0.0007	8585.5229	-0.0001
3	2	1	2	2	0	*a*	8725.0112	-0.0014	8725.0038	-0.0315	8725.0246	-0.0009
3	1	2	2	1	1	*a*	9120.6119	-0.0018	9120.6586	0.0169	9120.6352	-0.0041
4	0	4	3	1	3	*b*	9158.7954	0.0005	9158.8223	0.0022	9158.8088	-0.0003
3	2	2	3	1	3	*b*	9879.4161	0.0040	9879.4350	-0.0070	9879.4255	-0.0006
3	1	3	2	0	2	*b*	10400.5022	0.0027	10400.5145	0.0077	10400.5083	0.0027
4	1	4	3	1	3	*a*	10640.0842	0.0025	10640.0892	-0.0041	10640.0867	-0.0028
4	0	4	3	0	3	*a*	11112.0188	0.0063	11112.0286	-0.0003	11112.0237	0.0009
4	2	3	3	2	2	*a*	11419.0063	0.0023	11419.0258	-0.0021	11419.0161	-0.0012
4	3	2	3	3	1	*a*	11508.9168	0.0063	11508.9412	0.0067	11508.9290	0.0057
4	3	1	3	3	0	*a*	11521.5234	0.0055	11521.5478	0.0055	11521.5356	0.0047
4	2	2	3	2	1	*a*	11754.9575	0.0055	11754.9893	0.0041	11754.9734	0.0032
4	1	3	3	1	2	*a*	12113.2856	0.0050	12113.3149	-0.0016	12113.3003	0.0000
5	0	5	4	1	4	*b*	12199.7710	0.0014	12199.8003	0.0039	12199.7856	0.0013
4	1	4	3	0	3	*b*	12593.3002	0.0008	12593.3100	0.0079	12593.3051	0.0019
5	1	5	4	1	4	*a*	13245.9412	0.0010	13245.9510	0.0001	13245.9461	-0.0012
5	0	5	4	0	4	*a*	13681.0644	0.0080	13681.0693	-0.0003	13681.0669	0.0022
5	2	4	4	2	3	*a*	14228.4535	-0.0112	14228.4879	-0.0047	14228.4707	-0.0085
2	2	1	1	1	0	*b*	14283.2051	0.0113	14283.2149	-0.0027	14283.2100	0.0034
5	3	3	4	3	2	*a*	14404.7441	0.0003	14404.7734	-0.0003	14404.7588	0.0001
5	3	2	4	3	1	*a*	14448.2935	-0.0008	14448.3295	0.0037	14448.3115	0.0013
5	1	5	4	0	4	*b*	14727.2193	-0.0078	14727.2338	0.0098	14727.2265	-0.0012
5	2	3	4	2	2	*a*	14855.0879	0.0017	14855.1344	0.0029	14855.1112	0.0013
6	0	6	5	1	5	*b*	15131.2559	0.0030	15131.2803	0.0040	15131.2681	0.0025
5	1	4	4	1	3	*a*	15058.8647	0.0052	15058.9038	0.0022	15058.8842	0.0029
6	1	6	5	1	5	*a*	15825.1709	-0.0016	15825.1807	0.0010	15825.1758	-0.0012
6	2	5	5	2	4	*a*	17008.5025	-0.0071	17008.5270	-0.0126	17008.5147	-0.0090
6	1	5	5	1	4	*a*	17938.4075	0.0069	17938.4466	0.0006	17938.4270	0.0039
7	0	7	6	1	6	*b*	17942.4100	0.0010	17942.4295	0.0054	17942.4197	0.0038
6	2	4	5	2	3	*a*	17995.2803	0.0015	17995.3364	0.0004	17995.3083	0.0010
7	0	7	6	0	6	*a*	18636.3246	-0.0040	18636.3246	-0.0029	18636.3246	-0.0031
1	1	0	0	0	0	*c*	5961.9145*	-1.2981	5964.5270*	1.3003	5963.2210	-0.0001
2	1	1	1	0	1	*c*	9195.7120*	-1.2801	9198.3010*	1.2827	9197.0071	-0.0001
3	1	2	2	0	2	*c*	12626.8830*	-1.2562	12629.4392*	1.2585	12628.1611	-0.0011
2	2	0	1	1	0	*c*	14317.3120*	-1.2863	14319.9100*	1.2871	14318.6110	-0.0005
3	2	2	2	1	2	*c*	17886.1464*	-1.2735	17888.7344*	1.2742	17887.4404	-0.0006

Table III.3. Constants obtained for the Ar•••g-PA complex; by fitting the two different sets and the line centres of observed transitions.

Constants	*Lower set*	*Upper set*	*Line centre*
A/MHz	4346.1683(45)	4346.1784(32)	4346.1735(11)
B/MHz	1617.14984(93)	1617.15601(66)	1617.15334(24)
C/MHz	1245.41968(64)	1245.42057(46)	1245.42047(18)
D_J/kHz	7.3056(97)	7.3100(69)	7.3132(27)
D_{JK}/kHz	61.504(76)	61.580(54)	61.552(21)
D_K/kHz	-55.33(96)	-54.99(68)	-55.17(24)
d_1/kHz	-2.1764(67)	-2.1699(48)	-2.1738(18)
d_2/kHz	-0.7145(25)	-0.7157(18)	-0.71468(73)
# transitions	45	45	50
rms deviation /kHz	10.6	7.6	3.1

Table III.4. Calculated distortion constants for Ar•••g-PA complex and its isotopologues at MP2/6-311+G(3df,2p) level and their comparison with the experimentally observed distortion constants in this study.

Complex/Constants	*Ar…PA*		*Ar…PA-D(OD)*		*Ar•••PA-D(CD)*	
	Experimental	*Calculated*	*Experimental*	*Calculated*	*Experimental*	*Calculated*
D_J /kHz	7.3133(22)	28.52	7.1324(61)	26.85	6.98(29)	25.01
D_{JK} /kHz	61.537(17)	119.73	55.981(86)	101.89	58.10(33)	137
D_K /kHz	-55.28(19)	-132.16	-48.83(61)	-107.87	-	-148.08
d_1 /kHz	-2.1709(17)	-5.81	-2.1270(49)	-5.22	-2.53(13)	-5.64
d_2 /kHz	-0.7086(17)	-1.41	-0.6808(63)	1.29	-1.93(62)	-1.71

From the table it is clear that the *ab initio* calculations are able to reproduce the pattern and signs of distortion constants for all the three complexes. On the basis of the calculations the D_K value for Ar•••g-PA-D(CD) should be very close to the D_K value for Ar•••g-PA. Therefore, experimental D_K for the Ar•••g-PA was used in the fitting of Ar•••g-PA-D(CD) transitions. The rms deviation of the fit was an acceptable 8.7 kHz. Observed transitions for the Ar•••g-PA-D(OD) and Ar•••g-PA-D(CD) isotopologues are given in *Table III.5* along with the residues. Fitted constants for the two isotopologues are given in *Table III.6*.

Table III.5. Observed transitions for the Ar•••g-PA-D(OD) and Ar•••g-PA-D(CD) complexes. Residues (Obs-Calc) correspond to the line centres used in fitting.

Transition			*Ar…PA-D(OD)*		*Ar…PA-D(CD)*	
J K_{-1} K_{+1}	*J* K_{-1} K_{+1}	*type*	*Frequency (MHz)*	*obs -cal (MHz)*	*Frequency (MHz)*	*obs -cal (MHz)*
3 1 2	3 0 3	*b*	4108.1265	0.0000	-	-
4 1 3	4 0 4	*b*	5119.7511	-0.0009	-	-
2 1 2	2 1 1	*a*	5333.9315	0.0000	-	-
1 1 1	0 0 0	*b*	5500.2705 5500.3095	0.0098	-	-
2 0 2	1 0 1	*a*	5670.3490	-0.0031	-	-
1 1 0	0 0 0	*c*	5872.7509 5873.6706	-0.0005	-	-
2 1 1	1 1 0	*a*	6079.7160	0.0001	-	-
3 0 3	2 1 2	*b*	6105.4584	0.0053	-	-
5 1 4	5 0 5	*b*	6511.4680	-0.0025	-	-
3 1 3	2 1 2	*a*	7978.6900	-0.0022	7832.6500	-0.0094
2 1 2	1 0 1	*b*	7980.5925	0.0023	7698.7783	-0.0057
2 2 0	2 1 1	*b*	7976.6210	-0.0043	-	
3 0 3	2 0 2	*a*	8415.6888	-0.0024	8273.4140	-0.0017
3 2 2	2 2 1	*a*	8558.8636	-0.0030	-	-
3 2 1	2 2 0	*a*	8703.1900	0.0031	-	-
3 1 2	2 1 1	*a*	9094.8632	0.0113	8992.0253 8992.0497	0.0041
2 1 1	1 0 1	*c*	9098.8583 9099.7729	-0.0023	8860.3800 8862.4260	0.0054
4 0 4	3 1 3	*b*	9192.2500	-0.0118	9182.2820	0.0047
3 2 2	3 1 3	*b*	9638.8700	0.0050	-	-
3 1 3	2 0 2	*b*	10288.9168 10288.9339	-0.0048	9947.2740	0.0067
7 1 6	7 0 7	*b*	10387.0660	-0.0124	-	-
4 1 4	3 1 3	*a*	10599.8490	-0.0031	10399.9750	-0.0037
8 0 8	7 1 6	*c*	10599.8588	-0.0153	-	
4 0 4	3 0 3	*a*	11065.5027	0.0019	10856.1254	-0.0035
4 2 3	3 2 2	*a*	11382.5000	-0.0078	-	-
4 2 2	3 2 1	*a*	11729.2973	0.0095	-	-
6 1 5	5 2 4	*b*	11994.3200	-0.0029	-	-
4 1 3	3 1 2	*a*	12077.1198	-0.0065	11931.9500	0.0007
5 0 5	4 1 4	*b*	12211.0327	0.0017	12119.2670	0.0055
4 1 4	3 0 3	*b*	12473.0908	-0.0003	12073.8400	0.0097
3 1 2	2 0 2	*c*	12523.3673 12524.2680	-0.0001	12268.2437 12270.2558	-0.0055
5 1 5	4 1 4	*a*	13194.1880	0.0027	12937.6004	0.0045
5 0 5	4 0 4	*a*	13618.6246	0.0033	13336.9500	-0.0128
5 2 4	4 2 3	*a*	14181.3096	-0.0038	-	-
2 2 0	1 1 1	*b*	14429.2807	-0.0039	-	-
5 1 5	4 0 4	*b*	14601.7730	-0.0026	-	-

Table III.5 (continued)

5	1	4	4	1	3	*a*	15010.3377	-0.0021	-	-
5	2	3	4	2	2	*a*	14825.7375	-0.0010	-	-
6	0	6	5	1	5	*b*	15117.2246	0.0008	-	-
6	1	6	5	1	5	*a*	15761.4844	0.0064	-	-
6	1	5	5	1	4	*a*	17874.6520	-0.0035	-	-
7	0	7	6	1	6	*b*	17902.9815	0.0065	-	-
7	1	7	6	1	6	*a*	18304.0926	0.0093	-	-
7	0	7	6	0	6	*a*	18547.2392	0.0100	-	-

Table III.6. Fitted constants for the Ar●●●PA-D(OD) and Ar●●●PA-D(CD) complexes. Line centres for all the transitions were used in fitting.

Constants	*Ar…g-PA-D(OD)*	*Ar…g-PA-D(CD)*
A/MHz	4260.0118(22)	4060.5888(70)
B/MHz	1613.29915(55)	1600.4695(29)
C/MHz	1240.33875(34)	1212.8717(31)
D_J/kHz	7.1412(53)	7.199(46)
D_{JK}/kHz	55.890(76)	55.80(55)
D_K/kHz	-49.17(50)	-55.28
d_1/kHz	-2.1313(47)	-2.49(12)
d_2/kHz	-0.6822(62)	-1.56(47)
# transitions	45	15
rms deviation /kHz	6.3	8.7

III.4. Analysis

III.4.a. Structure

Using the rotational constants of the parent complex and the two deuterium substituted complexes, positions of substituted atoms can be found from the Kraitchman analysis.[32,33] The analysis shows, not surprisingly, that distances of H-4 and H-1(labelling as in *Figure III.3a*) from centre of mass of the complex, are 1.546(2) Å and 3.348(1) Å which are very close to the *ab initio* values 1.523 Å and 3.293 Å for the Ar●●●g-PA complex and very different from the *ab initio* values 1.411 Å and 4.747 Å for the Ar●●●t-PA complex. For further structural analysis we needed to make some assumptions due to limitations of the available data. The two assumptions made are (i) monomer PA geometry is the same as optimized at the MP2/6-311+G(3df,2p) level; (ii) monomer geometry does not change on

complexation with Ar. Both these approximations are reasonable. *Ab initio* calculations show that on complexation with Ar, change in O-H bond length and angle (C-O-H) of PA is only 0.001Å and 0.009^0 respectively. With these assumptions, position of Ar atom was determined from RGDFIT code.[34] The code is based on the fact that complexation of a molecule with a rare gas atom is equivalent to addition of a point mass to the molecule and co-ordinates of this point mass can be calculated from the rotational constants of the molecule and the complex. Rotational constants for the monomer PA were taken from the *ab initio* optimized geometry, in accordance with the assumption (i), and for the complex the experimental rotational constants were used. Although experimental rotational constants for the PA-monomer are also available, *ab initio* constants were used in the calculations because experimental rotational constants for the molecule are largely affected by tunnelling motion of molecule between two equivalent gauche-conformers. The tunnelling splitting was about 660 GHz[5,7] as compared to 2.6 MHz in the complex. Thus, in the Ar●●●PA complex the motion is very much restricted compared to that in the monomer. Ar position was calculated using the data from all three isotopologues separately and the other intermolecular parameters were determined using Ar position and *ab-initio* monomer geometry, see *Table III.7*. The values obtained are similar for all three isotopologue and the Ar to c.m. distance is 2.08 Å. The Ar●●●H-O bond distance (2.83 Å) is similar to that of Ar●●●methanol (2.87 Å) and less than Ar●●●butan-2-ol (2.97 Å) complex. Similar to the Ar●●●butan-2-ol complex, Ar is out of the carbon-hydrogen-oxygen plane (C-O-H-Ar dihedral angle ~36^0) in the Ar●●●PA complex also. The Ar●●●π distance is about 3.90 Å, and is comparable to that for Ar●●●acetylene complex.

Table III.7. Approximate Ar-position and intermolecular parameters for the Ar●●●PA alcohol complex calculated using data for all three isotopologues separately.

	r(Ar●●●c.m.) in A^0	*r(Ar●●●H/D-O) in A^0*	*r(Ar●●●π-bond) in A^0*	*Angle (Ar●●●H-O)*	*dihedral (COHAr)*
Ar…PA	2.079	2.834	3.901	144.8^0	35.6^0
Ar…PA-D(OD)	2.079	2.855	3.898	143.6^0	35.7^0
Ar…PA-D(CD)	2.079	2.816	3.920	144.7^0	37.2^0

III.4.b. Nature of interactions

To understand the nature of interactions in the Ar•••PA complex, it will be worth comparing its properties with the complexes in which Ar•••H-O or Ar•••π interaction is present. Simplest complexes with these interactions are Ar•••methanol and Ar•••acetylene complex and thus, were chosen for the purpose. In the Ar•••methanol complex the main interaction is between Ar and hydroxyl group while in the Ar•••acetylene complex the interaction is between Ar and π-electronic density. Comparing interaction energies of the Ar•••g-PA and Ar•••t-PA complexes with those of Ar•••methanol and Ar•••acetylene complexes, one would expect that Ar•••g-PA interaction energy would be nearly equal to the sum of interaction energies of Ar•••methanol and Ar•••acetylene complex while that for Ar•••t-PA it would be nearly same as that of Ar•••methanol. The Ar•••methanol and Ar•••acetylene complexes were optimized at the MP2/6-311+G(3df,2p) and interaction energies for them were calculated at the same level. These interaction energies are compared in *Table III.8*. The energies are corrected for the basis set superposition error (BSSE) and are given with and without zero-point energy correction. BSSE corrections were made using the counterpoise method[35]. Interaction energy for Ar•••g-PA is found to be slightly less (0.3 kJ mol^{-1}) than the sum of Ar•••methanol and Ar•••acetylene interaction energies while for Ar•••t-PA complex interaction energy is marginally (0.3 kJ mol^{-1}) greater than the Ar•••methanol complex.

Table III.8. BSSE corrected ΔE_{BSSE}, and BSSE+zero-point corrected $\Delta E_{(BSSE+ZPC)}$, interaction energies, calculated at MP2/6-311+G(3df,2p) level.

Complex	ΔE_{BSSE}	$\Delta E_{(BSSE+ZPE)}$
Ar…methanol	2.0	1.0
Ar…acetylene	1.2	0.8
Ar… g-PA	2.9	2.3
Ar…t-PA	2.3	1.5

The difference between Ar•••t-PA and Ar•••methanol could arise due to both dispersion contribution and the electrostatic contribution (difference in acidic nature of the two OH groups). From our calculations, the dispersion contribution was estimated as the difference between HF and MP2 interaction energies (after BSSE

correction) and it favours Ar•••methanol complex by 0.3 kJ.mol^{-1}. Clearly the electrostatic contribution should be little more than compensating. To explore this in detail, the *ab initio* wave functions were analyzed using AIM theory and were also used for calculating the electrostatic potentials.

Electron density topology and critical points obtained from the AIM calculations are shown in *Figure III.5*. The Ar•••g-PA complex has two inter-molecular bond critical points showing that Ar is bound to both the –OH group and the internal C atom from the C≡C group. For the Ar•••t-PA complex and the Ar•••methanol complex also, there are two inter-molecular bond critical points (i) between Ar and –OH group and (ii) between Ar and the carbon atom through CH_2O face. To the best of our knowledge, such Ar•••C interaction has not been reported before. This appears to be similar to the recently observed P•••N[36,37] and C•••S[38] interactions.

A ring critical point is also present in both the structures of Ar•••PA complex and Ar•••methanol complex, showing the presence of a cyclic structure involving Ar atom. In the case of Ar•••Acetylene complex, there is only one intermolecular bond critical point present showing the interaction between Ar and one of the C atoms in the π- bond of acetylene. For all these complexes electron density (ρ) and Laplacian of electron density ($\nabla^2\rho$) at intermolecular bond critical points, are given in *Table III.9*. The ρ and $\nabla^2\rho$ values are almost equal for the Ar•••HO interaction in the Ar•••g-PA and the Ar•••t-PA structures and these are slightly larger than those for the Ar•••methanol complex. The larger ρ value implies that the Ar•••HO interaction in the Ar•••PA complex is slightly stronger as compared to the Ar•••methanol complex. This is due to the electron withdrawing nature of the acetylenic group present in PA which makes the OH proton more acidic. Similar trend is present for the bond critical point present between Ar and CH_2O–face of Ar•••t-PA and Ar•••methanol. The Ar•••π bond critical points present in the Ar•••g-PA complex and Ar•••acetylene complex have very similar ρ and $\nabla^2\rho$ values as well. More interestingly, these values are almost similar to those for the Ar•••CH_2O interaction in Ar•••t-PA and Ar•••methanol complex, which implies that Ar•••CH_2O interaction is as strong as the Ar•••acetylene interaction!

Table III.9. Electron density (ρ) and Laplacian of electron density $\nabla^2(\rho)$ at the inter-molecular bond critical points. Both the quantities are reported in atomic units.

Complex/Interaction type	*Ar…g-PA*		*Ar…t-PA*		*Ar…methanol*		*Ar…acetylene*	
	ρ	*$\nabla^2(\rho)$*	*ρ*	*$\nabla^2(\rho)$*	*ρ*	*$\nabla^2(\rho)$*	*ρ*	*$\nabla^2(\rho)$*
Ar●●●H-O	0.0046	0.0203	0.0048	0.0213	0.004	0.0182	-	-
Ar●●●π--bond	-	-	0.0035	0.0116	-	-	0.0031	0.0117
Ar●●●C(CH_2O surface)	0.0034	0.0165	-	-	0.0031	0.0144	-	-

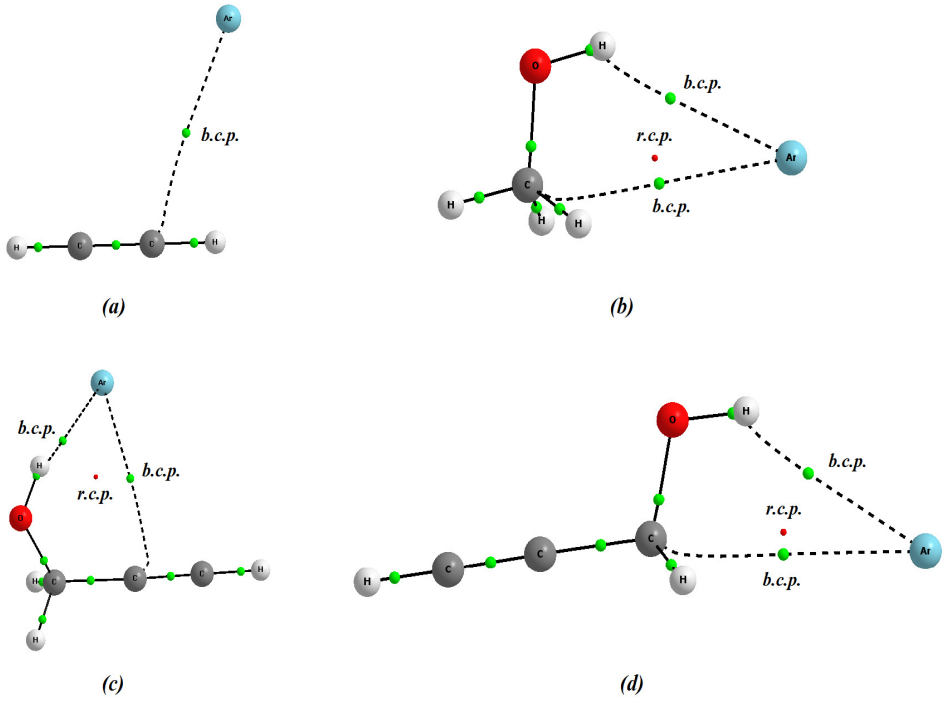

Figure III.5. Critical points for (a) Ar●●●acetylene, (b) Ar●●●methanol, (c) Ar●●●g-PA and (d) Ar●●●t-PA. Wave functions for the optimized geometries at MP2/6-311+G(3df,2p) level were used in the calculations.

In the Ar●●●t-PA complex, Ar interacts with the –OH group as well as the CH_2O face of the PA molecule. We were curious to know the nature of the CH_2O face. It is well established that tetrahedral face of methane is a -ve centre and thus, can act as hydrogen bond acceptor. [38-43] Question arises whether the CH_2O face in molecules like PA and methanol has a positive centre or a negative one? Locating surface minima and maxima on electrostatic potential surface of the molecules would be very helpful in understanding this property. The calculations were done for methane, methanol and both the conformers of PA molecule. Electrostatic potential (ESP) was mapped onto 0.001 e.Bohr^{-3} isosurface of electron density. *Figure III.6* shows the points where ESP maxima/minima occur on the isosurface. Values of ESP at the

maximum/minimum points and their positions are given in the *Supplementary Information.*

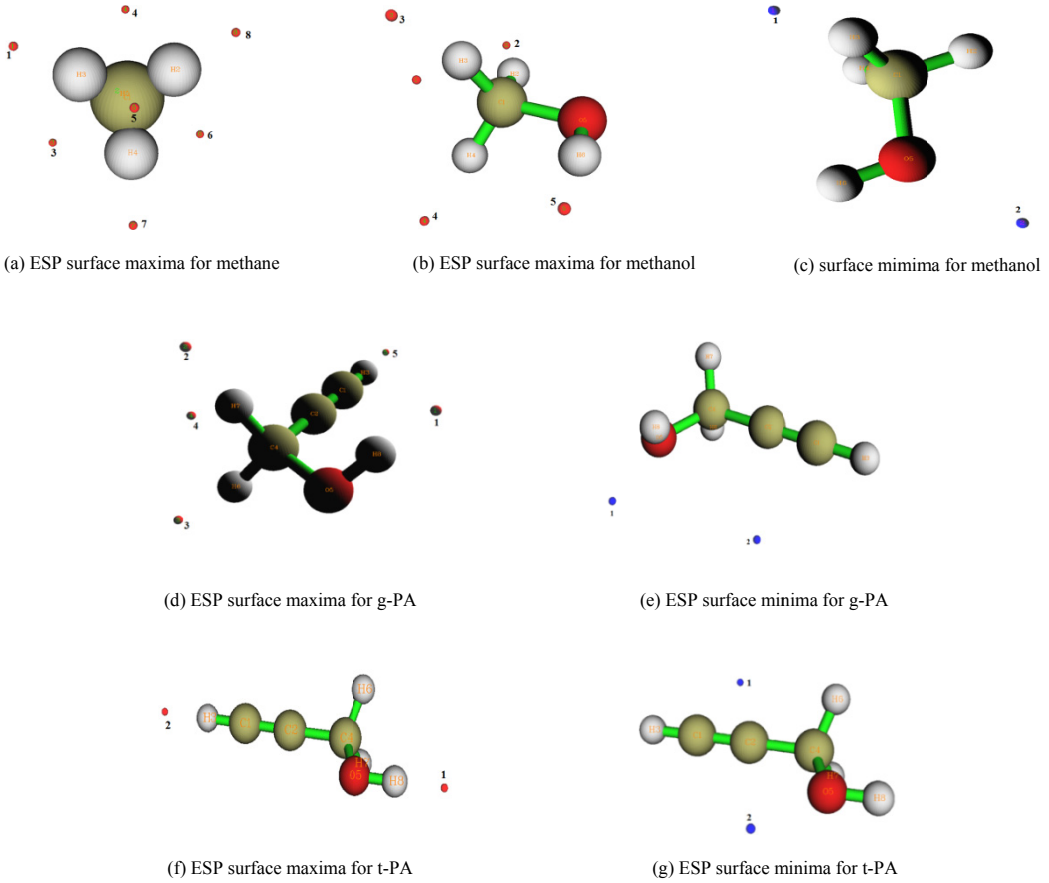

(a) ESP surface maxima for methane

(b) ESP surface maxima for methanol

(c) surface mimima for methanol

(d) ESP surface maxima for g-PA

(e) ESP surface minima for g-PA

(f) ESP surface maxima for t-PA

(g) ESP surface minima for t-PA

Figure III.6. ESP extremum points mapped on the 0.001 Bohr isosurface of electron density for different molecules.

Extremums with positive ESP values indicate electron deficiency while those with negative ESP values indicate an electron rich centre. For methane there are a total of 8 maximum and 15 minimum points on the isosurface. Maximum points 1, 2, 7 and 8 have +ve ESP values and these are in the direction of C-H bonds. These +ve values indicate electron deficiency and justify the already known fact that methane can form complexes having CH●●●O type of interactions.[40] On the other hand, maximum points 3,4,5 and 6 are located at the centre of the tetrahedral faces of methane and have –ve ESP value which shows that these are electron rich centres and can act as hydrogen bond acceptors as found in the case of CH_4●●●HF, CH_4●●●H_2O and CH_4●●●H_2S complexes.[38-43] For methanol, maximum #1 corresponds to the CH_3 face centre and its

positive value shows that the centre is electron deficient (unlike CH_3 faces of methane) and cannot act as hydrogen bond acceptor. This is due to the presence of electron withdrawing –OH group in methanol. Similarly, maximum points in the C-H bond direction are more +ve compared to those of methane, again due to the same reason. The two minimum points 1 and 2, in methanol are present at the CH_2 edge centre and near oxygen respectively. High –ve value of ESP at minimum point 2 is due to presence of lone pairs of electrons on oxygen. For gauche-conformer of PA there are 5 maximum points and 2 minimum points on the isosurface while for the trans-conformer of PA there are 2 minimum and 2 maximum points present. Maxima #1 and 5 in the gauche conformer correspond to O-H proton and acetylenic proton respectively. High positive value of ESP at these points shows acidic nature of the protons. It is clear from the ESP values that hydroxyl proton is more acidic than the acetylenic proton. Maxima #2 and 3 correspond to two C-H hydrogens and their ESP value is much less than that of acetylenic proton indicating lower acidity for these hydrogens. The two minima #1 and 2 correspond to the lone pair of oxygen and π-electron density of acetylenic bond respectively. For the trans conformer maxima #1 and 2 correspond to the hydroxyl and acetylenic protons respectively and minima #1 and 2 correspond to oxygen lone pair of electrons and π- electron density of acetylenic bond. Hydroxyl proton of t-PA has more +ve ESP value than that of methanol explaining the larger binding energy of Ar●●●t-PA complex than Ar●●●methanol complex.

In both the conformers there were no maxima or minima present on the CH_2O surface to draw any conclusion about its nature. However, AIM calculations show the presence of a bond critical point between Ar and the CH_2O face carbon in the *Structure* B . To explore this interaction another approach was adopted. A dummy atom was put in place of Ar and ESP was calculated along a line which extends from the dummy atom to the CH_2O face carbon atom. Throughout the line the ESP value was +ve which shows that Ar interacts with the face through an electron deficient path. Moreover, ESP surface plotted using GaussView software shows that the CH_2O surface for t-PA has positive ESP value, *Figure III.7*.

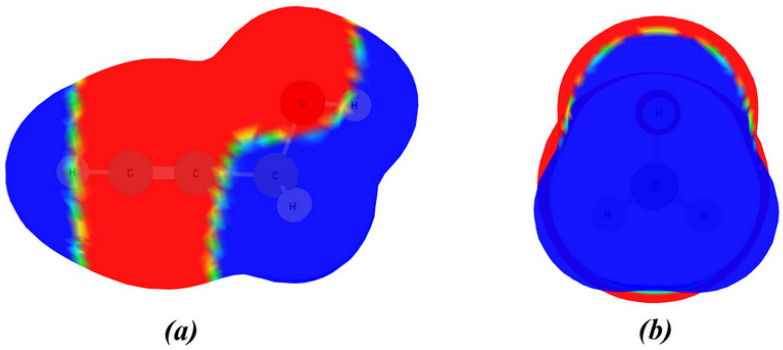

Figure III.7. ESP surface mapped on the 0.001 Bohr isosurface of electron density for (a) t-PA and (b) g-PA. Blue is positive and red is negative.

III.5. Discussions

Comparison of experimental and theoretical rotational constants and structural analysis on Ar•••PA complex, confirms the structure in which PA exists in gauche form and Ar atom is located in between -OH and -C≡C-H groups and enjoys the proximity of both the groups. The Ar•••H(-O) distance and Ar•••H-O angle is in good agreement with other similar complexes. Two sets of transitions were found for this complex similar to those for PA monomer. The rotational spectra of PA monomer show that the ground state of the molecule consists of two torsional substates resulting due to tunnelling motion of -OH proton between two equivalent gauche conformers.[5,7] The separation between the lowest two internal rotation states was found to be 21.49 cm^{-1}, as measured through the tunnelling splitting in the *c*-dipole transitions. For the monomer also, the *a*- and *b*-type transitions with low K_a values, can be fitted in two different sets giving two sets of rotational constants corresponding to the two vibrational-rotational-tunnelling states. Difference between rotational constants of the two subsets was found to be ~100MHz, ~20MHz and ~5MHz for A,B and C constants respectively. Analysing the normal modes for the monomer calculated from *ab initio* calculation, we found that there is no mode corresponding to a localized C-OH torsional motion. The low frequency mode dominated by large amplitude C-OH torsion is coupled with the carbon chain motion. The same trend is seen in the mode description of the Ar•••PA complexes. In the Ar•••PA complex, observed splitting of the transitions is many orders of magnitude lower than that of the monomer. The two sets of rotational constants, obtained by fitting two sets of frequencies for the complex, are not very different from each other (differ by only few kHz) which

indicates more localization of the large amplitude motions in the complex due to bonding with Ar.

The principal axis system in the Ar•••PA complex is different from that of the monomer, see *Figure III.1 and III.3* and no direct correlation can be drawn between the energy states of the two. However, the reduction in splitting of c-type transitions on going from Ar•••PA to Ar•••PA-D(OD) complex implies that the large amplitude motion responsible for the splitting involves -OH proton movement. Change in splitting on going from Ar•••PA complex to Ar•••PA-D(CD) complex shows that the motion responsible for splitting also involves movement of acetylenic proton. This observation is in accordance with the *ab initio* calculated normal modes in which all the large amplitude motions involve movements of both the -OH and the carbon chain of PA. Decrease in splitting on complexation with Ar could be because of two reasons (i) due to change in reduced mass of the corresponding large amplitude motion, (ii) due to increase in barrier height for the -OH motion. However, *ab initio* calculated reduced mass and barrier heights for the similar motions in PA monomer and Ar•••PA complex are nearly equal and cannot explain the observed huge reduction in the splitting.

During the experiments, attempts were made to observe transitions for the trans conformer of PA molecule, using both Ar and He as carrier gas, but no transition could be identified. Though there is no signature for the trans conformer experimentally, AIM calculations on the theoretical stable geometry for Ar•••t-PA complex show a novel Ar•••carbon interaction. This interaction is also present in the Ar•••methanol complex and is perhaps the main reason for the deviation from linearity of Ar•••H-O angle in this complex.

III.6. Conclusions

Rotational spectra of Ar•••PA complex and its two deuterium isotopologues were observed and fitted with a semi-rigid rotor Hamiltonian. The spectra reveal a small splitting due to a large amplitude vibrational-tunnelling motion dominated by, but not restricted to, C-OH torsion. The rotational constants confirm the geometry in which PA exists in gauche form and Ar acts as a bridging atom between OH and π groups. No evidence could be found for the structure in which PA exists in trans form. The observed signs and pattern of distortion constants could be reproduced from *ab initio*

calculations for all three isotopologues of the complex. The nature of interaction in this complex has been studied using AIM theory and ESP calculations. These confirm the Ar•••OH and Ar•••π interactions in the observed Ar•••g-PA complex. The other theoretically predicted Ar•••t-PA structure reveals Ar•••H-O and a novel Ar•••C interaction, through the CH_2O face which is also seen in the Ar•••methanol complex.

III.7. Supplementary Information

Coordinates of the optimized geometries and frequencies for the normal modes of vibrations for Ar•••PA complexes are given in the *Supplementary Information*. For different molecules, values of ESP at the maximum/minimum points and their positions are also given in the *Supplementary Information*.

III.8. References:

1. http://science.gsfc.nasa.gov/691/cosmicice/interstellar.html.

2. Miller, J. A.; Melius, C. F. *Combust. Flame* **1992**, *91*, 21-39.

3. Frenklach, M. *Phys. Chem. Chem. Phys.* **2002**, *4*, 2028-2037.

4. Tranter, R. S.; Yang, X.; Kiefer, J. H. *P Combust Inst.* **2011**, *33*, 259-265.

5. Hirota, E. *J. Mol. Spectrosc.* **1968**, *26*, 335-350.

6. Bolton, K.; Owen, N. L.; Sheridan, J. *Nature* **1968**, *217*, 164-164.

7. Pearson, J. C.; Drouin, B. J. *J. Mol. Spectrosc.* **2005**, *234*, 149-156.

8. Bolton, K.; Sheridan, J. *Spectrochim. Acta, Part A* **1970**, *26*, 1001-1006.

9. Mirri, A. M.; Scappini, F.; Cervellati, R.; Favero, P. G. *J. Mol. Spectrosc.* **1976**, *63*, 509-520.

10. Mirri, A. M.; Scappini, F.; Mäder, H. *J. Mol. Spectrosc.* **1975**, *57*, 264-270.

11. Scappini, F.; Favero, P. G.; Cervellati, R. *Chem. Phys. Lett.* **1975**, *33*, 499-501.

12. Møllendal, H.; Konovalov, A.; Guillemin, J.-C. *J. Phys. Chem. A* **2010**, *114*, 5537-5543.

13. Miller, B. J.; Lane, J. R.; Kjaergaard, H. G. *Phys. Chem. Chem. Phys.* **2011**, *13*, 14183-14193.

14. Maity, S.; Guin, M.; Singh, P. C.; Patwari, G. N. *ChemPhysChem* **2011**, *12*, 26-46.

15. Goswami, M.; Arunan, E. *Phys. Chem. Chem. Phys.* **2011**, *13*, 14153-14162.

16. Goswami, M.; Arunan, E. *J. Mol. Spectrosc.* **2011**, *268*, 147-156.

17. Arunan, E.; Emilsson, T.; Gutowsky, H. S.; Fraser, G. T.; de Oliveira, G.; Dykstra, C. E. *J. Chem. Phys.* **2002**, *117*, 9766-9776.

18. Brupbacher, T.; Makarewicz, J.; Bauder, A. *J. Chem. Phys.* **1994**, *101*, 9736-9746.

19. Cohen, R. C.; Saykally, R. J. *J. Chem. Phys.* **1993**, *98*, 6007-6030.

20. Gutowsky, H. S.; Emilsson, T.; Arunan, E. *J. Chem. Phys.* **1997**, *106*, 5309-5315.

21. King, A. K.; Howard, B. J. *J. Mol. Spectrosc.* **2002**, *214*, 97-102.

22. Liu, Y.; Jäger, W. *J. Mol. Spectrosc.* **2001**, *205*, 177-182.

23. Mani, D.; Aiswaryalakshmi, P.; Arunan, E. *Asian J. Spectro.* **2010**, 31-42.

24. Ohshima, Y.; Iida, M.; Endo, Y. *Chem. Phys. Lett.* **1989**, *161*, 202-206.

25. Suenram, R. D.; Lovas, F. J.; Fraser, G. T.; Gillies, J. Z.; Gillies, C. W.; Onda, M. *J. Mol. Spectrosc.* **1989**, *137*, 127-137.

26. Tan, X. Q.; Sun, L. H.; Kuczkowski, R. L. *J. Mol. Spectrosc.* **1995**, *171*, 248-264.

27. Frisch, M. J.; Trucks, G. W.; Schlegel, H. B.; Scuseria, G. E.; Robb, M. A.; Cheeseman, J. R.; Scalmani, G.; Barone, V.; Mennucci, B.; Petersson, G. A.; Nakatsuji, H.; Caricato, M.; Li, X.; Hratchian, H. P.; Izmaylov, A. F.; Bloino, J.; Zheng, G.; Sonnenberg, J. L.; Hada, M.; Ehara, M.; Toyota, K.; Fukuda, R.; Hasegawa, J.; Ishida, M.; Nakajima, T.; Honda, Y.; Kitao, O.; Nakai, H.; Vreven, T.; Montgomery, J. A.; Peralta, J. E.; Ogliaro, F.; Bearpark, M.; Heyd, J. J.; Brothers, E.; Kudin, K. N.; Staroverov, V. N.; Kobayashi, R.; Normand, J.; Raghavachari, K.; Rendell, A.; Burant, J. C.; Iyengar, S. S.; Tomasi, J.; Cossi, M.; Rega, N.; Millam, J. M.; Klene, M.; Knox, J. E.; Cross, J. B.; Bakken, V.; Adamo, C.; Jaramillo, J.; Gomperts, R.; Stratmann, R. E.; Yazyev, O.; Austin, A. J.; Cammi, R.; Pomelli, C.; Ochterski, J. W.; Martin, R. L.; Morokuma, K.; Zakrzewski, V. G.; Voth, G. A.; Salvador, P.; Dannenberg, J. J.; Dapprich, S.; Daniels, A. D.; Farkas; Foresman, J. B.; Ortiz, J. V.; Cioslowski, J.; Fox, D. J. Wallingford CT, 2009.

28. AIMAll (Version 13.02.26), K., Todd A.; TK Gristmill Software, : Overland Park KS, USA, 2012 (aim.tkgristmill.com).

29. Lu, T.; Chen, F. *J. Comput. Chem.* **2012**, *33*, 580-592.

30. Bew, S. P.; Hiatt-Gipson, G. D.; Lovell, J. A.; Poullain, C. *Org. Lett.* **2012**, *14*, 456-459.

31. Arunan, E.; Tiwari, A. P.; Mandal, P. K.; Mathias, P. C. *Curr. Sci.* **2002**, *82*, 533-540.

32. Kraitchman, J. *Am.J.Phys.* **1953**, *21*.

33. Gordy, W.; Cook, R. L. *Microwave Molecular Spectra*; Wiley: New York, **1984**.

34. Kisiel, Z. *in: J.Demaison et al. (Eds.), Spectroscopy from Space, Kluwer Academic Publishers, Dordrecht,* **2001**, 91-106.

35. Boys, S. F.; Bernardi, F. *Mol. Phys.* **1970**, *19*, 553.

36. Scheiner, S. *J. Chem. Phys.* **2011**, *134*, 094315-094319.

37. Scheiner, S. *J. Phys. Chem. A* **2011**, *115*, 11202-11209.

38. Aiswaryalakshmi, P.; Arunan, E. *to be published*.

39. Legon, A. C.; Roberts, B. P.; Wallwork, A. L. *Chem. Phys. Lett.* **1990**, *173*, 107-114.

40. Ohshima, Y.; Endo, Y. *J. Chem. Phys.* **1990**, *93*, 6256-6265.

41. Raghavendra, B.; Arunan, E. *Chem. Phys. Lett.* **2008**, *467*, 37-40.

42. Suenram, R. D.; Fraser, G. T.; Lovas, F. J.; Kawashima, Y. *J. Chem. Phys.* **1994**, *101*, 7230-7240.

43. Szczesniak, M. M.; Chalasinski, G.; Cybulski, S. M.; Cieplak, P. *J. Chem. Phys.* **1993**, *98*, 3078-3089.

Supplementary Information

Table III.S.1. Coordinates and geometry of Ar…g-PA complex, optimized at MP2/6-311+G(3df,2p) level.

Atom	*x (Å)*	*y (Å)*	*z (Å)*
C	1.3961	1.8759	0.2186
C	1.4543	0.7098	0.1147
H	1.3528	2.8963	0.5129
C	1.4893	0.7005	0.5071
O	1.0254	1.5711	0.5118
H	2.5157	1.0014	0.7100
H	0.9162	0.8316	1.4295
H	0.1483	1.2782	0.7735
Ar	2.1763	0.0818	0.0457

Table III.S.2. Coordinates and geometry of Ar…t-PA complex, optimized at MP2/6-311+G(3df,2p) level.

Atom	*x (Å)*	*y (Å)*	*z (Å)*
C	-3.4908	-0.4714	-0.0003
C	-2.2911	-0.2922	0.0000
H	-4.5435	-0.6164	-0.0006
C	-0.8443	-0.1099	0.0005
O	-0.5596	1.2822	0.0001
H	-0.4236	-0.5972	-0.8839
H	-0.4242	-0.5964	0.8856
H	0.3958	1.3854	-0.0011
Ar	2.7350	-0.2552	-0.0001

Table III.S.3. Coordinates of the approximate experimental geometry of Ar…g-PA complex; obtained by fitting Ar position by RGFIT program and using ab initio optimized geometry for gauche-PA monomer.

Atom	*x (Å)*	*y (Å)*	*z (Å)*
C	1.9149	-0.2483	-0.0072
C	0.7720	0.1612	-0.0059
H	2.9171	-0.6022	-0.0176
C	-0.6182	0.6184	0.0263
O	-1.5518	-0.4473	-0.0536
H	-0.8187	1.2546	-0.8338
H	-0.7798	1.2160	0.9276
H	-1.3209	-1.0949	0.6179
Ar	-0.3011	-1.4528	3.2381

Table III.S.4. Coordinates and geometry of Ar…methanol complex, optimized at MP2/6-311+G(3df,2p) level.

Atom	*x (Å)*	*y (Å)*	*z (Å)*
C	-1.8065	0.6513	0.0011
H	-2.8411	0.9779	-0.0399
H	-1.2802	1.0554	-0.8651
H	-1.3526	1.0495	0.9101
O	-1.8282	-0.7666	-0.0046
H	-0.9237	-1.0825	0.0330
Ar	1.7701	0.0125	-0.0005

Table III.S.5. Coordinates and geometry of Ar…acetylene complex, optimized at MP2/6-311+G(3df,2p) level.

Atom	*x (Å)*	*y (Å)*	*z (Å)*
C	-0.5304	-2.4929	0.0000
C	0.5303	-1.9090	0.0000
H	1.4628	-1.3992	0.0000
H	-1.4625	-3.0035	0.0000
Ar	0.0000	1.7119	0.0000

Table III.S.6. Frequencies for the normal modes of vibration for Ar...t-PA and Ar...g-PA complexes at MP2/6-311+G(3df,2p) level.

Ar●●●t-PA		Ar●●●g-PA	
Frequency (cm^{-1})	*IR intensity*	*Frequency (cm^{-1})*	*IR intensity*
32.1	5.5	9.0	1.8
35.4	0.5	34.7	0.2
51.7	0.1	56.3	1.0
206.0	9.0	191.3	4.6
235.6	111.6	267.9	43.7
313.9	0.1	332.8	75.6
550.0	2.5	557.1	11.5
645.3	44.5	646.0	46.1
675.5	35.9	671.2	37.1
923.1	8.3	924.0	21.6
1042.5	3.2	1002.0	17.0
1082.0	106.8	1081.1	102.2
1248.4	65.8	1227.5	17.7
1277.3	0.1	1365.7	3.1
1453.4	31.0	1422.1	46.5
1524.5	2.0	1516.1	3.0
2146.0	2.4	2132.3	1.9
3048.9	35.0	3064.0	26.8
3092.8	13.1	3145.8	6.2
3487.5	56.4	3484.4	56.2
3871.8	50.8	3870.5	59.0

Table III.S.7. Coordinates of methane, geometry optimized at MP2/6-311+G(3df,2p) level.

Atom	*x (Å)*	*y (Å)*	*z (Å)*
C	0.0000	0.0000	0.0000
H	0.6267	0.6267	0.6267
H	-0.6267	-0.6267	0.6267
H	0.6267	-0.6267	-0.6267
H	-0.6267	0.6267	-0.6267

Table III.S.8. Position of electrostatic potential (ESP) extrema, mapped on the 0.001 Bohr electron density surface of methane, and ESP value at the extremum points.

Number of surface minima: 15

#	*ESP value (kcal/mol)*	*x (Å)*	*y (Å)*	*z (Å)*
1	-2.2	-1.9639	0.3712	0.3712
2	-2.2	-1.9620	-0.3745	-0.3756
3	-2.2	-0.3764	0.3959	1.9563
4	-2.2	-0.3764	1.9563	0.3959
5	-2.2	-0.3704	-1.9631	-0.3755
6	-2.2	-0.3702	-0.3742	-1.9635
7	-2.2	-0.0634	0.0442	2.0533
8	-2.2	-0.0634	2.0533	0.0442
9	-2.2	0.3712	-1.9639	0.3712
10	-2.2	0.3959	-0.3764	1.9563
11	-2.2	0.3712	0.3712	-1.9639
12	-2.2	0.3959	1.9563	-0.3764
13	-2.2	1.9563	-0.3764	0.3959
14	-2.2	1.9563	0.3959	-0.3764
15	-2.2	2.0533	-0.0634	0.0442
Number of surface maxima:	8			
1	8.7	-1.4323	-1.4325	1.3448
2	8.7	-1.4323	1.3448	-1.4325
3	-1.8	-1.0866	-1.0866	-1.0866
4	-1.8	-1.1019	1.0788	1.0788
5	-1.8	1.0788	-1.1019	1.0788
6	-1.8	1.0788	1.0788	-1.1019
7	8.7	1.3448	-1.4323	-1.4325
8	8.8	1.4044	1.4044	1.4044

Table III.S.9. Coordinates of methanol, geometry optimized at MP2/6-311+G(3df,2p) level.

Atom	*x (Å)*	*y (Å)*	*z (Å)*
C	-0.6647	-0.0202	0.0000
H	-1.0781	0.9836	-0.0018
H	-1.0230	-0.5409	0.8894
H	-1.0228	-0.5440	-0.8877
O	0.7465	0.1219	0.0000
H	1.1398	-0.7525	0.0000

Table III.S.10. Position of electrostatic potential (ESP) extrema mapped on 0.001 Bohr electron density surface of methanol, and ESP value at the extremum points.

Number of surface minima: 2				
#	*ESP value (kcal/mol)*	*x (Å)*	*y (Å)*	*z (Å)*
1	7.5	-1.8088	-1.7097	-0.0014
2	-36.2	1.7718	1.6006	0.0037
Number of surface maxima: 5				
1	12.0	-2.4603	-0.1052	0.0052
2	11.2	-1.9178	2.0341	0.0071
3	13.6	-1.4281	-1.4378	1.8283
4	13.6	-1.4029	-1.4232	-1.8519
5	47.7	1.4831	-1.8594	-0.0110

Table III.S.13. Coordinates of t-PA, geometry optimized at MP2/6-311+G(3df,2p) level.

Atom	*x (Å)*	*y (Å)*	*z (Å)*
C	-1.9413	-0.2069	0.0000
C	-0.7769	0.1329	0.0001
H	-2.9581	-0.5157	-0.0002
C	0.6135	0.5725	0.0001
O	1.4546	-0.5732	0.0002
H	0.7914	1.1901	0.8852
H	0.7915	1.1901	-0.8850
H	2.3662	-0.2695	-0.0027

Table III.S.14. Position of electrostatic potential (ESP) extrema mapped on 0.001 Bohr electron density surface of t-PA, and ESP value at the extremum points.

Number of surface minima: 2				
#	*ESP value (kcal/mol)*	*x (Å)*	*y (Å)*	*z (Å)*
1	-15.5	-2.1668	1.9231	0.3032
2	-36.8	0.7136	-2.1968	0.0065
Number of surface maxima: 2				
1	53.5	3.4432	0.1451	-0.0308
2	31.9	-4.1485	-0.8524	-0.0145

Chapter IV. The X-C●●●Y ($X=O/F/Cl,Br,NO_2,NF_2$; $Y=O/S/F/Cl/Br/N/P$) 'Carbon Bond'.

(Part of this chapter has been published in Phys. Chem. Chem. Phys. 2013, 15, 14377-14383.)

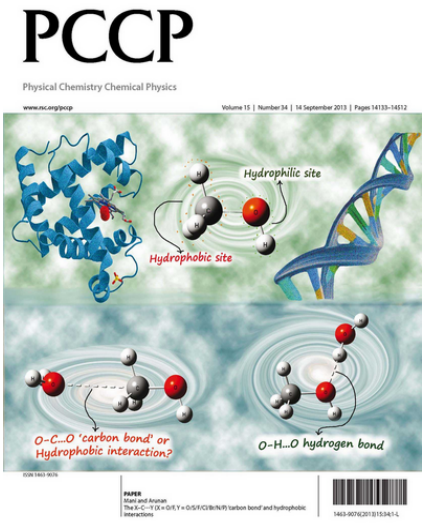

IV.1. Introduction

In the last few decades, due to the development of experimental and theoretical techniques, many non-conventional interactions have been reported and analysed, e.g. halogen bonds (group 17),[1-3] chalcogen bonds (group 16)[4,5] and pnicogen bonds (group 15),[6,7] and the realm of weak interactions is expanding continuously with improved understanding. Do similar interactions exist with group 14 (carbon group) elements as well? Politzer et al.[1,8,9] have mentioned that similar interactions can exist with group 14 elements also. However, they focused on Si and Ge compounds extensively and a few carbon compounds were included in one study.[10] No electron density or NBO analysis had been performed to explore the nature of interactions which could provide important insight about the nature of bonding.

Work reported in this chapter is an offshoot of our spectroscopic and *AIM* investigations on the Ar•••propargyl alcohol complex[11] discussed in *Chapter III*. As mentioned in the chapter, one of the structures of the complex was found to exhibit a unique Ar•••C bond which was also found to be present in the Ar•••methanol complex! This drew our attention and curiosity towards the different possible interactions in methanol, other than the well known hydrogen bonded ones with OH group as the acceptor or donor. Let us start the discussion with the bonding properties of methane molecule. Through many theoretical and experimental studies, it is now very well established that the tetrahedral face of methane molecule can act as hydrogen bond acceptor.[12-17] Rotational spectra of the complexes like CH_4•••HF[13]/HCl[14]/HCN[12] and CH_4•••H_2O[16] further helped confirm this fact. Atoms in molecules (AIM) theoretical calculations show a bond critical point (BCP) connecting the H from HX to the C of CH_4 through one of the faces, leading to a pentacoordinate C.[15]

Electrostatic potential calculations have been extensively used in locating sites of electrophilic and nucleophilic attacks on molecules.[18,19] Calculation of the electrostatic maxima and minima points, by Multiwfn software,[20] shows the presence of four equivalent maxima at the tetrahedral face centers of methane, *Figure IV.1.a*, with ESP value -7.5 kJ.mol^{-1} and four equivalent maxima along C-H bonds with ESP value of +36.4 kJ.mol^{-1}, at 0.001 a.u. isosurface of electron density. Clearly, methane can accept a hydrogen bond through the face centre. How would the substitution of

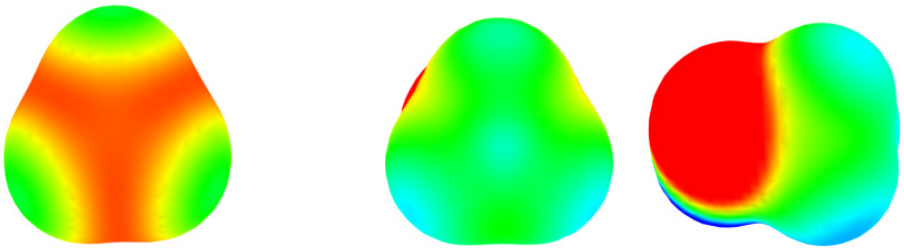

(a) (b)

Figure IV.1. ESP surfaces of (a) methane and (b) methanol at 0.001 a.u. isosurface of electron density. For methanol two different views are shown. Colour code is: blue more positive than green which is more positive than yellow which is more positive than red. Surfaces were plotted using GaussView software

one of the hydrogen atoms of methane, with some electron withdrawing group such as -OH/F/Cl/Br etc., affect the nature of the tetrahedral face? *Figure IV.1.b* shows ESP value mapped on the 0.001 a.u. electron density isosurface of methanol. The value throughout the CH_3 tetrahedral face is positive with maximum at the face centre, shown in light blue in the *Figure IV.1.b*. This positive face centre along the extension of C-O bond resembles a sigma hole which is often used to explain the origin of halogen bonding. ESP extrema calculations give the ESP value of +50.2 $kJ.mol^{-1}$ for the CH_3 face centre maxima of CH_3OH. The interesting follow-up question then is: being a positive centre can this face accept electron density from the atoms like oxygen in water?

IV.2. Computational details

Gaussian 09 software suite[21] was used to perform all the optimization and frequency calculations on the complexes. Møller-Plesset second order perturbation theory (MP2) was used to perform optimization and frequency calculations, which inherently takes care of electron correlations and is often regarded as one of the most suitable theory for weakly bonded complexes. Complexes were first optimized with 6-311+G(3df,2p) basis sets and the optimized minima geometries were used as starting geometries for the optimization with Aug-cc-pVTZ basis set. BSSE correction was done using Boys and Bernardi's counterpoise method.[22] To have a better estimate of the stabilization energies, counterpoise single point calculations were performed at CCSD-T/6-311+G(3df,2p) level on the geometries optimized at MP2/6-311+G(3df,2p) level. NBO calculations were performed using NBO-6.0 software suite.[23] AIMALL and

AIM2000 software suites[24,25] were used to do the Atoms in molecules analysis and the wave functions for the analysis were extracted from the Gaussian calculations at MP2/6-311+G(3df,2p) level. Electrostatic potential analysis was done using Multiwfn[20] and GaussView software.

IV.3. Results and discussions

IV.3.a. Complexes with CH_3OH

Methanol•••water complex was optimized at MP2/6-311+G(3df,2p) level, with the initial geometry in which oxygen of water faces the tetrahedral CH_3 face of methanol. The optimized structure was confirmed to be a minimum on the potential energy hyper surface by frequency calculations. Atoms in molecules (AIM) analyses show the presence of a BCP between oxygen of water and carbon atom of methanol, *Figure IV.2.a and IV.3.a*. Encouraged by this result, we further investigated complexes of other molecules with methanol taking the initial geometry in which the more electronegative atom of the other molecule points towards the CH_3 face of methanol. Structures were optimized for H_2S•••CH_3OH, HY••CH_3OH(Y=F/Cl/Br), LiY•••CH_3OH (Y=F/Cl/Br) ClF•••CH_3OH, H_3N•••CH_3OH and H_3P•••CH_3OH complexes at MP2/6-311+G(3df,2p) level. Optimized geometries for the complexes are given in *Figure IV.2*. All the complexes were confirmed to be minima by frequency calculations. Calculations were repeated at MP2/Aug-cc-pVTZ level to see the effect of basis sets and all the complexes were found to be stable minima at this level as well. CCSD-T/6-311+G(3df,2p) single point counterpoise calculations were also performed on the geometries optimized at MP2/6-311+G(3df,2p) level.

BSSE corrected stabilization energies $\Delta E_{(BSSE)}$, and BSSE and zero-point corrected stabilization energies $\Delta E_{(BSSE+ZPC)}$, at MP2/6-311+G(3df,2p) as well as MP2/Aug-cc-pVTZ level for all these complexes are given in *Table IV.1*. BSSE corrected binding energies at CCSD-T/6-311+G(3df,2p) level are also given. The stabilization energies at this level are not very different from those calculated at MP2/6-311+G(3df,2p) level.

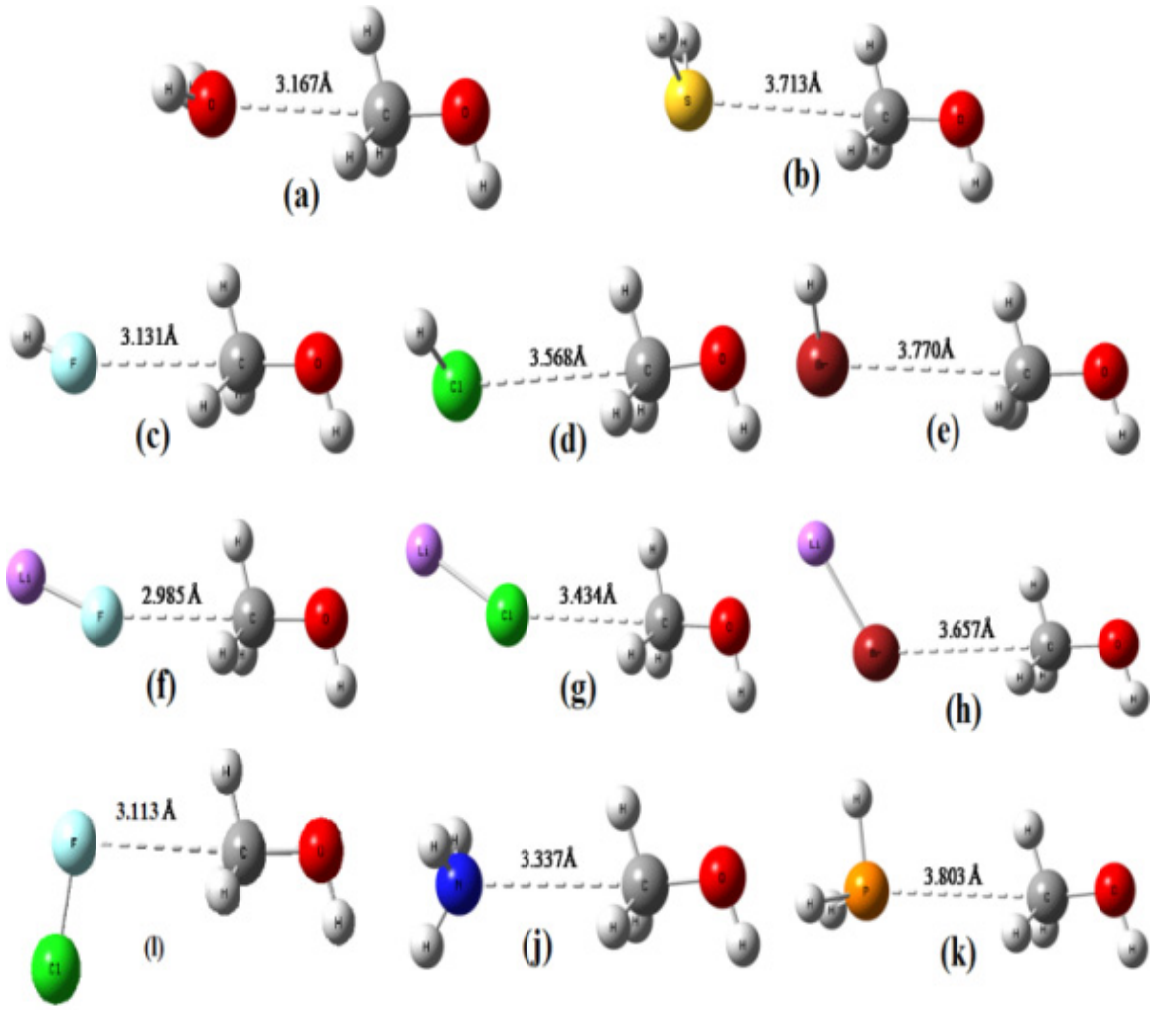

Figure IV.2. Optimized geometries for (a) H_2O•••CH_3OH, (b) H_2S•••CH_3OH, (c) HF•••CH_3OH, (d) HCl•••CH_3OH, (e) HBr•••CH_3OH, (f) LiF•••CH_3OH, (g) LiCl•••CH_3OH, (h) LiBr•••CH_3OH, (i) ClF•••CH_3OH, (j) H_3N•••CH_3OH, (k) H_3P•••CH_3OH complexes.

Table IV.1. BSSE corrected, $\Delta E_{(BSSE)}$, and BSSE and zero point corrected $\Delta E_{(BSSE+ZPC)}$, stabilization energies for different complexes of methanol in kJ mol^{-1}.

Complex	At MP2 /6-311+G(3df,2p)		At MP2 /Aug-cc-pVTZ		At CCSD-T /6-311+G(3df,2p)
	$\Delta E_{(BSSE)}$	$\Delta E_{(BSSE+ZPC)}$	$\Delta E_{(BSSE)}$	$\Delta E_{(BSSE+ZPC)}$	$\Delta E_{(BSSE)}$
$H_2O\bullet\bullet\bullet CH_3OH$	4.2	1.9	4.5	2.2	4.4
$H_2S\bullet\bullet\bullet CH_3OH$	2.5	1.0	3.5	2.3	2.7
$HF\bullet\bullet\bullet CH_3OH$	2.9	1.2	3.1	1.7	3.1
$HCl\bullet\bullet\bullet CH_3OH$	2.4	1.1	3.0	1.8	2.2
$HBr\bullet\bullet\bullet CH_3OH$	2.5	1.4	2.9	1.5	2.6
$ClF\bullet\bullet\bullet CH_3OH$	2.4	1.1	2.9	1.5	2.3
$LiF\bullet\bullet\bullet CH_3OH$	9.0	7.6	9.7	8.4	9.7
$LiCl\bullet\bullet\bullet CH_3OH$	7.2	6.0	8.1	7.0	7.0
$LiBr\bullet\bullet\bullet CH_3OH$	6.9	6.0	7.5	6.6	6.7
$H_3N\bullet\bullet\bullet CH_3OH$	4.3	2.2	4.7	2.7	4.5
$H_3P\bullet\bullet\bullet CH_3OH$	2.8	1.6	3.3	1.7	2.6

Electron density topologies for the complexes, calculated using AIM theory, are shown in *Figure IV.3*. In all these complexes, a bond critical point is found between C of methanol and the interacting atom of the other molecule which confirms the presence of C•••Y (Y= O/S/F/Cl/Br/N/P) bond in all these complexes.

Electron density ρ(r), and Laplacian of electron density $\nabla^2\rho(r)$ values at the intermolecular BCPs as well as mutual penetration between interacting atoms are given in *Table IV.2*. For all the complexes $\nabla^2\rho(r)$ values are positive which is characteristic of the closed shell interactions. Mutual penetration is calculated as the sum of the difference between bonded and non-bonded radii of the two interacting atoms, Y and C, along the bond path connecting them. Significant positive values of mutual penetration for all the complexes further confirm the bonded interaction. Moreover, both ρ(r) and $\nabla^2\rho(r)$ values at the BCP are within the range prescribed for the C-H•••O hydrogen bonds.[26]

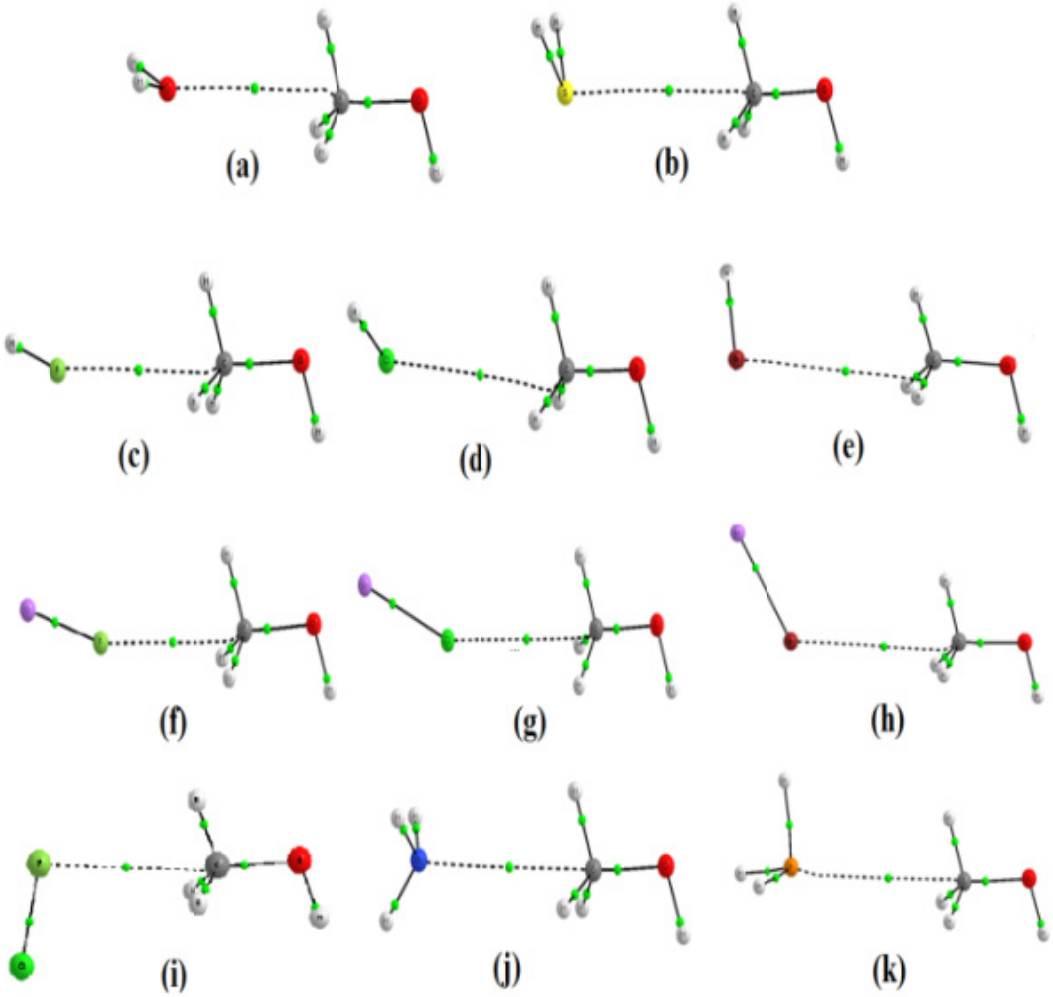

Figure IV.3. Electron density topologies for (a) H_2O•••CH_3OH, (b) H_2S•••CH_3OH, (c) HF•••CH_3OH, (d) HCl•••CH_3OH, (e) HBr•••CH_3OH, (f) LiF•••CH_3OH, (g) LiCl•••CH_3OH, (h) LiBr•••CH_3OH, (i) ClF•••CH_3OH, (j) H_3N•••CH_3OH, (k) H_3P•••CH_3OH. Bond critical points are shown in green.

Table IV.2. Electron density, ρ(r), and Laplacian of electron density, $\nabla^2\rho(r)$, at the intermolecular bond critical point of various complexes of methanol. Mutual penetration between the interacting atoms is also given. Wave functions used in the calculations are those of the optimized structures at MP2/6-311+G(3df,2p) level.

Complex	*ρ(r) in a.u.*	*$\nabla^2\rho(r)$ in a.u.*	*Mutual penetration (Å)*
$H_2O\bullet\bullet\bullet CH_3OH$	0.0050	0.0248	0.41
$H_2S\bullet\bullet\bullet CH_3OH$	0.0037	0.0164	0.30
$HF\bullet\bullet\bullet CH_3OH$	0.0037	0.0230	0.28
$HCl\bullet\bullet\bullet CH_3OH$	0.0038	0.0174	0.34
$HBr\bullet\bullet\bullet CH_3OH$	0.0034	0.0140	0.31
$ClF\bullet\bullet\bullet CH_3OH$	0.0050	0.0299	0.39
$LiF\bullet\bullet\bullet CH_3OH$	0.0063	0.0350	0.54
$LiCl\bullet\bullet\bullet CH_3OH$	0.0049	0.0228	0.48
$LiBr\bullet\bullet\bullet CH_3OH$	0.0042	0.0181	0.42
$H_3N\bullet\bullet\bullet CH_3OH$	0.0044	0.0201	0.43
$H_3P\bullet\bullet\bullet CH_3OH$	0.0035	0.0143	0.34

IV.3.b. Complexes with halomethanes (CH_3F, CH_3Cl and CH_3Br)

ESP surfaces for the CH_3F, CH_3Cl and CH_3Br are shown in the *Figure IV.4.* It is clear from the figure that the sigma hole present along the C-X(X=F/Cl/Br) bond in these molecules is more positive as compared to that in methanol.

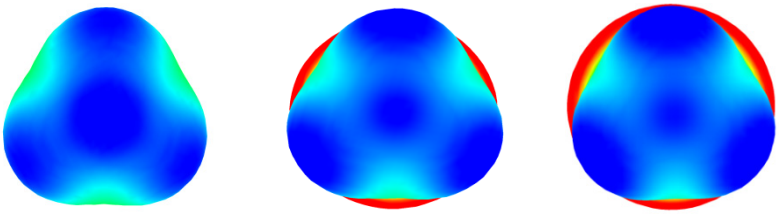

(a) (b) (c)

Figure IV.4. Electrostatic potential surfaces for (a) CH_3F, (b) CH_3Cl and (b) CH_3Br respectively. The potentials were mapped at the 0.001a.u. isosurface of electron density.

The size of sigma hole decreases in the order $CH_3F< CH_3Cl<CH_3Br$ as expected. The ESP values corresponding to the maxima at the tetrahedral face centre of CH_3F (+ 97.8 kJ.mol^{-1}), CH_3Cl (+82.3 kJ.mol^{-1}) and CH_3Br (+78.6 kJ.mol^{-1}) are much higher than that for CH_3OH (+50.2 kJ.mol^{-1}) and thus the C•••Y bonding interactions are

expected to be stronger with these molecules. Complexes with these halomethane molecules were optimized with similar starting geometries as those of methanol complexes, in which more electronegative atom of the other molecule faces CH_3 face centre of CH_3X. Complexes were optimized at both MP2/6-311+G(3df,2p) and MP2/Aug-cc-pVTZ levels. All the complexes were confirmed to be minima by frequency calculations. *Table IV.3* lists stabilization energy with BSSE correction, $\Delta E_{(BSSE)}$, and BSSE+Zero-point-energy correction, $\Delta E_{(BSSE+ZPC)}$, for all the complexes under consideration. The BSSE corrected interaction energy values at CCSD-T/6-311+G(3df,2p) level are also given. Comparison of stabilization energies of CH_3F complexes with corresponding CH_3OH complexes clearly shows that the C•••Y bonding interaction is significantly stronger with CH_3F. Complexes with CH_3Cl and CH_3Br are also stronger than the methanol complexes. Among the haloalkanes, with most of the molecules CH_3F complexes are the most stable ones. CH_3Cl complexes are slightly stronger than or equal in stability to the CH_3Br complexes which is in accordance with the nearly equal ESP value at the CH_3 face centre of CH_3Cl and CH_3Br molecules.

The AIM analysis was performed for all the complexes on the geometries optimized at mp2/6-311+G(3df,2p) level. In each case a BCP was found to be present between the Y atom and the C atom and a bond path was also found which connects the two atoms leading to the C•••Y interaction. The electron density $\rho(r)$ and the Laplacian of the electron density $\nabla^2\rho(r)$, for all the halomethane complexes are given in *Table IV.4*. Electron density $\rho(r)$ for the CH_3X complexes are also more than those for the CH_3OH complex which are consistent with the higher stabilization energies for the CH_3X complexes. For all the complexes mutual penetration was also calculated which has significant positive value and thus, confirms the bonding between C and Y atom in all these complexes, *Table IV.4*.

Table IV.3. BSSE corrected, $\Delta E_{(BSSE)}$, and BSSE and zero point corrected $\Delta E_{(BSSE+ZPC)}$, stabilization energies for the different complexes of CH_3X (X=F/Cl/Br) molecules, in kJ mol^{-1}.

Complex	At MP2 /6-311+G(3df,2p)		At MP2 /Aug-cc-pVTZ		At CCSD-T /6-311+G(3df,2p)
	$\Delta E_{(BSSE)}$	$\Delta E_{(BSSE+ZPC)}$	$\Delta E_{(BSSE)}$	$\Delta E_{(BSSE+ZPC)}$	$\Delta E_{(BSSE)}$
Complexes with CH_3F					
$H_2O\bullet\bullet\bullet CH_3F$	8.6	6.0	7.5	4.7	7.3
$H_2S\bullet\bullet\bullet CH_3F$	3.7	1.6	4.8	2.8	3.8
$HF\bullet\bullet\bullet CH_3F$	4.7	2.7	5.1	3.0	5.0
$HCl\bullet\bullet\bullet CH_3F$	5.0	3.5	3.7	2.2	2.8
$HBr\bullet\bullet\bullet CH_3F$	4.1	2.8	3.6	2.0	3.2
$ClF\bullet\bullet\bullet CH_3F$	2.6	1.0	3.7	2.2	3.1
$LiF\bullet\bullet\bullet CH_3F$	15.9	14.0	16.8	15.0	16.7
$LiCl\bullet\bullet\bullet CH_3F$	11.6	10.1	12.6	11.3	11.3
$LiBr\bullet\bullet\bullet CH_3F$	10.4	9.3	11.3	10.2	10.0
$H_3N\bullet\bullet\bullet CH_3F$	7.6	4.6	8.2	5.2	7.9
$H_3P\bullet\bullet\bullet CH_3F$	4.1	2.5	4.8	3.1	3.8
Complexes with CH_3Cl					
$H_2O\bullet\bullet\bullet CH_3Cl$	6.7	4.2	7.1	4.8	6.8
$H_2S\bullet\bullet\bullet CH_3Cl$	3.6	1.9	4.7	3.1	3.6
$HF\bullet\bullet\bullet CH_3Cl$	4.6	2.6	4.9	3.2	4.8
$HCl\bullet\bullet\bullet CH_3Cl$	3.1	1.8	3.7	2.4	2.7
$HBr\bullet\bullet\bullet CH_3Cl$	3.2	2.1	3.7	2.4	3.1
$ClF\bullet\bullet\bullet CH_3Cl$	3.2	1.9	3.8	2.5	3.0
$LiF\bullet\bullet\bullet CH_3Cl$	15.8	14.2	16.6	15.2	16.5
$LiCl\bullet\bullet\bullet CH_3Cl$	12.1	10.9	13.1	12.1	11.5
$LiBr\bullet\bullet\bullet CH_3Cl$	11.1	10.1	11.9	11.0	10.4
$H_3N\bullet\bullet\bullet CH_3Cl$	7.1	4.6	7.5	5.1	7.3
$H_3P\bullet\bullet\bullet CH_3Cl$	4.1	2.7	4.7	3.5	3.7

Table IV.3. (Continued)

Complexes with CH_3Br					
H_2O●●●CH_3Br	6.4	4.2	6.8	4.6	6.4
H_2S●●● CH_3Br	3.5	1.5	4.6	3.1	3.3
HF●●● CH_3Br	4.4	2.9	4.8	3.0	4.5
HCl●●● CH_3Br	3.1	2.0	3.7	2.7	2.5
HBr●●● CH_3Br	3.2	2.3	3.7	2.5	2.1
ClF●●● CH_3Br	3.2	2.1	3.8	2.6	2.7
LiF●●● CH_3Br	15.4	14.0	16.2	14.7	16.0
$LiCl$●●● CH_3Br	12.0	10.9	13.0	12.2	11.3
$LiBr$●●● CH_3Br	11.1	10.2	11.9	11.1	9.7
H_3N●●● CH_3Br	6.8	4.4	7.2	5.0	6.8
H_3P●●● CH_3Br	4.0	2.8	4.7	3.6	3.4

Table IV.4. Electron density, ρ(r), and Laplacian of electron density, $\nabla^2\rho(r)$, at the intermolecular bond critical point of various halomethane (CH_3X) complexes. Mutual penetration for the interacting atoms is also reported. Wave functions used in the calculations are those of the optimized structures at MP2/6-311+G(3df,2p) level.

Complex	*ρ(r) (a.u.)*	*$\nabla^2\rho(r)$ (a.u.)*	*Mutual penetration (Å)*
Complexes with CH_3F			
H_2O●●●CH_3F	0.0056	0.0307	0.50
H_2S●●● CH_3F	0.0042	0.0184	0.45
HF●●● CH_3F	0.0048	0.0298	0.38
HCl●●●CH_3F	0.0041	0.0196	0.39
HBr●●●CH_3F	0.0036	0.0164	0.32
ClF●●● CH_3F	0.0051	0.0305	0.41
LiF●●● CH_3F	0.0081	0.0459	0.67
$LiCl$●●●H_3F	0.0058	0.0287	0.58
$LiBr$●●●CH_3F	0.005	0.0227	0.49
H_3N●●●H_3F	0.0056	0.0262	0.55
H_3P●●● CH_3F	0.004	0.0163	0.42

Table IV.4. (Continued)

Complexes with CH_3Cl			
$H_2O\bullet\bullet\bullet CH_3Cl$	0.0055	0.0282	0.52
$H_2S\bullet\bullet\bullet CH_3Cl$	0.0042	0.0172	0.46
$HF\bullet\bullet\bullet CH_3Cl$	0.0044	0.026	0.37
$HCl\bullet\bullet\bullet CH_3Cl$	0.0041	0.0186	0.54
$HBr\bullet\bullet\bullet CH_3Cl$	0.0038	0.0157	0.36
$ClF\bullet\bullet\bullet CH_3Cl$	0.0049	0.0281	0.4
$LiF\bullet\bullet\bullet CH_3Cl$	0.0081	0.0442	0.69
$LiCl\bullet\bullet\bullet CH_3Cl$	0.0061	0.0287	0.46
$LiBr\bullet\bullet\bullet CH_3Cl$	0.0052	0.0227	0.53
$H_3N\bullet\bullet\bullet CH_3Cl$	0.0053	0.0232	0.53
$H_3P\bullet\bullet\bullet CH_3Cl$	0.0039	0.015	0.4
Complexes with CH_3Br			
$H_2O\bullet\bullet\bullet CH_3Br$	0.0055	0.0264	0.51
$H_2S\bullet\bullet\bullet CH_3Br$	0.0042	0.0167	0.46
$HF\bullet\bullet\bullet CH_3Br$	0.0044	0.0252	0.39
$HCl\bullet\bullet\bullet CH_3Br$	0.0042	0.0185	0.43
$HBr\bullet\bullet\bullet CH_3Br$	0.0039	0.0153	0.37
$ClF\bullet\bullet\bullet CH_3Br$	0.0057	0.0321	0.41
$LiF\bullet\bullet\bullet CH_3Br$	0.0082	0.0435	0.7
$LiCl\bullet\bullet\bullet CH_3Br$	0.0062	0.0284	0.64
$LiBr\bullet\bullet\bullet H_3Br$	0.0054	0.0227	0.57
$H_3N\bullet\bullet\bullet H_3Br$	0.0052	0.0222	0.55
$H_3P\bullet\bullet\bullet CH_3Br$	0.0041	0.0148	0.43

IV.3.c. Complexes with CH_3NO_2 and CH_3NF_2

The ESP values at the CH_3 face centre of CH_3NO_2 and CH_3NF_2 molecules are 146.3 and 107.4 $kJ.mol^{-1}$ respectively. Again the calculations were started with the initial geometries in which electron rich atom of the other molecule points towards the CH_3 face centre. The complexes were optimized at MP2/6-311+G(3df,2p) and MP2/Aug-cc-pVTZ levels and the structures were confirmed to be minima by obtaining all real frequency. The interaction energies were corrected for basis set superposition as well as zero-point corrections. The BSSE and BSSE+zero-point corrected energies at MP2/6-311+G(3df,2p) and MP2/Aug-cc-pVTZ levels are given in *Table IV.5*. For all the complexes, the BSSE corrected single point interaction energies at CCSD-T/6-311+G(3df,2p) are also given.

The AIM analysis was performed on these complexes. Wave functions used for the analysis were those of the optimized geometries at MP2/6-311+G(3df,2p) level. Again in all the complexes a BCP was found to be present between C of the CH_3X molecule and the electron rich atom (Y) of the other molecule. A bond path connecting the C and Y atom was also found to be present in each complex. The electron density and Laplacian of electron density values at the intermolecular BCP are given in *Table IV.6*. These values are within the range prescribed for the C-H•••O hydrogen bonds. For both the CH_3NO_2 and CH_3NF_2 complexes mutual penetration between C atom and the Y atom is also reported in *Table IV.6*. Significant positive value of the mutual penetration in each case confirms bonding interaction between Y and C atom in these complexes as well.

Table IV.5. BSSE corrected, ΔE(BSSE), and BSSE and zero point corrected ΔE(BSSE+ZPC), stabilization energies for different complexes of CH_3NO_2/CH_3NF_2 in kJ mol^{-1}.

Complex	At MP2 /6-311+G(3df,2p)		At MP2 /Aug-cc-pVTZ		At CCSD-T /6-311+G(3df,2p)
	$\Delta E_{(BSSE)}$	$\Delta E_{(BSSE+ZPC)}$	$\Delta E_{(BSSE)}$	$\Delta E_{(BSSE+ZPC)}$	$\Delta E_{(BSSE)}$
Complexes with CH_3NO_2					
$H_2O\bullet\bullet\bullet CH_3NO_2$	10.4	7.4	10.6	7.8	11.0
$H_2S\bullet\bullet\bullet CH_3NO_2$	5.0	3.0	6.1	4.3	5.3
$HF\bullet\bullet\bullet CH_3NO_2$	7.2	5.1	7.3	5.4	7.7
$HCl\bullet\bullet\bullet CH_3NO_2$	4.1	2.6	4.7	3.2	4.0
$HBr\bullet\bullet\bullet CH_3NO_2$	4.1	2.8	4.5	3.0	4.2
$ClF\bullet\bullet\bullet CH_3NO_2$	3.9	2.7	4.4	3.3	4.0
$LiF\bullet\bullet\bullet CH_3NO_2$	24.6	23.0	25.3	23.8	26.3
$LiCl\bullet\bullet\bullet CH_3NO_2$	18.1	16.9	19.1	18.1	18.2
$LiBr\bullet\bullet\bullet CH_3NO_2$	16.3	15.4	17.1	16.3	16.3
$H_3N\bullet\bullet\bullet CH_3NO_2$	10.7	7.8	11.1	8.3	11.4
$H_3P\bullet\bullet\bullet CH_3NO_2$	5.3	3.7	6.0	4.5	5.3
Complexes with CH_3NF_2					
$H_2O\bullet\bullet\bullet CH_3NF_2$	8.5	5.8	8.8	6.3	8.7
$H_2S\bullet\bullet\bullet CH_3NF_2$	4.1	2.5	5.2	3.6	4.3
$HF\bullet\bullet\bullet CH_3NF_2$	5.9	4.1	6.2	4.3	6.2
$HCl\bullet\bullet\bullet CH_3NF_2$	3.5	2.3	4.1	2.9	3.3
$HBr\bullet\bullet\bullet CH_3NF_2$	3.5	2.4	3.9	2.7	3.6
$ClF\bullet\bullet\bullet CH_3NF_2$	3.1	2.1	3.7	3.2	3.3
$LiF\bullet\bullet\bullet CH_3NF_2$	20.0	18.7	20.8	19.6	20.9
$LiCl\bullet\bullet\bullet CH_3NF_2$	14.8	13.8	15.8	15.0	14.4
$LiBr\bullet\bullet\bullet CH_3NF_2$	13.3	12.6	14.1	13.4	12.9
$H_3N\bullet\bullet\bullet CH_3NF_2$	8.7	6.2	9.1	6.6	9.0
$H_3P\bullet\bullet\bullet CH_3NF_2$	4.5	3.1	5.1	3.9	4.3

Table IV.6. Electron density, ρ(r), and Laplacian of electron density, $\nabla^2\rho(r)$, at the intermolecular bond critical point for different complexes of CH_3NO_2/CH_3NF_2. Wave functions used in the calculations are those of the optimized structures at MP2/6-311+G(3df,2p) level.

Complex	*ρ(r) in a.u.*	*∇^2.υ.α νι)ρ()*	*Mutual penetration (Å)*
Complexes with CH_3NO_2			
H_2O●●●CH_3NO_2	0.0063	0.0317	0.52
H_2S●●● CH_3NO_2	0.0044	0.0176	0.39
HF●●● CH_3NO_2	0.0052	0.0308	0.4
HCl●●● CH_3NO_2	0.0042	0.0187	0.38
HBr●●● CH_3NO_2	0.0038	0.0155	0.32
ClF●●● CH_3NO_2	0.0052	0.0290	0.39
LiF●●● CH_3NO_2	0.0096	0.0509	0.72
LiCl●●● CH_3NO_2	0.0067	0.0314	0.63
LiBr●●● CH_3NO_2	0.0058	0.0247	0.55
H_3N●●● CH_3NO_2	0.0058	0.0254	0.57
H_3P●●● CH_3NO_2	0.0040	0.0148	0.37
Complexes with CH_3NF_2			
H_2O●●●CH_3NF_2	0.0060	0.0284	0.55
H_2S●●● CH_3NF_2	0.0042	0.0163	0.42
HF●●● CH_3NF_2	0.0050	0.0291	0.42
HCl●●● CH_3NF_2	0.0039	0.0179	0.39
HBr●●● CH_3NF_2	0.0036	0.0145	0.32
ClF●●● CH_3NF_2	0.0057	0.0326	0.46
LiF●●● CH_3NF_2	0.0088	0.0463	0.71
LiCl●●● CH_3NF_2	0.0062	0.0290	0.62
LiBr●●● CH_3NF_2	0.0053	0.0227	0.53
H_3N●●● CH_3NF_2	0.0053	0.0234	0.56
H_3P●●● CH_3NF_2	0.0037	0.0138	0.36

IV.3.d. Electron density vs. stabilization energy

The electron density at the BCP is a good measure of the stabilization energies in complexes bound by hydrogen bonding and other non-covalent interactions.[16] *Figure IV.5* shows plots of stabilization energy vs. electron density (ρ) for the CH_3OH, CH_3F, CH_3Cl, CH_3Br, CH_3NO_2 and CH_3NF_2 complexes. In the figures, dashed line shows

correlation for the $H_nY\bullet\bullet\bullet CH_3X$ (Y= O/S/F/Cl/Br/N/P) complexes and the solid line shows correlation for the $LiY\bullet\bullet\bullet CH_3X$ (Y=F/Cl/Br) complexes. Clearly, the electron density at the BCP is a good measure of C•••Y interaction as well, though correlation does depend on the nature of the acceptors. In none of the fits, data for the complexes with ClF was included since it was worsening the fit.

IV.3.e. Koch and Popelier Criteria

Koch and Popelier have proposed a set of criteria for C-H•••O hydrogen bonds on the basis of AIM theory[16]. The Y•••C-X interactions found in CH_3OH and CH_3F complexes were subjected to these criteria and the conclusions are given below:

1. According to the first criterion a BCP should be present between H and O and a bond path should connect the BCP to the two interacting atoms (H and O). It is clear from the earlier discussions that there does appear a BCP between Y and C atoms in case of Y••• C-X interactions and a bond path connecting it to the Y and C atoms.

2,3. According to the second and third criteria the electron density, $\rho(r)$, and the Laplacian of electron density, $\nabla^2\rho(r)$, should be within the range of 0.002-0.034 a.u. and 0.024-0.139 a.u. respectively. Small deviations from these ranges are expected depending on the basis set used. As mentioned earlier the $\rho(r)$ and $\nabla^2\rho(r)$ values lie within these ranges for the CH_3OH as well as for the CH_3F complexes, *Table IV.2 and IV.4*.

4. Fourth criterion says there should be positive mutual penetration between H atom and the H-bond acceptor atom. This criterion was found to be the necessary and sufficient condition for the H-bonding. Calculated mutual penetrations between acceptor atom Y and C are given in *Table IV.2 and IV.4* for the CH_3OH complexes and the CH_3F complexes respectively. The significant positive values of mutual penetration complexes confirm the bonding between Y and C in these complexes.

5. According to the fifth criteria for hydrogen bonding there should be loss of charge of the hydrogen atom on complex formation. This can be calculated by subtracting the population on the concerned atom in monomer, N(monomer), from the population on

the atom in the complex, N (complex) i.e.

$$\Delta N = N(complex) - N(monomer) = negative$$

ΔN values for the C are given in *Table IV.7* for the CH_3OH and the CH_3F complexes. All the complexes follow this criterion except H_2O••• CH_3OH for which value is nearly zero.

6. According to the sixth criterion, hydrogen should destabilize on complex formation i.e.

$$\Delta E = E(complex) - E(monomer) = positive$$

ΔE values for the C are given in *Table IV.7* for the CH_3OH and the CH_3F complexes. All the complexes follow this criterion except the H_2O••• CH_3OH and the LiCl••• CH_3OH complexes for which ΔE value is negative.

7. According to the seventh criterion, magnitude of dipolar polarization (M) of hydrogen should decrease on complex formation i.e.

$$\Delta|M| = |M(complex)| - |M(monomer)| = negative$$

Δ|M| values for the C are given in *Table IV.7* for all the complexes. It is clear from the table that many of the CH_3OH complexes (with HF, HCl, HBr, ClF) do not follow this criterion since their |ΔM| values are positive. However most of the CH_3F complexes follow this criterion except the ClF••• CH_3F complex.

8. According to the eighth and final criterion, atomic volume of H should decrease on complex formation. i.e.

$$\Delta V = V(complex) - V(monomer) = negative$$

Changes in the atomic volume of C (ΔV_C) for all the complexes are given in *Table IV.7* and they follow this criterion.

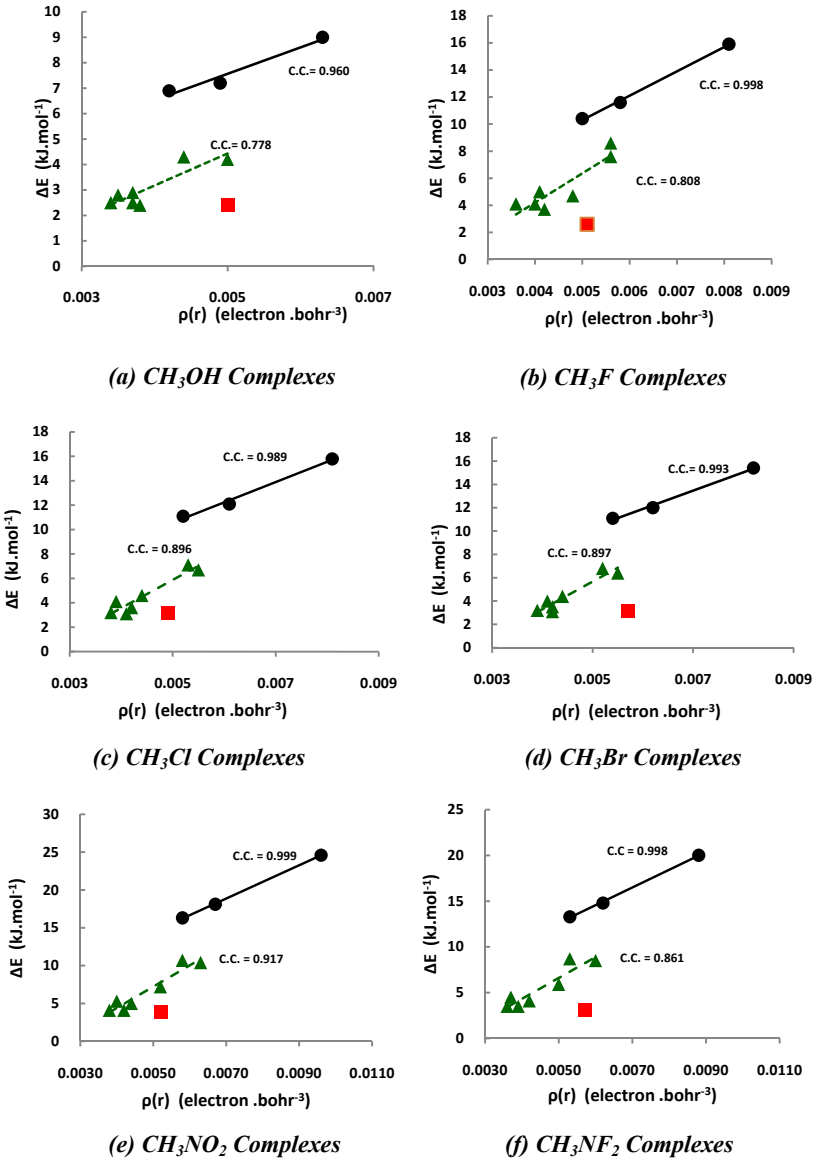

(a) CH_3OH Complexes *(b) CH_3F Complexes*

(c) CH_3Cl Complexes *(d) CH_3Br Complexes*

(e) CH_3NO_2 Complexes *(f) CH_3NF_2 Complexes*

Figure IV.5. Plots between ρ(r) and stabilization energy for the (a) CH_3OH, (b) CH_3F, (c) CH_3Cl, (d) CH_3Br, (e) CH_3NO_2 and (f) CH_3NF_2 complexes. Data points for $LiY\bullet\bullet\bullet CH_3X$ complexes are marked with solid circles, for $H_nY\bullet\bullet\bullet CH_3X$ with solid triangles and for $ClF\bullet\bullet\bullet CH_3X$ with solid square. The $ClF\bullet\bullet\bullet CH_3X$ complexes were not included in the fits.

Table IV.7. Change in bonded carbon's population, ΔN_C, energy ΔE_C ,dipolar polarization $\Delta|M_C|$, and volume ΔV_C on complexation in different CH_3OH and CH_3F complexes, calculated by AIM theory. All the properties are given in atomic units.

CH_3OH complexes	*ΔN_C*	*ΔE_C*	*$\Delta\|M_C\|$*	*ΔV_C*	*CH_3F complexes*	*ΔN_C*	*ΔE_C*	*$\Delta\|M_C\|$*	*ΔV_C*
$H_2O\cdots CH_3OH$	0.002	-0.0270	-0.030	-3.44	$H_2O\cdots CH_3F$	-0.163	0.1906	-0.025	-8.92
$H_2S\cdots CH_3OH$	-0.204	0.2323	-0.011	-8.79	$H_2S\cdots CH_3F$	-0.163	0.2309	-0.029	-7.96
$HF\cdots CH_3OH$	-0.204	0.2323	0.006	-9.09	$HF\cdots CH_3F$	-0.164	0.2026	-0.006	-8.62
$HCl\cdots CH_3OH$	-0.204	0.2046	0.004	-8.22	$HCl\cdots CH_3F$	-0.164	0.2366	-0.009	-8.04
$HBr\cdots CH_3OH$	-0.205	0.2370	0.000	-8.56	$HBr\cdots CH_3F$	-0.163	0.2279	-0.013	-7.59
$ClF\cdots CH_3OH$	-0.205	0.2249	0.018	-9.89	$ClF\cdots CH_3F$	-0.168	0.2303	0.007	-9.37
$LiF\cdots CH_3OH$	-0.193	0.1919	-0.046	-9.74	$LiF\cdots CH_3F$	-0.168	0.1866	-0.036	-9.41
$LiCl\cdots CH_3OH$	-0.190	-0.4515	-0.040	-9.00	$LiCl\cdots CH_3F$	-0.151	0.2156	-0.050	-8.35
$LiBr\cdots CH_3OH$	-0.193	0.2259	-0.038	-9.16	$LiBr\cdots CH_3F$	-0.148	0.2184	-0.054	-8.11
$H_3N\cdots CH_3OH$	-0.203	0.1937	-0.020	-9.24	$H_3N\cdots CH_3F$	-0.162	0.1848	-0.043	-8.64
$H_3P\cdots CH_3OH$	-0.202	0.2325	-0.004	-7.57	$H_3P\cdots CH_3F$	-0.162	0.2315	-0.033	-7.56

It is clear that the complexes with the CH_3OH and the CH_3F molecules follow the necessary and sufficient criterion proposed by Koch and Popelier. Most of these complexes follow other criteria as well. More data from these analyses are given in the *Supplementary Information*.

The complexes with other CH_3X molecules also fulfil the necessary and sufficient criteria as has already been discussed.

IV.3.f. NBO analysis

To estimate the charge transfer from the electron donor to the electron acceptor unit, Natural bond orbital analysis (NBO) has been performed on all the complexes at MP2/6-311+G(3df,2p) and MP2/Aug-cc-pVTZ levels. The charge transfer from the AY fragment to the CH_3X fragment (ΔQ) is given in *Table IV.8*. $\Delta Q < 0$ shows that charge is transferred from the AY fragment to the CH_3X fragment.

Moreover, the table also contains second order perturbation energies which give information on the natural orbitals involved in the charge transfer. For all the complexes the interaction is between lone-pair(s) of Y and the σ^*(C-O/C-F/C-Cl/C-Br/C-N) anti-bonding orbital. In the case of complexes where more than one lone pairs of Y are involved in the Y•••C interaction, the reported value is sum of the energies from individual contributions, e.g. in case of $LiBr\bullet\bullet\bullet CH_3F$ complex all three

lone-pairs of Br interact with σ^*(C-F) orbital and the second order perturbation energies are 2.3, 1.8 and 0.8 kJ/mol and the reported value 4.9 kJ/mol is the sum of these three contributions. It is clear that the charge is transferred from the lone pair(s) of Y to the C-X anti-bonding orbital. This is very similar to what is found in hydrogen bonding, in which the lone pair charge is transferred to the H-X anti-bonding orbital. Charges on each of the atoms, resulting from natural population analysis, in all the complexes, can be found in the *Supplementary Information*. The charge transfer from the lone-pair(s) of Y to the C-X anti-bonding orbital of CH_3X is also reflected in C-X vibrational frequency shift after complex formation as discussed below.

Table IV.8. Charge transferred (ΔQ, e) from AY to CH_3X fragment and second order interaction energy for the corresponding donor-acceptor interaction, E^2 (l.p. -->C-O/C-Cl/C-Br/C-N anti-bonding) in kJ.mol^{-1}, for the CH_3X complexes.

Complex	MP2/6-311+G(3df,2p)		MP2/Aug-cc-pVTZ	
	ΔQ	E^2[l.p. –> σ^* (C-O)]	ΔQ	E^2[l.p. –> σ^* (C-O)]
CH_3OH complexes				
$H_2O\cdots CH_3OH$	-0.0014	2.6	-0.0021	2.8
$H_2S\cdots CH_3OH$	-0.0011	2.4	-0.0016	3.0
$HF\cdots CH_3OH$	-0.0010	1.5	-0.0016	1.6
$HCl\cdots CH_3OH$	-0.0007	2.0	-0.0013	2.3
$HBr\cdots CH_3OH$	-0.0007	2.0	-0.0018	3.3
$ClF\cdots CH_3OH$	-0.0018	2.3	-0.0027	2.2
$LiF\cdots CH_3OH$	-0.0022	3.6	-0.0027	3.6
$LiCl\cdots CH_3OH$	-0.0021	3.0	-0.0036	3.1
$LiBr\cdots CH_3OH$	-0.0019	2.9	-0.0040	3.9
$H_3N\cdots CH_3OH$	-0.0017	3.0	-0.0019	2.8
$H_3P\cdots CH_3OH$	-0.0009	1.9	-0.0006	1.8
CH_3F complexes				
$H_2O\cdots CH_3F$	-0.0020	3.6	-0.0026	3.6
$H_2S\cdots CH_3F$	-0.0017	3.3	-0.0023	4.0
$HF\cdots CH_3F$	-0.0014	2.3	-0.0018	2.5
$HCl\cdots CH_3F$	-0.0009	2.8	-0.0015	3.1
$HBr\cdots CH_3F$	-0.0010	2.5	-0.0022	4.1
$ClF\cdots CH_3F$	-0.0020	3.3	-0.0026	2.9
$LiF\cdots CH_3F$	-0.0035	5.9	-0.0038	5.6
$LiCl\cdots CH_3F$	-0.0029	4.1	-0.0029	4.1
$LiBr\cdots CH_3F$	-0.0033	3.6	-0.0050	4.9
$H_3N\cdots CH_3F$	-0.0027	5.1	-0.0029	4.9
$H_3P\cdots CH_3F$	-0.0016	2.8	-0.0020	3.5
CH_3Cl complexes				
$H_2O\cdots CH_3Cl$	-0.0016	2.5	-0.0031	2.9
$H_2S\cdots CH_3Cl$	-0.0011	2.6	-0.0029	3.3

Table IV.8. (Continued)

$HF\cdots CH_3Cl$	-0.0015	1.5	-0.0033	2.3
$HCl\cdots CH_3Cl$	-0.0007	2.1	-0.0027	2.8
$HBr\cdots CH_3Cl$	-0.0006	2.0	-0.0035	3.8
$ClF\cdots CH_3Cl$	-0.0027	2.3	-0.0066	3.1
$LiF\cdots CH_3Cl$	-0.0027	4.3	-0.0046	5.0
$LiCl\cdots CH_3Cl$	-0.0024	3.1	-0.0061	4.0
$LiBr\cdots CH_3Cl$	-0.0026	2.5	-0.0073	4.0
$H_3N\cdots CH_3Cl$	-0.0023	3.6	-0.0032	4.3
$H_3P\cdots CH_3Cl$	-0.0009	1.9	-0.0024	2.6
CH_3Br complexes				
$H_2O\cdots CH_3Br$	-0.0017	2.7	-0.0034	3.1
$H_2S\cdots CH_3Br$	-0.0016	3.0	-0.0037	3.9
$HF\cdots CH_3Br$	-0.0017	1.3	-0.0032	1.6
$HCl\cdots CH_3Br$	-0.0009	2.3	-0.0030	2.8
$HBr\cdots CH_3Br$	-0.0008	2.2	-0.0039	4.0
$ClF\cdots CH_3Br$	-0.0028	2.5	-0.0068	2.6
$LiF\cdots CH_3Br$	-0.0031	4.8	-0.0051	5.6
$LiCl\cdots CH_3Br$	-0.0029	3.4	-0.0064	4.0
$LiBr\cdots CH_3Br$	-0.0031	2.7	-0.0079	4.1
$H_3N\cdots CH_3Br$	-0.0026	3.9	-0.0035	4.4
$H_3P\cdots CH_3Br$	-0.0014	2.2	-0.0029	2.9
CH_3NO_2 complexes				
$H_2O\cdots CH_3NO_2$	-0.0029	4.4	-0.0028	4.2
$H_2S\cdots CH_3NO_2$	-0.0023	3.6	-0.0027	4.0
$HF\cdots CH_3NO_2$	-0.0026	2.4	-0.0030	2.4
$HCl\cdots CH_3NO_2$	-0.0016	2.9	-0.0021	3.0
$HBr\cdots CH_3NO_2$	-0.0014	2.5	-0.0026	3.8
$ClF\cdots CH_3NO_2$	-0.0041	3.0	-0.0063	2.5
$LiF\cdots CH_3NO_2$	-0.0039	6.5	-0.0040	6.2
$LiCl\cdots CH_3NO_2$	-0.0036	5.0	-0.0050	5.1
$LiBr\cdots CH_3NO_2$	-0.0038	4.1	-0.0060	5.1
$H_3N\cdots CH_3NO_2$	-0.0035	5.4	-0.0028	5.4
$H_3P\cdots CH_3NO_2$	-0.0023	2.8	-0.0023	3.2

Table IV.8. (Continued)

CH_3NF_2 complexes				
$H_2O\cdots CH_3NF_2$	-0.0019	2.8	-0.0024	2.6
$H_2S\cdots CH_3NF_2$	-0.0013	2.2	-0.0018	2.4
$HF\cdots CH_3NF_2$	-0.0019	1.5	-0.0029	1.7
$HCl\cdots CH_3NF_2$	-0.0010	1.9	-0.0016	1.9
$HBr\cdots CH_3NF_2$	-0.0008	1.8	-0.0020	2.5
$ClF\cdots CH_3NF_2$	-0.0025	2.3	-0.0042	2.0
$LiF\cdots CH_3NF_2$	-0.0024	4.3	-0.0032	3.9
$LiCl\cdots CH_3NF_2$	-0.0023	3.3	-0.0045	3.1
$LiBr\cdots CH_3NF_2$	-0.0025	2.6	-0.0054	3.2
$H_3N\cdots CH_3NF_2$	-0.0023	3.4	-0.0022	3.5
$H_3P\cdots CH_3NF_2$	-0.0013	1.7	-0.0015	1.9

IV.3.g. Red shift in the C-X vibrational frequency

Vibrational frequency shifts corresponding to C-X stretching motion for all the complexes are given in *Table IV.9*. For $CH_3F/CH_3Cl/CH_3Br$ the C-X stretching is a local mode of vibration but in the case of CH_3OH there is no mode which is a pure C-O stretching mode. However, there were two normal modes with significant contribution from C-O stretching. Frequency shifts on complex formation for both these modes were very similar and one of these values is reported in *Table IV.9*. As expected, the C-X stretching frequencies decrease upon complex formation.

In the case of CH_3NO_2/CH_3NF_2 molecules also there is no pure C-N stretching mode. There are two normal modes which are close to the C-N stretch but they are strongly coupled with the NO_2/NF_2 scissoring motions. The coupling is weaker in CH_3NF_2 as compared to CH_3NO_2 due to higher mass of fluorine but it is still quite significant. The frequency shift for one of these modes is reported in *Table IV.9* for both the CH_3NO_2 and the CH_3NF_2 complexes. In many of the CH_3NO_2 complexes the mode is slightly blue shifted upon complex formation while most of the CH_3NF_2 complexes show the expected red shift. Due to high contribution from the scissoring motions these modes should not be used to draw any conclusions about the X-C•••Y bond formation.

IV.3.h. Correlation between charge transfer & frequency shift and second order perturbation energy & frequency shift

Hyperconjugation is considered to be one of the major reasons for the observed red shift in frequency upon hydrogen/halogen bond formation. The molecular orbitals involved in the hyperconjugation are usually lone pair orbitals of the hydrogen/halogen bond acceptor and the sigma antibonding orbital of the hydrogen/halogen bond donor (σ*(H-X/X'-X). The electron transfer from the lone pairs to the antibonding orbital results in the weakening of the H-X/X'-X sigma bond and thus, results in the decrease of the stretching frequency. As clear from the NBO data given in *Table IV.9*, the orbitals involved in the X-C•••Y interactions are l.p(s). of Y and antibonding C-X sigma orbital (σ*(C-X)). Correlations between (i) total charge transfer from H_nY moiety to CH_3X moiety (ΔQ) and C-X frequency shift (Δν) and (ii) second order perturbation energy for the l.p(s). - σ*(C-X) orbital interaction and the C-X frequency shift (Δν), are discussed below. These correlations were not

checked for the CH_3NO_2 and CH_3NF_2 complexes since the C-X frequencies are largely affected by mode mixings in these molecules.

IV.3.h. (i). Charge transfer (ΔQ) vs. C-X stretching frequency shift (Δν)

The C-X stretching frequency shifts were plotted against the charge transfer (ΔQ) obtained from the NBO results. The plots are given in the *Figure IV.6.a-d* for the CH_3X (X=OH/F/Cl/Br) complexes. Correlation coefficients resulting from the linear fit are also given in the plots. In none of the plots data for the $ClF\bullet\bullet\bullet CH_3X$ complexes was included since the frequency shift for these complexes are very small and the fit was worsening on including the data. In all the cases correlation coefficient is more than 0.8 which shows the correlation between these two properties is quite good.

IV.3.h. (ii). Perturbation energy vs. C-X stretching frequency shift

Other set of correlation diagrams were plotted between second order perturbation energy, ΔE (l.p.--> σ*(C-X)), and the C-X stretch frequency shift (Δν). The plots are shown in *Figure IV.7.a-d* for the CH_3X (X=OH/F/Cl/Br) complexes. Correlation coefficient is also given in each case. Again the data points for the ClF complexes were not included in the fit. The correlation coefficient for the CH_3OH and the CH_3F complexes is nearly 0.8 but is poorer for the CH_3Cl and the CH_3Br complexes, ~0.74

Table IV.9. Shifts in C-X vibrational frequencies on Y●●●C bond formation for different H_nY●●●CH_3X complexes at MP2/Aug-cc-pVTZ and MP2/6-311+G(3df,2p) levels.

Complex	Δν/cm^{-1}		Complex	Δν/cm^{-1}	
	MP2 /6-311+G(3df,2p)	MP2 /Aug-cc-pVTZ		MP2 /6-311+G(3df,2p)	MP2 /Aug-cc-pVTZ
CH_3OH complexes			*CH_3F complexes*		
H_2O●●●CH_3OH	-9.1	-7.8	H_2O●●●CH_3F	-16.3	-14.8
H_2S●●●CH_3OH	-5.5	-5.2	H_2S●●●CH_3F	-10.4	-11
HF●●●CH_3OH	-6.3	-6.5	HF●●●CH_3F	-10.2	-7.8
HCl●●●CH_3OH	-4	-3.2	HCl●●●CH_3F	-6.5	-4.3
HBr···CH_3OH	-3.3	-4.1	HBr●●●CH_3F	-6.3	-5.7
ClF●●●CH_3OH	-2.8	-3.1	ClF●●●CH_3F	-4.9	-3.1
LiF●●●CH_3OH	-20.9	-20.3	LiF●●●CH_3F	-40.4	-39
LiCl●●●CH_3OH	-14.8	-14.5	LiCl●●●CH_3F	-29.1	-26.3
LiBr●●●CH_3OH	-12.5	-14.3	LiBr●●●CH_3F	-24.3	-24.8
H_3N●●●CH_3OH	-18.8	-9.9	H_3N●●●CH_3F	-22.9	-20.3
H_3P●●●CH_3OH	-3.9	-1	H_3P●●●CH_3F	-9.9	-8.9
CH_3Cl complexes			*CH_3Br complexes*		
H_2O●●●CH_3Cl	-9.2	-9.9	H_2O●●●CH_3Br	-6.6	-6.8
H_2S●●●CH_3Cl	-6.3	-7	H_2S●●●CH_3Br	-5.5	-5.5
HF●●●CH_3Cl	-5.3	-5.6	HF●●●CH_3Br	-3.4	-3
HCl●●●CH_3Cl	-2.4	-2.8	HCl●●●CH_3Br	-2	-1.7
HBr●●●CH_3Cl	-3.4	-3.9	HBr●●●CH_3Br	-2.4	-2.6
ClF●●●CH_3Cl	-1.3	-1.3	ClF●●●CH_3Br	-0.2	0.3
LiF●●●CH_3Cl	-27.9	-27.8	LiF●●●CH_3Br	-19.8	-21.3
LiCl●●●CH_3Cl	-18.7	-18.7	LiCl●●●CH_3Br	-13.6	-13.9
LiBr●●●CH_3Cl	-16.6	-17.6	LiBr●●●CH_3Br	-11.5	-13.4
H_3N●●●CH_3Cl	-14.1	-14.9	H_3N●●●CH_3Br	-10.5	-11.5
H_3P●●●CH_3Cl	-6.4	-7.1	H_3P●●●CH_3Br	-5.3	-5.6
CH_3NO_2 complexes			*CH_3NF_2 complexes*		
H_2O●●●CH_3NO_2	0.6	0.5	H_2O●●●CH_3NF_2	-2.4	-2.9
H_2S●●●CH_3NO_2	-0.1	-0.4	H_2S●●●CH_3NF_2	-0.9	-1.7
HF●●●CH_3NO_2	1.1	1.1	HF●●●CH_3NF_2	-0.6	-1.2
HCl●●●CH_3NO_2	0.6	0.2	HCl●●●CH_3NF_2	-0.4	-0.7
HBr●●●CH_3NO_2	0.2	0.2	HBr●●●CH_3NF_2	-0.7	-0.9
ClF●●●CH_3NO_2	1.1	1.1	ClF●●●CH_3NF_2	0.8	0.4
LiF●●●CH_3NO_2	-0.9	-1.2	LiF●●●CH_3NF_2	-9.4	-10.1
LiCl●●●CH_3NO_2	-0.1	-0.6	LiCl●●●CH_3NF_2	-6.4	-6.8
LiBr●●●CH_3NO_2	-0.5	-1.1	LiBr●●●CH_3NF_2	-5.9	-6.2
H_3N●●●CH_3NO_2	-1.2	-1.1	H_3N●●●CH_3NF_2	-3.8	-4.2
H_3P●●●CH_3NO_2	-0.2	-1.2	H_3P●●●CH_3NF_2	-1.4	-1.7

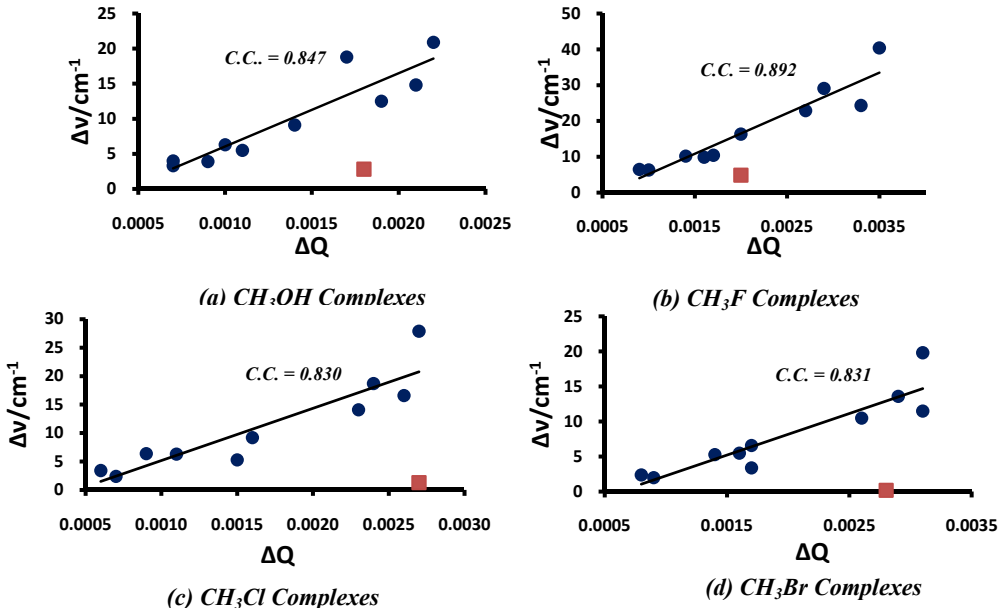

Figure IV.6. Plots between NBO charge transfer (ΔQ) and C-X frequency shift (Δν) for the (a) CH_3OH, (b) CH_3F, (c) CH_3Cl and (d) CH_3Br complexes. Data points for the $ClF\bullet\bullet\bullet CH_3X$ complexes are marked with brown squares and these points were not included in the fit.

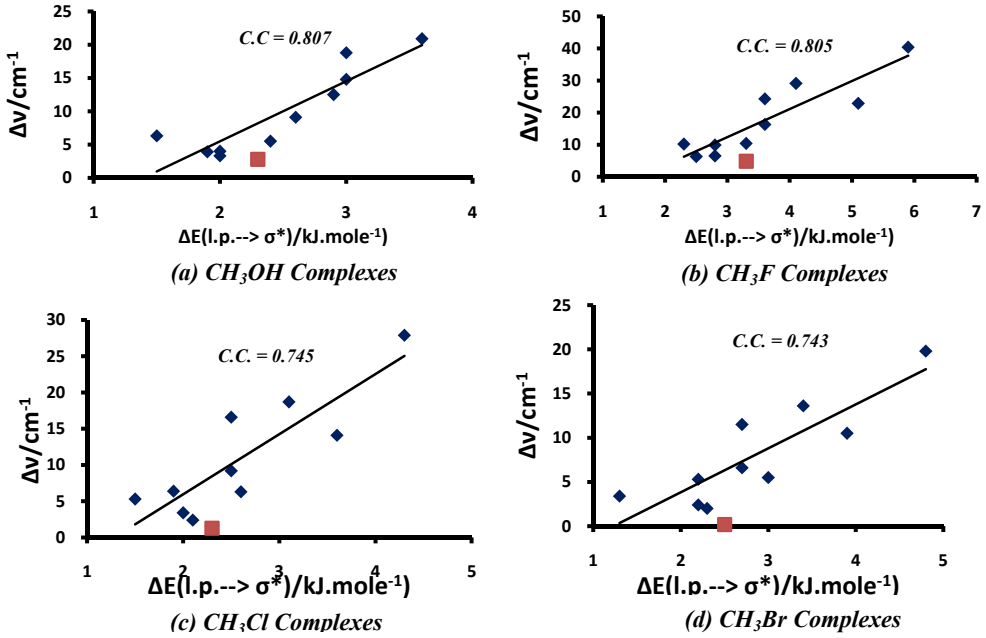

Figure IV.7. Plots between second order perturbation energy, ΔE(l.p.--> σ), and C-X frequency shift (Δν) for the (a) CH_3OH, (b) CH_3F, (c) CH_3Cl and (d) CH_3Br complexes. Data points for the $ClF\bullet\bullet\bullet CH_3X$ complexes are marked with brown squares and these points were not included in the fit.*

Often 'hydrophobic interactions' is the term that would be used to describe structures such as those given in *Figure IV.2.a* for the H_2O•••CH_3OH complex,[27,28] though it remains an ill-defined term, more imaginative chemists may call it a trifurcated hydrogen bond. Several experts have pointed out that 'hydrophobic effect' is a better term as it is largely an entropy effect.[29,30] Chandler pointed out that "*hydrophobic molecules exert weak attractive forces on water molecules by means of van der Waals interactions"*.[31] Our work shows that there is a specific binding between the hydrophobic site and the H_2O molecule in several H_2O•••CH_3X complexes. This work also shows that the hydrophobic effect includes the enthalpic contribution, however small, stabilizing the H_2O•••CH_3X complexes. Presence of an electron deficient face in the CH_3X leading to the H_2O•••CH_3X interaction may be compared to the 'sigma hole' which contributes to the formation of a halogen bond in H_2O•••$ClCF_3$ complex.[1,8,10,32]

Based on recent definitions of hydrogen bond[33,34] and halogen bond[35] by IUPAC, we can call the X-C•••Y interaction as "carbon bond" in which the participating carbon atom, being electron deficient, is bonded with an electron rich region of an acceptor. Comparison of carbon bond with hydrogen and halogen bond is shown in *Figure IV.8*.

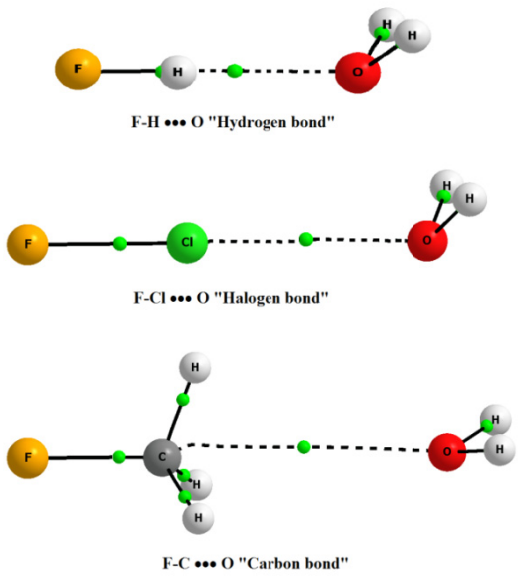

Figure IV.8. Cartoon showing F-H•••O hydrogen bond, F-Cl•••O halogen bond and similar F-C•••O carbon bond in F-H•••H_2O, F-Cl•••H_2O and F-H_3C•••H_2O complexes respectively.

The X-C•••Y interactions discussed here, could mistakenly be termed as blue shifted hydrogen bonds since the C-H stretch for the CH_3X moiety shows significant blue shift in all the cases. However, AIM analysis shows that there is no critical point

between the CH_3 hydrogens and the Y atom. Similarly NBO analysis also does not show any significant interaction between the C-H bonds and the lone pairs of Y atom. Abundance of alkyl groups bonded to more electronegative atoms in biological and organic molecules implies that these interactions, though weak, could be prevalent and together play a significant role in their functioning. In amino acids ($NH_2RCHCOOH$) the middle carbon atom is positively charged and can participate in similar kind of interactions. This possibility was indeed checked in the glycine•••FH complex and we found that fluorine of HF interacts with CH_2 carbon of glycine. Alanine (R=CH_3) has a CH_3 group and thus presents a closer example to the already discussed complexes. ESP calculations show a maximum with ESP value 19.6 $kJ.mol^{-1}$ at this CH_3 face which implies that this face of alanine can interact with electron rich centers via carbon bonding interactions. HF•••alanine complex was optimized at MP2/6-311+G(3df,2p) with the initial geometry in which F faces CH_3 of alanine. The optimized structure was confirmed to be a minimum by getting all real frequencies.

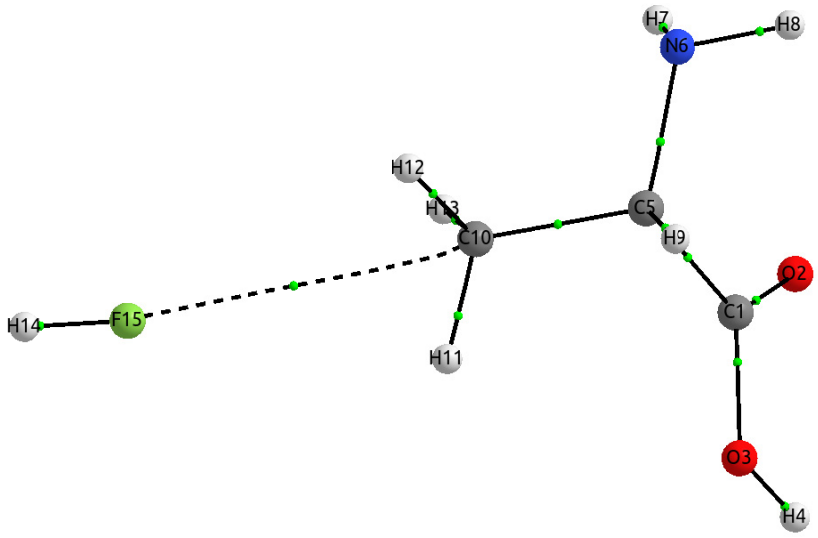

Figure IV.9. X-C•••Y carbon bonding interaction in the HF•••alanine complex.

The stabilization energy for the complex is 2.0 $kJ.mole^{-1}$. The AIM calculations show the presence of a BCP between F and C and a bond path connecting them, *Figure IV.8*. The value of $\rho(r)$ and $\nabla^2\rho(r)$ at the BCP is respectively 0.0039 and +0.0205 a.u. respectively. This example shows that the X-C•••Y interactions could also be present in the biological systems and can play an important role in the biological processes such as protein folding.

It may be noted that S_N2 reactions often involve a pentacoordinate C with two nucleophilic groups and indeed the C•••Y interaction could play a stabilizing role in the intermediate to S_N2 reactions. All the complexes discussed are like entrance channel complexes for the S_N2 reactions which would eventually lead to the intermediate for S_N2 reactions.

Following our work, Grabowski has analysed the role of X-Z•••Y (Z=C,Si,Ge) interactions in the S_N2 reactions.[36] Grabowski[36] and, simultaneously and independently, Frontela et al.[37] have named similar interactions by heavier 16th group elements as tetrel bond. The X-C•••Y carbon bond interactions can be considered as the most important subclass of the tetrel bonds.

More recently, Guru Row et al. have examined the crystal structure of dimethylammonium-4-hydroxybenzoate using X-rays.[38] Their analysis provided the first experimental evidence of the carbon bond. Crystal structure database search for the carbon bonded structures also suggests the ubiquitous nature of these interactions.

Similar interaction with corresponding silicon containing molecules (SiH_3X) complexes are stronger than with the CH_3X molecules, e.g. interaction energy for the H_2O•••SiH_3F is 13.7 kJ.mole^{-1} at MP22/6-311+G(3df,2p) which is much more than the value 8.6 kJ.mole^{-1} for the H_2O•••CH_3F complex. The weak nature of carbon bonding makes the carbon compounds more stable in comparison to silicon compounds, which are more prone to nucleophilic substitution reactions. This could well be another reason for life based on carbon compounds.

IV.4. Conclusions

Substitution of one of the hydrogens of methane by an electron withdrawing group (like OH/F/Cl/Br/NO_2/NF_2 etc.) drastically affects the bonding properties of the tetrahedral CH_3 face and it no longer remains a hydrogen bond acceptor. Rather it interacts with negative centers of molecules like H_2O, H_2S , NH_3 etc. and gives rise to a novel C•••Y bond, which could be called carbon bond. The AIM analysis, NBO calculations and frequency shift confirms the presence of this interaction. The carbon bond could play an important role in hydrophobic interactions as well as in the stabilization of intermediate to the S_N2 reaction. Moreover, given the abundance of alkyl groups in biological systems, the carbon bonding interactions could play a significant role in these systems as well which is yet to be recognised.

IV.5. Supplementary Information:

Coordinates of the optimized geometries and their vibrational frequencies are given in the *Supplementary Information*. AIM and NBO parameters for the complexes are also given.

IV.6. References

1. Politzer, P.; Murray, J. S. *ChemPhysChem* **2013**, *14*, 278-294.

2. Legon, A. C. *Phys. Chem. Chem. Phys.* **2010**, *12*, 7736-7747.

3. Metrangolo, P.; Resnati, G. *Chemistry – A European Journal* **2001**, *7*, 2511-2519.

4. Wang, W.; Ji, B.; Zhang, Y. *J. Phys. Chem. A* **2009**, *113*, 8132-8135.

5. Manna, D.; Mugesh, G. *J. Am. Chem. Soc.* **2012**, *134*, 4269-4279.

6. Scheiner, S. *J. Chem. Phys.* **2011**, *134*, 094315-094319.

7. Del Bene, J. E.; Alkorta, I.; Sanchez-Sanz, G.; Elguero, J. *J. Phys. Chem. A* **2011**, *115*, 13724-13731.

8. Politzer, P.; Murray, J. S.; Clark, T. *Phys. Chem. Chem. Phys.* **2013**.

9. Murray, J.; Lane, P.; Politzer, P. *J. Mol. Model.* **2009**, *15*, 723-729.

10. Bundhun, A.; Ramasami, P.; Murray, J.; Politzer, P. *J. Mol. Model.* **2012**, 1-8.

11. Mani, D.; Arunan, E. *ChemPhysChem* **2013**, *14*, 754-763.

12. Legon, A. C.; Wallwork, A. L. *J. Chem. Soc., Faraday Trans.* **1992**, *88*, 1-9.

13. Legon, A. C.; Roberts, B. P.; Wallwork, A. L. *Chem. Phys. Lett.* **1990**, *173*, 107-114.

14. Ohshima, Y.; Endo, Y. *J. Chem. Phys.* **1990**, *93*, 6256-6265.

15. Raghavendra, B.; Arunan, E. *Chem. Phys. Lett.* **2008**, *467*, 37-40.

16. Suenram, R. D.; Fraser, G. T.; Lovas, F. J.; Kawashima, Y. *J. Chem. Phys.* **1994**, *101*, 7230-7240.

17. Szczesniak, M. M.; Chalasinski, G.; Cybulski, S. M.; Cieplak, P. *J. Chem. Phys.* **1993**, *98*, 3078-3089.

18. Gadre, S. R.; Shirsat, R. N. *Electrostatics of Atoms and Molecules*; Universities Press: Hyderabad,, **2000**.

19. *Chemical applications of atomic and molecular electrostatic potentials : reactivity, structure, scattering, and energetics of organic, inorganic, and biological systems / edited by Peter Politzer and Donald G. Truhlar*; Plenum Press: New York :, **1981**.

20. Lu, T.; Chen, F. *J. Comput. Chem.* **2012**, *33*, 580-592.

21. Frisch, M. J.; Trucks, G. W.; Schlegel, H. B.; Scuseria, G. E.; Robb, M. A.; Cheeseman, J. R.; Scalmani, G.; Barone, V.; Mennucci, B.; Petersson, G. A.; Nakatsuji, H.; Caricato, M.; Li, X.; Hratchian, H. P.; Izmaylov, A. F.; Bloino, J.; Zheng, G.; Sonnenberg, J. L.; Hada, M.; Ehara, M.; Toyota, K.; Fukuda, R.; Hasegawa, J.; Ishida, M.; Nakajima, T.; Honda, Y.; Kitao, O.; Nakai, H.; Vreven, T.; Montgomery, J. A.; Peralta, J. E.; Ogliaro, F.; Bearpark, M.; Heyd, J. J.; Brothers, E.; Kudin, K. N.; Staroverov, V. N.; Kobayashi, R.; Normand, J.; Raghavachari, K.; Rendell, A.; Burant, J. C.; Iyengar, S. S.; Tomasi, J.; Cossi, M.; Rega, N.; Millam, J. M.; Klene, M.; Knox, J. E.; Cross, J. B.; Bakken, V.; Adamo, C.; Jaramillo, J.; Gomperts, R.; Stratmann, R. E.; Yazyev, O.; Austin, A. J.; Cammi, R.; Pomelli, C.; Ochterski, J. W.; Martin, R. L.; Morokuma, K.; Zakrzewski, V. G.; Voth, G. A.; Salvador, P.; Dannenberg, J. J.; Dapprich, S.; Daniels, A. D.; Farkas; Foresman, J. B.; Ortiz, J. V.; Cioslowski, J.; Fox, D. J. Wallingford CT, 2009.

22. Boys, S. F.; Bernardi, F. *Mol. Phys.* **1970**, *19*, 553.

23. Glendening, E.; Badenhoop, J.; Reed, A.; Carpenter, J.; Bohmann, J.; Morales, C.; Landis, C.; Weinhold, F. In *(Theoretical Chemistry Institute, University of Wisconsin, Madison, WI, 2013); http://nbo6.chem.wisc.edu/*.

24. AIMAll (Version 13.02.26), K., Todd A.; TK Gristmill Software, : Overland Park KS, USA, 2012 (aim.tkgristmill.com).

25. Biegler-König, F.; Schönbohm, J. *J. Comput. Chem.* **2002**, *23*, 1489-1494.

26. Koch, U.; Popelier, P. L. A. *J. Phys. Chem.* **1995**, *99*, 9747-9754.

27. Ben-Naim, A. *Hydrophobic interactions*; Plenum Press: New York and London, **1980**.

28. Berne, B. J.; Weeks, J. D.; Zhou, R. *Annu. Rev. Phys. Chem.* **2009**, *60*, 85-103.

29. Tanford, C. *The Hydrophobic Effect: Formation of Micelles and Biological Membranes 2d Ed*; John Wiley & Sons, **1980**.

30. Southall, N. T.; Dill, K. A.; Haymet, A. D. J. *J. Phys. Chem. B* **2001**, *106*, 521-533.

31. Chandler, D. *Nature* **2005**, *437*, 640-647.

32. Politzer, P.; Lane, P.; Concha, M.; Ma, Y.; Murray, J. *J. Mol. Model.* **2007**, *13*, 305-311.

33. Arunan, E.; Desiraju, G. R.; Klein, R. A.; Sadlej, J.; Scheiner, S.; Alkorta, I.; Clary, D. C.; Crabtree, R. H.; Dannenberg, J. J.; Hobza, P.; Kjaergaard, H. G.; Legon, A. C.; Mennucci, B.; Nesbitt, D. J. *Pure Appl. Chem.* **2011**, *83*, 1637-1641.

34. Arunan, E.; Desiraju, G. R.; Klein, R. A.; Sadlej, J.; Scheiner, S.; Alkorta, I.; Clary, D. C.; Crabtree, R. H.; Dannenberg, J. J.; Hobza, P.; Kjaergaard, H. G.; Legon, A. C.; Mennucci, B.; Nesbitt, D. J. *Pure Appl. Chem.*, *83*, 1619-1636.

35. http://www.iupac.org/home/publications/provisional-recommendations/currently-under-public-review/currently-under-public-review-container/definition-of-the-halogen-bond.html.

36. Grabowski, S. J. *Phys. Chem. Chem. Phys.* **2014**.

37. Bauzá, A.; Mooibroek, T. J.; Frontera, A. *Angew. Chem.* **2013**, *125*, 12543-12547.

38. Thomas, S. P.; Pavan, M. S.; Guru Row, T. N. *Chem. Commun.* **2013**.

Supplementary Information

Table.IV.S.1 Coordinates of the optimized geometries for different molecules and complexes at MP2/6-311+G(3df,2p) and MP2/Aug-cc-pVTZ levels.

H_2O

	MP2/6-311+G(3df,2p)				MP2/Aug-cc-pVTZ		
Atom	x(Å)	y(Å)	z(Å)	Atom	x(Å)	y(Å)	z(Å)
O	0.0000	0.1175	0.0000	O	0.0000	0.1181	0.0000
H	0.7581	-0.4702	0.0000	H	0.7584	-0.4723	0.0000
H	-0.7581	-0.4702	0.0000	H	-0.7584	-0.4723	0.0000

H_2S

	MP2/6-311+G(3df,2p)				MP2/Aug-cc-pVTZ		
Atom	x(Å)	y(Å)	z(Å)	Atom	x(Å)	y(Å)	z(Å)
S	0.0000	0.1026	0.0000	S	0.0000	0.1029	0.0000
H	0.9617	-0.8211	0.0000	H	0.9634	-0.8233	0.0000
H	-0.9617	-0.8211	0.0000	H	-0.9634	-0.8233	0.0000

HF

	MP2/6-311+G(3df,2p)				MP2/Aug-cc-pVTZ		
Atom	x(Å)	y(Å)	z(Å)	Atom	x(Å)	y(Å)	z(Å)
H	0.0000	0.0000	-0.8261	H	0.0000	0.0000	-0.8295
F	0.0000	0.0000	0.0918	F	0.0000	0.0000	0.0922

HCl

	MP2/6-311+G(3df,2p)				MP2/Aug-cc-pVTZ		
Atom	x(Å)	y(Å)	z(Å)	Atom	x(Å)	y(Å)	z(Å)
H	0.0000	0.0000	-1.2016	H	0.0000	0.0000	-1.2041
Cl	0.0000	0.0000	0.0707	Cl	0.0000	0.0000	0.0708

HBr

	MP2/6-311+G(3df,2p)				MP2/Aug-cc-pVTZ		
Atom	x(Å)	y(Å)	z(Å)	Atom	x(Å)	y(Å)	z(Å)
H	0.0000	0.0000	-1.3759	H	0.0000	0.0000	-1.3675
Br	0.0000	0.0000	0.0393	Br	0.0000	0.0000	0.0391

ClF

	MP2/6-311+G(3df,2p)				MP2/Aug-cc-pVTZ		
Atom	x(Å)	y(Å)	z(Å)	Atom	x(Å)	y(Å)	z(Å)
Cl	0.0000	0.0000	0.5654	Cl	0.0000	0.0000	0.5672
F	0.0000	0.0000	-1.0680	F	0.0000	0.0000	-1.0713

LiF

	MP2/6-311+G(3df,2p)				MP2/Aug-cc-pVTZ		
Atom	x(Å)	y(Å)	z(Å)	Atom	x(Å)	y(Å)	z(Å)
Li	0.0000	0.0000	-1.1939	Li	0.0000	0.0000	-1.1960
F	0.0000	0.0000	0.3980	F	0.0000	0.0000	0.3987

LiCl

	MP2/6-311+G(3df,2p)				MP2/Aug-cc-pVTZ		
Atom	x(Å)	y(Å)	z(Å)	Atom	x(Å)	y(Å)	z(Å)
Li	0.0000	0.0000	-1.7358	Li	0.0000	0.0000	-1.7413
Cl	0.0000	0.0000	0.3063	Cl	0.0000	0.0000	0.3073

LiBr

	MP2/6-311+G(3df,2p)				MP2/Aug-cc-pVTZ		
Atom	x(Å)	y(Å)	z(Å)	Atom	x(Å)	y(Å)	z(Å)
Li	0.0000	0.0000	-2.0266	Li	0.0000	0.0000	-2.0238
Br	0.0000	0.0000	0.1737	Br	0.0000	0.0000	0.1735

NH_3

	MP2/6-311+G(3df,2p)				MP2/Aug-cc-pVTZ		
Atom	x(Å)	y(Å)	z(Å)	Atom	x(Å)	y(Å)	z(Å)
N	0.0000	0.0000	-0.1123	N	0.0000	-0.0001	-0.1139
H	-0.5672	-0.7483	0.2620	H	-0.0008	0.9384	0.2656
H	-0.3644	0.8654	0.2620	H	0.8133	-0.4680	0.2659
H	0.9316	-0.1171	0.2620	H	-0.8125	-0.4695	0.2659

PH_3

	MP2/6-311+G(3df,2p)				MP2/Aug-cc-pVTZ		
Atom	x(Å)	y(Å)	z(Å)	Atom	x(Å)	y(Å)	z(Å)
P	0.0000	0.1266	0.0000	P	0.0000	0.1269	0.0000
H	1.1865	-0.6332	0.0000	H	1.1899	-0.6345	0.0000
H	-0.5932	-0.6332	1.0275	H	-0.5950	-0.6345	1.0305
H	-0.5932	-0.6332	-1.0275	H	-0.5950	-0.6345	-1.0305

CH_3OH

	MP2/6-311+G(3df,2p)				MP2/Aug-cc-pVTZ		
Atom	x(Å)	y(Å)	z(Å)	Atom	x(Å)	y(Å)	z(Å)
C	-0.0464	0.6631	0.0000	C	-0.0467	0.6657	0.0000
O	-0.0464	-0.7546	0.0000	O	-0.0467	-0.7576	0.0000
H	-1.0867	0.9723	0.0000	H	-1.0878	0.9751	0.0000
H	0.4367	1.0722	0.8886	H	0.4373	1.0731	0.8893
H	0.4367	1.0722	-0.8886	H	0.4373	1.0731	-0.8893
H	0.8629	-1.0584	0.0000	H	0.8675	-1.0546	0.0000

$H_2O \bullet\bullet\bullet CH_3OH$

	MP2/6-311+G(3df,2p)				MP2/Aug-cc-pVTZ		
Atom	x(Å)	y(Å)	z(Å)	Atom	x(Å)	y(Å)	z(Å)
C	0.7430	0.0028	0.0014	C	0.7417	0.0028	0.0024
H	0.3494	-0.0253	1.0115	H	0.3484	-0.0254	1.0132
H	0.3676	-0.8666	-0.5386	H	0.3669	-0.8671	-0.5377
H	0.3735	0.9047	-0.4868	H	0.3728	0.9053	-0.4858
O	2.1605	-0.0051	0.1096	O	2.1640	-0.0051	0.1113
H	2.5297	0.0199	-0.7746	H	2.5279	0.0200	-0.7778
O	-2.4241	0.0015	-0.0448	O	-2.4251	0.0015	-0.0476
H	-2.9961	0.7475	0.1459	H	-2.9999	0.7478	0.1467
H	-2.9733	-0.7682	0.1164	H	-2.9770	-0.7687	0.1173

H_2S•••CH_3OH

MP2/6-311+G(3df,2p)				MP2/Aug-cc-pVTZ			
Atom	x(Å)	y(Å)	z(Å)	Atom	x(Å)	y(Å)	z(Å)
C	-1.5435	0.0076	0.0054	C	-1.5317	0.0077	0.0055
H	-1.1555	0.9623	0.3452	H	-1.1445	0.9749	0.3109
H	-1.1673	-0.1781	-1.0016	H	-1.1559	-0.2146	-0.9945
H	-1.1701	-0.7719	0.6709	H	-1.1600	-0.7475	0.6998
O	-2.9595	0.1048	0.0373	O	-2.9529	0.1067	0.0330
H	-3.3266	-0.7288	-0.2620	H	-3.3139	-0.7425	-0.2359
S	2.1674	-0.0966	-0.0393	S	2.1585	-0.0985	-0.0358
H	2.5688	0.3221	1.1614	H	2.5546	0.3700	1.1515
H	2.5094	1.0564	-0.6154	H	2.4971	1.0359	-0.6559

HF•••CH_3OH

MP2/6-311+G(3df,2p)				MP2/Aug-cc-pVTZ			
Atom	x(Å)	y(Å)	z(Å)	Atom	x(Å)	y(Å)	z(Å)
C	0.7208	0.0392	-0.0002	C	-0.7068	0.0195	0.0002
H	0.3757	1.0680	-0.0019	H	-0.3415	1.0415	0.0008
H	0.3243	-0.4546	0.8877	H	-0.3245	-0.4842	-0.8881
H	0.3270	-0.4581	-0.8869	H	-0.3250	-0.4851	0.8882
O	2.1409	0.0827	0.0000	O	-2.1311	0.0937	-0.0001
H	2.4699	-0.8175	0.0026	H	-2.4737	-0.8041	-0.0004
H	-3.2655	0.2755	0.0042	H	3.3023	0.0596	-0.0020
F	-2.4092	-0.0567	-0.0005	F	2.3835	-0.0216	0.0002

HCl•••CH_3OH

MP2/6-311+G(3df,2p)				MP2/Aug-cc-pVTZ			
Atom	x(Å)	y(Å)	z(Å)	Atom	x(Å)	y(Å)	z(Å)
C	1.4630	0.0025	-0.0206	C	1.4584	0.0004	-0.0157
H	1.0878	0.7917	-0.6642	H	1.0784	0.7774	-0.6721
H	1.0609	0.1525	0.9822	H	1.0637	0.1690	0.9873
H	1.1057	-0.9539	-0.4056	H	1.1021	-0.9645	-0.3807
O	2.8793	0.0914	-0.0472	O	2.8793	0.0923	-0.0528
H	3.2363	-0.5969	0.5166	H	3.2359	-0.5886	0.5241
H	-2.5267	1.0895	0.2906	H	-2.5254	1.0912	0.2925
Cl	-2.1045	-0.0723	-0.0128	Cl	-2.1023	-0.0721	-0.0138

HBr•••CH_3OH

MP2/6-311+G(3df,2p)				MP2/Aug-cc-pVTZ			
Atom	x(Å)	y(Å)	z(Å)	Atom	x(Å)	y(Å)	z(Å)
C	-2.2944	-0.0145	-0.0257	C	-2.1885	-0.0146	-0.0120
H	-1.9143	0.6955	-0.7535	H	-1.7982	0.5934	-0.8225
H	-1.9515	-1.0115	-0.3070	H	-1.8434	-1.0404	-0.1531
H	-1.8828	0.2379	0.9526	H	-1.7926	0.3663	0.9306
O	-3.7091	0.0907	-0.0531	O	-3.6083	0.0834	-0.0736
H	-4.0712	-0.5304	0.5811	H	-3.9740	-0.4515	0.6361
H	1.6094	1.3487	0.2418	H	1.6433	1.3287	0.2382
Br	1.4757	-0.0394	-0.0039	Br	1.4218	-0.0393	-0.0048

ClF•••CH$_3$OH

	MP2/6-311+G(3df,2p)				MP2/Aug-cc-pVTZ		
Atom	x(Å)	y(Å)	z(Å)	Atom	x(Å)	y(Å)	z(Å)
C	-1.7844	0.1418	-0.0165	C	-1.7506	0.1433	-0.0191
H	-1.7031	1.2222	-0.0808	H	-1.6619	1.2227	-0.0944
H	-1.2833	-0.2945	-0.8820	H	-1.2539	-0.3067	-0.8805
H	-1.2782	-0.1889	0.8917	H	-1.2484	-0.1832	0.8931
O	-3.1699	-0.1626	0.0057	O	-3.1440	-0.1512	0.0064
H	-3.2708	-1.1139	0.0656	H	-3.2441	-1.1046	0.0767
Cl	1.9240	-0.4769	-0.0017	Cl	1.8768	-0.4949	-0.0019
F	1.2103	0.9924	0.0099	F	1.2398	1.0149	0.0112

LiF•••CH$_3$OH

	MP2/6-311+G(3df,2p)				MP2/Aug-cc-pVTZ		
Atom	x(Å)	y(Å)	z(Å)	Atom	x(Å)	y(Å)	z(Å)
C	0.9443	0.0321	0.0064	C	0.9426	0.0322	0.0064
H	0.5690	-0.4879	0.8858	H	0.5684	-0.4884	0.8864
H	0.5539	-0.4601	-0.8823	H	0.5531	-0.4605	-0.8829
H	0.5670	1.0480	0.0255	H	0.5661	1.0490	0.0255
O	2.3693	0.1180	-0.0044	O	2.3724	0.1186	-0.0044
H	2.7183	-0.7742	-0.0219	H	2.7161	-0.7785	-0.0218
Li	-3.5705	0.2860	-0.0123	Li	-3.5736	0.2865	-0.0122
F	-2.0352	-0.1467	0.0030	F	-2.0352	-0.1470	0.0029

LiCl•••CH$_3$OH

	MP2/6-311+G(3df,2p)				MP2/Aug-cc-pVTZ		
Atom	x(Å)	y(Å)	z(Å)	Atom	x(Å)	y(Å)	z(Å)
C	1.6385	0.0584	0.0082	C	1.6376	0.0590	0.0081
H	1.2657	-0.4488	0.8976	H	1.2654	-0.4486	0.8980
H	1.2472	-0.4466	-0.8743	H	1.2468	-0.4463	-0.8750
H	1.2633	1.0761	0.0131	H	1.2635	1.0777	0.0131
O	3.0608	0.1414	-0.0065	O	3.0648	0.1419	-0.0066
H	3.4097	-0.7512	-0.0133	H	3.4078	-0.7557	-0.0131
Li	-3.6965	0.5837	-0.0047	Li	-3.7024	0.5855	-0.0046
Cl	-1.7890	-0.1566	-0.0003	Cl	-1.7894	-0.1572	-0.0003

LiBr•••CH$_3$OH

	MP2/6-311+G(3df,2p)				MP2/Aug-cc-pVTZ		
Atom	x(Å)	y(Å)	z(Å)	Atom	x(Å)	y(Å)	z(Å)
C	2.3323	0.0854	0.0003	C	-2.2677	0.1103	0.0004
H	1.9553	-0.4229	0.8875	H	-1.8741	-0.3890	-0.8850
H	1.9547	-0.4255	-0.8853	H	-1.8750	-0.3853	0.8882
H	1.9476	1.0999	-0.0011	H	-1.9176	1.1377	-0.0016
O	3.7525	0.1837	-0.0004	O	-3.6962	0.1603	-0.0005
H	4.1120	-0.7049	0.0009	H	-4.0189	-0.7447	0.0011
Li	-2.6491	1.5755	0.0001	Li	3.0829	1.0752	0.0002
Br	-1.3153	-0.1787	0.0000	Br	1.2461	-0.1368	-0.0001

NH_3 ●●●CH_3OH

	MP2/6-311+G(3df,2p)				MP2/Aug-cc-pVTZ		
Atom	x(Å)	y(Å)	z(Å)	Atom	x(Å)	y(Å)	z(Å)
C	0.8174	0.0078	0.0055	C	-0.8181	0.0173	0.0004
H	0.4390	0.5229	-0.8772	H	-0.4531	0.5355	0.8872
H	0.4513	0.5210	0.8945	H	-0.4538	0.5365	-0.8862
H	0.4213	-1.0021	0.0069	H	-0.4120	-0.9891	-0.0003
N	-2.5598	0.0254	-0.0022	N	2.5655	0.0275	-0.0011
H	-2.8235	-0.5135	-0.8164	H	2.8036	-0.5234	0.8145
H	-3.1481	0.8480	0.0081	H	3.1969	0.8191	-0.0090
H	-2.8111	-0.5250	0.8082	H	2.7998	-0.5364	-0.8089
O	2.2348	-0.1066	-0.0043	O	-2.2393	-0.1136	0.0009
H	2.6073	0.7765	-0.0073	H	-2.6166	0.7701	0.0017

PH_3●●●CH_3OH

	MP2/6-311+G(3df,2p)				MP2/Aug-cc-pVTZ		
Atom	x(Å)	y(Å)	z(Å)	Atom	x(Å)	y(Å)	z(Å)
C	1.6276	-0.0244	-0.0079	C	1.5044	-0.0649	-0.1210
H	1.2114	0.9781	0.0074	H	1.0162	0.8956	0.0200
H	1.2597	-0.5641	0.8659	H	1.0772	-0.7800	0.5843
H	1.2755	-0.5300	-0.9081	H	1.3074	-0.4096	-1.1374
O	3.0396	0.1200	0.0077	O	2.8926	0.1500	0.1121
H	3.4328	-0.7541	-0.0066	H	3.3464	-0.6888	-0.0070
P	-2.1758	-0.0450	-0.0053	P	-2.0962	-0.0828	-0.0363
H	-3.0097	-0.2345	1.1146	H	-1.9987	0.1809	1.3481
H	-2.4294	1.3392	-0.0774	H	-1.9656	1.2771	-0.3956
H	-3.1858	-0.3735	-0.9311	H	-3.5079	-0.0435	-0.0382

CH_3F

	MP2/6-311+G(3df,2p)				MP2/Aug-cc-pVTZ		
Atom	x(Å)	y(Å)	z(Å)	Atom	x(Å)	y(Å)	z(Å)
C	0.0000	0.6331	0.0000	C	0.0000	-0.6360	0.0000
F	0.0000	-0.7496	0.0000	F	0.0000	0.7522	0.0000
H	-1.0290	0.9827	0.0000	H	1.0297	-0.9848	0.0000
H	0.5145	0.9827	0.8911	H	-0.5148	-0.9847	0.8918
H	0.5145	0.9827	-0.8911	H	-0.5148	-0.9847	-0.8918

H_2O●●● CH_3F

	MP2/6-311+G(3df,2p)				MP2/Aug-cc-pVTZ		
Atom	x(Å)	y(Å)	z(Å)	Atom	x(Å)	y(Å)	z(Å)
C	0.7213	0.0083	-0.0067	C	0.7198	0.0084	-0.0068
H	0.3680	-0.7915	-0.6501	H	0.3668	-0.7919	-0.6506
H	0.3842	0.9666	-0.3897	H	0.3831	0.9673	-0.3897
H	0.3577	-0.1373	1.0055	H	0.3566	-0.1377	1.0059
O	-2.3244	0.0012	-0.0015	O	-2.3257	0.0012	-0.0016
H	-2.8836	-0.7780	0.0141	H	-2.8883	-0.7787	0.0145
H	-2.9393	0.7373	0.0161	H	-2.9434	0.7382	0.0167
F	2.1090	-0.0063	0.0063	F	2.1124	-0.0063	0.0063

H_2S●●● CH_3F

	MP2/6-311+G(3df,2p)				MP2/Aug-cc-pVTZ		
Atom	x(Å)	y(Å)	z(Å)	Atom	x(Å)	y(Å)	z(Å)
C	1.5164	0.0010	-0.0086	C	1.5092	0.0019	-0.0177
F	2.9015	-0.0013	0.0211	F	2.8996	-0.0016	0.0263
H	1.1774	-0.8179	-0.6368	H	1.1693	1.0053	-0.2604
H	1.1423	-0.1254	1.0032	H	1.1819	-0.6986	-0.7815
H	1.1757	0.9486	-0.4164	H	1.1271	-0.2976	0.9542
S	-2.1078	-0.0022	-0.0983	S	-2.1132	0.0002	-0.0998
H	-2.4742	0.9796	0.7265	H	-2.4134	0.9585	0.7820
H	-2.5071	-0.9439	0.7574	H	-2.4060	-0.9685	0.7731

HF●●● CH_3F

	MP2/6-311+G(3df,2p)				MP2/Aug-cc-pVTZ		
Atom	x(Å)	y(Å)	z(Å)	Atom	x(Å)	y(Å)	z(Å)
C	0.6914	0.0319	0.0000	C	0.6900	0.0316	0.0000
F	2.0765	-0.0210	0.0000	F	2.0799	-0.0206	0.0000
H	0.3208	-0.4689	-0.8894	H	0.3206	-0.4701	-0.8899
H	0.3209	-0.4670	0.8905	H	0.3207	-0.4682	0.8911
H	0.3808	1.0725	-0.0011	H	0.3794	1.0727	-0.0011
H	-3.1878	0.1874	-0.0001	H	-3.1935	0.1879	-0.0001
F	-2.2968	-0.0363	0.0000	F	-2.2984	-0.0362	0.0000

HCl●●● CH_3F

	MP2/6-311+G(3df,2p)				MP2/Aug-cc-pVTZ		
Atom	x(Å)	y(Å)	z(Å)	Atom	x(Å)	y(Å)	z(Å)
C	1.4454	0.0110	-0.0115	C	1.4437	0.0112	-0.0116
F	2.8297	0.0048	0.0099	F	2.8328	0.0047	0.0100
H	1.0785	0.0627	1.0097	H	1.0770	0.0634	1.0102
H	1.1073	0.8763	-0.5748	H	1.1058	0.8769	-0.5755
H	1.0984	-0.9018	-0.4882	H	1.0967	-0.9022	-0.4882
H	-2.5686	1.0901	0.0025	H	-2.5700	1.0921	0.0024
Cl	-2.0503	-0.0727	0.0018	Cl	-2.0510	-0.0729	0.0018

HBr●●● CH_3F

	MP2/6-311+G(3df,2p)				MP2/Aug-cc-pVTZ		
Atom	x(Å)	y(Å)	z(Å)	Atom	x(Å)	y(Å)	z(Å)
C	-2.2581	0.0196	0.0038	C	-2.1648	0.0238	0.0023
F	-3.6422	-0.0049	-0.0032	F	-3.5539	-0.0078	-0.0019
H	-1.8934	-0.5190	-0.8666	H	-1.7996	-0.5141	-0.8688
H	-1.9256	1.0535	-0.0317	H	-1.8379	1.0598	-0.0351
H	-1.9034	-0.4550	0.9145	H	-1.8064	-0.4482	0.9134
H	1.8159	1.3218	-0.0009	H	1.7792	1.3099	-0.0006
Br	1.4353	-0.0421	-0.0003	Br	1.3897	-0.0423	-0.0002

ClF●●● CH_3F

	MP2/6-311+G(3df,2p)				MP2/Aug-cc-pVTZ		
Atom	x(Å)	y(Å)	z(Å)	Atom	x(Å)	y(Å)	z(Å)
C	-1.7791	0.1474	0.0009	C	-1.7775	0.1485	0.0008
H	-1.7737	1.2338	0.0016	H	-1.7740	1.2354	0.0016
H	-1.2832	-0.2282	-0.8899	H	-1.2815	-0.2275	-0.8904
H	-1.2847	-0.2295	0.8920	H	-1.2830	-0.2288	0.8924
F	-3.0912	-0.2935	-0.0007	F	-3.0940	-0.2948	-0.0007
Cl	1.9182	-0.4594	0.0000	Cl	1.9191	-0.4610	0.0000
F	1.1364	0.9767	-0.0003	F	1.1361	0.9800	-0.0003

LiF●●● CH_3F

	MP2/6-311+G(3df,2p)				MP2/Aug-cc-pVTZ		
Atom	x(Å)	y(Å)	z(Å)	Atom	x(Å)	y(Å)	z(Å)
C	-0.9105	-0.0050	0.0002	C	-0.9088	-0.0049	0.0001
F	-2.3058	0.0094	-0.0004	F	-2.3093	0.0092	-0.0001
H	-0.5486	0.8974	-0.4789	H	-0.5485	0.9162	-0.4445
H	-0.5597	-0.0462	1.0250	H	-0.5586	-0.0857	1.0232
H	-0.5675	-0.8773	-0.5443	H	-0.5662	-0.8557	-0.5784
Li	3.5213	0.0397	-0.0016	Li	3.5255	0.0394	-0.0001
F	1.9252	-0.0164	0.0006	F	1.9259	-0.0163	0.0000

LiCl●●● CH_3F

	MP2/6-311+G(3df,2p)				MP2/Aug-cc-pVTZ		
Atom	x(Å)	y(Å)	z(Å)	Atom	x(Å)	y(Å)	z(Å)
C	-1.6043	0.0054	0.0000	C	-1.6038	0.0052	0.0000
F	-2.9959	0.0344	0.0000	F	-2.9999	0.0346	0.0000
H	-1.2321	1.0193	-0.1058	H	-1.2314	1.0197	-0.1058
H	-1.2622	-0.4210	0.9375	H	-1.2614	-0.4214	0.9379
H	-1.2660	-0.6041	-0.8317	H	-1.2652	-0.6047	-0.8321
Li	3.7377	0.2496	0.0000	Li	3.7446	0.2495	0.0000
Cl	1.7139	-0.0638	0.0000	Cl	1.7145	-0.0638	0.0000

LiBr●●● CH_3F

	MP2/6-311+G(3df,2p)				MP2/Aug-cc-pVTZ		
Atom	x(Å)	y(Å)	z(Å)	Atom	x(Å)	y(Å)	z(Å)
C	2.2908	0.0252	0.0012	C	2.2269	0.0232	0.0012
F	3.6807	0.0563	-0.0010	F	3.6222	0.0562	-0.0010
H	1.9467	-0.2381	0.9966	H	1.8836	-0.2350	0.9985
H	1.9547	-0.7162	-0.7170	H	1.8924	-0.7231	-0.7132
H	1.9170	1.0064	-0.2745	H	1.8525	1.0029	-0.2802
Li	-3.3530	0.4909	0.0001	Li	-3.3273	0.4691	0.0000
Br	-1.2180	-0.0624	-0.0001	Br	-1.1888	-0.0599	-0.0001

H_3N●●● CH_3F

	MP2/6-311+G(3df,2p)				MP2/Aug-cc-pVTZ		
Atom	x(Å)	y(Å)	z(Å)	Atom	x(Å)	y(Å)	z(Å)
C	-0.7861	0.0001	0.0000	C	-0.7845	0.0001	0.0000
H	-0.4340	-0.3232	0.9743	H	-0.4333	-0.2266	1.0021
H	-0.4343	1.0057	-0.2073	H	-0.4334	0.9813	-0.3049
H	-0.4341	-0.6821	-0.7673	H	-0.4333	-0.7545	-0.6974
N	2.4451	0.0000	0.0000	N	2.4457	0.0000	0.0000
H	2.8255	-0.9162	0.1979	H	2.8306	-0.8919	0.2864
H	2.8255	0.6296	0.6944	H	2.8306	0.6940	0.6291
H	2.8249	0.2867	-0.8926	H	2.8302	0.1979	-0.9157
F	-2.1748	-0.0001	0.0001	F	-2.1783	0.0000	0.0000

H_3P●●● CH_3F

	MP2/6-311+G(3df,2p)				MP2/Aug-cc-pVTZ		
Atom	x(Å)	y(Å)	z(Å)	Atom	x(Å)	y(Å)	z(Å)
C	-1.6143	0.0171	0.0005	C	-1.5912	0.0104	0.0005
H	-1.2492	-0.5626	-0.8426	H	-1.2351	-0.3452	-0.9628
H	-1.2538	-0.4115	0.9313	H	-1.2320	-0.6391	0.7944
H	-1.2859	1.0490	-0.0867	H	-1.2542	1.0296	0.1704
F	-2.9993	-0.0143	-0.0004	F	-2.9815	-0.0085	-0.0003
P	2.1225	0.0009	0.0003	P	2.1016	0.0014	0.0009
H	2.8450	-1.0955	-0.5098	H	2.8304	-0.9316	-0.7685
H	2.9031	0.9565	-0.6791	H	2.8833	1.1008	-0.4160
H	2.8832	0.0770	1.1834	H	2.8638	-0.2210	1.1684

CH_3Cl

MP2/6-311+G(3df,2p)				MP2/Aug-cc-pVTZ			
Atom	x(Å)	y(Å)	z(Å)	Atom	x(Å)	y(Å)	z(Å)
C	-1.1191	0.0000	0.0000	C	1.1247	0.0000	0.0000
Cl	0.6536	0.0000	0.0000	Cl	-0.6557	0.0000	0.0000
H	-1.4654	0.9973	-0.2453	H	1.4663	-0.5031	0.8974
H	-1.4654	-0.7111	-0.7411	H	1.4663	-0.5257	-0.8844
H	-1.4654	-0.2862	0.9864	H	1.4663	1.0288	-0.0131

$H_2O \bullet\bullet\bullet CH_3Cl$

MP2/6-311+G(3df,2p)				MP2/Aug-cc-pVTZ			
Atom	x(Å)	y(Å)	z(Å)	Atom	x(Å)	y(Å)	z(Å)
C	-0.0826	0.0186	-0.0358	C	0.0829	-0.0013	-0.0711
Cl	-1.8584	-0.0070	0.0136	Cl	1.8650	0.0007	0.0267
H	0.2416	0.9918	-0.3834	H	-0.2323	0.8843	-0.6090
H	0.2989	-0.1678	0.9601	H	-0.2301	-0.8935	-0.5995
H	0.2587	-0.7507	-0.7174	H	-0.3191	0.0039	0.9341
O	3.0114	-0.0075	0.0091	O	-3.0238	0.0041	0.0202
H	3.5927	0.7554	0.0318	H	-3.6411	0.7414	0.0417
H	3.6054	-0.7606	0.0197	H	-3.5891	-0.7738	0.0429

$H_2S \bullet\bullet\bullet CH_3Cl$

MP2/6-311+G(3df,2p)				MP2/Aug-cc-pVTZ			
Atom	x(Å)	y(Å)	z(Å)	Atom	x(Å)	y(Å)	z(Å)
C	0.8553	0.0010	-0.0270	C	0.8496	0.0011	-0.0265
Cl	2.6298	-0.0006	0.0169	Cl	2.6320	-0.0006	0.0167
H	0.5220	-0.8168	-0.6548	H	0.5203	-0.8181	-0.6550
H	0.4810	-0.1251	0.9817	H	0.4801	-0.1253	0.9842
H	0.5183	0.9464	-0.4352	H	0.5169	0.9482	-0.4350
S	-2.8112	-0.0021	-0.0945	S	-2.8110	-0.0021	-0.0948
H	-3.1750	0.9783	0.7332	H	-3.1760	0.9800	0.7351
H	-3.2056	-0.9453	0.7619	H	-3.2063	-0.9471	0.7637

$HF \bullet\bullet\bullet CH_3Cl$

MP2/6-311+G(3df,2p)				MP2/Aug-cc-pVTZ			
Atom	x(Å)	y(Å)	z(Å)	Atom	x(Å)	y(Å)	z(Å)
C	-0.0647	0.0291	-0.0039	C	-0.0520	-0.0399	0.0008
Cl	-1.8395	-0.0138	0.0014	Cl	-1.8345	0.0119	-0.0003
H	0.2576	1.0629	-0.0054	H	0.3214	0.9768	-0.0176
H	0.2983	-0.4737	0.8838	H	0.2753	-0.5472	0.9003
H	0.2928	-0.4762	-0.8927	H	0.2755	-0.5794	-0.8797
H	3.8541	-0.2994	0.0004	H	3.8565	-0.2243	-0.0019
F	2.9953	0.0274	0.0015	F	2.9743	0.0456	-0.0001

$HCl \bullet\bullet\bullet CH_3Cl$

MP2/6-311+G(3df,2p)				MP2/Aug-cc-pVTZ			
Atom	x(Å)	y(Å)	z(Å)	Atom	x(Å)	y(Å)	z(Å)
C	0.7949	-0.0432	0.0093	C	0.7910	-0.0428	0.0087
Cl	2.5673	0.0229	-0.0035	Cl	2.5711	0.0227	-0.0033
H	0.4860	-1.0812	-0.0351	H	0.4849	-1.0820	-0.0359
H	0.4353	0.4149	0.9230	H	0.4348	0.4166	0.9235
H	0.4198	0.4951	-0.8530	H	0.4197	0.4970	-0.8548
H	-3.2275	1.1118	0.0028	H	-3.2311	1.1136	0.0023
Cl	-2.7368	-0.0630	-0.0020	Cl	-2.7389	-0.0632	-0.0018

HBr•••CH$_3$Cl

	MP2/6-311+G(3df,2p)				MP2/Aug-cc-pVTZ		
Atom	x(Å)	y(Å)	z(Å)	Atom	x(Å)	y(Å)	z(Å)
C	-1.6978	-0.0433	-0.0104	C	1.6219	-0.0364	-0.0004
Cl	-3.4706	0.0224	0.0041	Cl	3.4029	0.0194	0.0002
H	-1.3321	0.6028	-0.7998	H	1.2616	0.4627	0.8915
H	-1.3903	-1.0666	-0.1925	H	1.3119	-1.0753	-0.0036
H	-1.3292	0.2933	0.9514	H	1.2620	0.4680	-0.8896
H	2.3912	1.3311	-0.0039	H	-2.3280	1.3249	-0.0001
Br	2.0242	-0.0366	0.0011	Br	-1.9740	-0.0369	0.0000

ClF•••CH$_3$Cl

	MP2/6-311+G(3df,2p)				MP2/Aug-cc-pVTZ		
Atom	x(Å)	y(Å)	z(Å)	Atom	x(Å)	y(Å)	z(Å)
C	-1.1650	0.2911	0.0001	C	-1.1425	0.2921	0.0000
H	-1.1001	1.3728	-0.0009	H	-1.0783	1.3740	-0.0004
H	-0.6949	-0.1135	-0.8886	H	-0.6787	-0.1163	-0.8906
H	-0.6955	-0.1118	0.8899	H	-0.6788	-0.1157	0.8909
Cl	-2.8755	-0.1775	0.0000	Cl	-2.8625	-0.1712	0.0000
Cl	2.4614	-0.5181	0.0000	Cl	2.4210	-0.5335	0.0000
F	1.8356	0.9923	-0.0001	F	1.8662	1.0095	0.0000

LiF•••CH$_3$Cl

	MP2/6-311+G(3df,2p)				MP2/Aug-cc-pVTZ		
Atom	x(Å)	y(Å)	z(Å)	Atom	x(Å)	y(Å)	z(Å)
C	0.2587	0.0032	-0.0036	C	0.2541	0.0031	-0.0033
H	-0.0875	1.0205	-0.1240	H	-0.0882	1.0233	-0.1131
H	-0.0952	-0.4004	0.9350	H	-0.0948	-0.4112	0.9329
H	-0.0902	-0.6073	-0.8250	H	-0.0904	-0.6001	-0.8324
Cl	2.0431	-0.0013	0.0015	Cl	2.0462	-0.0013	0.0013
Li	-4.1995	-0.0025	0.0028	Li	-4.2041	-0.0024	0.0026
F	-2.6016	-0.0002	0.0003	F	-2.6027	-0.0002	0.0002

LiCl•••CH$_3$Cl

	MP2/6-311+G(3df,2p)				MP2/Aug-cc-pVTZ		
Atom	x(Å)	y(Å)	z(Å)	Atom	x(Å)	y(Å)	z(Å)
C	0.9439	0.0002	0.0001	C	-0.6629	-0.3243	-0.5833
H	0.5949	-0.6482	-0.7932	H	0.2917	-0.7416	-0.8790
H	0.5950	1.0119	-0.1643	H	-0.9114	-0.6299	0.4254
H	0.5958	-0.3629	0.9587	H	-0.6404	0.7559	-0.6551
Cl	2.7246	0.0003	0.0000	Cl	-1.9224	-0.9425	-1.6920
Li	-4.4300	0.0056	0.0011	Li	3.1227	1.5317	2.7570
Cl	-2.3810	-0.0014	-0.0003	Cl	1.6794	0.8229	1.4766

LiBr•••CH$_3$Cl

	MP2/6-311+G(3df,2p)				MP2/Aug-cc-pVTZ		
Atom	x(Å)	y(Å)	z(Å)	Atom	x(Å)	y(Å)	z(Å)
C	-1.7326	-0.0015	-0.0003	C	-1.6768	-0.0001	0.0000
H	-1.3848	-0.5326	-0.8776	H	-1.3324	-0.8276	-0.6079
H	-1.3846	-0.4960	0.8981	H	-1.3325	-0.1127	1.0207
H	-1.3832	1.0238	-0.0215	H	-1.3327	0.9403	-0.4127
Cl	-3.5123	0.0002	0.0000	Cl	-3.4645	-0.0004	0.0000
Li	3.9868	-0.0045	-0.0016	Li	3.9496	-0.0053	0.0003
Br	1.7799	0.0007	0.0002	Br	1.7459	0.0007	0.0000

H_3N●●●CH_3Cl

	MP2/6-311+G(3df,2p)				MP2/Aug-cc-pVTZ		
Atom	x(Å)	y(Å)	z(Å)	Atom	x(Å)	y(Å)	z(Å)
C	-0.1364	0.0001	0.0003	C	-0.1323	0.0003	0.0003
Cl	-1.9145	-0.0001	-0.0001	Cl	-1.9184	-0.0001	-0.0001
H	0.2132	-0.3850	0.9497	H	0.2122	-0.7709	0.6778
H	0.2134	-0.6294	-0.8080	H	0.2125	-0.2005	-1.0062
H	0.2125	1.0152	-0.1408	H	0.2118	0.9727	0.3297
N	3.1586	0.0000	0.0001	N	3.1618	-0.0002	0.0000
H	3.5373	0.3317	-0.8773	H	3.5446	0.6894	-0.6352
H	3.5390	-0.9253	0.1504	H	3.5460	-0.8942	-0.2803
H	3.5403	0.5932	0.7251	H	3.5475	0.2049	0.9137

H_3P●●●CH_3Cl

	MP2/6-311+G(3df,2p)				MP2/Aug-cc-pVTZ		
Atom	x(Å)	y(Å)	z(Å)	Atom	x(Å)	y(Å)	z(Å)
C	-0.9385	0.0013	0.0018	C	-0.0058	-0.0515	-0.9197
H	-0.5912	-0.1312	1.0196	H	-1.0303	-0.1067	-0.5706
H	-0.5905	0.9492	-0.3912	H	0.4421	0.8917	-0.6295
H	-0.5884	-0.8129	-0.6215	H	0.5721	-0.8807	-0.5287
Cl	-2.7134	-0.0005	-0.0006	Cl	-0.0081	-0.1530	-2.6996
P	2.8480	0.0003	0.0018	P	0.0079	0.1604	2.8261
H	3.6233	-0.1174	1.1720	H	-1.1667	0.1535	3.6097
H	3.5870	-0.9706	-0.7024	H	0.6597	-0.8067	3.6220
H	3.5988	1.0796	-0.5041	H	0.5774	1.2524	3.5167

CH_3Br

	MP2/6-311+G(3df,2p)				MP2/Aug-cc-pVTZ		
Atom	x(Å)	y(Å)	z(Å)	Atom	x(Å)	y(Å)	z(Å)
C	0.0000	-1.5124	0.0000	C	0.0000	-1.5087	0.0000
Br	0.0000	0.4178	0.0000	Br	0.0000	0.4166	0.0000
H	1.0293	-1.8501	0.0000	H	1.0304	-1.8430	0.0000
H	-0.5147	-1.8501	0.8914	H	-0.5152	-1.8430	0.8923
H	-0.5147	-1.8501	-0.8914	H	-0.5152	-1.8430	-0.8923

H_2O●●●CH_3Br

	MP2/6-311+G(3df,2p)				MP2/Aug-cc-pVTZ		
Atom	x(Å)	y(Å)	z(Å)	Atom	x(Å)	y(Å)	z(Å)
C	-0.6360	-0.0074	-0.0715	C	-0.6348	0.0612	-0.0479
Br	1.2962	0.0012	0.0124	Br	1.2922	-0.0103	0.0083
H	-1.0231	-0.0037	0.9389	H	-0.9729	-0.5916	-0.8421
H	-0.9561	0.8778	-0.6060	H	-1.0139	-0.2689	0.9102
H	-0.9493	-0.9006	-0.5965	H	-0.9265	1.0850	-0.2440
O	-3.7447	-0.0006	0.0206	O	-3.7322	-0.0172	0.0141
H	-4.3089	0.7751	0.0420	H	-4.2872	-0.8028	0.0058
H	-4.3553	-0.7399	0.0514	H	-4.3597	0.7107	0.0541

H_2S•••CH_3Br

	MP2/6-311+G(3df,2p)				MP2/Aug-cc-pVTZ		
Atom	x(Å)	y(Å)	z(Å)	Atom	x(Å)	y(Å)	z(Å)
C	-0.0040	0.0177	-0.0167	C	0.0035	0.0294	-0.0665
Br	-1.9370	-0.0032	0.0057	Br	-1.9222	-0.0053	0.0140
H	0.3310	-0.5415	-0.8819	H	0.3119	-0.4856	-0.9679
H	0.3229	1.0487	-0.0787	H	0.3204	1.0647	-0.0877
H	0.3515	-0.4416	0.8975	H	0.3868	-0.4716	0.8135
S	3.6737	-0.0017	-0.0973	S	3.6521	0.0014	-0.0904
H	4.0097	-0.9785	0.7467	H	3.8861	-1.0223	0.7365
H	4.0246	0.9454	0.7741	H	3.9181	0.9006	0.8621

HF•••CH_3Br

	MP2/6-311+G(3df,2p)				MP2/Aug-cc-pVTZ		
Atom	x(Å)	y(Å)	z(Å)	Atom	x(Å)	y(Å)	z(Å)
C	0.6489	0.0257	-0.0212	C	0.6532	-0.0001	-0.0035
Br	-1.2833	-0.0059	0.0035	Br	-1.2742	-0.0002	0.0006
H	1.0074	-0.4144	0.9006	H	0.9911	-0.2892	0.9836
H	0.9863	-0.5473	-0.8755	H	0.9874	-0.7109	-0.7485
H	0.9705	1.0568	-0.1023	H	0.9883	1.0000	-0.2476
H	4.5699	-0.3197	-0.0107	H	4.6005	-0.0393	0.0028
F	3.7211	0.0307	0.0103	F	3.6790	0.0052	0.0011

HCl•••CH_3Br

	MP2/6-311+G(3df,2p)				MP2/Aug-cc-pVTZ		
Atom	x(Å)	y(Å)	z(Å)	Atom	x(Å)	y(Å)	z(Å)
C	-0.0401	-0.0282	-0.0034	C	-0.0379	-0.0278	-0.0036
Br	1.8913	0.0083	0.0006	Br	1.8881	0.0083	0.0006
H	-0.3580	-1.0562	-0.1288	H	-0.3533	-1.0566	-0.1292
H	-0.3890	0.3674	0.9425	H	-0.3843	0.3683	0.9430
H	-0.3894	0.5825	-0.8267	H	-0.3844	0.5837	-0.8275
H	-4.1453	1.0713	-0.0007	H	-4.1421	1.0728	-0.0008
Cl	-3.5689	-0.0639	0.0007	Cl	-3.5642	-0.0641	0.0008

HBr•••CH_3Br

	MP2/6-311+G(3df,2p)				MP2/Aug-cc-pVTZ		
Atom	x(Å)	y(Å)	z(Å)	Atom	x(Å)	y(Å)	z(Å)
C	-0.8488	-0.0563	-0.0346	C	-0.7891	-0.0393	-0.0037
Br	-2.7789	0.0130	0.0062	Br	-2.7152	0.0097	0.0007
H	-0.5518	-1.0848	-0.2008	H	-0.4808	-1.0779	-0.0096
H	-0.5038	0.5762	-0.8432	H	-0.4413	0.4701	-0.8938
H	-0.4757	0.3009	0.9174	H	-0.4375	0.4612	0.8900
H	3.2908	1.3182	-0.0136	H	3.1868	1.3159	-0.0009
Br	2.8742	-0.0351	0.0037	Br	2.7983	-0.0364	0.0004

ClF•••CH_3Br

	MP2/6-311+G(3df,2p)				MP2/Aug-cc-pVTZ		
Atom	x(Å)	y(Å)	z(Å)	Atom	x(Å)	y(Å)	z(Å)
C	0.3350	0.3415	-0.0003	C	0.3244	0.3922	0.0009
H	-0.1088	-0.0860	-0.8911	H	-0.1288	-0.0213	-0.8918
H	0.2328	1.4198	-0.0013	H	0.2585	1.4732	0.0024
H	-0.1088	-0.0843	0.8914	H	-0.1285	-0.0238	0.8926
Br	2.2179	-0.0880	0.0001	Br	2.1884	-0.0929	-0.0001
Cl	-3.2603	-0.5389	0.0000	Cl	-3.1844	-0.5638	0.0000
F	-2.6916	0.9938	0.0001	F	-2.7116	1.0062	-0.0004

LiF●●●CH$_3$Br

	MP2/6-311+G(3df,2p)				MP2/Aug-cc-pVTZ		
Atom	x(Å)	y(Å)	z(Å)	Atom	x(Å)	y(Å)	z(Å)
C	-0.4959	0.0123	0.0000	C	-0.4967	-0.0001	0.0000
H	-0.8420	-0.5002	-0.8867	H	-0.8339	-1.0132	0.1678
H	-0.8255	1.0419	-0.0025	H	-0.8340	0.3612	-0.9612
H	-0.8398	-0.4952	0.8903	H	-0.8339	0.6518	0.7935
Br	1.4447	-0.0008	0.0000	Br	1.4396	0.0000	0.0000
Li	-4.9538	0.0426	-0.0001	Li	-4.9432	0.0001	0.0000
F	-3.3578	-0.0243	0.0000	F	-3.3417	0.0000	0.0000

LiCl●●●CH$_3$Br

	MP2/6-311+G(3df,2p)				MP2/Aug-cc-pVTZ		
Atom	x(Å)	y(Å)	z(Å)	Atom	x(Å)	y(Å)	z(Å)
C	-0.0914	-0.0032	-0.0004	C	-0.0934	-0.0022	-0.0002
Br	-2.0291	0.0010	0.0002	Br	-2.0258	0.0008	0.0000
H	0.2486	-0.4840	0.9075	H	0.2430	-0.2795	0.9902
H	0.2475	-0.5506	-0.8702	H	0.2421	-0.7222	-0.7351
H	0.2502	1.0229	-0.0391	H	0.2449	0.9933	-0.2558
Li	5.2827	0.0132	0.0027	Li	5.2830	0.0128	0.0001
Cl	3.2338	-0.0026	-0.0006	Cl	3.2286	-0.0027	0.0000

LiBr●●●CH$_3$Br

	MP2/6-311+G(3df,2p)				MP2/Aug-cc-pVTZ		
Atom	x(Å)	y(Å)	z(Å)	Atom	x(Å)	y(Å)	z(Å)
C	-0.8918	-0.0014	0.0002	C	-0.8490	-0.0006	0.0000
Br	-2.8281	0.0008	-0.0001	Br	-2.7812	0.0006	0.0000
H	-0.5523	-0.1247	1.0205	H	-0.5127	-0.2614	0.9951
H	-0.5528	-0.8239	-0.6165	H	-0.5130	-0.7323	-0.7232
H	-0.5507	0.9433	-0.4034	H	-0.5119	0.9912	-0.2719
Li	4.8216	0.0148	-0.0023	Li	4.7661	0.0133	-0.0001
Br	2.6150	-0.0017	0.0003	Br	2.5622	-0.0015	0.0000

H$_3$N●●●CH$_3$Br

	MP2/6-311+G(3df,2p)				MP2/Aug-cc-pVTZ		
Atom	x(Å)	y(Å)	z(Å)	Atom	x(Å)	y(Å)	z(Å)
C	-0.6013	0.0051	0.0011	C	0.5993	0.0046	-0.0022
Br	1.3338	-0.0009	-0.0002	Br	-1.3314	-0.0008	0.0004
H	-0.9461	-0.9885	-0.2530	H	0.9396	-0.9044	0.4760
H	-0.9411	0.2832	0.9901	H	0.9347	0.0459	-1.0301
H	-0.9409	0.7240	-0.7329	H	0.9345	0.8751	0.5461
N	-3.9107	-0.0015	-0.0003	N	3.9041	-0.0013	0.0006
H	-4.2907	-0.4224	0.8374	H	4.2877	-0.6064	-0.7151
H	-4.2885	-0.5188	-0.7833	H	4.2856	-0.3209	0.8826
H	-4.2941	0.9330	-0.0564	H	4.2911	0.9200	-0.1635

H_3P●●●CH_3Br

	MP2/6-311+G(3df,2p)				MP2/Aug-cc-pVTZ		
Atom	x(Å)	y(Å)	z(Å)	Atom	x(Å)	y(Å)	z(Å)
C	-0.0597	0.0018	0.0018	C	-0.0491	-0.0002	-0.0020
H	0.2789	0.1148	1.0242	H	0.2862	0.1494	-1.0208
H	0.2797	0.8311	-0.6064	H	0.2877	-0.9571	0.3771
H	0.2814	-0.9393	-0.4115	H	0.2882	0.8068	0.6364
Br	-1.9925	-0.0003	-0.0003	Br	-1.9769	0.0000	0.0003
P	3.7217	0.0006	0.0016	P	3.6861	-0.0004	-0.0017
H	4.4972	0.1639	1.1662	H	4.4642	0.1364	-1.1720
H	4.4608	-1.1094	-0.4522	H	4.4286	0.9601	0.7194
H	4.4725	0.9291	-0.7458	H	4.4395	-1.0900	0.4870

CH_3NO_2

	MP2/6-311+G(3df,2p)				MP2/Aug-cc-pVTZ		
Atom	x(Å)	y(Å)	z(Å)	Atom	x(Å)	y(Å)	z(Å)
C	-1.3154	-0.0445	-0.0001	C	-1.3170	-0.0449	-0.0001
H	-1.6544	0.4914	-0.8803	H	-1.6553	0.4912	-0.8807
H	-1.6232	-1.0818	-0.0121	H	-1.6240	-1.0828	-0.0120
H	-1.6527	0.4690	0.8941	H	-1.6537	0.4691	0.8944
N	0.1680	0.0009	-0.0004	N	0.1674	0.0011	-0.0004
O	0.7737	-1.0657	0.0001	O	0.7750	-1.0680	-0.0001
O	0.6821	1.1134	0.0001	O	0.6828	1.1160	0.0002

H_2O●●● CH_3NO_2

	MP2/6-311+G(3df,2p)				MP2/Aug-cc-pVTZ		
Atom	x(Å)	y(Å)	z(Å)	Atom	x(Å)	y(Å)	z(Å)
C	0.2535	-0.0824	0.0162	C	0.2521	-0.1032	0.0110
H	0.6061	0.4583	0.8865	H	0.6148	0.4281	0.8834
H	0.5345	-1.1258	0.0501	H	0.5165	-1.1518	0.0394
H	0.6194	0.4008	-0.8823	H	0.6223	0.3795	-0.8864
N	-1.2270	0.0042	0.0011	N	-1.2279	0.0060	0.0009
O	-1.8656	-1.0442	-0.0070	O	-1.8842	-1.0349	-0.0048
O	-1.7137	1.1299	-0.0052	O	-1.6986	1.1415	-0.0037
O	3.2767	0.0021	-0.0061	O	3.2808	0.0031	-0.0034
H	3.8807	-0.7433	-0.0067	H	3.8971	-0.7355	-0.0102
H	3.848446	0.77251	-0.006223	H	3.848218	0.779877	-0.00338

H_2S●●● CH_3NO_2

	MP2/6-311+G(3df,2p)				MP2/Aug-cc-pVTZ		
Atom	x(Å)	y(Å)	z(Å)	Atom	x(Å)	y(Å)	z(Å)
C	-0.4846	0.0381	-0.0240	C	0.4805	-0.0569	-0.0264
H	-0.1647	-0.4639	-0.9307	H	0.1481	0.5070	-0.8913
H	-0.1689	1.0725	-0.0046	H	0.1807	-1.0954	-0.0790
H	-0.1266	-0.5100	0.8403	H	0.1196	0.4199	0.8788
N	-1.9675	-0.0003	0.0046	N	1.9638	0.0018	0.0019
O	-2.5697	1.0689	0.0163	O	2.5818	-1.0617	0.0193
O	-2.4887	-1.1099	0.0129	O	2.4715	1.1207	0.0112
H	3.5846	-0.9402	0.7522	H	-3.5093	0.9087	0.8270
S	3.1526	-0.0026	-0.0922	S	-3.1538	0.0082	-0.0945
H	3.5810	0.9843	0.6960	H	-3.5341	-1.0140	0.6782

HF●●● CH_3NO_2

	MP2/6-311+G(3df,2p)				MP2/Aug-cc-pVTZ		
Atom	x(Å)	y(Å)	z(Å)	Atom	x(Å)	y(Å)	z(Å)
C	0.2749	0.0220	0.0097	C	0.2764	0.0230	0.0092
H	0.6130	-0.4940	-0.8820	H	0.6138	-0.4933	-0.8831
H	0.6028	1.0524	0.0265	H	0.6031	1.0542	0.0257
H	0.6030	-0.5213	0.8887	H	0.6044	-0.5205	0.8886
N	-1.2079	0.0010	0.0003	N	-1.2076	0.0009	0.0005
O	-1.7983	1.0770	-0.0037	O	-1.8004	1.0789	-0.0034
O	-1.7431	-1.1021	-0.0035	O	-1.7436	-1.1050	-0.0035
H	4.1589	-0.0010	-0.0098	H	4.1631	-0.0014	-0.0095
F	3.2399	0.0029	-0.0029	F	3.2402	0.0028	-0.0028

HCl●●● CH_3NO_2

	MP2/6-311+G(3df,2p)				MP2/Aug-cc-pVTZ		
Atom	x(Å)	y(Å)	z(Å)	Atom	x(Å)	y(Å)	z(Å)
C	0.4364	-0.1004	0.0082	C	-0.4351	-0.1007	-0.0080
H	0.0720	0.3759	-0.8957	H	-0.0710	0.3765	0.8959
H	0.1731	-1.1494	0.0438	H	-0.1723	-1.1503	-0.0431
H	0.0737	0.4392	0.8760	H	-0.0730	0.4388	-0.8766
N	1.9158	0.0097	0.0011	N	-1.9157	0.0098	-0.0009
O	2.5691	-1.0288	-0.0048	O	-2.5711	-1.0311	0.0046
O	2.3816	1.1437	-0.0019	O	-2.3829	1.1464	0.0019
H	-3.5596	1.1120	-0.0138	H	3.5606	1.1142	0.0132
Cl	-3.0820	-0.0684	-0.0008	Cl	3.0828	-0.0686	0.0008

HBr●●● CH_3NO_2

	MP2/6-311+G(3df,2p)				MP2/Aug-cc-pVTZ		
Atom	x(Å)	y(Å)	z(Å)	Atom	x(Å)	y(Å)	z(Å)
C	1.3548	-0.1255	0.0104	C	-1.2912	-0.1265	-0.0084
H	0.9803	0.3480	-0.8908	H	-0.9166	0.3535	0.8896
H	1.1099	-1.1791	0.0422	H	-1.0472	-1.1809	-0.0332
H	0.9847	0.4038	0.8815	H	-0.9207	0.3967	-0.8835
N	2.8321	0.0107	0.0009	N	-2.7695	0.0108	-0.0007
O	3.5036	-1.0161	-0.0063	O	-3.4435	-1.0179	0.0048
O	3.2776	1.1528	-0.0021	O	-3.2156	1.1557	0.0019
H	-2.6159	1.3549	-0.0157	H	2.5599	1.3462	0.0093
Br	-2.3618	-0.0384	-0.0005	Br	2.3066	-0.0381	0.0006

ClF●●● CH_3NO_2

	MP2/6-311+G(3df,2p)				MP2/Aug-cc-pVTZ		
Atom	x(Å)	y(Å)	z(Å)	Atom	x(Å)	y(Å)	z(Å)
C	-0.8376	-0.4082	0.0001	C	-0.8302	-0.4784	0.0000
H	-0.3583	-0.0078	-0.8867	H	-0.3320	-0.1014	-0.8870
H	-0.3582	-0.0072	0.8867	H	-0.3320	-0.1011	0.8870
H	-0.8483	-1.4901	0.0004	H	-0.8959	-1.5589	0.0002
N	-2.2402	0.0748	0.0000	N	-2.2079	0.0745	0.0000
O	-2.4016	1.2900	0.0000	O	-2.3086	1.2991	-0.0002
O	-3.1362	-0.7633	-0.0001	O	-3.1471	-0.7193	0.0001
F	2.1581	-1.0214	0.0000	F	2.2041	-1.0442	0.0001
Cl	2.7735	0.4947	0.0000	Cl	2.6944	0.5218	-0.0001

LiF●●● CH_3NO_2

	MP2/6-311+G(3df,2p)				MP2/Aug-cc-pVTZ		
Atom	x(Å)	y(Å)	z(Å)	Atom	x(Å)	y(Å)	z(Å)
C	-0.0916	-0.0402	-0.0123	C	-0.0932	-0.0405	-0.0112
H	-0.4342	0.5143	-0.8766	H	-0.4354	0.5143	-0.8761
H	-0.4102	-1.0711	-0.0470	H	-0.4109	-1.0722	-0.0460
H	-0.4444	0.4535	0.8846	H	-0.4448	0.4534	0.8865
N	1.3911	0.0011	-0.0012	N	1.3906	0.0012	-0.0011
O	2.0017	-1.0652	0.0051	O	2.0033	-1.0675	0.0046
O	1.9177	1.1099	0.0044	O	1.9189	1.1125	0.0039
Li	-4.4717	0.0161	0.0047	Li	-4.4746	0.0162	0.0041
F	-2.8710	-0.0077	0.0034	F	-2.8708	-0.0077	0.0033

LiCl●●● CH_3NO_2

	MP2/6-311+G(3df,2p)				MP2/Aug-cc-pVTZ		
Atom	x(Å)	y(Å)	z(Å)	Atom	x(Å)	y(Å)	z(Å)
C	0.5651	-0.0324	0.0006	C	0.5642	-0.0336	0.0001
H	0.2229	0.4930	-0.8836	H	0.2219	0.4919	-0.8845
H	0.2430	-1.0643	0.0021	H	0.2435	-1.0662	0.0016
H	0.2237	0.4953	0.8837	H	0.2230	0.4943	0.8836
N	2.0479	0.0019	-0.0001	N	2.0481	0.0021	-0.0010
O	2.6512	-1.0678	-0.0006	O	2.6539	-1.0697	0.0001
O	2.5770	1.1089	-0.0004	O	2.5780	1.1119	0.0003
Li	-4.7558	0.0462	-0.0047	Li	-4.7622	0.0469	-0.0044
Cl	-2.7043	-0.0123	0.0010	Cl	-2.7047	-0.0125	0.0009

LiBr●●● CH_3NO_2

	MP2/6-311+G(3df,2p)				MP2/Aug-cc-pVTZ		
Atom	x(Å)	y(Å)	z(Å)	Atom	x(Å)	y(Å)	z(Å)
C	1.3695	-0.0251	0.0005	C	1.3248	-0.0320	0.0015
H	1.0319	0.5014	-0.8852	H	0.9836	0.4928	-0.8841
H	1.0421	-1.0555	0.0033	H	1.0028	-1.0645	0.0046
H	1.0324	0.5062	0.8835	H	0.9853	0.4978	0.8847
N	2.8527	0.0003	-0.0001	N	2.8089	0.0011	-0.0002
O	3.4487	-1.0733	-0.0003	O	3.4122	-1.0719	-0.0010
O	3.3877	1.1042	-0.0006	O	3.3402	1.1101	-0.0009
Li	-4.2978	0.0240	-0.0056	Li	-4.2588	0.0267	-0.0060
Br	-2.0883	-0.0035	0.0006	Br	-2.0522	-0.0036	0.0006

H_3N●●● CH_3NO_2

	MP2/6-311+G(3df,2p)				MP2/Aug-cc-pVTZ		
Atom	x(Å)	y(Å)	z(Å)	Atom	x(Å)	y(Å)	z(Å)
C	-0.2059	0.0322	-0.0019	C	0.2067	-0.0323	-0.0017
H	-0.5477	-0.5059	0.8743	H	0.5475	0.5058	0.8754
H	-0.5283	1.0637	0.0099	H	0.5281	-1.0646	0.0097
H	-0.5437	-0.4833	-0.8933	H	0.5437	0.4841	-0.8933
N	1.2774	0.0003	0.0004	N	-1.2775	-0.0002	0.0004
O	1.8771	1.0715	0.0007	O	-1.8788	-1.0740	0.0006
O	1.8058	-1.1066	0.0006	O	-1.8076	1.1090	0.0005
N	-3.4402	0.0018	0.0008	N	3.4413	-0.0018	0.0007
H	-3.8261	0.5576	-0.7516	H	3.8314	-0.5560	-0.7521
H	-3.8260	0.3717	0.8600	H	3.8313	-0.3728	0.8588
H	-3.8164	-0.9313	-0.1067	H	3.8216	0.9310	-0.1053

H_3P●●● CH_3NO_2

	MP2/6-311+G(3df,2p)				MP2/Aug-cc-pVTZ		
Atom	x(Å)	y(Å)	z(Å)	Atom	x(Å)	y(Å)	z(Å)
C	-0.5626	0.0204	-0.0038	C	-0.5508	0.0250	-0.0079
H	-0.2277	-0.5843	-0.8391	H	-0.2149	-0.6050	-0.8241
H	-0.2336	1.0476	-0.0865	H	-0.2259	1.0508	-0.1222
H	-0.2332	-0.4309	0.9262	H	-0.2188	-0.3953	0.9361
N	-2.0461	0.0013	-0.0028	N	-2.0354	0.0006	-0.0034
O	-2.6335	1.0787	0.0021	O	-2.6284	1.0784	0.0038
O	-2.5818	-1.1016	0.0020	O	-2.5698	-1.1059	0.0035
P	3.2143	0.0023	0.0016	P	3.1963	0.0013	0.0017
H	3.9519	-0.6418	-1.0106	H	3.9550	1.1701	-0.2232
H	3.9773	1.1847	-0.0537	H	3.9536	-0.3950	1.1250
H	3.9709	-0.5577	1.0492	H	3.9452	-0.7801	-0.9043

CH_3NF_2

	MP2/6-311+G(3df,2p)				MP2/Aug-cc-pVTZ		
Atom	x(Å)	y(Å)	z(Å)	Atom	x(Å)	y(Å)	z(Å)
C	-1.2878	0.0000	0.1022	C	-1.2898	0.0000	0.1042
H	-1.7896	0.8901	-0.2637	H	-1.7924	0.8907	-0.2606
H	-1.2265	-0.0001	1.1883	H	-1.2226	0.0000	1.1899
H	-1.7896	-0.8901	-0.2638	H	-1.7924	-0.8907	-0.2606
N	0.0431	0.0000	-0.4869	N	0.0398	0.0000	-0.4917
F	0.6795	-1.0849	0.1186	F	0.6815	-1.0890	0.1193
F	0.6795	1.0849	0.1186	F	0.6815	1.0890	0.1193

H_2O●●●CH_3NF_2

	MP2/6-311+G(3df,2p)				MP2/Aug-cc-pVTZ		
Atom	x(Å)	y(Å)	z(Å)	Atom	x(Å)	y(Å)	z(Å)
C	0.2681	-0.0855	0.1860	C	0.2692	-0.0864	0.1881
H	0.7459	0.7547	0.6773	H	0.7473	0.7541	0.6798
H	0.4293	-0.0529	-0.8885	H	0.4278	-0.0534	-0.8869
H	0.6372	-1.0155	0.6049	H	0.6372	-1.0172	0.6072
N	-1.1505	-0.0139	0.4984	N	-1.1504	-0.0141	0.5039
F	-1.7209	-1.0359	-0.2659	F	-1.7232	-1.0398	-0.2687
F	-1.5908	1.1283	-0.1765	F	-1.5915	1.1332	-0.1787
O	3.3279	0.0078	-0.0816	O	3.3293	0.0077	-0.0826
H	3.7892	0.3793	-0.8364	H	3.7929	0.3792	-0.8391
H	4.0253	-0.3486	0.4725	H	4.0310	-0.3485	0.4704

H_2S●●●CH_3NF_2

	MP2/6-311+G(3df,2p)				MP2/Aug-cc-pVTZ		
Atom	x(Å)	y(Å)	z(Å)	Atom	x(Å)	y(Å)	z(Å)
C	-0.4508	-0.0647	0.2472	C	-0.4495	-0.0648	0.2499
H	-0.0064	0.7909	0.7445	H	-0.0051	0.7916	0.7470
H	-0.2439	-0.0477	-0.8204	H	-0.2443	-0.0479	-0.8181
H	-0.0935	-0.9840	0.7000	H	-0.0920	-0.9842	0.7034
N	-1.8828	-0.0024	0.4957	N	-1.8829	-0.0025	0.5013
F	-2.4067	-1.0433	-0.2739	F	-2.4077	-1.0476	-0.2769
F	-2.3018	1.1226	-0.2183	F	-2.3025	1.1272	-0.2209
H	3.4826	0.8789	-0.9406	H	3.4828	0.8804	-0.9438
S	3.2076	-0.0941	-0.0710	S	3.2078	-0.0944	-0.0717
H	3.8001	0.5579	0.9302	H	3.8028	0.5600	0.9304

HF•••CH$_3$NF$_2$

	MP2/6-311+G(3df,2p)				MP2/Aug-cc-pVTZ		
Atom	x(Å)	y(Å)	z(Å)	Atom	x(Å)	y(Å)	z(Å)
C	0.2918	-0.0127	0.1902	C	0.2935	-0.0128	0.1908
H	0.7211	0.8708	0.6509	H	0.7231	0.8711	0.6514
H	0.4546	-0.0119	-0.8847	H	0.4524	-0.0120	-0.8848
H	0.7046	-0.9057	0.6475	H	0.7063	-0.9065	0.6479
N	-1.1297	-0.0005	0.4980	N	-1.1287	-0.0005	0.5035
F	-1.6436	-1.0797	-0.2255	F	-1.6453	-1.0841	-0.2275
F	-1.6244	1.0897	-0.2219	F	-1.6257	1.0943	-0.2238
F	3.2789	0.0192	-0.0912	F	3.2794	0.0191	-0.0918
H	4.1786	-0.1368	-0.1937	H	4.1830	-0.1360	-0.1962

HCl•••CH$_3$NF$_2$

	MP2/6-311+G(3df,2p)				MP2/Aug-cc-pVTZ		
Atom	x(Å)	y(Å)	z(Å)	Atom	x(Å)	y(Å)	z(Å)
C	0.4012	-0.0392	-0.2667	C	-0.4095	-0.1600	0.2624
H	-0.0139	0.8265	-0.7726	H	0.0771	0.6416	0.8093
H	0.1779	-0.0158	0.7974	H	-0.1868	-0.1036	-0.8007
H	0.0312	-0.9518	-0.7231	H	-0.1188	-1.1221	0.6735
N	1.8382	-0.0094	-0.4917	N	-1.8401	-0.0205	0.4978
F	2.3251	-1.0606	0.2879	F	-2.4154	-0.9899	-0.3395
F	2.2701	1.1071	0.2275	F	-2.1758	1.1678	-0.1718
Cl	-3.1396	-0.0157	-0.0052	Cl	3.1459	-0.0440	-0.0141
H	-3.4537	0.2915	1.1899	H	3.4061	0.8351	-0.9007

HBr•••CH$_3$NF$_2$

	MP2/6-311+G(3df,2p)				MP2/Aug-cc-pVTZ		
Atom	x(Å)	y(Å)	z(Å)	Atom	x(Å)	y(Å)	z(Å)
C	-1.3112	-0.1105	0.2977	C	-1.2509	-0.1441	0.2895
H	-0.8717	0.7092	0.8569	H	-0.7869	0.6607	0.8512
H	-1.0593	-0.0456	-0.7583	H	-1.0074	-0.0778	-0.7685
H	-0.9940	-1.0602	0.7169	H	-0.9540	-1.1044	0.7003
N	-2.7509	-0.0269	0.4896	N	-2.6879	-0.0269	0.4969
F	-3.2632	-1.0149	-0.3536	F	-3.2319	-0.9988	-0.3582
F	-3.1140	1.1425	-0.1821	F	-3.0271	1.1610	-0.1715
Br	2.4256	-0.0219	-0.0031	Br	2.3694	-0.0276	-0.0103
H	2.5461	0.8657	-1.1000	H	2.4706	1.0801	-0.8722

ClF•••CH$_3$NF$_2$

	MP2/6-311+G(3df,2p)				MP2/Aug-cc-pVTZ		
Atom	x(Å)	y(Å)	z(Å)	Atom	x(Å)	y(Å)	z(Å)
C	-1.0098	-0.0003	0.2820	C	-1.0245	0.0008	0.2223
H	-0.6258	0.8888	0.7717	H	-0.6201	0.8910	0.6945
H	-0.7682	-0.0001	-0.7784	H	-0.8337	0.0009	-0.8486
H	-0.6264	-0.8900	0.7712	H	-0.6192	-0.8889	0.6945
N	-2.4506	0.0001	0.4820	N	-2.4561	0.0001	0.4904
F	-2.8980	-1.0841	-0.2756	F	-2.9372	-1.0888	-0.2543
F	-2.8972	1.0852	-0.2750	F	-2.9383	1.0885	-0.2543
Cl	3.5408	0.0012	-0.0845	Cl	3.5773	0.0009	-0.0748
F	1.9107	-0.0030	0.0624	F	1.9420	-0.0025	0.0601

LiF●●●CH₃NF₂

MP2/6-311+G(3df,2p)				MP2/Aug-cc-pVTZ			
Atom	x(Å)	y(Å)	z(Å)	Atom	x(Å)	y(Å)	z(Å)
C	-0.1079	0.0086	0.2072	C	0.1100	-0.0079	0.2036
H	-0.5351	-0.8712	0.6736	H	0.5383	0.8725	0.6687
H	-0.2940	0.0069	-0.8625	H	0.2894	-0.0062	-0.8675
H	-0.5235	0.8964	0.6688	H	0.5272	-0.8962	0.6640
N	1.3180	0.0000	0.4918	N	-1.3159	0.0001	0.4973
F	1.8239	1.0797	-0.2427	F	-1.8264	-1.0846	-0.2429
F	1.8093	-1.0914	-0.2361	F	-1.8126	1.0955	-0.2367
Li	-4.5062	-0.0258	-0.2900	Li	4.5107	0.0251	-0.2889
F	-2.9341	0.0110	0.0015	F	2.9350	-0.0108	0.0016

LiCl●●●CH₃NF₂

MP2/6-311+G(3df,2p)				MP2/Aug-cc-pVTZ			
Atom	x(Å)	y(Å)	z(Å)	Atom	x(Å)	y(Å)	z(Å)
C	0.5345	0.0096	0.2413	C	0.5336	-0.0018	0.2124
H	0.1242	-0.8708	0.7239	H	0.1214	-0.8900	0.6799
H	0.3175	0.0048	-0.8235	H	0.3426	-0.0003	-0.8577
H	0.1384	0.9020	0.7135	H	0.1185	0.8834	0.6830
N	1.9686	-0.0002	0.4829	N	1.9632	0.0001	0.4885
F	2.4511	1.0763	-0.2694	F	2.4527	1.0915	-0.2527
F	2.4337	-1.0940	-0.2556	F	2.4563	-1.0871	-0.2565
Li	-4.7871	-0.0599	-0.3634	Li	-4.7991	0.0192	-0.3753
Cl	-2.7747	0.0145	0.0219	Cl	-2.7830	-0.0047	0.0300

LiBr●●●CH₃NF₂

MP2/6-311+G(3df,2p)				MP2/Aug-cc-pVTZ			
Atom	x(Å)	y(Å)	z(Å)	Atom	x(Å)	y(Å)	z(Å)
C	1.3367	0.0094	0.2393	C	-1.2919	-0.0055	0.2014
H	0.9284	-0.8713	0.7239	H	-0.8700	0.8795	0.6666
H	1.1190	0.0035	-0.8257	H	-1.1133	-0.0054	-0.8711
H	0.9427	0.9033	0.7114	H	-0.8772	-0.8947	0.6653
N	2.7714	-0.0001	0.4784	N	-2.7184	-0.0002	0.4935
F	3.2516	1.0758	-0.2754	F	-3.2217	-1.0868	-0.2449
F	3.2346	-1.0943	-0.2597	F	-3.2131	1.0917	-0.2430
Li	-4.3272	-0.0643	-0.4240	Li	4.3254	-0.0060	-0.2166
Br	-2.1658	0.0077	0.0198	Br	2.1308	0.0008	-0.0023

H₃N●●●CH₃NF₂

MP2/6-311+G(3df,2p)				MP2/Aug-cc-pVTZ			
Atom	x(Å)	y(Å)	z(Å)	Atom	x(Å)	y(Å)	z(Å)
C	0.2178	-0.0029	0.2485	C	-0.2186	0.0029	0.2505
H	0.6247	0.8827	0.7238	H	-0.6253	-0.8833	0.7260
H	0.4270	-0.0027	-0.8179	H	-0.4257	0.0028	-0.8164
H	0.6209	-0.8908	0.7228	H	-0.6216	0.8914	0.7251
N	-1.2154	0.0000	0.4974	N	1.2157	0.0000	0.5032
F	-1.6927	-1.0836	-0.2458	F	1.6941	1.0879	-0.2484
F	-1.6881	1.0865	-0.2444	F	1.6894	-1.0908	-0.2470
N	3.4830	-0.0003	-0.0987	N	-3.4844	0.0003	-0.0996
H	3.7620	0.7784	-0.6813	H	-3.7650	-0.7785	-0.6829
H	3.7896	-0.8405	-0.5715	H	-3.7927	0.8405	-0.5735
H	4.0238	0.0667	0.7537	H	-4.0289	-0.0666	0.7517

$H_3P\bullet\bullet\bullet CH_3NF_2$

MP2/6-311+G(3df,2p)				MP2/Aug-cc-pVTZ			
Atom	x(Å)	y(Å)	z(Å)	Atom	x(Å)	y(Å)	z(Å)
C	-0.5345	0.0127	-0.3214	C	-0.5185	-0.0075	-0.2831
H	-0.1520	-0.8709	-0.8222	H	-0.1341	-0.8994	-0.7681
H	-0.2682	0.0106	0.7329	H	-0.2863	-0.0072	0.7795
H	-0.1686	0.9070	-0.8154	H	-0.1247	0.8787	-0.7709
N	-1.9795	-0.0001	-0.4896	N	-1.9592	-0.0001	-0.4976
F	-2.4206	1.0782	0.2815	F	-2.4073	1.0925	0.2632
F	-2.3996	-1.0917	0.2735	F	-2.4192	-1.0852	0.2667
P	3.2676	-0.0045	0.0463	P	3.2545	-0.0039	0.0413
H	3.8188	-0.4816	1.2515	H	3.8087	-0.4718	1.2524
H	3.9848	1.2072	0.0822	H	3.9784	1.2079	0.0644
H	4.2176	-0.6579	-0.7627	H	4.2036	-0.6695	-0.7644

Table.IV.S.2 Frequencies for the normal modes of vibration for different molecules and complexes at MP2/6-311+G(3df,2p) and MP2/Aug-cc-pVTZ levels.

H_2O				*H_2S*			
MP2/6-311+G(3df,2p)		*MP2/Aug-cc-pVTZ*		*MP2/6-311+G(3df,2p)*		*MP2/Aug-cc-pVTZ*	
ν (cm^{-1})	IR intensities	ν (cm^{-1})	IR intensities	ν (cm^{-1})	IR intensities	ν (cm^{-1})	IR intensities
1624.2	72.3	1627.0	71.9	1217.3	0.8	1211.4	0.7
3853.9	9.9	3824.7	5.6	2775.9	0.4	2771.8	0.1
3982.0	76.5	3951.2	75.9	2794.9	0.7	2791.8	0.5

Molecule	*MP2/6-311+G(3df,2p)*		*MP2/Aug-cc-pVTZ*	
	ν (cm^{-1})	IR intensities	ν (cm^{-1})	IR intensities
HF	4164.6	125.4	4125.7	120.6
HCl	3047.6	54.4	3043.0	49.9
HBr	2708.3	16.9	2762.1	17.2
ClF	795.0	29.1	799.5	27.2
LiF	883.5	151.5	876.3	152.5
LiCl	629.2	130.9	628.0	130.5
LiBr	553.0	115.3	556.6	114.9

H_3N				*H_3P*			
MP2/6-311+G(3df,2p)		*MP2/Aug-cc-pVTZ*		*MP2/6-311+G(3df,2p)*		*MP2/Aug-cc-pVTZ*	
ν (cm^{-1})	IR intensities	ν (cm^{-1})	IR intensities	ν (cm^{-1})	IR intensities	ν (cm^{-1})	IR intensities
1032.6	157.3	1037.3	139.3	1023.4	22.0	1011.3	20.6
1672.7	17.8	1668.8	14.3	1165.8	14.2	1159.2	14.0
1672.7	17.8	1669.4	14.3	1165.8	14.2	1159.2	14.0
3531.9	2.6	3501.1	3.4	2475.5	26.7	2468.4	28.0
3676.1	9.4	3647.8	8.4	2486.5	50.7	2481.5	51.4
3676.1	9.4	3648.6	8.5	2486.5	50.7	2481.5	51.4

CH_3OH				*$H_2O...CH_3OH$*			
MP2/6-311+G(3df,2p)		*MP2/Aug-cc-pVTZ*		*MP2/6-311+G(3df,2p)*		*MP2/Aug-cc-pVTZ*	
ν (cm^{-1})	IR intensities	ν (cm^{-1})	IR intensities	ν (cm^{-1})	IR intensities	ν (cm^{-1})	IR intensities
293.1	110.2	294.4	102.9	22.3	0.2	38.6	0.2
1069.2	114.4	1057.9	116.5	55.4	9.1	48.7	5.7
1097.2	6.7	1089.6	2.0	64.8	39.8	69.8	32.5
1193.0	0.4	1184.4	0.4	73.1	29.3	72.5	17.6
1375.9	21.2	1372.5	21.0	85.0	38.7	86.1	40.5
1500.1	3.5	1492.6	3.4	88.8	208.0	91.6	204.3
1528.2	3.2	1525.7	2.9	293.9	116.8	293.5	108.9
1538.5	5.3	1536.2	5.2	1060.1	129.5	1050.1	131.8
3060.3	54.4	3053.1	53.6	1087.5	6.5	1080.7	3.2
3130.5	41.0	3124.1	39.4	1184.8	0.6	1175.9	0.5
3191.1	19.2	3182.1	18.7	1370.0	21.3	1366.3	20.6
3899.2	41.6	3857.8	39.3	1486.9	2.5	1479.5	2.2
				1526.3	3.0	1522.4	2.5
				1533.6	5.4	1530.2	5.0
				1627.0	74.3	1630.5	72.0
				3070.4	53.4	3063.7	53.4
				3142.5	38.3	3136.3	36.9
				3203.4	17.3	3195.2	16.8
				3854.0	11.3	3817.4	7.5
				3900.9	37.8	3860.8	35.8
				3981.9	80.8	3942.5	78.3

$H_2S...CH_3OH$				*$HF...CH_3OH$*			
MP2/6-311+G(3df,2p)		*MP2/Aug-cc-pVTZ*		*MP2/6-311+G(3df,2p)*		*MP2/Aug-cc-pVTZ*	
ν (cm^{-1})	IR intensities	ν (cm^{-1})	IR intensities	ν (cm^{-1})	IR intensities	ν (cm^{-1})	IR intensities
20.0	27.9	11.7	13.9	45.4	5.6	32.0	23.1
32.7	23.7	22.4	25.7	50.6	17.1	37.9	60.4
39.4	4.0	31.7	15.7	58.6	5.9	59.1	106.2
54.4	3.9	52.1	2.1	68.8	167.4	63.9	0.2
59.5	3.0	56.3	2.2	74.8	166.5	65.9	146.6
74.4	0.9	71.4	1.0	288.7	112.8	287.7	105.6
294.3	107.4	292.9	100.3	1062.9	123.6	1051.4	126.3
1063.7	133.8	1052.7	136.6	1090.7	5.8	1082.8	2.2
1091.8	7.0	1084.2	3.4	1188.1	0.5	1179.0	0.5
1189.2	0.2	1179.7	0.2	1372.1	21.6	1367.9	20.6
1216.8	0.4	1210.5	0.5	1494.0	2.7	1485.9	2.3
1372.2	20.8	1368.1	20.0	1527.3	3.3	1523.5	2.9
1489.4	1.9	1480.4	1.7	1537.2	5.0	1533.4	4.8
1524.9	2.1	1521.0	1.7	3066.9	51.5	3062.9	51.3
1534.1	3.9	1530.6	3.6	3139.6	36.4	3136.6	35.2
2776.0	0.9	2772.1	0.4	3195.2	19.1	3191.9	17.4
2795.0	1.4	2792.0	1.1	3901.8	39.3	3862.0	36.7
3061.9	64.9	3055.7	64.5	4154.2	139.4	4115.5	134.9
3133.5	33.6	3128.2	32.1				
3195.3	15.8	3187.4	15.4				
3898.8	42.2	3859.4	39.9				

HCl…CH$_3$OH				*HBr…CH$_3$OH*			
MP2/6-311+G(3df,2p)		*MP2/Aug-cc-pVTZ*		*MP2/6-311+G(3df,2p)*		*MP2/Aug-cc-pVTZ*	
ν (cm^{-1})	IR intensities	ν (cm^{-1})	IR intensities	ν (cm^{-1})	IR intensities	ν (cm^{-1})	IR intensities
22.2	35.0	21.8	28.1	24.1	24.5	35.4	14.1
33.3	34.7	32.0	36.9	35.0	20.7	46.9	16.7
54.5	3.9	49.5	3.8	42.8	1.0	54.1	2.0
58.8	0.3	54.6	0.2	51.4	1.9	61.6	8.5
69.6	8.7	65.2	10.7	60.8	4.5	73.4	6.0
293.5	108.2	290.5	100.9	292.8	106.7	290.9	99.5
1065.2	129.6	1054.7	131.1	1065.9	131.0	1053.8	135.5
1093.7	5.7	1086.4	3.2	1094.2	6.9	1085.8	3.2
1191.0	0.2	1181.8	0.2	1190.3	0.2	1181.3	0.2
1373.5	20.9	1369.3	20.2	1373.7	20.7	1368.5	19.8
1493.1	2.3	1484.4	2.1	1493.2	2.0	1480.2	1.9
1526.0	2.3	1522.1	1.9	1526.0	2.0	1521.0	1.6
1535.9	3.9	1532.2	3.7	1535.7	3.6	1529.8	3.4
3042.0	59.0	3040.6	54.7	2703.2	18.9	2758.4	19.7
3061.1	61.8	3055.0	61.5	3059.8	64.4	3054.6	65.7
3132.7	33.8	3127.5	32.6	3131.3	33.1	3127.4	31.2
3193.0	16.3	3185.6	15.8	3190.8	16.1	3186.0	14.7
3898.7	42.4	3860.2	40.2	3899.1	43.1	3860.2	41.0

ClF… *CH$_3$OH*				LiF… *CH$_3$OH*			
MP2/6-311+G(3df,2p)		*MP2/Aug-cc-pVTZ*		*MP2/6-311+G(3df,2p)*		*MP2/Aug-cc-pVTZ*	
ν (cm^{-1})	IR intensities	ν (cm^{-1})	IR intensities	ν (cm^{-1})	IR intensities	ν (cm^{-1})	IR intensities
7.7	15.7	30.8	12.2	28.3	111.9	24.9	108.8
34.6	0.3	40.5	1.5	32.7	117.5	34.4	106.5
52.2	6.2	51.2	4.9	55.4	10.5	49.5	12.2
60.6	1.4	62.9	4.5	66.4	13.9	58.1	22.5
67.9	4.4	65.7	2.3	85.5	2.8	84.8	3.1
289.2	104.6	293.4	99.1	287.8	111.4	289.8	105.1
794.8	28.8	798.8	26.3	877.1	180.5	867.7	180.6
1066.4	126.4	1054.8	129.9	1048.3	134.1	1037.6	135.1
1095.2	7.6	1087.0	2.3	1074.0	2.6	1067.6	0.7
1194.5	0.1	1184.9	0.1	1171.5	0.9	1162.3	0.8
1373.3	21.8	1370.0	21.4	1364.1	22.1	1360.3	21.2
1495.3	2.9	1487.2	2.6	1475.1	1.6	1467.7	1.5
1526.5	3.0	1522.5	2.6	1523.2	3.7	1519.0	3.2
1536.5	3.3	1531.7	3.1	1531.4	5.4	1527.6	4.9
3059.5	64.3	3053.8	64.1	3087.2	40.5	3080.9	39.2
3130.8	35.1	3125.7	33.2	3164.2	32.4	3158.5	31.3
3192.7	15.1	3186.5	14.3	3211.3	20.7	3203.6	20.1
3900.5	40.4	3859.1	38.2	3903.4	31.8	3862.3	29.6

LiCl… CH_3OH				LiBr… CH_3OH			
MP2/6-311+G(3df,2p)		*MP2/Aug-cc-pVTZ*		*MP2/6-311+G(3df,2p)*		*MP2/Aug-cc-pVTZ*	
ν (cm^{-1})	IR intensities	ν (cm^{-1})	IR intensities	ν (cm^{-1})	IR intensities	ν (cm^{-1})	IR intensities
16.2	79.9	10.4	79.7	10.2	70.5	9.9	68.0
21.9	86.8	27.5	80.9	14.3	49.0	13.5	60.8
55.9	6.8	46.4	6.8	48.1	3.8	46.4	5.1
68.6	5.7	58.8	9.7	54.6	1.5	61.7	4.6
71.6	1.7	68.1	1.3	59.9	7.1	63.5	0.8
289.8	106.0	291.5	100.5	290.2	105.4	288.1	98.1
624.5	143.4	623.4	143.4	549.4	121.9	552.7	124.1
1054.4	143.1	1043.4	143.8	1056.7	144.3	1043.6	147.9
1082.5	3.3	1075.3	1.5	1083.9	4.4	1076.1	1.9
1182.5	0.3	1172.1	0.3	1182.5	0.2	1172.7	0.1
1368.3	21.7	1364.2	21.0	1369.4	21.8	1364.1	21.4
1485.6	1.1	1477.1	1.0	1486.3	0.9	1474.9	0.8
1524.7	2.7	1520.4	2.3	1523.8	2.2	1519.8	2.0
1533.9	3.9	1529.9	3.5	1534.5	3.4	1528.8	2.8
3075.3	52.9	3068.4	51.3	3072.4	56.5	3067.2	56.3
3151.2	26.8	3144.9	26.1	3148.3	24.7	3144.2	23.5
3202.1	15.6	3194.3	15.3	3197.8	17.2	3192.3	14.8
3901.3	36.3	3860.5	34.0	3900.4	39.3	3862.1	35.9

H_3N… CH_3OH				H_3P… CH_3OH			
MP2/6-311+G(3df,2p)		*MP2/Aug-cc-pVTZ*		*MP2/6-311+G(3df,2p)*		*MP2/Aug-cc-pVTZ*	
ν (cm^{-1})	IR intensities	ν (cm^{-1})	IR intensities	ν (cm^{-1})	IR intensities	ν (cm^{-1})	IR intensities
25.9	5.5	28.4	4.2	13.4	3.1	14.8	11.2
53.9	15.4	48.0	17.7	23.1	8.5	38.6	5.5
56.4	7.6	49.9	10.5	26.6	5.2	48.2	5.0
69.5	4.1	64.8	7.0	52.6	1.3	52.1	1.4
79.5	34.7	77.8	29.1	58.5	4.6	63.1	3.6
89.3	39.0	82.3	37.4	62.6	3.2	80.1	4.0
289.9	114.1	287.9	106.3	290.7	106.5	288.1	99.7
1050.5	235.3	1048.0	218.2	1021.8	32.7	1011.1	19.3
1060.2	66.7	1055.4	69.9	1065.3	130.7	1056.8	136.7
1085.5	4.6	1078.5	1.3	1092.8	5.7	1088.6	1.5
1181.2	0.6	1172.6	0.5	1164.6	11.5	1158.1	15.8
1369.4	21.4	1365.6	20.6	1164.8	12.3	1158.5	10.0
1482.5	2.2	1475.4	2.0	1187.9	0.4	1180.4	0.3
1524.0	3.1	1520.1	2.6	1373.3	20.5	1371.7	18.4
1533.2	4.7	1529.8	4.4	1490.8	1.8	1485.9	1.8
1673.4	18.7	1669.3	13.7	1525.0	1.9	1521.4	1.5
1673.4	16.3	1669.5	16.2	1534.5	3.6	1532.3	3.7
3072.2	54.8	3066.4	54.0	2474.5	29.5	2469.7	24.4
3146.1	34.9	3141.3	33.4	2486.4	44.4	2482.0	42.8
3199.2	19.8	3192.1	19.4	2486.4	44.9	2484.2	58.1
3526.4	2.3	3498.5	2.7	3061.6	65.4	3053.3	64.3
3669.2	10.3	3643.7	9.2	3134.2	30.9	3126.7	28.9
3669.5	10.3	3644.2	9.0	3189.2	17.0	3176.5	17.9
3901.0	38.4	3862.1	36.4	3899.3	43.3	3859.6	43.4

HCl…CH$_3$F				*HBr… CH$_3$F*			
MP2/6-311+G(3df,2p)		*MP2/Aug-cc-pVTZ*		*MP2/6-311+G(3df,2p)*		*MP2/Aug-cc-pVTZ*	
ν (cm^{-1})	IR intensities	ν (cm^{-1})	IR intensities	ν (cm^{-1})	IR intensities	ν (cm^{-1})	IR intensities
8.6	25.0	18.7	24.4	-3.8	8.7	23.8	7.8
52.9	5.5	51.4	5.4	44.1	0.4	51.4	1.8
60.2	3.2	56.3	2.1	52.1	6.5	57.3	5.1
64.0	5.2	58.7	4.4	59.3	8.6	64.3	8.5
92.6	28.7	93.1	29.3	86.9	15.0	92.6	13.7
1076.4	124.6	1069.1	126.6	1076.6	127.6	1067.7	132.0
1217.2	0.8	1207.2	0.9	1216.8	0.7	1206.6	0.7
1218.7	0.7	1208.7	0.8	1218.0	0.7	1207.9	0.7
1503.5	0.6	1497.4	0.6	1503.2	0.5	1493.3	0.5
1525.2	4.1	1523.8	3.6	1524.9	3.7	1522.1	3.2
1526.2	3.8	1524.8	3.4	1526.3	3.6	1523.7	3.0
3040.5	60.6	3038.3	56.2	2702.5	20.0	2757.5	20.6
3095.4	38.8	3088.0	39.4	3094.4	41.2	3088.1	42.9
3198.0	19.3	3190.5	18.6	3197.9	19.0	3192.0	17.7
3200.8	18.2	3193.1	17.6	3198.8	17.4	3193.3	16.0

ClF… CH$_3$F				*LiF… CH$_3$F*			
MP2/6-311+G(3df,2p)		*MP2/Aug-cc-pVTZ*		*MP2/6-311+G(3df,2p)*		*MP2/Aug-cc-pVTZ*	
ν (cm^{-1})	IR intensities	ν (cm^{-1})	IR intensities	ν (cm^{-1})	IR intensities	ν (cm^{-1})	IR intensities
31.3	0.6	30.5	1.5	38.0	96.2	37.6	94.4
33.4	1.7	33.7	0.4	38.3	96.6	37.7	93.7
61.1	3.8	60.2	5.0	93.7	23.4	86.7	25.3
74.0	2.6	67.7	7.3	93.9	23.1	86.9	24.7
77.0	7.2	72.3	1.5	105.7	0.6	103.4	0.6
792.8	30.0	797.6	28.1	873.9	185.4	863.3	185.9
1078.0	121.2	1070.3	122.8	1042.6	136.0	1034.3	137.6
1217.7	1.0	1208.7	1.1	1198.0	1.9	1188.5	1.9
1221.9	0.5	1211.3	0.6	1198.4	1.9	1188.5	1.9
1505.8	0.9	1499.8	0.9	1477.9	0.2	1472.3	0.2
1526.1	3.8	1523.6	3.5	1521.6	5.4	1519.2	4.7
1526.3	5.0	1524.2	4.6	1521.8	5.4	1519.4	4.8
3095.0	36.7	3087.6	37.2	3120.9	24.0	3114.0	23.7
3198.6	20.0	3190.5	19.3	3229.4	21.5	3222.3	20.5
3199.1	20.0	3191.7	19.2	3229.7	21.6	3222.5	20.7

LiCl... CH_3F				*LiBr... CH_3F*			
MP2/6-311+G(3df,2p)		*MP2/Aug-cc-pVTZ*		*MP2/6-311+G(3df,2p)*		*MP2/Aug-cc-pVTZ*	
ν (cm^{-1})	IR intensities	ν (cm^{-1})	IR intensities	ν (cm^{-1})	IR intensities	ν (cm^{-1})	IR intensities
16.3	62.9	13.2	74.8	10.5	40.4	2.1	41.2
16.5	74.4	16.4	62.6	12.6	63.3	10.9	64.2
80.5	0.1	73.0	10.4	62.6	0.1	69.3	0.1
82.0	10.8	73.2	11.2	71.8	8.1	71.6	7.7
82.8	10.9	77.2	0.6	73.2	8.4	73.0	7.7
622.2	145.3	620.7	145.5	547.5	125.7	550.0	126.1
1053.8	145.3	1047.1	147.3	1058.6	148.1	1048.6	152.9
1207.9	1.0	1197.3	1.0	1209.3	0.8	1198.0	0.8
1208.2	1.0	1197.3	1.0	1209.8	0.8	1198.7	0.8
1492.2	0.1	1486.2	0.1	1495.6	0.1	1485.3	0.1
1523.4	4.0	1521.3	3.6	1523.8	3.6	1520.7	3.0
1523.5	4.1	1521.4	3.6	1524.0	3.7	1520.8	3.2
3108.1	33.9	3099.9	33.3	3104.2	37.9	3098.6	37.6
3215.8	16.2	3207.2	15.8	3211.1	15.0	3206.1	13.9
3216.0	15.7	3207.4	15.3	3211.2	15.0	3206.2	14.3

H3N... CH_3F				*H3P... CH_3F*			
MP2/6-311+G(3df,2p)		*MP2/Aug-cc-pVTZ*		*MP2/6-311+G(3df,2p)*		*MP2/Aug-cc-pVTZ*	
ν (cm^{-1})	IR intensities	ν (cm^{-1})	IR intensities	ν (cm^{-1})	IR intensities	ν (cm^{-1})	IR intensities
28.7	0.0	39.7	0.0	1.3	0.0	4.6	0.0
75.6	0.4	70.8	0.8	45.6	0.0	43.6	0.0
75.6	0.4	70.8	0.8	46.6	0.0	44.0	0.0
86.1	0.1	83.2	0.1	53.8	0.1	56.4	0.0
130.5	50.6	124.2	48.5	77.1	8.8	77.7	8.9
130.6	50.6	124.2	48.5	78.0	8.9	78.3	8.9
1060.0	283.2	1053.1	185.4	1020.8	38.9	1009.8	39.8
1065.2	16.0	1065.8	100.7	1073.0	124.0	1064.5	126.8
1207.9	1.4	1199.3	1.4	1164.3	11.6	1157.7	11.6
1207.9	1.4	1199.3	1.4	1164.3	11.7	1157.7	11.6
1486.8	0.6	1481.6	0.5	1214.8	0.9	1205.1	1.0
1522.6	4.8	1520.8	4.3	1215.0	0.8	1205.3	0.9
1522.6	4.8	1520.8	4.3	1498.3	0.4	1490.7	0.4
1674.5	17.7	1670.0	15.2	1523.8	3.5	1521.8	3.0
1674.5	17.7	1670.0	15.2	1523.9	3.4	1521.9	3.1
3107.0	34.6	3099.2	34.9	2477.3	28.0	2473.0	29.7
3213.4	21.2	3205.6	20.2	2489.4	41.3	2486.5	42.2
3213.4	21.2	3205.6	20.2	2489.4	41.2	2486.6	42.1
3525.5	1.8	3497.8	2.1	3096.1	43.0	3089.3	43.6
3666.8	11.2	3642.0	10.1	3200.8	17.6	3194.2	16.7
3666.8	11.2	3642.0	10.1	3201.1	17.6	3194.4	16.7

CH_3Cl				*$H_2O...CH_3Cl$*			
MP2/6-311+G(3df,2p)		*MP2/Aug-cc-pVTZ*		*MP2/6-311+G(3df,2p)*		*MP2/Aug-cc-pVTZ*	
ν (cm^{-1})	IR intensities	ν (cm^{-1})	IR intensities	ν (cm^{-1})	IR intensities	ν (cm^{-1})	IR intensities
776.9	23.5	764.3	23.6	15.6	0.8	9.6	0.0
1054.1	2.4	1050.3	2.0	50.1	1.7	39.9	2.0
1054.1	2.4	1050.3	2.0	56.6	0.3	50.9	0.1
1408.6	11.3	1401.4	11.4	80.3	0.3	76.8	0.3
1513.6	5.8	1511.1	5.7	106.9	73.6	101.5	68.8
1513.6	5.8	1511.1	5.7	115.1	239.5	117.4	221.6
3114.4	21.9	3110.4	22.0	767.7	35.1	754.4	35.7
3223.2	2.4	3221.4	2.3	1046.8	2.1	1040.4	1.9
3223.2	2.4	3221.5	2.3	1048.5	2.2	1042.5	1.9
				1395.8	10.3	1387.8	9.9
				1509.0	5.6	1505.2	5.4
				1511.0	5.3	1507.3	4.9
				1630.3	73.9	1632.5	70.9
				3125.5	21.5	3122.7	21.6
				3234.1	2.3	3233.4	2.3
				3238.4	1.4	3238.7	1.3
				3852.7	12.5	3816.6	8.7
				3979.6	83.4	3940.3	80.5

$H_2S...CH_3Cl$				*$HF...CH_3Cl$*			
MP2/6-311+G(3df,2p)		*MP2/Aug-cc-pVTZ*		*MP2/6-311+G(3df,2p)*		*MP2/Aug-cc-pVTZ*	
ν (cm^{-1})	IR intensities	ν (cm^{-1})	IR intensities	ν (cm^{-1})	IR intensities	ν (cm^{-1})	IR intensities
12.6	6.4	15.1	6.8	33.6	1.5	33.0	3.8
42.5	3.5	38.8	3.2	39.6	3.7	36.2	1.2
43.5	2.2	39.0	1.6	63.2	2.9	65.5	22.2
52.4	1.1	50.2	0.9	104.0	165.9	82.7	158.7
74.4	23.8	69.2	23.0	107.8	171.1	83.6	144.8
87.1	1.0	82.6	1.0	771.6	30.6	758.8	31.4
770.6	34.2	757.3	35.0	1049.2	2.2	1045.3	2.0
1050.5	2.8	1044.5	2.6	1050.0	2.2	1045.7	1.9
1052.1	2.9	1046.1	2.6	1402.2	10.2	1395.3	9.9
1216.5	0.5	1210.2	0.5	1511.4	5.7	1508.1	5.2
1397.7	9.1	1389.0	9.2	1511.6	5.7	1508.3	5.4
1509.3	4.2	1505.7	4.0	3123.9	20.7	3118.9	21.0
1509.8	3.8	1506.2	3.6	3233.7	1.8	3231.2	1.9
2775.1	1.1	2770.7	0.6	3235.2	1.8	3232.2	1.6
2794.1	1.6	2790.6	1.3	4146.0	148.2	4112.0	144.3
3118.7	30.4	3114.7	30.6				
3227.9	1.5	3226.4	1.4				
3230.3	1.3	3228.5	1.3				

HCl…CH$_3$Cl				*HBr…CH$_3$Cl*			
MP2/6-311+G(3df,2p)		*MP2/Aug-cc-pVTZ*		*MP2/6-311+G(3df,2p)*		*MP2/Aug-cc-pVTZ*	
ν (cm^{-1})	IR intensities	ν (cm^{-1})	IR intensities	ν (cm^{-1})	IR intensities	ν (cm^{-1})	IR intensities
22.4	27.5	34.3	18.5	14.2	13.7	24.1	14.4
37.5	5.8	36.7	4.0	33.4	4.0	37.3	4.1
44.4	0.5	48.5	8.3	40.3	0.7	47.0	0.4
52.5	1.0	51.1	0.8	41.2	0.8	47.9	0.0
74.7	27.7	84.2	29.1	72.0	14.3	77.7	13.3
774.5	30.6	761.5	31.2	773.5	31.5	760.4	33.1
1052.8	2.9	1047.4	2.6	1052.3	3.1	1047.1	2.8
1054.2	2.9	1048.8	2.6	1053.4	3.0	1048.7	2.8
1402.2	9.4	1394.5	9.5	1401.4	8.8	1389.8	9.2
1510.7	4.5	1507.3	4.2	1510.5	4.2	1505.7	3.8
1511.5	4.1	1508.1	3.9	1511.3	3.8	1506.6	3.3
3039.8	61.2	3036.7	56.8	2702.0	20.4	2757.9	21.0
3117.1	28.1	3111.8	28.4	3116.0	30.1	3112.4	31.5
3225.2	1.7	3221.8	1.6	3224.5	1.6	3223.2	1.4
3228.6	1.4	3224.9	1.3	3227.4	1.2	3226.7	1.1

ClF…CH$_3$Cl				*LiF…CH$_3$Cl*			
MP2/6-311+G(3df,2p)		*MP2/Aug-cc-pVTZ*		*MP2/6-311+G(3df,2p)*		*MP2/Aug-cc-pVTZ*	
ν (cm^{-1})	IR intensities	ν (cm^{-1})	IR intensities	ν (cm^{-1})	IR intensities	ν (cm^{-1})	IR intensities
24.8	0.8	27.5	2.4	35.9	69.8	35.4	60.6
28.1	1.9	32.2	1.1	35.9	70.0	35.4	60.5
49.0	2.0	50.6	3.4	63.9	50.3	59.0	59.1
56.3	3.6	51.2	1.7	64.0	49.9	59.2	58.9
62.3	1.0	61.5	0.9	95.6	0.8	93.5	0.8
775.6	30.3	763.0	30.0	749.1	54.0	736.5	55.2
792.7	28.1	797.7	26.4	871.7	184.5	861.4	184.9
1053.5	2.6	1048.5	2.2	1035.2	1.7	1029.2	1.5
1057.8	3.4	1052.6	3.2	1035.8	1.7	1029.6	1.5
1404.4	10.4	1397.1	10.0	1380.1	9.6	1373.1	9.6
1511.0	4.2	1506.5	4.1	1505.5	6.1	1501.2	5.5
1511.7	5.4	1508.0	5.2	1505.5	6.1	1501.2	5.5
3115.8	26.3	3112.1	26.5	3142.1	14.3	3137.0	14.0
3225.4	1.9	3223.4	1.8	3255.1	1.5	3252.2	1.4
3226.0	1.8	3224.9	1.7	3255.7	1.5	3252.5	1.4

LiCl…CH$_3$Cl				*LiBr…CH$_3$Cl*			
MP2/6-311+G(3df,2p)		*MP2/Aug-cc-pVTZ*		*MP2/6-311+G(3df,2p)*		*MP2/Aug-cc-pVTZ*	
ν (cm^{-1})	IR intensities	ν (cm^{-1})	IR intensities	ν (cm^{-1})	IR intensities	ν (cm^{-1})	IR intensities
17.9	72.6	16.7	73.2	15.7	63.8	16.7	64.6
18.0	73.0	16.7	73.2	15.9	64.3	16.7	64.6
52.4	12.5	50.1	12.5	49.3	8.7	50.3	7.9
53.0	12.1	50.2	12.5	50.6	8.2	50.3	7.9
73.9	0.2	71.1	0.2	55.6	0.1	61.7	0.1
620.9	152.0	619.1	152.7	546.2	129.9	549.4	130.7
758.2	43.0	745.6	43.8	760.3	43.1	746.7	45.5
1045.9	2.6	1038.9	2.4	1047.2	2.9	1040.6	2.7
1046.3	2.6	1039.0	2.4	1047.9	2.9	1040.6	2.7
1392.6	7.9	1384.3	8.1	1395.3	7.2	1382.9	7.6
1507.4	4.3	1503.5	4.0	1508.1	3.8	1503.1	3.4
1507.6	4.3	1503.5	4.0	1508.6	3.8	1503.1	3.4
3129.1	22.3	3123.8	21.7	3123.2	25.8	3122.3	25.5
3240.9	0.6	3238.5	0.7	3233.8	0.6	3237.2	0.5
3242.6	0.6	3238.6	0.7	3237.1	0.6	3237.2	0.5

H$_3$N…CH$_3$Cl				*H$_3$P…CH$_3$Cl*			
MP2/6-311+G(3df,2p)		*MP2/Aug-cc-pVTZ*		*MP2/6-311+G(3df,2p)*		*MP2/Aug-cc-pVTZ*	
ν (cm^{-1})	IR intensities	ν (cm^{-1})	IR intensities	ν (cm^{-1})	IR intensities	ν (cm^{-1})	IR intensities
26.0	0.0	35.7	0.0	16.5	0.0	10.0	0.0
48.0	0.0	46.7	0.0	36.0	0.1	31.8	0.0
48.1	0.0	46.7	0.0	36.2	0.1	31.8	0.0
76.5	0.2	74.6	0.3	48.6	0.0	49.6	0.1
115.1	48.3	108.8	47.0	58.0	6.0	51.9	6.4
115.8	48.3	109.0	46.9	58.2	6.0	52.0	6.2
762.8	39.7	749.5	40.4	770.5	35.9	757.3	36.9
1044.3	2.1	1039.4	1.9	1020.7	31.1	1009.5	32.2
1044.5	2.1	1039.4	1.9	1050.7	3.2	1045.2	2.9
1062.2	166.2	1062.7	151.1	1050.8	3.2	1045.4	2.9
1388.6	10.4	1381.4	10.4	1164.1	11.3	1157.4	11.4
1507.9	5.4	1504.2	5.0	1164.1	11.4	1157.4	11.5
1508.0	5.4	1504.2	5.0	1397.6	8.8	1388.9	9.0
1673.9	17.6	1669.7	15.2	1509.5	3.8	1505.5	3.6
1673.9	17.6	1669.8	15.2	1509.5	3.8	1505.5	3.6
3128.2	24.5	3124.1	24.6	2476.5	31.3	2472.5	32.9
3239.5	1.8	3238.0	1.7	2488.7	40.8	2486.2	41.8
3239.7	1.8	3238.0	1.7	2488.8	40.8	2486.3	41.8
3524.1	1.7	3497.7	1.9	3117.8	31.7	3114.1	32.1
3666.3	11.1	3642.3	10.0	3228.1	1.3	3226.9	1.2
3666.6	11.1	3642.3	10.0	3228.3	1.3	3227.0	1.2

CH_3Br				H_2O... CH_3Br			
MP2/6-311+G(3df,2p)		*MP2/Aug-cc-pVTZ*		*MP2/6-311+G(3df,2p)*		*MP2/Aug-cc-pVTZ*	
ν (cm^{-1})	IR intensities	ν (cm^{-1})	IR intensities	ν (cm^{-1})	IR intensities	ν (cm^{-1})	IR intensities
651.3	8.6	651.9	8.9	-4.2	0.1	8.1	0.1
989.2	4.0	988.3	3.5	39.1	0.8	35.4	0.6
989.2	4.0	988.3	3.5	49.8	0.1	51.9	2.1
1363.3	16.5	1359.8	16.8	72.8	0.4	72.6	0.8
1504.8	5.5	1501.5	5.3	100.9	72.7	92.4	66.5
1504.8	5.5	1501.5	5.3	119.0	239.9	127.4	219.8
3118.3	15.3	3117.1	15.8	644.7	16.7	645.0	17.5
3233.4	0.7	3233.4	0.7	981.8	3.7	980.7	3.4
3233.4	0.7	3233.4	0.7	984.0	3.8	981.9	3.5
				1351.4	17.0	1347.7	16.3
				1500.2	5.3	1496.5	4.9
				1502.3	5.0	1498.1	4.6
				1629.3	73.3	1632.5	70.4
				3129.6	14.7	3128.4	15.4
				3244.3	0.7	3244.1	0.6
				3249.2	0.3	3248.8	0.2
				3851.6	12.6	3816.3	8.7
				3978.3	82.9	3939.8	79.9

H_2S... CH_3Br				HF... CH_3Br			
MP2/6-311+G(3df,2p)		*MP2/Aug-cc-pVTZ*		*MP2/6-311+G(3df,2p)*		*MP2/Aug-cc-pVTZ*	
ν (cm^{-1})	IR intensities	ν (cm^{-1})	IR intensities	ν (cm^{-1})	IR intensities	ν (cm^{-1})	IR intensities
40.8	1.5	7.2	6.0	29.5	1.5	31.1	1.9
41.8	2.9	36.4	2.4	33.1	1.4	31.2	1.9
46.4	0.4	37.5	3.0	54.9	27.1	62.2	0.4
55.2	5.5	48.1	0.2	67.7	165.2	93.0	164.8
85.1	24.9	66.2	25.0	73.8	146.7	94.3	164.9
92.6	0.6	76.1	0.4	647.9	13.5	648.9	14.3
645.7	15.1	646.4	16.1	985.8	3.8	984.8	3.5
987.2	4.6	984.2	4.4	986.0	3.9	984.9	3.5
988.3	4.6	985.1	4.2	1357.9	16.4	1355.7	15.7
1216.8	0.5	1210.3	0.4	1502.6	5.3	1499.2	4.9
1352.7	15.5	1347.8	15.2	1503.3	5.3	1499.2	4.9
1501.0	3.8	1496.2	3.6	3124.8	14.2	3124.6	14.6
1501.5	3.7	1496.8	3.4	3239.4	0.4	3242.0	0.4
2772.4	1.1	2770.6	0.6	3243.7	0.4	3242.1	0.4
2791.4	1.5	2790.4	1.2	4152.6	150.1	4110.9	145.6
3119.6	22.1	3121.3	23.1				
3235.5	0.3	3237.9	0.2				
3237.4	0.2	3240.0	0.3				

HCl…CH$_3$Br				*HBr…CH$_3$Br*			
MP2/6-311+G(3df,2p)		*MP2/Aug-cc-pVTZ*		*MP2/6-311+G(3df,2p)*		*MP2/Aug-cc-pVTZ*	
ν (cm^{-1})	IR intensities	ν (cm^{-1})	IR intensities	ν (cm^{-1})	IR intensities	ν (cm^{-1})	IR intensities
18.7	26.3	19.8	24.4	11.7	13.3	24.4	13.0
32.1	7.2	31.1	6.0	29.3	2.7	33.3	3.7
40.4	0.3	38.1	1.2	35.1	1.2	40.4	0.6
44.9	2.1	44.2	1.7	37.9	0.2	44.8	0.2
65.0	23.2	61.2	23.7	62.4	13.5	65.5	11.8
649.3	12.7	650.1	13.4	648.8	13.1	649.2	14.4
988.0	4.6	986.8	4.3	987.4	4.9	986.8	4.5
990.0	4.7	988.7	4.3	988.8	4.8	988.6	4.5
1356.6	15.2	1353.9	15.1	1356.0	14.4	1349.5	15.0
1501.7	4.1	1497.8	3.9	1501.8	4.0	1496.1	3.5
1502.6	3.9	1498.6	3.6	1502.6	3.5	1497.2	3.1
3040.0	62.1	3038.4	57.6	2702.2	20.6	2758.0	21.2
3120.8	20.3	3118.7	21.1	3120.0	21.9	3118.7	23.8
3235.6	0.4	3234.0	0.3	3234.8	0.3	3234.5	0.3
3239.1	0.2	3237.3	0.2	3238.2	0.2	3237.9	0.1

ClF…CH$_3$Br				*LiF…CH$_3$Br*			
MP2/6-311+G(3df,2p)		*MP2/Aug-cc-pVTZ*		*MP2/6-311+G(3df,2p)*		*MP2/Aug-cc-pVTZ*	
ν (cm^{-1})	IR intensities	ν (cm^{-1})	IR intensities	ν (cm^{-1})	IR intensities	ν (cm^{-1})	IR intensities
22.6	0.9	20.5	1.7	31.1	64.7	36.2	42.9
24.7	1.4	33.3	1.0	31.6	65.8	36.2	43.0
44.7	1.4	48.7	2.3	57.1	55.0	58.6	77.1
49.3	2.3	50.7	0.9	57.6	55.2	58.6	77.1
55.3	1.2	58.7	1.4	86.6	0.9	87.2	0.9
651.0	12.0	652.1	12.5	631.5	30.5	630.5	31.7
792.8	28.9	797.6	26.4	872.7	193.6	861.3	194.4
988.7	4.4	987.6	3.7	972.8	3.2	970.1	2.9
992.6	5.3	992.4	5.0	974.9	3.2	970.2	2.9
1358.6	16.2	1355.8	15.8	1337.4	18.0	1333.7	17.5
1502.0	3.9	1496.9	4.1	1496.9	5.6	1492.2	5.0
1502.7	5.0	1498.8	4.9	1497.0	5.5	1492.2	5.0
3119.9	18.9	3118.4	19.2	3143.1	9.0	3143.6	8.9
3235.9	0.5	3235.0	0.4	3262.5	0.3	3263.9	0.2
3236.7	0.4	3235.9	0.5	3263.5	0.2	3263.9	0.2

LiCl...CH$_3$Br				*LiBr...CH$_3$Br*			
MP2/6-311+G(3df,2p)		*MP2/Aug-cc-pVTZ*		*MP2/6-311+G(3df,2p)*		*MP2/Aug-cc-pVTZ*	
ν (cm^{-1})	IR intensities	ν (cm^{-1})	IR intensities	ν (cm^{-1})	IR intensities	ν (cm^{-1})	IR intensities
16.4	74.5	9.4	74.2	14.4	65.9	16.9	65.8
16.5	74.7	9.5	74.3	14.4	65.9	16.9	65.8
53.0	11.4	44.6	12.0	46.4	7.1	45.9	7.2
53.3	11.1	44.7	12.0	46.4	7.2	45.9	7.3
64.9	0.2	62.6	0.2	46.8	0.1	52.1	0.1
620.7	162.3	620.3	161.9	546.4	132.4	549.1	133.2
637.7	14.6	638.0	16.1	639.8	21.0	638.5	23.0
982.8	4.4	979.0	4.1	983.9	4.8	980.9	4.4
983.2	4.4	979.0	4.0	984.0	4.8	980.9	4.4
1348.8	15.1	1344.1	14.8	1350.9	13.9	1342.9	14.2
1498.7	3.9	1494.1	3.6	1499.5	3.5	1493.4	3.1
1499.0	4.0	1494.2	3.6	1499.6	3.5	1493.4	3.1
3131.9	15.1	3130.3	15.0	3128.7	18.0	3128.0	18.1
3250.2	0.0	3249.9	0.0	3247.1	0.0	3247.8	0.0
3251.1	0.0	3250.0	0.0	3247.2	0.0	3247.9	0.0

H$_3$N...CH$_3$Br				*H$_3$P...CH$_3$Br*			
MP2/6-311+G(3df,2p)		*MP2/Aug-cc-pVTZ*		*MP2/6-311+G(3df,2p)*		*MP2/Aug-cc-pVTZ*	
ν (cm^{-1})	IR intensities	ν (cm^{-1})	IR intensities	ν (cm^{-1})	IR intensities	ν (cm^{-1})	IR intensities
20.0	0.0	31.0	0.0	18.8	0.0	5.3	0.0
42.9	0.1	40.3	0.1	32.2	0.0	26.6	0.5
42.9	0.1	40.4	0.1	32.4	0.0	26.7	0.5
70.2	0.3	68.2	0.3	44.2	0.0	42.8	4.8
116.9	47.4	101.5	45.7	48.4	5.0	43.0	4.8
117.0	47.4	101.9	45.7	48.7	5.1	45.9	0.1
640.7	19.5	640.4	20.3	646.0	15.7	646.3	16.8
980.0	3.7	979.2	3.4	986.1	5.0	984.9	4.5
980.2	3.7	979.4	3.4	986.3	5.0	985.0	4.5
1062.4	167.7	1061.5	152.7	1020.4	34.4	1009.3	35.4
1345.1	17.9	1341.4	17.4	1164.0	11.3	1157.4	11.3
1499.2	4.9	1495.3	4.5	1164.1	11.4	1157.4	11.3
1499.2	5.0	1495.3	4.6	1352.3	15.2	1347.3	15.3
1674.1	17.7	1669.6	15.3	1500.7	3.5	1496.1	3.3
1674.1	17.7	1669.6	15.4	1500.8	3.5	1496.1	3.3
3131.8	17.3	3129.9	17.8	2476.3	32.7	2472.1	34.6
3249.2	0.4	3248.4	0.4	2488.5	40.7	2485.9	41.6
3249.4	0.4	3248.6	0.3	2488.6	40.7	2486.0	41.6
3524.3	1.6	3497.6	1.9	3122.0	23.4	3120.3	24.4
3665.8	11.0	3642.3	10.0	3238.8	0.2	3238.0	0.2
3665.8	11.0	3642.3	10.0	3238.9	0.2	3238.1	0.2

CH_3NO_2				$H_2O...CH_3NO_2$			
MP2/6-311+G(3df,2p)		*MP2/Aug-cc-pVTZ*		*MP2/6-311+G(3df,2p)*		*MP2/Aug-cc-pVTZ*	
ν (cm^{-1})	IR intensities	ν (cm^{-1})	IR intensities	ν (cm^{-1})	IR intensities	ν (cm^{-1})	IR intensities
34.8	0.0	28.4	0.0	18.4	1.7	11.8	1.5
482.1	0.9	478.7	1.0	34.2	0.0	31.0	0.2
615.1	1.7	610.4	1.8	35.5	0.1	37.4	0.1
674.7	23.4	669.9	23.9	68.5	3.4	69.6	5.3
948.8	4.6	940.6	4.3	89.4	0.3	86.9	0.4
1130.4	3.3	1127.5	3.5	134.6	71.3	131.7	66.2
1151.7	0.1	1149.2	0.0	144.6	241.9	145.3	222.7
1423.4	43.9	1412.3	51.8	485.7	1.1	481.6	1.1
1435.2	9.8	1430.7	0.7	615.9	2.1	610.6	2.1
1491.7	24.1	1492.1	24.2	675.3	31.5	670.3	32.4
1504.0	12.3	1502.8	11.9	949.4	2.1	941.4	1.9
1759.9	171.0	1745.9	165.6	1126.4	3.6	1123.0	3.7
3120.8	1.7	3115.6	1.7	1145.7	0.1	1142.0	0.1
3226.8	0.1	3221.7	0.1	1414.7	15.8	1411.6	30.5
3253.7	0.9	3248.1	0.9	1436.1	36.6	1424.5	21.3
				1488.4	23.0	1487.9	22.8
				1497.8	11.4	1495.9	10.9
				1632.6	75.4	1634.9	72.3
				1752.3	180.0	1738.4	174.2
				3133.6	1.3	3127.4	1.4
				3241.0	0.0	3234.9	0.0
				3265.0	1.7	3257.9	1.8
				3852.4	14.5	3816.3	10.6
				3977.5	86.4	3938.2	83.4

$H_2S...CH_3NO_2$				$HF...\ CH_3NO_2$			
MP2/6-311+G(3df,2p)		*MP2/Aug-cc-pVTZ*		*MP2/6-311+G(3df,2p)*		*MP2/Aug-cc-pVTZ*	
ν (cm^{-1})	IR intensities	ν (cm^{-1})	IR intensities	ν (cm^{-1})	IR intensities	ν (cm^{-1})	IR intensities
13.6	8.5	13.5	7.4	25.1	1.3	25.3	2.0
28.2	4.9	20.4	2.7	29.8	2.5	26.3	2.4
29.9	4.2	26.5	7.0	40.2	6.1	32.3	6.2
45.8	4.4	39.9	5.3	73.1	0.2	72.6	0.2
53.9	0.9	52.4	0.4	102.5	172.4	96.4	164.9
91.3	25.7	90.3	25.0	112.6	174.3	104.1	166.4
110.7	0.7	110.0	0.4	484.5	0.8	480.4	0.9
484.5	0.9	480.5	1.0	616.2	1.9	610.9	2.0
616.4	1.6	610.7	1.7	675.8	29.1	671.0	29.8
674.5	30.1	669.5	31.1	950.2	2.7	941.9	2.5
948.7	3.2	940.3	2.9	1127.8	3.5	1124.1	3.6
1127.8	2.4	1123.8	2.5	1149.3	0.1	1145.8	0.1
1148.9	0.2	1144.8	0.2	1421.9	24.8	1415.2	47.0
1216.1	0.5	1209.8	0.5	1435.7	27.8	1427.4	4.8
1417.3	26.0	1411.2	46.7	1489.4	23.6	1489.0	23.4
1433.2	33.4	1422.7	12.0	1501.6	11.8	1499.7	11.2
1487.8	19.1	1487.3	18.8	1754.8	177.7	1740.8	172.2
1498.9	9.1	1497.0	8.7	3128.6	1.2	3122.7	1.3
1755.9	174.6	1741.7	169.0	3234.5	0.0	3228.3	0.0
2774.8	1.4	2770.5	0.9	3262.6	1.1	3256.2	1.1
2793.7	2.1	2790.3	1.7	4143.8	155.3	4106.5	151.4
3125.5	3.6	3120.0	3.7				
3231.9	0.0	3226.5	0.0				
3259.0	1.4	3252.6	1.4				

HCl…CH_3NO_2				*HBr…CH_3NO_2*			
MP2/6-311+G(3df,2p)		*MP2/Aug-cc-pVTZ*		*MP2/6-311+G(3df,2p)*		*MP2/Aug-cc-pVTZ*	
ν (cm^{-1})	IR intensities	ν (cm^{-1})	IR intensities	ν (cm^{-1})	IR intensities	ν (cm^{-1})	IR intensities
23.5	4.7	22.9	4.5	19.7	5.3	22.2	5.2
29.6	1.3	25.5	7.8	26.8	6.9	25.6	5.1
36.1	40.4	36.4	24.7	33.2	19.5	32.8	18.3
51.8	0.3	50.2	0.1	38.8	0.1	44.7	0.0
52.9	1.1	52.7	9.2	52.1	0.0	61.0	1.9
99.9	31.0	102.7	30.1	100.1	15.9	107.0	15.3
484.4	1.0	480.4	1.0	483.9	0.9	480.6	1.0
616.5	1.7	611.2	1.7	616.2	1.6	611.1	1.6
675.2	28.3	670.1	29.2	674.9	28.9	670.1	30.0
949.3	3.6	940.8	3.3	949.0	3.7	940.9	3.3
1130.1	2.6	1126.2	2.8	1129.3	2.5	1125.5	2.6
1149.8	0.2	1146.2	0.2	1149.6	0.3	1146.0	0.3
1420.5	32.9	1412.4	54.2	1420.0	35.3	1411.7	52.8
1433.5	25.8	1425.2	3.5	1433.2	25.9	1423.4	7.2
1489.5	19.7	1489.2	19.6	1489.4	18.7	1488.1	18.1
1500.6	9.9	1499.0	9.4	1500.6	9.5	1497.9	8.8
1757.2	173.3	1742.6	167.6	1757.3	172.2	1743.1	167.2
3037.2	63.4	3035.6	59.1	2700.0	21.5	2755.9	22.2
3123.7	3.0	3117.8	3.0	3123.0	3.4	3117.9	3.8
3231.4	0.0	3225.3	0.0	3230.4	0.0	3225.7	0.0
3255.0	1.3	3248.6	1.3	3254.6	1.2	3248.8	1.3

ClF…CH_3NO_2				*LiF…CH_3NO_2*			
MP2/6-311+G(3df,2p)		*MP2/Aug-cc-pVTZ*		*MP2/6-311+G(3df,2p)*		*MP2/Aug-cc-pVTZ*	
ν (cm^{-1})	IR intensities	ν (cm^{-1})	IR intensities	ν (cm^{-1})	IR intensities	ν (cm^{-1})	IR intensities
10.4	0.2	9.5	4.2	10.2	0.0	21.8	0.4
15.9	3.9	10.7	0.0	33.6	37.6	32.1	31.7
31.5	5.6	30.2	7.1	43.3	50.6	41.5	35.8
41.5	1.4	48.9	1.1	65.6	80.6	64.8	85.9
64.9	1.1	61.6	3.6	70.8	73.8	66.8	87.2
66.6	5.0	63.4	1.1	107.9	0.6	105.8	0.7
483.6	0.9	479.5	0.9	486.2	1.0	481.8	1.1
618.3	1.4	612.9	1.5	615.0	2.2	609.5	2.3
675.8	28.0	670.9	28.3	673.8	40.3	668.7	41.5
791.1	29.0	796.2	26.4	865.5	190.5	856.0	190.9
949.9	3.7	941.8	3.5	947.1	0.4	938.7	0.3
1129.0	3.1	1125.5	3.7	1117.0	4.6	1112.9	4.6
1154.0	0.4	1150.3	0.4	1137.9	0.0	1134.0	0.0
1422.0	36.6	1413.2	55.4	1397.7	11.7	1395.4	14.9
1434.0	21.7	1428.0	2.2	1441.1	35.8	1428.0	31.5
1488.8	21.2	1487.9	23.2	1481.4	24.3	1479.6	23.9
1501.8	11.3	1499.7	11.2	1492.7	12.2	1489.8	11.4
1757.6	170.2	1743.7	163.9	1741.7	193.1	1727.1	187.7
3122.9	2.4	3117.2	2.3	3147.4	0.1	3141.0	0.1
3229.7	0.1	3223.7	0.1	3251.8	0.1	3245.0	0.1
3255.9	0.8	3249.4	0.7	3282.8	1.4	3275.7	1.4

LiCl...CH_3NO_2				*LiBr... CH_3NO_2*			
MP2/6-311+G(3df,2p)		*MP2/Aug-cc-pVTZ*		*MP2/6-311+G(3df,2p)*		*MP2/Aug-cc-pVTZ*	
ν (cm^{-1})	IR intensities	ν (cm^{-1})	IR intensities	ν (cm^{-1})	IR intensities	ν (cm^{-1})	IR intensities
18.4	60.5	14.1	61.0	12.0	59.2	14.7	57.2
20.6	50.1	17.4	46.2	14.9	56.2	16.9	41.5
30.1	18.0	24.4	19.9	30.0	7.2	22.5	17.0
47.3	24.3	42.1	24.3	40.3	13.9	38.1	15.8
58.9	22.0	49.7	25.0	51.3	15.0	47.2	19.8
78.5	0.2	75.7	0.2	58.3	0.1	63.4	0.1
486.4	1.0	481.6	1.1	485.5	1.0	481.3	1.1
616.7	156.0	611.2	1.9	543.2	133.0	545.9	133.5
617.5	1.8	615.4	156.4	617.0	1.7	611.4	1.8
674.6	33.5	669.3	34.4	674.2	35.0	669.3	36.3
948.0	1.5	939.6	1.3	947.9	2.0	939.5	1.6
1124.3	2.8	1118.6	3.0	1124.9	2.4	1119.3	2.5
1145.6	0.2	1140.2	0.2	1146.2	0.3	1141.2	0.3
1411.9	21.0	1407.8	30.6	1414.3	26.0	1407.0	33.8
1438.0	37.2	1425.5	26.4	1436.8	36.6	1424.6	27.4
1484.6	19.9	1483.4	19.7	1485.2	18.6	1483.2	17.9
1496.3	9.3	1493.7	8.6	1497.0	8.4	1493.8	7.6
1747.3	186.1	1732.8	180.5	1749.0	183.3	1734.2	178.6
3133.4	1.2	3127.5	1.2	3129.6	2.0	3125.2	2.0
3238.3	0.0	3232.2	0.0	3234.8	0.0	3230.4	0.0
3269.0	1.8	3262.4	1.7	3265.2	1.8	3260.1	1.9

$H_3N...CH_3NO_2$				*$H_3P...CH_3NO2$*			
MP2/6-311+G(3df,2p)		*MP2/Aug-cc-pVTZ*		*MP2/6-311+G(3df,2p)*		*MP2/Aug-cc-pVTZ*	
ν (cm^{-1})	IR intensities	ν (cm^{-1})	IR intensities	ν (cm^{-1})	IR intensities	ν (cm^{-1})	IR intensities
17.5	0.1	12.2	0.1	21.7	0.0	11.5	0.0
35.5	1.3	34.6	1.4	27.9	2.8	22.0	1.0
37.4	0.6	35.2	0.4	33.2	4.6	26.0	2.2
51.3	2.0	46.3	1.7	41.0	1.6	34.0	4.8
84.6	0.2	82.1	0.2	49.3	0.0	50.5	0.0
147.1	50.6	141.3	49.4	71.5	5.8	64.8	6.4
149.6	46.6	143.6	45.6	74.2	4.3	66.6	5.0
485.1	0.9	481.4	1.0	484.6	0.9	480.6	0.9
615.5	1.9	610.7	2.0	615.7	1.7	610.3	1.9
673.5	33.3	668.6	34.2	674.4	31.0	669.7	31.9
947.8	2.0	939.7	1.8	948.5	3.2	940.3	3.0
1076.5	165.7	1077.0	150.8	1020.6	31.3	1009.3	32.2
1123.0	3.5	1120.0	3.6	1127.5	1.8	1123.5	1.8
1144.2	0.1	1141.4	0.1	1148.5	0.8	1144.7	1.0
1408.0	12.9	1405.8	20.8	1163.8	11.6	1157.1	11.8
1435.6	38.7	1423.1	29.8	1163.9	11.0	1157.3	10.9
1485.1	22.3	1484.5	22.1	1417.5	27.6	1411.4	47.6
1496.7	11.1	1494.6	10.5	1433.0	33.1	1422.7	11.8
1674.9	17.5	1670.5	15.1	1487.5	18.6	1486.7	18.5
1674.9	16.8	1670.5	14.6	1499.1	8.6	1496.9	8.2
1751.5	180.8	1737.3	175.3	1755.7	174.3	1741.7	169.1
3134.9	2.2	3129.1	2.2	2478.7	27.9	2475.3	29.2
3240.7	0.1	3234.9	0.1	2490.9	38.3	2488.9	39.2
3269.3	1.3	3263.1	1.3	2491.1	37.5	2489.2	38.5
3522.7	1.2	3496.4	1.4	3124.4	3.9	3119.1	4.0
3662.8	11.8	3638.8	10.7	3230.5	0.1	3225.2	0.2
3662.9	11.8	3638.8	10.7	3258.8	1.3	3252.8	1.2

CH_3NF_2				$H_2O...CH_3NF_2$			
MP2/6-311+G(3df,2p)		*MP2/Aug-cc-pVTZ*		*MP2/6-311+G(3df,2p)*		*MP2/Aug-cc-pVTZ*	
ν (cm^{-1})	IR intensities	ν (cm^{-1})	IR intensities	ν (cm^{-1})	IR intensities	ν (cm^{-1})	IR intensities
285.1	0.0	278.1	0.0	24.9	0.2	25.4	0.1
426.3	2.5	422.7	2.7	36.7	0.4	35.6	0.5
474.2	4.3	468.0	4.4	48.4	0.2	57.0	0.1
570.9	2.6	564.6	2.9	86.1	0.3	84.6	0.5
884.0	108.2	869.2	109.0	122.6	73.8	117.4	69.5
898.2	26.0	888.6	26.7	131.9	239.0	124.0	220.3
1102.2	31.2	1089.2	30.2	288.0	0.0	281.0	0.0
1167.5	19.9	1161.3	18.5	428.3	2.4	424.4	2.6
1206.2	0.7	1200.3	0.7	475.1	5.5	468.3	5.6
1444.8	3.9	1440.9	3.9	571.2	3.4	564.4	3.9
1499.7	9.6	1497.9	9.6	878.9	109.7	863.8	109.9
1502.9	6.1	1500.9	5.8	896.3	33.8	886.1	34.7
3099.2	4.4	3094.2	3.9	1099.8	28.3	1086.4	27.3
3209.6	3.1	3204.6	3.0	1158.6	20.8	1151.6	19.7
3224.3	0.5	3217.1	0.4	1203.3	0.7	1196.5	0.7
				1431.6	5.5	1428.1	5.9
				1495.5	8.4	1492.0	8.1
				1498.3	6.4	1495.1	5.9
				1631.1	75.8	1633.1	73.1
				3109.1	4.1	3103.4	3.8
				3219.2	3.7	3213.3	3.5
				3236.4	0.4	3228.6	0.4
				3852.2	13.1	3816.6	9.4
				3978.2	85.1	3940.0	82.3

$H_2S...CH_3NF_2$				$HF...CH_3NF_2$			
MP2/6-311+G(3df,2p)		*MP2/Aug-cc-pVTZ*		*MP2/6-311+G(3df,2p)*		*MP2/Aug-cc-pVTZ*	
ν (cm^{-1})	IR intensities	ν (cm^{-1})	IR intensities	ν (cm^{-1})	IR intensities	ν (cm^{-1})	IR intensities
-2.8	10.6	10.9	10.2	28.1	0.9	26.1	1.3
24.6	2.5	23.5	3.4	32.6	2.3	29.3	2.7
31.1	2.3	29.3	1.6	71.1	5.7	70.4	4.3
54.1	3.1	51.8	2.5	94.6	172.6	97.6	166.1
79.8	23.5	75.2	22.5	100.1	168.9	104.2	161.2
97.3	1.2	93.8	1.3	286.8	0.0	278.8	0.0
286.7	0.0	278.5	0.0	428.2	2.5	424.1	2.6
428.2	2.5	424.2	2.6	475.0	5.2	468.3	5.3
475.2	5.0	468.5	5.1	571.1	3.3	564.3	3.7
571.7	3.2	565.0	3.7	881.3	109.2	865.9	109.7
882.3	104.1	867.1	104.4	897.8	31.3	887.6	32.1
897.6	31.9	887.4	32.7	1101.6	29.2	1088.1	28.2
1101.3	30.7	1087.5	29.7	1163.2	20.6	1156.0	19.5
1163.3	22.2	1155.6	21.1	1204.6	0.6	1197.7	0.6
1204.6	0.8	1197.5	0.8	1439.1	5.2	1435.7	5.4
1216.3	0.4	1210.1	0.4	1497.2	9.2	1494.2	8.9
1434.9	7.2	1430.4	7.5	1500.6	5.9	1497.5	5.5
1495.8	6.9	1492.9	6.6	3105.5	3.7	3100.5	3.4
1498.3	4.2	1495.3	3.9	3216.3	3.0	3211.1	2.8
2775.3	1.2	2771.0	0.7	3230.7	0.4	3223.6	0.3
2794.2	1.8	2790.8	1.5	4147.3	149.8	4108.1	146.0
3102.3	7.2	3096.8	6.7				
3212.9	2.6	3207.0	2.5				
3229.0	0.3	3221.3	0.2				

HCl…CH_3NF_2				*HBr…CH_3NF_2*			
MP2/6-311+G(3df,2p)		*MP2/Aug-cc-pVTZ*		*MP2/6-311+G(3df,2p)*		*MP2/Aug-cc-pVTZ*	
ν (cm^{-1})	IR intensities	ν (cm^{-1})	IR intensities	ν (cm^{-1})	IR intensities	ν (cm^{-1})	IR intensities
3.5	13.7	12.7	7.0	14.1	6.6	19.3	3.0
31.7	9.0	24.8	15.3	25.3	12.1	23.0	14.2
33.8	17.4	33.4	17.6	29.7	4.7	36.3	5.9
50.1	1.8	50.1	0.8	40.4	1.7	46.4	1.1
92.2	30.8	90.5	30.8	87.6	15.7	90.8	15.3
286.2	0.0	279.5	0.0	286.6	0.0	279.8	0.0
428.6	2.6	424.4	2.6	427.9	2.5	424.6	2.6
475.4	4.8	468.9	5.0	475.2	4.9	469.0	5.0
571.9	3.0	565.4	3.5	571.7	3.1	565.6	3.6
882.9	104.7	868.2	105.5	882.9	103.7	868.2	104.0
897.9	30.2	888.4	30.8	897.7	30.1	888.3	31.1
1101.8	30.8	1088.5	29.8	1101.6	31.2	1088.3	30.2
1165.9	21.9	1158.4	20.2	1165.4	21.9	1157.6	20.7
1205.0	0.7	1198.1	0.7	1204.8	0.6	1197.6	0.6
1438.5	6.2	1434.2	6.6	1438.3	7.1	1431.2	7.3
1497.2	7.3	1494.5	7.2	1497.0	6.9	1492.9	6.5
1499.4	4.4	1497.1	4.2	1499.9	4.0	1495.8	3.5
3038.9	60.9	3037.8	56.2	2701.2	20.4	2757.0	21.0
3101.4	6.4	3096.0	5.7	3100.6	7.1	3095.6	6.8
3211.8	2.8	3206.3	2.6	3211.1	2.6	3206.2	2.3
3226.1	0.2	3219.2	0.3	3225.3	0.3	3218.8	0.3

ClF… CH_3NF_2				*LiF… CH_3NF_2*			
MP2/6-311+G(3df,2p)		*MP2/Aug-cc-pVTZ*		*MP2/6-311+G(3df,2p)*		*MP2/Aug-cc-pVTZ*	
ν (cm^{-1})	IR intensities	ν (cm^{-1})	IR intensities	ν (cm^{-1})	IR intensities	ν (cm^{-1})	IR intensities
22.5	0.3	2.4	2.5	28.8	24.8	27.1	17.1
24.5	0.0	8.4	1.6	34.2	48.5	32.9	39.9
30.4	3.3	17.9	2.0	55.4	93.0	55.3	100.1
33.0	4.8	18.7	2.8	61.2	72.3	60.0	80.3
56.5	1.2	50.7	0.7	103.5	1.3	101.3	1.2
286.2	0.0	278.7	0.0	288.2	0.0	280.1	0.0
428.9	2.6	424.3	2.7	427.7	2.6	423.0	2.8
475.8	5.1	469.0	5.2	474.3	6.8	467.4	7.0
572.4	3.3	565.2	3.6	569.3	4.7	562.1	5.3
791.3	35.4	797.0	33.2	868.8	195.8	855.4	112.3
883.9	105.8	869.3	106.3	870.6	112.4	858.6	197.2
899.5	30.6	889.6	31.6	892.3	30.2	881.7	30.3
1103.0	31.2	1089.7	30.2	1092.9	25.5	1079.2	24.5
1167.6	21.1	1159.6	20.0	1146.5	21.0	1138.2	20.2
1206.8	0.6	1199.1	0.8	1197.2	0.4	1190.0	0.4
1441.5	7.4	1438.0	7.6	1415.4	6.4	1411.4	6.7
1498.6	8.2	1495.3	8.1	1489.3	9.7	1484.8	9.1
1501.9	5.0	1498.5	4.8	1492.4	6.6	1488.2	6.0
3101.2	6.4	3095.2	5.9	3121.7	1.7	3116.3	1.5
3211.9	2.6	3205.4	2.4	3232.6	3.9	3226.9	3.8
3225.9	0.3	3218.2	0.3	3246.4	0.3	3239.2	0.3

LiCl... CH_3NF_2				*LiBr... CH_3NF_2*			
MP2/6-311+G(3df,2p)		*MP2/Aug-cc-pVTZ*		*MP2/6-311+G(3df,2p)*		*MP2/Aug-cc-pVTZ*	
ν (cm^{-1})	IR intensities	ν (cm^{-1})	IR intensities	ν (cm^{-1})	IR intensities	ν (cm^{-1})	IR intensities
18.1	61.0	15.2	58.5	13.4	60.0	15.8	54.4
18.7	67.6	15.3	65.6	13.7	60.5	16.6	60.6
41.7	22.4	35.4	25.5	35.3	12.5	32.9	17.2
47.6	17.5	40.7	20.6	38.3	9.3	37.3	11.6
77.9	1.5	74.4	1.0	59.9	2.8	64.1	2.0
286.1	0.0	279.3	0.0	286.7	0.0	278.6	0.0
429.5	2.7	424.6	2.9	428.8	2.7	424.6	2.8
474.6	6.3	467.9	6.5	474.3	6.5	468.1	6.6
570.6	4.9	563.5	5.3	545.3	129.2	547.9	130.3
619.3	148.5	617.7	148.9	570.4	3.3	563.8	3.4
875.5	106.7	860.8	106.7	876.7	104.6	861.6	104.5
894.7	37.7	884.7	39.1	895.0	37.4	885.3	39.6
1095.8	29.3	1082.5	28.1	1096.3	30.5	1083.1	29.1
1157.1	22.7	1147.9	22.0	1158.7	23.3	1149.2	22.9
1200.8	0.4	1193.4	0.6	1201.3	0.5	1194.1	0.7
1429.2	8.9	1424.8	9.3	1431.9	10.2	1424.1	10.6
1492.3	7.0	1488.6	6.7	1493.0	6.3	1488.5	5.8
1495.8	4.5	1492.1	4.2	1496.6	3.9	1491.9	3.6
3110.8	3.7	3104.4	3.2	3107.0	4.7	3102.2	4.2
3222.0	2.1	3215.4	2.2	3218.3	1.8	3213.3	1.8
3234.8	0.1	3227.1	0.1	3230.8	0.1	3225.0	0.0

H_3N... CH_3NF_2				*H_3P... CH_3NF_2*			
MP2/6-311+G(3df,2p)		*MP2/Aug-cc-pVTZ*		*MP2/6-311+G(3df,2p)*		*MP2/Aug-cc-pVTZ*	
ν (cm^{-1})	IR intensities	ν (cm^{-1})	IR intensities	ν (cm^{-1})	IR intensities	ν (cm^{-1})	IR intensities
21.6	0.0	28.6	0.1	19.4	0.0	3.2	0.0
31.2	0.2	34.7	0.0	24.0	1.4	21.9	1.2
42.5	0.6	40.0	0.5	31.0	1.8	27.2	1.4
81.0	0.4	79.4	0.4	48.3	0.9	50.4	0.5
130.4	46.7	121.5	44.6	64.2	3.8	56.2	4.2
131.4	48.5	123.8	47.7	66.9	4.8	59.5	5.9
286.8	0.0	279.4	0.0	285.9	0.0	278.2	0.0
428.0	2.5	424.6	2.6	427.8	2.4	424.4	2.5
474.7	5.6	468.3	5.8	474.8	5.0	468.6	5.3
570.9	3.7	564.6	4.3	571.4	3.4	565.1	3.8
878.4	108.6	863.6	108.9	881.9	103.0	867.5	103.4
895.1	35.0	885.4	35.5	897.0	32.4	887.6	33.6
1069.5	166.7	1065.5	153.6	1021.1	28.7	1009.7	29.5
1098.4	27.2	1085.0	25.7	1100.9	30.9	1087.6	29.8
1157.1	20.8	1150.3	19.7	1162.6	33.4	1155.2	32.3
1200.8	0.5	1194.3	0.4	1164.0	11.2	1157.3	11.5
1425.5	5.7	1422.7	5.9	1165.1	1.2	1158.3	1.1
1493.1	8.7	1489.9	8.3	1203.9	0.5	1197.4	0.6
1496.2	5.6	1493.0	5.1	1435.1	7.6	1430.2	7.8
1674.4	17.9	1669.8	15.6	1495.2	6.6	1492.1	6.3
1674.5	17.0	1670.0	14.8	1498.6	3.7	1495.3	3.6
3111.5	5.1	3105.7	4.7	2477.6	28.2	2474.2	29.6
3222.3	3.2	3216.3	3.0	2489.7	39.7	2487.7	40.4
3236.5	0.4	3228.8	0.4	2490.0	39.9	2488.0	40.9
3523.9	1.5	3498.2	1.7	3102.4	7.6	3096.8	7.1
3664.5	11.3	3642.2	10.5	3213.3	2.4	3207.5	2.3
3664.9	11.3	3642.7	10.5	3227.2	0.3	3220.5	0.2

A.VI.3. Population on bonded carbon, N_C, its energy E_C, dipolar polarization M_C, and volume V_C in different complexes and monomers calculated from AIM analysis. Δ represents the change in the properties on complex formation. All the properties are given in atomic units.

	N_C	E_C	$\|M_C\|$	V_C	ΔN_C	ΔE_C	$\Delta\|M_C\|$	ΔV_C
CH_3OH complexes								
CH_3OH	5.426	-37.5259	0.109	69.10	-	-	-	-
$H_2O\cdots CH_3OH$	5.428	-37.5529	0.079	65.65	0.002	-0.0270	-0.030	-3.44
$H_2S\cdots CH_3OH$	5.222	-37.2936	0.098	60.30	-0.204	0.2323	-0.011	-8.79
$HF\cdots CH_3OH$	5.222	-37.3213	0.115	60.01	-0.204	0.2323	0.006	-9.09
$HCl\cdots CH_3OH$	5.222	-37.2889	0.112	60.87	-0.204	0.2046	0.004	-8.22
$HBr\cdots CH_3OH$	5.222	-37.9601	0.109	60.53	-0.205	0.2370	0.000	-8.56
$ClF\cdots CH_3OH$	5.221	-37.3010	0.126	59.20	-0.205	0.2249	0.018	-9.89
$LiF\cdots CH_3OH$	5.233	-37.3339	0.063	59.36	-0.193	0.1919	-0.046	-9.74
$LiCl\cdots CH_3OH$	5.236	-37.9774	0.069	60.09	-0.190	-0.4515	-0.040	-9.00
$LiBr\cdots CH_3OH$	5.233	-37.3000	0.071	59.93	-0.193	0.2259	-0.038	-9.16
$H_3N\cdots CH_3OH$	5.223	-37.3322	0.089	59.86	-0.203	0.1937	-0.020	-9.24
$H_3P\cdots CH_3OH$	5.224	-37.2934	0.105	61.52	-0.202	0.2325	-0.004	-7.57
CH_3F complexes								
CH_3F	5.376	-37.5134	0.055	69.53	-	-	-	-
$H_2O\cdots CH_3F$	5.213	-37.3229	0.030	60.62	-0.163	0.1906	-0.025	-8.92
$H_2S\cdots CH_3F$	5.213	-37.2826	0.026	61.58	-0.163	0.2309	-0.029	-7.96
$HF\cdots CH_3F$	5.212	-37.3108	0.049	60.92	-0.164	0.2026	-0.006	-8.62
$HCl\cdots CH_3F$	5.212	-37.2768	0.046	61.50	-0.164	0.2366	-0.009	-8.04
$HBr\cdots CH_3F$	5.213	-37.2856	0.042	61.94	-0.163	0.2279	-0.013	-7.59
$ClF\cdots CH_3F$	5.208	-37.2832	0.062	60.16	-0.168	0.2303	0.007	-9.37
$LiF\cdots CH_3F$	5.225	-37.3269	0.019	60.13	-0.168	0.1866	-0.036	-9.41
$LiCl\cdots CH_3F$	5.229	-37.2979	0.005	61.18	-0.151	0.2156	-0.050	-8.35
$LiBr\cdots CH_3F$	5.228	-37.2951	0.001	61.42	-0.148	0.2184	-0.054	-8.11
$H_3N\cdots CH_3F$	5.214	-37.3286	0.012	60.90	-0.162	0.1848	-0.043	-8.64
$H_3P\cdots CH_3F$	5.214	-37.2819	0.022	61.98	-0.162	0.2315	-0.033	-7.56

Table.IV.S.4. Natural charges on atoms (q), charge transferred (ΔQ, e) and second order interaction energy for the corresponding donor-acceptor interaction, E^2 (l.p. ⟶ C-O anti-bonding) in kJ.mol^{-1}, for CH_3OH complexes.

at MP2/6-311+G(3df,2p)								
Complex	q(C)	q(H)	q(H)	q(H)	q(O)	q(H)	ΔQ	E^2[l.p. ⟶ (σ^* (C-O)]
CH_3OH	-0.091	0.1492	0.1283	0.1283	-0.7728	0.4581	-	-
$H_2O\cdots CH_3OH$	-0.087	0.1505	0.1297	0.1299	-0.7797	0.4551	-0.0014	2.6
$H_2S\cdots CH_3OH$	-0.089	0.1496	0.1288	0.1292	-0.7766	0.4568	-0.0011	2.4
$HF\cdots CH_3OH$	-0.0893	0.1482	0.1307	0.1307	-0.7775	0.4562	-0.001	1.5
$HCl\cdots CH_3OH$	-0.0904	0.1494	0.1297	0.1286	-0.7752	0.4573	-0.0007	2
$HBr\cdots CH_3OH$	-0.0907	0.149	0.1293	0.1292	-0.7749	0.4575	-0.0007	2
$ClF\cdots CH_3OH$	-0.0912	0.1518	0.1271	0.1275	-0.7739	0.457	-0.0018	2.3
$LiF\cdots CH_3OH$	-0.0847	0.1359	0.1365	0.1469	-0.7883	0.4514	-0.0022	3.6
$LiCl\cdots CH_3OH$	-0.0913	0.1344	0.1351	0.1495	-0.7832	0.4534	-0.0021	3
$LiBr\cdots CH_3OH$	-0.0907	0.1352	0.1353	0.1455	-0.7822	0.455	-0.0019	2.9
$H_3N\cdots CH_3OH$	-0.0861	0.1316	0.131	0.147	-0.7803	0.4551	-0.0017	3
$H_3P\cdots CH_3OH$	-0.0899	0.147	0.1303	0.1309	-0.7762	0.4571	-0.0009	1.9
at MP2/Aug-cc-pVTZ								
CH_3OH	-0.1115	0.152	0.1309	0.1309	-0.758	0.4558	-	-
$H_2O\cdots CH_3OH$	-0.1067	0.1529	0.1319	0.132	-0.7652	0.453	-0.0021	2.8
$H_2S\cdots CH_3OH$	-0.1094	0.1521	0.1314	0.1318	-0.7621	0.4545	-0.0016	3
$HF\cdots CH_3OH$	-0.1094	0.1523	0.1325	0.1325	-0.7631	0.4536	-0.0016	1.6
$HCl\cdots CH_3OH$	-0.1105	0.1521	0.1321	0.131	-0.7609	0.455	-0.0013	2.3
$HBr\cdots CH_3OH$	-0.1112	0.1525	0.1312	0.1316	-0.761	0.455	-0.0018	3.3
$ClF\cdots CH_3OH$	-0.1113	0.1547	0.129	0.1294	-0.7592	0.4546	-0.0027	2.2
$LiF\cdots CH_3OH$	-0.1034	0.1382	0.1388	0.1492	-0.7747	0.4492	-0.0027	3.6
$LiCl\cdots CH_3OH$	-0.1108	0.1366	0.1372	0.1516	-0.7693	0.4511	-0.0036	3.1
$LiBr\cdots CH_3OH$	-0.1119	0.1371	0.1371	0.1504	-0.7686	0.4518	-0.004	3.9
$H_3N\cdots CH_3OH$	-0.1059	0.134	0.134	0.149	-0.766	0.453	-0.0019	2.8
$H_3P\cdots CH_3OH$	-0.1137	0.1474	0.1333	0.1356	-0.7591	0.4559	-0.0006	1.8

Table.IV.S.5. Natural charges on different atoms (q), charge transferred (ΔQ, e) and second order interaction energy for the corresponding donor-acceptor interaction, E^2 (l.p. –> C-F anti-bonding) in kJ.mol^{-1}, for CH_3F complexes.

Complex	q(C)	q(F)	q(H)	q(H)	q(H)	ΔQ	E^2[l.p. —> σ^* (C-F)]
at MP2/6-311+G(3df,2p)							
CH_3F	0.0428	-0.4371	0.1314	0.1314	0.1314	-	-
$H_2O\cdots CH_3F$	0.0463	-0.4471	0.1323	0.1318	0.1347	-0.002	3.6
$H_2S\cdots CH_3F$	0.0441	-0.4424	0.1323	0.1327	0.1316	-0.0017	3.3
$HF\cdots CH_3F$	0.0441	-0.4438	0.1336	0.1336	0.1311	-0.0014	2.3
$HCl\cdots CH_3F$	0.0428	-0.4404	0.1335	0.1315	0.1318	-0.0009	2.8
$HBr\cdots CH_3F$	0.0427	-0.4401	0.1329	0.1306	0.1329	-0.001	2.5
$ClF\cdots CH_3F$	0.0425	-0.4396	0.134	0.1306	0.1306	-0.002	3.3
$LiF\cdots CH_3F$	0.0502	-0.4601	0.1354	0.1355	0.1356	-0.0035	5.9
$LiCl\cdots CH_3F$	0.0418	-0.4523	0.1353	0.1361	0.1362	-0.0029	4.1
$LiBr\cdots CH_3F$	0.0404	-0.4499	0.1355	0.1358	0.1349	-0.0033	3.6
$H_3N\cdots CH_3F$	0.048	-0.4485	0.1326	0.1326	0.1326	-0.0027	5.1
$H_3P\cdots CH_3F$	0.0445	-0.4426	0.1322	0.1322	0.1321	-0.0016	2.8
at MP2/Aug-cc-pVTZ							
CH_3F	0.0194	-0.4249	0.1352	0.1352	0.1352	-	-
$H_2O\cdots CH_3F$	0.0243	-0.4353	0.1354	0.135	0.138	-0.0026	3.6
$H_2S\cdots CH_3F$	0.0208	-0.4308	0.1357	0.1366	0.1355	-0.0023	4
$HF\cdots CH_3F$	0.0218	-0.4318	0.1368	0.1368	0.1346	-0.0018	2.5
$HCl\cdots CH_3F$	0.0195	-0.4284	0.1371	0.1351	0.1352	-0.0015	3.1
$HBr\cdots CH_3F$	0.0185	-0.4287	0.1368	0.1343	0.1369	-0.0022	4.1
$ClF\cdots CH_3F$	0.0201	-0.4277	0.1376	0.1337	0.1337	-0.0026	2.9
$LiF\cdots CH_3F$	0.0294	-0.4493	0.1386	0.1387	0.1388	-0.0038	5.6
$LiCl\cdots CH_3F$	0.0411	-0.4536	0.136	0.1368	0.1369	-0.0029	4.1
$LiBr\cdots CH_3F$	0.0178	-0.4396	0.1391	0.1393	0.1384	-0.005	4.9
$H_3N\cdots CH_3F$	0.0256	-0.4369	0.1361	0.1361	0.1361	-0.0029	4.9
$H_3P\cdots CH_3F$	0.0211	-0.4309	0.1359	0.1359	0.136	-0.002	3.5

Chapter V.

Propargyl Alcohol Dimer: Rotational Spectra and AIM Analysis.

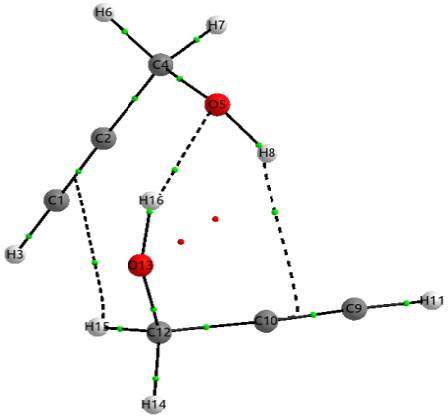

V.1. Introduction

Propargyl alcohol (PA) contains a hydroxyl group and acetylenic group and can form weakly bound complexes with other molecules/atoms. As we discussed in the *Chapter III*, the rotational spectra of the Ar•••g-PA complex[1] affirm a structure in which Ar interacts with both the hydroxyl and acetylenic groups of PA. Moreover, the *ab-initio* and AIM analysis of the Ar•••t-PA complex revealed the presence of a unique Ar•••C interaction which led us to the carbon bond[2], which has been discussed in the *Chapter IV*.

Since both the groups, hydroxyl and acetylenic, of the PA molecule can act as hydrogen bond acceptors as well as hydrogen bond donors, hydrogen bonded complexes of the PA molecule offer many different possibilities. If the other interacting entity is also multifunctional then the number of dimers will increase many fold and the resulting complex will have several local minima.

Microwave spectroscopy carried out in molecular beams has been used to explore the presence of different conformers of molecules and different possible minima of weakly bound complexes[3]. However, cooling due to the supersonic expansion often populates only few, the most stable, conformers. Sometimes, varying the stagnation pressure and changing the carrier gas, may help in stabilization of the other conformers as well and depending on their concentration in the molecular beam, these species can also be identified experimentally. Comparison of the experimental rotational constants of different isotopologues of the species under study, with the *ab initio* calculated rotational constants usually provides ample information to distinguish different conformers/structures. At the same time these comparisons also provide a test for the reliability of the different *ab initio* methods. Methanol•••water is one of the most interesting hetero-dimer solved via rotational spectroscopy. In the complex both methanol and water can act as hydrogen bond acceptor as well as hydrogen bond donor. Calculations at some levels of theory predicted that the structure in which methanol acts as hydrogen bond donor is more stable while at other levels of theory the structure in which water acts as the hydrogen bond donor was predicted to be more stable and thus the results of these calculations were ambiguous[4-7]. Microwave spectrum in molecular beam deterministically revealed that the complex in which water acts as hydrogen bond donor is more stable[8]. Later high level *ab initio* calculations could also predict this structural preference.[9] Other interesting dimer

solved by MW spectroscopy is the benzene-dimer, for which the potential energy surface is very shallow. The *ab initio* calculations predict three minima for the dimer, parallel displaced, pi-stacked and T-shaped. Rotational spectrum led to the unambiguous identification of the T-shaped structure and the intermolecular distance was very similar to that found in the solid.[10] Other structures could not be probed by microwave spectroscopy since they have no-permanent dipole moment.

Many other homo and hetero molecular complexes bound with O-H•••O, O-H•••π and C-H•••π interactions have been identified by microwave spectroscopy in molecular beams. The $(CH_3OH)_2$ and CH_3OH•••H_2O complexes were found to be bound with O-H•••O hydrogen bonds.[8,11] The C_6H_6•••H_2O complex[12] was found to be bound with O-H•••π hydrogen bond. The $(C_6H_6)_2$ dimer[10] and C_6H_6•••C_2H_4 complex[13] were found to be bound with C-H•••π interactions. Since PA molecule contains all the three groups, namely O-H, C-H and π-electron density, all three interactions can be present in the PA-dimer. As shown in the upcoming sections, due to the possibility of PA monomer existing in two different conformers, gauche and trans, and due to the presence of multiple hydrogen bond acceptor and hydrogen-bond donor groups, several structures are possible for the PA-dimer. We report here microwave spectra of the most stable PA-dimer and its two mono-deuterated and one bi-deuterated isotopologues for the first time. The AIM analysis shows that the observed dimer is bound by O-H•••O, O-H•••π and C-H•••π interactions.

V.2. Theoretical and Experimental details

V.2.a. Theoretical methods

Gaussian 09 software suite[14] was used to perform all the optimization and frequency calculations on the complexes. The optimization and frequency calculations were performed using *ab initio* Møller-Plesset second order perturbation theory (MP2) with 6-311+G(3df,2p) basis sets. For all the optimized geometries, BSSE correction was done using Boys and Bernardi's counterpoise method[15]. AIMALL and AIM2000 software suites[16,17] were used to perform the Atoms in Molecules *(AIM)* analysis. The wave functions for the *AIM* analysis were extracted from the Gaussian calculations at MP2/6-311+G (3df,2p) level.

V.2.b. Experimental Section

Pure rotational spectra of PA-dimer was observed using the home-built PN-FTMW spectrometer.[18] The details of the spectrometer have been discussed in *Chapter II*. Helium was used as the carrier gas instead of argon to avoid formation of unwanted complexes with argon. The gas was expanded from a high back pressure of 1.5-2.0 bar into the vacuum chamber which led to the formation of the PA-dimer in the molecular beams. Microwave pulse of 1μs duration was used and a total of 15 FIDs were collected per gas pulse during the search for the rotational transitions. The observed PA-dependent signals were reasonably strong and therefore, a total of 500-700 gas pulses were averaged in the scanning mode. A total of 256 points were sampled during the data acquisition. Once a signal was observed, it was re-sampled with 1024 or 2048 points for better resolution. The optimum microwave pulse durations for the *a-, b-* and *c-* type transitions were found to be 0.4 μs, 0.4 μs and 1.3 μs respectively. The OD isotopologue of PA was formed by simple mixing of PA and D_2O in 9:4 ratio.

V.3. Geometry optimization; search, assignment and fitting of the rotational spectra

V.3.a Geometry optimization

Exploration of the potential energy surface (PES) of weakly bound complexes comprised of multifunctional molecules is not straight forward since many local minima can exist for such complexes. Electrostatic calculations are often useful in locating the points of interactions in the monomer entities. Legon-Millen rules,[19] can be handy in choosing the starting geometries for geometry optimization. These rules were derived from the analysis of several microwave studies and are based on electrostatic interaction between two interacting molecules. Structures for the PA-dimer were optimized starting with geometries in which O-H•••O hydrogen bonds were given the most importance. Possibility of the stabilization of the t-PA conformer on complexation was also taken into account. The starting geometries taken for the optimization of the dimer can be classified into following three groups:

(i) g-PA-dimer

(ii) t-PA (donor) ••• g-PA (acceptor) and g-PA (donor)••• t-PA (acceptor)

(iii) t-PA dimer

Optimizations were done starting with different geometries taken according to the above mentioned possibilities. Seven different structures could be located for the PA-dimer, *Figure V.1*. Each of the seven structures was confirmed to be a minimum on the PES by confirming the presence of all real frequencies for the normal modes of vibration. In the *Structures 1 to 5*, both the PA units are in gauche form. In the *Structure 6*, one PA unit is in gauche form and the other is in trans form whereas in the *Structure 7*, both the units are in trans form. For all the structures, BSSE corrected *(ΔE_{BSSE})* and BSSE+ zero-point corrected *($\Delta E_{BSSE+ZPC}$)* interaction energies are given in *Table V.1*. Interaction energies of these structures are comparable. However, *Structure 1* is the most stable one amongst all the structures. Geometrical parameters for the anticipated hydrogen bonding interactions in these different structures are given in the *Table V.2*. All the angles and distances are within the accepted range for these interactions.[20] AIM analysis reported later, confirms the presence of these interactions. It should be noted that many other structures are possible for the dimer e.g. structures in which acetyenic group of one of the units acts as the hydrogen bond donor and hydroxyl group of the other unit acts as the hydrogen bond acceptor. However, these structures are less stable as compared to the structures considered here and thus, are less likely to be found. For the seven structures, rotational constants and dipole moment components along the principal axes *a, b and c* are given in the *Table V.3*. These calculated rotational constants were used to predict the rotational spectra for all the seven structures. The predicted spectra served as an aid to the experimental search of the rotational transitions.

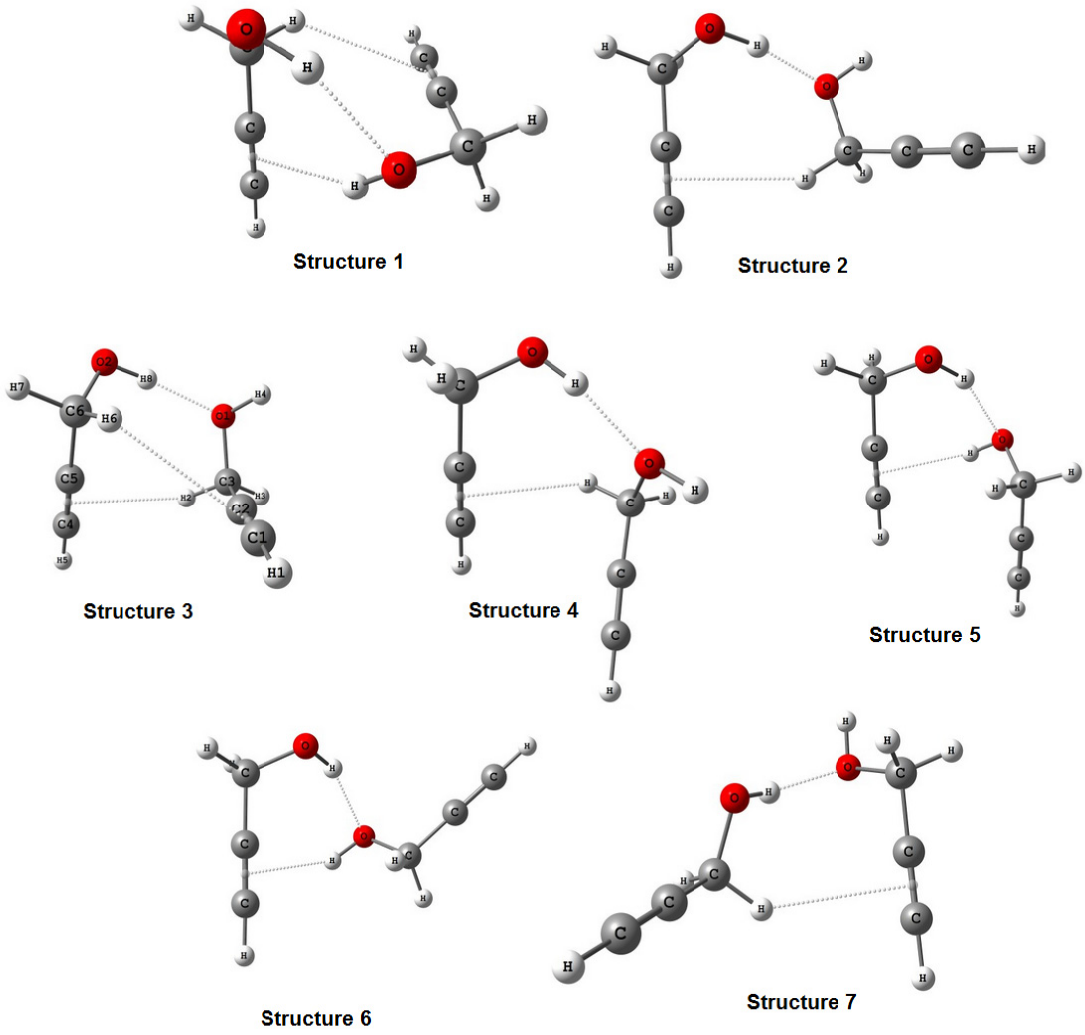

Figure V.1. Optimized structures for the PA-dimer at MP2/6-311+G(3df,2p) level. Structure 1 to 5 are for g-PA dimer, Structure 6 is for t-PA●●●g-PA dimer and Structure 7 is for t-PA dimer.

Table V.1. BSSE corrected and BSSE+Zero-point corrected interaction energies for the different structures of PA-dimer.

	ΔE_{BSSE} ($kJ.mol^{-1}$)	$\Delta E_{BSSE+ZPC}$ ($kJ.mol^{-1}$)
Structure 1	31.6	25.6
Structure 2	26.6	21.6
Structure 3	27.8	22.6
Structure 4	27.7	23.0
Structure 5	30.8	24.6
Structure 6	30.9	24.8
Structure 7	27.0	21.5

Table V.2. Parameters for the different possible hydrogen bonding interactions in the optimized structures of PA-dimer.

	O-H•••O		O-H•••π		C-H•••π		C-H•••π	
	r(H…O) (Å)	∠O-H-O (degree)	r (H…π) (Å)	∠O-H-π (degree)	r(H…π) (Å)	∠C-H-π (degree)	r(H…π) (Å)	∠C-H-π (degree)
Structure 1	1.957	155.2	2.286	145.9	2.930	125.2	-	-
Structure 2	1.871	169.7	-	-	2.724	150.0	-	-
Structure 3	1.899	170.7	-	-	2.800 (H2... π)	126.9 (C3-H2-π)	3.049 (H6... π)	123.6 (C6-H6- π)
Structure 4	1.871	164.0	-	-	2.811	118.2	-	-
Structure 5	1.947	154.7	2.424	131.2	-	-	-	-
Structure 6	1.955	152.3	2.359	139.2	-	-	-	-
Structure 7	1.924	155.9	-	-	2.860	133.3	-	-

Table V.3. Rotational constants and dipole moment components along the principal axes for different the possible structures of PA-dimer, optimized at MP2/6-311+G(3df,2p) level.

	Structure 1	*Structure 2*	*Structure 3*	*Structure 4*	*Structure 5*	*Structure 6*	*Structure 7*
A/MHz	2286.1	2828.0	2165.5	2760	3247.7	3373.6	3056.5
B/ MHz	1234.4	934.5	1317.2	1186	1099.9	996.5	925.0
C/ MHz	1209.1	832.3	1106.2	887	882.0	828.8	770.7
$\lvert\mu_a\rvert$/D	1.8	2.1	3.2	2.9	0.9	1.0	2.6
$\lvert\mu_b\rvert$/D	1.5	0.9	1.6	0.5	2.0	0.1	0.2
$\lvert\mu_c\rvert$/D	2.1	1.8	0.4	1.1	0.3	2.2	0.2

V.3.b. Search, assignments and fitting of the rotational spectra

While searching for the Ar•••PA transitions, many other transitions were observed which depended only on PA concentration. These transitions could not be fit with the PA-monomer transitions and thus we anticipated that these transitions could be due to some higher clusters of PA like PA-dimer/trimer etc. The *ab initio* rotational

constants were used to predict the spectra for the different structures of PA-dimer. In the 8-10 GHz range, *a*-type transitions were predicted for these different structures and thus this region was selected to start the search. During the search three very strong transitions were observed at 9101.8119, 9049.0136 and 9096.8586 MHz. The signal at 9049.0136 MHz was the strongest signal and signals at 9101.8119 and 9096.8586 MHz were slightly weaker and had similar intensities. Considering the signal at 9049.0136 MHz as an *a*-type K_a=0 transitions for a particular J value, next corresponding transition was searched for different combinations of J values. Very soon a very strong transition at 11367.6588 MHz was observed. The difference between the transition at 9049.0136 MHz and the transition at 11367.6588 MHz was close to the predicted difference between the $3_{0,3}$-$4_{0,4}$ and $4_{0,4}$-$5_{0,5}$ transitions for the *Structure 1* as well as for the *Structure 3* . Considering transition at 9049.0136 MHz as $3_{0,3}$-$4_{0,4}$ (*a*-type) transition and transition at 11367.6588 MHz as $4_{0,4}$-$5_{0,5}$ (*a*-type) transition other *a*-type transitions were searched and were observed immediately. Once all the *a*-type transitions were collected, the *b*- and *c*-type transitions were searched and were observed. A total of 51 transitions out of all observed transitions, could be fitted with a semi-rigid rotor asymmetric top Hamiltonian. The transitions and their residues are given in the *Table V.4*. No splitting was observed in any of these transitions. The rotational and distortion constants obtained from the fitting of these 51 transitions are given in the *Table V.5*.

The experimental rotational constants are closer to the *Structure 1 and Structure 3* and are significantly different from other structures. Both the Structures were scaled to the experimental rotational constants and these scaled geometries were used to predict the spectra for deuterium substituted species. There are three possible -OD isotopologues (i) H-8 as D (ii) H-16 as D (iii) H-8 and H-16 both as D. The predicted rotational constants for these species on the basis of the scaled geometries are given in the *Table V.6*. The labelling of atoms is shown in the *Figure V.2*.

Table V.4. Experimentally observed rotational transitions and their assignments for the PA-dimer. Residues from the fit are also given.

$J\ K_{-1}\ K_{+1}$	$J\ K_{-1}\ K_{+1}$	*Frequency (MHz)*	*Residue (MHz)*	*Type*
2 1 2	1 1 1	4525.0904	0.0026	*a*
2 0 2	1 0 1	4550.2612	0.0003	*a*
2 1 1	1 1 0	4576.2612	0.0011	*a*
3 0 3	2 1 1	5601.3099	0.0078	*c*
2 1 2	1 0 1	5696.4442	-0.0001	*b*
2 1 1	1 0 1	5773.2026	-0.0013	*c*
3 1 3	2 1 2	6787.2685	0.0018	*a*
3 0 3	2 0 2	6824.2441	-0.0010	*a*
3 2 2	2 2 1	6825.9070	-0.0010	*a*
3 2 1	2 2 0	6827.5363	-0.0005	*a*
3 1 2	2 1 1	6864.0172	0.0014	*a*
4 0 4	3 1 2	7834.1436	-0.0013	*c*
3 1 3	2 0 2	7933.4491	-0.0011	*b*
4 0 4	3 1 3	7987.6514	-0.0022	*b*
5 1 4	4 2 3	8012.6465	-0.0007	*b*
3 1 2	2 0 2	8086.9612	0.0024	*c*
2 2 1	1 1 0	8090.3430	0.0014	*b*
2 2 0	1 1 0	8090.7486	-0.0004	*c*
2 2 0	1 1 1	8116.3340	-0.0023	*b*
4 2 3	3 2 2	9100.6989	0.0002	*a*
4 2 2	3 2 1	9104.7685	0.0032	*a*
4 3 2	3 3 1	9101.7826	-0.0050	*a*
4 3 1	3 3 0	9101.8119	0.0008	*a*
4 1 4	3 1 3	9049.0136	0.0003	*a*
4 0 4	3 0 3	9096.8586	0.0000	*a*
4 1 3	3 1 2	9151.3160	-0.0009	*a*
6 1 6	5 2 3	9810.4390	0.0031	*b*
5 0 5	4 1 3	10050.4868	0.0000	*c*
5 0 5	4 1 4	10306.2977	-0.0014	*b*
3 2 2	2 1 1	10339.9928	0.0033	*b*
3 2 1	2 1 1	10342.0246	-0.0011	*c*
4 1 3	3 0 3	10414.0309	0.0003	*c*
3 2 1	2 1 2	10418.7855	0.0002	*b*
4 1 4	3 0 3	10158.2185	0.0002	*b*
5 1 5	4 1 4	11310.1924	0.0000	*a*
5 0 5	4 0 4	11367.6588	0.0000	*a*
5 2 4	4 2 3	11375.0490	-0.0019	*a*
5 4 1	4 4 0	11376.7770	0.0009	*a*
5 4 2	4 4 1	11376.7770	0.0012	*a*
5 2 3	4 2 2	11383.1636	0.0007	*a*
5 3 3	4 3 2	11377.2647	-0.0004	*a*
5 3 2	4 3 1	11377.3477	0.0006	*a*

Table V.4 (continued)

5 1 4	4 1 3	11438.0039	0.0011	*a*
5 1 5	4 0 4	12371.5539	0.0018	*b*
4 2 3	3 1 2	12576.6710	-0.0015	*b*
6 0 6	5 1 5	12632.3367	0.0027	*b*
4 2 2	3 1 3	12736.2806	-0.0033	*b*
3 3 1	2 2 0	12746.5296	-0.0011	*b*
3 3 0	2 2 0	12746.5296	-0.0050	*c*
3 3 1	2 2 1	12746.9447	0.0066	*c*
5 1 4	4 0 4	12755.1770	0.0023	*c*

Table V.5. Experimental rotational and distortion constants for the PA-dimer.

A /MHz	2321.83350(42)
B /MHz	1150.47741(21)
C /MHz	1124.88979(16)
D_J */kHz*	1.8422(31)
D_{JK} */kHz*	0.375(11)
D_K */kHz*	-0.982(40)
d_1 */kHz*	-0.0457(27)
d_2 */kHz*	-0.1498(22)
σ*/kHz*	2.5
# transitions	51

Table V.6. Predicted rotational constants for the three deuterated (OD) species of PA-dimer. Scaled geometries of Structure 1 and Structure 3 to the experimental rotational constants of the parent PA-dimer were used for these predictions.

Rotational constants	*On the basis of scaled structure 1*			*On the basis of scaled structure 3*		
	H-8 as D	*H-16 as D*	*H-8 and H-16 both as D*	*H-8 as D*	*H-16 as D*	*H-8 and H-16 both as D*
A/MHz	2303.2	2297.2	2278.9	2293.1	2302.3	2274.2
B/MHz	1147.2	1147.9	1144.2	1141.9	1149.0	1140.5
C/MHz	1123.5	1118.9	1118.0	1110.0	1119.0	1104.3

Rotational spectra were predicted on the basis of these rotational constants. For the search of transitions corresponding to the mono-deuterated isotopologues, helium was flown through two different bubblers which contained the pure PA sample and the PA-D(OD) sample respectively whereas for the search of transitions corresponding to the bi-deuterated isotopologue helium was flown only through the PA-D (OD) bubbler. Three sets of rotational transitions corresponding to the three isotopologues were observed readily. The transitions are given in *Table V.7, V.8 and V.9* for the H-8 as D, H-16 as D and H-8 and H-16 both as D species respectively. For the H-8 as D

species a total of 14, for the H-16 as D species a total of 19 and for the H-8 and H-16 both as D a total of 17 lines were observed and fitted within experimental uncertainty. The fitted rotational and distortion constants for all three species are given in the *Table V.10*. The uncertainty in the fit was increasing on including D_K in the fit. Therefore, D_K was kept constant to the value for the parent dimer (1.00 MHz) in the fitting of spectra for each of the three isotopologues.

Table V.7. Experimentally observed rotational transitions and their assignments for mono deuterated isotopologue of PA-dimer (H-8 as D). Residues from the fit are also given.

$J\ K_{-1}\ K_{+1}$	$J\ K_{-1}\ K_{+1}$	*Frequency (MHz)*	*obs -cal (MHz)*
3 1 3	2 1 2	6801.512	0.0030
3 0 3	2 0 2	6828.098	-0.0050
3 1 2	2 1 1	6856.137	0.0006
4 1 4	3 1 3	9068.237	-0.0006
4 0 4	3 0 3	9102.9418	-0.0001
4 2 3	3 2 2	9104.9295	-0.0009
4 2 2	3 2 1	9107.0125	0.0013
4 1 3	3 1 2	9141.06	0.0021
4 1 4	3 0 3	10178.2245	0.0000
5 1 5	4 1 4	11334.593	0.0007
5 0 5	4 0 4	11376.7613	0.0001
5 2 4	4 2 3	11380.595	-0.0001
5 2 3	4 2 2	11384.749	-0.0012
5 1 4	4 1 3	11425.5832	-0.0001

Table V.8. Experimentally observed rotational transitions and their assignments for mono-deuterated isotopologue of PA-dimer(H-16 as D). Residues from the fit are also given.

$J\ K_{-1}\ K_{+1}$	$J\ K_{-1}\ K_{+1}$	*Frequency (MHz)*	*obs -cal (MHz)*
2 1 1	1 0 1	5748.995	-0.0007
3 1 3	2 1 2	6749.679	-0.0055
3 0 3	2 0 2	6797.907	-0.0005
3 1 2	2 1 1	6851.091	0.0018
3 1 3	2 0 2	7864.025	0.0043
4 0 4	3 1 3	7994.144	0.0013
4 1 4	3 1 3	8998.544	-0.0008
4 0 4	3 0 3	9060.247	-0.0095
4 2 3	3 2 2	9067.065	0.014
4 2 2	3 2 1	9074.314	0.008
4 1 3	3 1 2	9133.683	-0.0103
4 1 4	3 0 3	10064.66	-0.0021
5 0 5	4 1 4	10315.15	0.0041
5 1 5	4 1 4	11246.55	-0.0021
5 0 5	4 0 4	11319.56	0.004
5 2 4	4 2 3	11332.59	-0.0098
5 2 3	4 2 2	11347.03	-0.0068
5 1 4	4 1 3	11415.34	0.0065
5 1 5	4 0 4	12250.95	0.0038

Table V.9. Experimentally observed rotational transitions and their assignments for bi-deuterated isotopologue of PA-dimer (H-8 and H-16 both as D). Residues from the fit are also given.

$J\ K_{-1}\ K_{+1}$	$J\ K_{-1}\ K_{+1}$	*Frequency (MHz)*	*obs -cal (MHz)*
3 1 3	2 1 2	6764.8930	-0.0016
3 0 3	2 0 2	6802.1560	-0.0008
3 2 2	2 2 1	6803.9150	0.0000
3 2 1	2 2 0	6805.6330	-0.0010
3 1 2	2 1 1	6842.3510	-0.0094
2 2 1	1 1 1	7992.9680	0.0025
4 0 4	3 1 3	7994.1390	-0.7342
4 1 4	3 1 3	9019.1860	0.0162
4 0 4	3 0 3	9067.3170	-0.0018
4 2 3	3 2 2	9071.3630	-0.0005
4 2 2	3 2 1	9075.6600	0.0053
4 1 3	3 1 2	9122.4200	-0.0051
5 0 5	4 1 4	10306.3045	0.0074
5 1 5	4 1 4	11272.8660	-0.0012
5 0 5	4 0 4	11330.5803	-0.0135
5 2 3	4 2 2	11346.9195	-0.0024
5 1 4	4 1 3	11401.8630	0.0051

Table V.10. Experimental rotational and distortion constants for the two mono and one bi deuterated isotopologues of PA-dimer.

Constants	*H-8 as D*	*H-16 as D*	*H-8 and H-16 both as D*
A /MHz	2301.8767(51)	2297.8207(52)	2282.0237(32)
B /MHz	1147.29807(87)	1150.4122(13)	1146.9285(19)
C /MHz	1129.08541(85)	1116.6032(14)	1121.1011(21)
D_J /kHz	1.7851(72)	1.826(20)	1.764(25)
D_{JK} /kHz	0.233(51)	0.40(14)	-0.21(18)
D_K /kHz	-1.00	-1.00	-1.00
d_1 /kHz	-0.042(10)	-0.059(17)	-0.054(25)
d_2 /kHz	-0.1130(33)	-0.174(10)	-0.118(17)
σ/kHz	2.5	7.9	8.7
#transitions	14	19	17

V.4. Structure of the PA-dimer

Comparison of the observed rotational constants with the calculated rotational constants gives a meaningful insight into the structure of the dimer. The observed rotational constants for the parent dimer are close to the *Structure 1* and *Structure 3* and are very different from other optimized structures and thus structures other than 1 and 3 can be excluded. The observed A and B rotational constants are closer to the calculated A and B rotational constants for the *Structure 1* while C rotational constant is closer to the calculated C rotational constant for the *Structure 3*, see *Table V.3* and *Table V.5*. Isotopic substitution of hydrogen by deuterium provides more information about the structure. The observed constants for the two mono deuterated (either H-8 or H-16 as D) and one bi-deuterated (H-8 and H-16 both as D) are closer to the predicted constants on the basis of *Structure 1* as compared to *Structure 3,* see *Table V.6* and Table *V.10*, and hence the observed spectra is more likely to be corresponding to the *Structure 1*. In the *Figure V.2*, principal axes systems for the *ab initio* optimized *Structure 1* and *Structure 3* are shown.

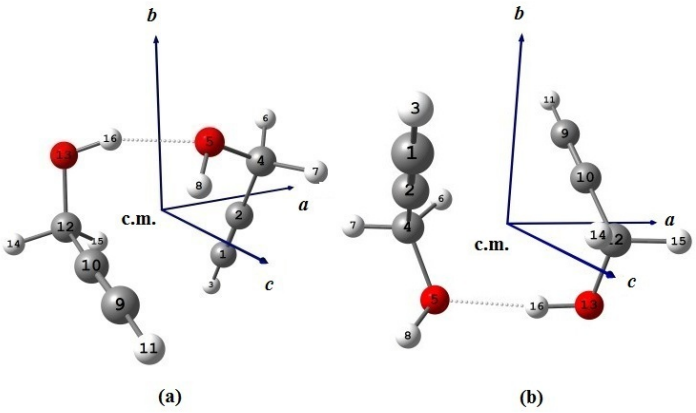

Figure V.2. Principal axes system for the ab initio optimized (a) Structure 1 and (b) Structure 3 of the PA-dimer.

In the *Structure 1*, H8 is close to the *c*-axis while in the *Structure 3* it is much far away. Thus the substitution of H-8 by D would change the C rotational constant much more significantly in *Structure 3* than in *Structure 1*, as predicted by the calculations, *Table V.6*. However, the experimental C rotational constant for the isotopologue in which H-8 is substituted by D is not very different from that of the parent dimer. This gives another indication that the observed structure is closer to the *Structure 1*.

Kraitchman analysis can be used to locate the position of the substituted atom. The

difference in the rotational constants of the different isotopologues depends on the position of the substitution. Thus the observed rotational constants of the different isotopologues can be used to locate the coordinates of the substituted atom which in turn gives the distance of the substitution from the centre of mass (c.m.) of the complex. Using this analysis distances of H8 and H16 atoms from the centre of mass of the complex were calculated and are given in the *Table V.11*. The table also gives *ab initio* calculated distances for these atoms from the centre of mass for the *Structure 1* and *Structure 3*.

Table V.11. Centre of mass to H-8 and H-16 atom distances for the Structure 1 and Structure 3. Experimental values as well as the ab initio calculated values at MP2/6-311+G(3df,2p) level are given.

	c.m. to H-8 distance (Å)	*c.m. to H-16 distance (Å)*
Experimental values	0.8482±0.0031	1.6806±0.0016
Structure 1	1.3509	1.6829
Structure 3	2.5840	1.7261

These values again put weight in favor of the *Structure 1* since both the distances are close to the calculated values for this structure. It should be noted that the values obtained experimentally are zero-point averaged distances and not the equilibrium distances. Moreover, the H16 distance from the centre of mass is closer to the calculated value as compared to the H8 distance in *Structure 1*. This is because H16 is involved in the H-bonding and thus is more localized in the complex as compared to the H-8.

V.5. Atoms in molecules (AIM) theoretical analysis:

Once the structure was confirmed, the AIM calculations were performed to explore the nature and strength of the intermolecular interactions present in the PA-dimer. The analysis was performed on all the structures of PA-dimer. However, results for only *Structure 1* are discussed here since it is the closest structure to the experimental data. Results for the other structures are summarized in the *Supplementary Information* given at the end of the chapter. Wave-function for the analysis was extracted from the Gaussian calculations at MP2/6-311+G(3df,2p) level.

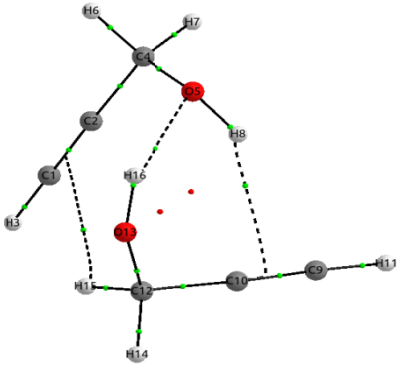

Figure V.3. Electron density topology for the Structure 1 of PA-dimer. Bond critical points are shown in green and ring critical points in red. The intermolecular bond paths are shown by dashed lines.

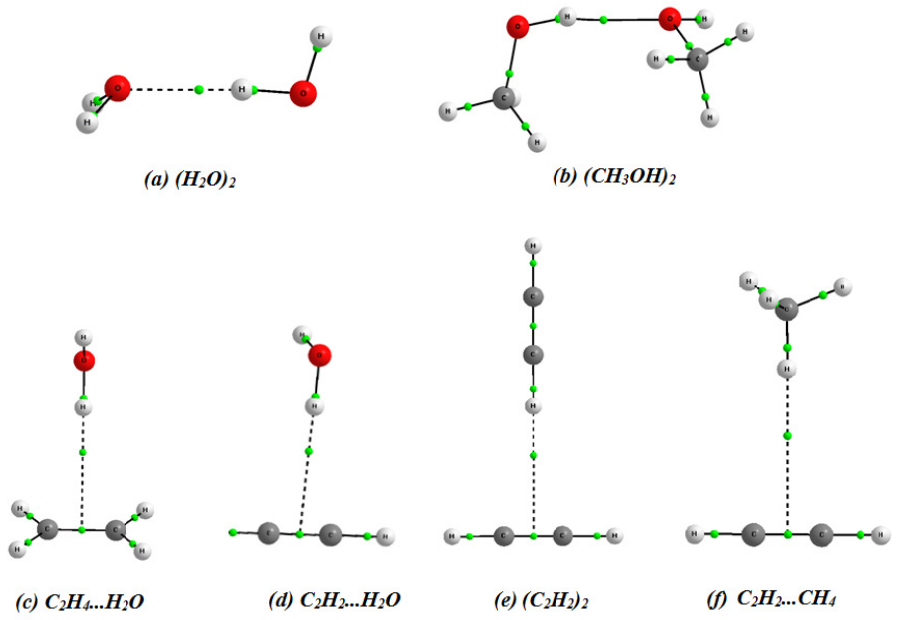

Figure V.4. Electron density topology for different O-H●●●O, O-H●●●π and C-H●●●π bonded dimers. The wave functions used in these calculations were of the optimized geometries at MP2/6-311+G(3df,2p) level. BCPs are shown in green and the intermolecular bond paths are shown with dashed lines.

The electron density topology resulting from the AIM analysis is shown in *Figure V.3*. There are three intermolecular bond critical points (BCPs) and two corresponding ring critical points (RCPs) present in the dimer. The BCPs are present between O-H and O, O-H and π-electron density and C-H and π-electron density. Each intermolecular BCP is linked by the interacting atoms/groups by the corresponding bond paths. Thus, the topology confirms the presence of O-H•••O, O-H•••π and C-H•••π intermolecular interactions in the dimer. The electron density and Laplacian of electron density values for these interactions in the dimer are given in *Table V.12*.

Table V.12. Electron density, ρ(r), and Laplacian of electron density, $\nabla^2\rho(r)$, values at intermolecular BCPs present in the PA-dimer. The wave function for the optimized geometry at MP2/6-311+G(3df,2p) level was used.

Contact	*ρ(r) in a.u.*	*$\nabla^2\rho(r)$ in a.u.*
O-H•••O	0.0233	0.0921
O-H•••π	0.0156	0.0501
C-H•••π	0.0058	0.0166

The positive values of the Laplacian indicate that these interactions are closed shell interactions. The ρ(r) and $\nabla^2\rho(r)$ values are within the range defined by Koch and Popelier[21] for the C-H•••O hydrogen bonds. Also, in the case of hydrogen bonds the electron density is linearly correlated to the bond strength[21] and thus the electron density can be used to predict the strength of a typical hydrogen bond. The electron density values at the BCPs suggest that OH•••O hydrogen bond is strongest and the C-H•••π hydrogen bond is weakest in the PA-dimer.

It will be worthwhile to compare these interactions with the similar interactions present in other complexes. We chose O-H•••O hydrogen bonded $(H_2O)_2$ and $(CH_3OH)_2$ dimers, C-H•••O hydrogen bonded C_2H_4•••H_2O and C_2H_2••• H_2O dimers and C-H•••π hydrogen bonded $(C_2H_2)_2$ and C_2H_2•••CH_4 dimers for the comparisons. All these dimers were optimized at the same MP2/6-311+G(3df,2p) level and the wave functions extracted from these calculations were used to perform the *AIM* calculations. The calculated topologies for these dimers are shown in the *Figure V.4*.

The ρ(r) and $\nabla^2\rho(r)$ values at the intermolecular BCPs present in these dimers are given in the *Table V.13*. For the sake of comparison, values for the PA dimer structure have also been included. Electron density values suggest that the O-H•••O interaction in the PA-dimer is slightly stronger than that in $(H_2O)_2$ and slightly weaker than that

in the $(CH_3OH)_2$. The O-H•••π interaction in the dimer is stronger than that in the C_2H_4•••H_2O and C_2H_2••• H_2O complexes. The C-H•••π interaction in the PA-dimer is much stronger than the C_2H_2•••CH_4 and slightly weaker than the $(C_2H_2)_2$ dimer.

Table V.13. Electron density ρ(r) and Laplacian of electron density ∇2ρ(r) values at the intermolecular BCPs of different complexes.

Contact	*Complex*	*ρ(r) in a.u.*	*$\nabla^2\rho(r)$ in a.u.*
OH•••O	PA-dimer	0.0233	0.0921
	$(H_2O)_2$	0.0215	0.096
	$(CH_3OH)_2$	0.0256	0.1018
OH•••π	PA-dimer	0.0156	0.0501
	C_2H_4•••H_2O	0.0100	0.0291
	C_2H_2•••H_2O	0.0100	0.0324
CH•••π	PA-dimer	0.0058	0.0166
	$(C_2H_2)_2$	0.0064	0.0178
	C_2H_2•••CH_4	0.0042	0.0109

V.6. Conclusions

Rotational spectra of PA-dimer and its two mono-deuterated and one bi-deuterated isotopologues have been observed and fitted within experimental uncertainty. The experimental rotational constants and Kraitchman analysis confirm the structure to be close to one of the *ab-initio* predicted structure. *Ab initio* calculations predict this structure to be the most stable structure for the dimer. The AIM calculations show that the observed dimer is bound with O-H•••O, O-H•••π and C-H•••π hydrogen bonds. These interactions could be compared to similar interactions present in other dimers. The other un-observed *ab initio* predicted dimer structures are not very different in terms of stabilization energies and there is a possibility that they could also be found. During this work many other 'only' PA dependent signals were also observed which could belong to any one of these different possible structures for the dimer or may also be due to some other higher PA-clusters.

V.7. Supplementary Information

The *Supplementary Information* contains coordinates for all the *ab initio* as well as scaled structures for the PA-dimer. The calculated harmonic frequencies for these structures are also given. AIM properties for all the structures have been summarized.

The observed transitions which could not be assigned as of now are also listed. The *Supplementary Information* also contains the total searched regions using argon as well as helium as carrier gases.

V.8. References:

1. Mani, D.; Arunan, E. *ChemPhysChem* **2013**, *14*, 754-763.

2. Mani, D.; Arunan, E. *Phys. Chem. Chem. Phys.* **2013**, *15*, 14377-14383.

3. Evangelisti, L.; Feng, G.; Rizzato, R.; Caminati, W. *ChemPhysChem* **2011**, *12*, 1916-1920.

4. Bene, J. E. D. *J.Chem.Phys.* **1971**, *55*, 4633-4636.

5. Tse, Y. C.; Newton, M. D.; Allen, L. C. *Chem. Phys. Lett.* **1980**, *75*, 350-356.

6. Bolis, G.; Clementi, E.; Wertz, D. H.; Scheraga, H. A.; Tosi, C. *J. Am. Chem. Soc.* **1983**, *105*, 355-360.

7. Kim, S.; Jhon, M. S.; Scheraga, H. A. *The Journal of Physical Chemistry* **1988**, *92*, 7216-7223.

8. Stockman, P. A.; Blake, G. A.; Lovas, F. J.; Suenram, R. D. *J.Chem.Phys.* **1997**, *107*, 3782-3790.

9. González, L.; Mó, O.; Yáñez, M. *J.Chem.Phys.* **1998**, *109*, 139-150.

10. Arunan, E.; Gutowsky, H. S. *J.Chem.Phys.* **1993**, *98*, 4294-4296.

11. Lovas, F. J.; Belov, S. P.; Tretyakov, M. Y.; Stahl, W.; Suenram, R. D. *J. Mol. Spectrosc.* **1995**, *170*, 478-492.

12. Gutowsky, H. S.; Emilsson, T.; Arunan, E. *J.Chem.Phys.* **1993**, *99*, 4883-4893.

13. Aiswaryalakshmi, P.; Arunan, E. *To be published*.

14. Frisch, M. J.; Trucks, G. W.; Schlegel, H. B.; Scuseria, G. E.; Robb, M. A.; Cheeseman, J. R.; Scalmani, G.; Barone, V.; Mennucci, B.; Petersson, G. A.; Nakatsuji, H.; Caricato, M.; Li, X.; Hratchian, H. P.; Izmaylov, A. F.; Bloino, J.; Zheng, G.; Sonnenberg, J. L.; Hada, M.; Ehara, M.; Toyota, K.; Fukuda, R.; Hasegawa, J.; Ishida, M.; Nakajima, T.; Honda, Y.; Kitao, O.; Nakai, H.; Vreven, T.; Montgomery, J. A.; Peralta, J. E.; Ogliaro, F.; Bearpark, M.; Heyd, J. J.; Brothers, E.; Kudin, K. N.; Staroverov, V. N.; Kobayashi, R.; Normand, J.; Raghavachari, K.; Rendell, A.; Burant, J. C.; Iyengar, S. S.; Tomasi, J.; Cossi, M.; Rega, N.; Millam, J. M.; Klene, M.; Knox, J. E.; Cross, J. B.; Bakken, V.; Adamo, C.; Jaramillo, J.; Gomperts, R.; Stratmann, R. E.; Yazyev, O.; Austin, A. J.; Cammi, R.; Pomelli, C.; Ochterski, J. W.; Martin, R. L.; Morokuma, K.; Zakrzewski, V. G.; Voth, G. A.; Salvador, P.; Dannenberg, J. J.; Dapprich, S.; Daniels, A. D.; Farkas; Foresman, J. B.; Ortiz, J. V.; Cioslowski, J.; Fox, D. J. Wallingford CT, 2009.

15. Boys, S. F.; Bernardi, F. *Mol. Phys.* **1970**, *19*, 553.

16. AIMAll (Version 13.02.26), K., Todd A.; TK Gristmill Software, : Overland Park KS, USA, 2012 (aim.tkgristmill.com).

17. Biegler-König, F.; Schönbohm, J. *J. Comput. Chem.* **2002**, *23*, 1489-1494.

18. Arunan, E.; Tiwari, A. P.; Mandal, P. K.; Mathias, P. C. *Curr. Sci.* **2002**, *82*, 533-540.

19. Legon, A. C.; Millen, D. J. *Chem. Soc. Rev.* **1987**, *16*, 467-498.

20. Desiraju, G. R., Steiner, T. *The weak hydrogen bond in structural chemistry and biology* Oxford University Press: Oxford, **1999**.

21. Koch, U.; Popelier, P. L. A. *J. Phys. Chem.* **1995**, *99*, 9747-9754.

Supplementary Information

Table.V.S.1 Coordinates of the optimized geometries for different structures of propargyl alcohol-dimer at MP2/6-311+G(3df,2p) level.

Structure-1				*Structure-2*			
Atom	x(Å)	y(Å)	z(Å)	Atom	x(Å)	y(Å)	z(Å)
C	-1.881336	1.794258	-0.100865	C	-1.9602	1.9598	-0.0859
C	-1.936115	0.583975	-0.017193	C	-2.1532	0.7600	-0.1014
H	-1.838113	2.854008	-0.17573	H	-1.8022	3.0111	-0.0838
C	-1.984543	-0.874394	0.102107	C	-2.3794	-0.6917	-0.1188
O	-0.695479	-1.472954	0.06286	O	-1.3276	-1.4105	-0.7242
H	-2.53713	-1.296675	-0.735259	H	-3.2771	-0.9030	-0.6988
H	-2.509379	-1.147783	1.020611	H	-2.5599	-1.0322	0.9054
H	-0.160265	-1.094715	0.77528	H	-0.5435	-1.2995	-0.1649
C	1.635468	0.063602	1.893083	C	3.3660	0.1946	-1.0084
C	1.664472	0.335524	0.707637	C	2.4682	0.3147	-0.2002
H	1.64556	-0.16149	2.932523	H	4.1424	0.0956	-1.7278
C	1.65804	0.634814	-0.731618	C	1.4017	0.4185	0.7919
O	1.482384	-0.51275	-1.53311	O	0.7904	-0.8438	1.0656
H	2.619132	1.066128	-1.009065	H	0.6001	1.0567	0.4246
H	0.883931	1.383203	-0.924997	H	1.7927	0.8553	1.7134
H	0.665109	-0.943722	-1.240271	H	1.4865	-1.4852	1.2387
Structure-3				*Structure-4*			
Atom	x(Å)	y(Å)	z(Å)	Atom	x(Å)	y(Å)	z(Å)
C	-2.0250	1.2814	1.2302	C	3.0210	0.8480	-0.4068
C	-1.8108	0.6136	0.2388	C	2.2274	0.0709	0.0839
H	-2.2031	1.8774	2.0925	H	3.7081	1.5375	-0.8344
C	-1.5706	-0.2308	-0.9293	C	1.2960	-0.9058	0.6423
O	-1.1083	-1.5328	-0.5686	O	0.5400	-1.5736	-0.3667
H	-0.7835	0.2018	-1.5433	H	0.5652	-0.4071	1.2762
H	-2.4800	-0.3029	-1.5296	H	1.8434	-1.6315	1.2482
H	-1.7332	-1.9101	0.0586	H	1.1389	-1.8664	-1.0593
C	1.6672	1.6186	-1.1147	C	-0.5661	2.0496	0.2888
C	1.6751	0.8155	-0.2026	C	-1.4223	1.2347	0.0064
H	1.6740	2.3217	-1.9120	H	0.1857	2.7597	0.5341
C	1.6792	-0.1608	0.8944	C	-2.4302	0.2281	-0.3470
O	1.5635	-1.4956	0.4504	O	-2.1634	-1.0424	0.2097
H	0.8813	0.0998	1.5968	H	-2.5100	0.1774	-1.4373
H	2.6264	-0.0917	1.4284	H	-3.4009	0.5370	0.0387
H	0.6848	-1.5938	0.0531	H	-1.2981	-1.3313	-0.1159

Table.V.S.1 (continued)

Structure-5				*Structure-6*			
Atom	x(Å)	y(Å)	z(Å)	Atom	x(Å)	y(Å)	z(Å)
C	3.3107	0.6174	-0.0851	C	0.2325	0.5028	2.1148
C	2.3650	-0.1335	-0.2126	C	0.2001	0.2386	0.9314
H	4.1478	1.2632	0.0264	H	0.2676	0.7277	3.1530
C	1.2054	-1.0123	-0.3485	C	0.1599	-0.0612	-0.4938
O	0.4428	-1.0912	0.8562	O	0.5491	-1.4227	-0.6861
H	1.5270	-2.0289	-0.5671	H	0.8436	0.6065	-1.0255
H	0.5784	-0.6640	-1.1734	H	-0.8513	0.1030	-0.8742
H	0.2612	-0.1801	1.1214	H	0.6687	-1.5446	-1.6375
H	-1.3443	-1.3313	0.1223	H	2.4639	-1.2467	-0.3323
O	-2.1133	-1.0807	-0.4135	O	3.3639	-0.9897	-0.5870
C	-2.5350	0.1939	0.0248	C	3.6392	-1.6101	-1.8227
H	-3.3211	0.5149	-0.6573	H	4.6346	-1.2848	-2.1223
H	-2.9678	0.1493	1.0291	H	3.6619	-2.7005	-1.7308
C	-1.4529	1.1886	0.0185	C	2.6817	-1.2472	-2.8791
C	-0.5260	1.9761	0.0267	C	1.8679	-0.9560	-3.7352
H	0.2795	2.6709	0.0137	H	1.1839	-0.6902	-4.5052

Structure-7			
Atom	x(Å)	y(Å)	z(Å)
C	-3.6337	0.4713	-0.5660
C	-2.6351	0.0919	0.0099
H	-4.5045	0.7970	-1.0804
C	-1.4447	-0.3500	0.7312
O	-0.6855	-1.2113	-0.0990
H	-1.7557	-0.8621	1.6474
H	-0.8595	0.5280	1.0187
H	0.1986	-1.2933	0.2874
C	1.4341	2.1437	0.3316
C	1.8147	1.0825	-0.1168
H	1.0987	3.0725	0.7257
C	2.2755	-0.1794	-0.6798
O	2.1202	-1.1986	0.3140
H	3.3246	-0.0884	-0.9695
H	1.6811	-0.4162	-1.5653
H	2.4745	-2.0181	-0.0454

Table.V.S.2 Coordinates of the scaled geometries of propargyl alcohol-dimer on the basis of observed rotational constants and ab-initio optimized structure 1 and structure 3.

Scaled geometry on the basis of Structure-1				*Scaled geometry on the basis of Structure-3*			
Atom	x(Å)	y(Å)	z(Å)	Atom	x(Å)	y(Å)	z(Å)
C	-2.0316	1.5584	-0.7968	C	-2.1753	1.0876	1.3698
C	-2.0612	0.4917	-0.2321	C	-1.9284	0.5095	0.2486
H	-2.0107	2.4917	-1.2926	H	-2.3817	1.6036	2.3449
C	-2.0784	-0.7858	0.4649	C	-1.6493	-0.2214	-1.0720
O	-0.7088	-1.3195	0.6603	O	-1.1456	-1.3348	-0.6460
H	-2.6493	-1.5213	-0.1155	H	-0.8227	0.1586	-1.7654
H	-2.6245	-0.6711	1.4085	H	-2.5975	-0.2995	-1.7655
H	-0.1551	-0.6752	1.1458	H	-1.8028	-1.6649	0.0638
C	1.7059	0.8683	1.6714	C	1.7246	1.4155	-1.2603
C	1.7307	0.6337	0.4918	C	1.7366	0.7288	-0.2154
H	1.7212	1.0869	2.7001	H	1.7286	2.0168	-2.1734
C	1.7178	0.3200	-0.9277	C	1.7454	-0.1060	1.0411
O	1.5601	-1.0523	-1.1860	O	1.6509	-1.2603	0.5446
H	2.7186	0.6184	-1.3603	H	0.8950	0.1115	1.8297
H	0.8864	0.9056	-1.3978	H	2.7340	-0.0304	1.6595
H	0.7104	-1.3413	-0.7408	H	0.7332	-1.3592	0.0830

Table.V.S.3.Frequencies for the normal modes of vibration for different structures of propargyl alcohol-dimer at MP2/6-311+G(3df,2p) level.

Structure 1		*Structure 2*		*Structure 3*		*Structure 4*	
ν (cm^{-1})	IR intensities	ν (cm^{-1})	IR intensities	ν (cm^{-1})	IR intensities	ν (cm^{-1})	IR intensities
28.7	1.2	10.5	0.3	26.9	0.8	22.5	0.8
48.2	1.6	19.1	0.9	43.4	0.4	49.0	1.3
67.4	0.5	63.8	2.8	69.0	0.6	72.7	1.0
108.1	2.4	70.3	2.1	91.5	2.2	76.4	5.9
126.3	0.6	91.5	2.1	112.8	1.3	114.9	1.4
157.8	4.2	187.4	3.3	183.5	2.5	160.2	13.1
211.1	1.1	194.4	6.1	193.4	1.3	197.9	12.4
225.1	0.9	215.0	4.6	211.3	1.8	225.1	30.2
301.1	5.9	290.6	13.4	286.9	13.0	231.6	49.8
314.5	7.1	307.4	4.8	307.2	3.8	303.8	7.9
522.3	79.1	349.8	111.3	357.6	126.9	316.7	35.4
561.2	7.7	558.4	11.0	558.7	3.0	557.9	4.2
575.8	68.2	560.2	9.3	559.2	9.1	559.3	10.8
634.6	33.7	634.0	42.0	634.5	44.0	631.3	58.0
645.4	35.6	650.4	46.0	648.8	41.9	647.3	35.3
652.4	58.4	662.2	43.3	659.7	37.3	663.6	33.6
670.9	54.0	679.4	37.9	674.1	75.7	675.4	40.6
675.0	52.7	690.4	70.4	676.9	60.7	679.9	101.2
917.7	12.6	924.4	20.0	925.5	14.1	925.6	11.6
930.9	28.9	928.5	17.7	929.5	24.1	928.7	35.9
1005.9	14.3	1003.8	11.4	1002.5	0.8	1007.1	20.7
1010.1	17.0	1013.1	16.7	1007.7	22.5	1009.2	4.5
1073.7	106.9	1063.0	103.3	1061.1	60.9	1067.5	87.6
1093.6	98.7	1095.4	100.4	1093.1	116.7	1092.2	101.2
1239.8	19.4	1225.9	26.1	1224.8	14.8	1228.0	21.4
1257.9	11.9	1261.2	9.1	1261.1	15.1	1253.3	9.1
1377.2	4.0	1355.1	5.2	1360.7	4.9	1352.8	5.8
1385.9	6.1	1393.5	11.1	1393.9	13.9	1387.0	5.9
1422.5	46.8	1428.5	47.1	1424.8	43.2	1431.9	59.4
1461.6	43.9	1466.1	32.3	1463.3	43.1	1446.6	21.8
1507.1	4.0	1508.3	2.1	1506.6	2.4	1512.2	0.9
1515.1	2.1	1521.0	0.6	1513.0	6.2	1514.2	7.2
2115.7	0.8	2122.4	0.8	2122.4	0.8	2124.5	0.7
2130.7	2.8	2136.4	2.8	2133.1	3.5	2134.3	2.4
3064.2	23.1	3058.4	32.7	3057.7	25.3	3056.1	35.4
3076.4	28.6	3081.0	22.1	3081.9	24.8	3078.8	24.0
3139.0	8.0	3136.2	10.8	3135.2	11.4	3136.7	10.8
3150.1	4.2	3155.5	3.9	3160.8	0.2	3156.5	0.3
3477.1	62.2	3482.0	53.9	3481.7	61.5	3482.6	54.1
3481.3	56.1	3483.5	62.1	3482.7	51.2	3484.4	53.0
3707.7	118.6	3701.4	501.2	3708.9	387.3	3726.4	394.9
3747.6	364.2	3853.6	50.7	3851.1	53.0	3866.0	52.9

Structure 5		*Structure 6*		*Structure 7*	
ν (cm^{-1})	IR intensities	ν (cm^{-1})	IR intensities	ν (cm^{-1})	IR intensities
41.4	0.0	25.4	0.1	7.8	0.0
45.6	3.0	38.0	1.0	31.5	6.1
87.3	1.7	59.0	7.7	57.5	5.3
99.5	3.6	96.2	3.2	86.7	15.6
119.8	3.2	105.3	1.5	97.4	1.5
153.4	1.8	179.5	9.6	153.7	6.8
212.7	4.2	208.5	7.9	205.0	12.5
238.0	11.3	224.3	3.0	225.5	4.6
304.9	3.4	304.2	10.9	300.0	33.4
311.3	6.1	314.3	5.9	308.3	6.1
491.0	191.9	470.6	152.8	343.0	83.1
560.6	14.7	558.2	0.4	542.4	23.4
567.0	18.7	571.5	31.2	557.9	3.1
645.8	45.1	638.3	35.3	636.7	39.8
647.6	36.1	647.0	43.6	638.6	165.0
658.0	134.3	664.1	102.3	646.1	35.8
663.7	56.3	668.2	55.6	667.2	35.6
672.3	36.4	679.4	47.5	682.3	34.1
918.6	11.5	916.8	14.7	925.0	7.1
931.5	24.8	929.3	4.7	931.1	10.1
1004.5	9.5	1008.7	9.4	1036.3	6.5
1014.9	10.0	1041.2	4.5	1040.3	3.8
1061.5	93.5	1064.4	110.9	1057.9	96.8
1090.2	92.5	1094.2	102.1	1092.7	100.6
1240.9	10.2	1256.2	5.0	1245.0	62.1
1260.6	7.6	1274.8	9.0	1278.3	6.2
1375.7	4.1	1288.1	30.2	1282.2	2.5
1385.1	2.9	1386.9	7.7	1320.1	59.2
1432.0	48.1	1456.5	12.2	1451.2	21.5
1471.6	28.3	1464.5	51.5	1472.0	14.3
1512.9	5.9	1511.3	1.8	1518.8	2.4
1515.0	2.2	1523.3	1.6	1522.3	0.8
2117.2	0.9	2115.3	1.4	2140.7	0.6
2133.4	1.8	2146.0	3.2	2144.9	3.9
3056.9	32.3	3058.0	29.0	3045.2	34.5
3077.3	12.2	3058.4	22.5	3067.4	23.7
3139.9	7.2	3106.9	8.9	3091.6	9.8
3151.9	4.5	3139.8	6.7	3119.2	7.3
3475.9	52.2	3475.7	63.1	3483.0	56.0
3483.1	62.3	3486.5	59.4	3488.2	56.4
3688.7	281.3	3696.3	247.8	3722.9	391.3
3785.6	138.1	3774.2	237.1	3853.1	54.1

Table.V.S.4. Observed but unassigned PA dependent signals. He was used as the carrier gas at a back pressure of 1.5 bar. MW pulse duration was 1.0 μs.

Freq(MHz)	Intensity	Freq(MHz)	Intensity	Freq(MHz)	Intensity	Freq(MHz)	Intensity
4764.343	strong	7724.417	medium	8796.824	medium	9698.107	medium
4764.795	strong	7858.918	medium	8816.049	medium	9763.786	medium
4830.522	very strong	8370.178	medium	8816.986	medium	9807.988	weak
4830.579	strong	8382.517	medium	8927.440	weak	9822.256	strong
4863.461	medium	8386.721	very strong	8942.597	weak	9822.343	strong
4955.008	medium	8386.829	very strong	8970.817	strong	9828.651	weak
4955.047	medium	8387.000	very strong	8970.826	strong	9878.610	strong
4955.764	medium	8387.104	very strong	8972.195	medium	9878.641	strong
6744.035	strong	8424.295	medium	8975.560	strong	9878.700	strong
6812.863	very strong	8427.500	medium	8987.275	medium	10225.508	very strong
6864.027	very strong	8427.620	medium	8987.600	medium	10225.525	very strong
6872.941	medium	8427.800	medium	9037.007	medium	10225.869	very strong
6944.890	weak	8433.425	strong	9046.643	medium	10414.031	strong
7109.870	very strong	8433.866	medium	9145.217	strong	10416.746	strong
7110.010	very strong	8434.217	strong	9151.326	very strong	10418.785	strong
7132.510	medium	8441.610	medium	9154.511	strong	10777.217	weak
7227.130	medium	8444.416	weak	9155.100	strong	11419.000	strong
7240.270	medium	8444.544	medium	9192.378	strong	11449.990	medium
7240.424	medium	8444.769	weak	9232.378	medium	11812.100	weak
7246.186	strong	8659.373	medium	9310.220	medium		
7253.200	medium	8672.290	medium	9325.805	very strong		
7255.875	medium	8713.621	medium	9411.205	strong		
7256.051	medium	8735.922	very strong	9477.943	strong		
7257.850	strong	8743.324	very strong	9516.363	medium		
7266.450	medium	8743.353	very strong	9516.656	medium		
7304.990	medium	8743.402	very strong	9568.785	strong		
7305.295	medium	8756.795	weak	9587.800	medium		
7354.880	medium	8756.825	weak	9592.135	medium		
7356.370	medium	8762.256	weak	9592.193	medium		
7453.195	medium	8772.798	medium	9596.120	medium		
8762.164	weak	8772.832	medium	9608.015	medium		
7475.984	medium	8796.795	medium	9645.985	medium		

Table.V.S.5. Overall scanned regions. He was used as the carrier gas at 1.5 bar back pressure. MW pulse length was 1.0 μs.

5689.0-5693.5 MHz	9756.5-9808.0 MHz
5950.0-5981.0 MHz	9808.5-9839.0 MHz
7093.0-7363.0 MHz	9839.0-9855.5 MHz
7452.0-7479.0 MHz	9880.0-9881.5 MHz
7584.0-7587.0 MHz	9955.5-9975.5 MHz
7525.0-7527.0 MHz	10007.0-10017.0 MHz
7651.0-7658.0 MHz	10218.0-10292.5 MHz
7684.5-7727.0 MHz	10399.0-10455.0 MHz
7833.5-7895.0 MHz	10669.0-10667.0 MHz
8347.0-8385.5 MHz	10618.0-10640.0 MHz
8410.0-8446.0 MHz	10752.0-10800.0 MHz
8638.5-8838.0 MHz	11188.0-11198.0 MHz
8940.5-9035.0 MHz	11277.0-11313.0 MHz
9351.5-9482.0 MHz	11355.0-11371.0 MHz
9477.0-9614.0 MHz	11457.0-11467.0 MHz
9620.0-9651.0 MHz	11670.0-11710.0 MHz
9640.0-9784.0 MHz	11803.0-11849.5 MHz

Table.V.S.6. AIM properties at the intermolecular BCPs for different structures of PA-dimer. The structures and interactions are shown in the Figure V.1 of the main text.

	O-H•••O		*O-H•••π*		*C-H•••π*		*C-H•••π*	
	ρ(r) in a.u.	*∇^2. ρ(r) in a.u.*	*ρ(r) in a.u.*	*∇^2. ρ(r) in a.u.*	*ρ(r) in a.u.*	*∇^2 ρ(r) in a.u.*	*ρ(r) in a.u.*	*∇^2. ρ(r) in a.u.*
Structure 2	0.0290	0.1001	-	-	0.0075	0.0207	-	-
Structure 3	0.0275	0.0942	-	-	0.0047 (H2... π)	0.0133 (C3-H2-π)	0.007 (H6... π)	0.0199 (C6-H6- π)
Structure 4	0.0258	0.1074	-	-	0.0071	0.0218	-	-
Structure 5	0.0269	0.0876	0.0131	0.0409	-	-	-	-
Structure 6	0.0266	0.0870	0.0142	0.0443	-	-	-	-
Structure 7	0.0252	0.0979	-	-	0.0063	0.0177	-	-

Chapter VI.

Measuring Rotational Constant of a Molecule Without Dipole Moment and Confirming Low Frequency Vibrations Using Microwave Spectroscopy: $^{13}CC_5H_6$/ C_6H_5D•••Ar Complex.

(This work has been published in Asian J. Spectro. 2010, 31-42.)

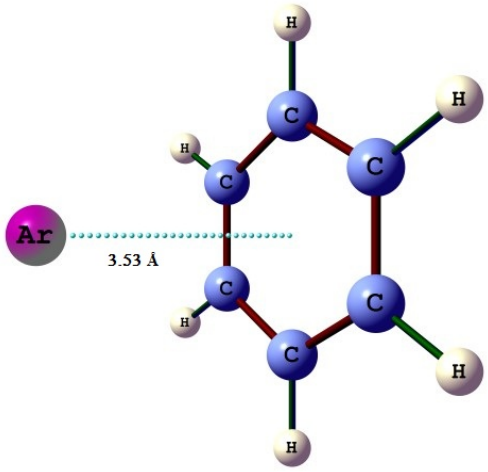

VI.1. Introduction

Microwave spectroscopy has been valuable in the determination of accurate structures of small molecules with appreciable dipole moments.[1,2] As there were not many of these molecules, interest in microwave spectroscopy was vanishing in the 1970s. Then came the introduction of the pulsed nozzle Fourier transform microwave (PNFTMW) spectrometer by Balle and Flygare.[3] This technique had high sensitivity and resolution and it opened up several avenues. Several groups built this spectrometer all over the world expanding the horizons of microwave spectroscopy research and in an earlier review the advances and applications of the Balle-Flygare spectrometer have been summarized.[4] While the sensitivity and resolution of this technique enabled numerous investigations that would not have been possible earlier, there remained a major disadvantage: narrow bandwidth. Within two years after this review was published Pate has given the next fillip to the field introducing chirped pulse Fourier transform microwave (CPFTMW) spectrometer.[5,6] This enabled the collection of 'microwave spectrum' rather than the observation of one line at a time and searching laboriously for all the lines. One could start seeing a broad band spectrum in papers, rather than many Tables listing numerous transition frequencies. There still remains one problem that cannot be solved by microwave spectroscopy: Experimentally measuring the rotational constants of a molecule that has no dipole moment, benzene for example or can it be?

We had proposed the concept of an electrophore as an atom or molecule, which could combine with another molecule having no dipole moment thereby forming a complex with a dipole moment.[4] Let us look at the structure of C_6H_6 , *Figure VI.1*. It is an oblate top with the *a*- and *b*-axes in the plane and the *c*-axis perpendicular to the plane. As it has no dipole moment, these constants can not be determined by microwave spectroscopy. If benzene were to form a complex with an atom which approaches along its *c*-axis, *Figure VI.2*, the resulting complex would also be a symmetric top. However, the complex will have a dipole moment due to polarization. The *c*-axis of benzene would become the *a*-axis for the complex. However, this does not help in measuring the rotational constants of C_6H_6 as the experiment can only determine the B rotational constant for the complex. It will depend on the intermolecular distance and the masses of C_6H_6 and the atom. Moreover, this does not give any structural details about benzene, as one often assumes the monomer structure

to be unaffected when interpreting the complex rotational constants. If a complex of C_6H_6 can be formed with an atom approaching it along the *a*- or *b*-axis (both being equivalent for C_6H_6), the complex would become an asymmetric top and experiment will give all three rotational constants. More importantly, the *a*-axis for the complex is the same as the *a*- or *b*-axes for C_6H_6 and the rotational constants for the complex and C_6H_6 along these axes would be the same as the atom approaching in this axis would not contribute to the moments of inertia about this axis, *Figure VI.3*. This would give a microwave spectrum from which the A rotational constant of C_6H_6 can be determined.

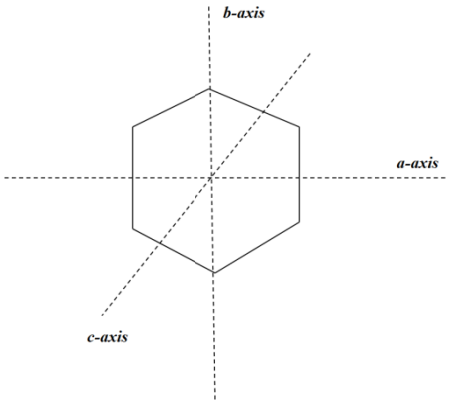

Figure VI.1. Principal axes system for the benzene molecule

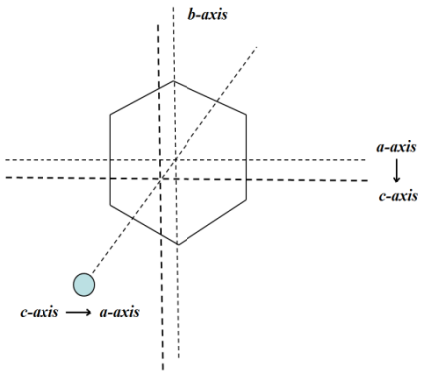

Figure VI.2. An atom approaching along c-axis of benzene and forming a complex. Principal axes change following this as shown in the figure. Darker lines are for the complex.

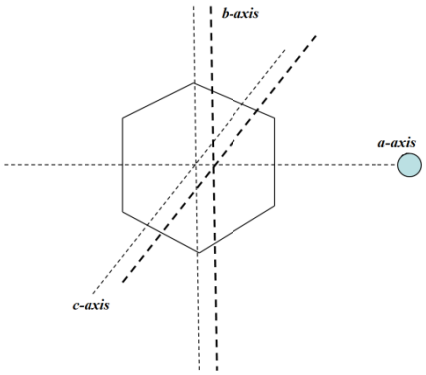

Figure VI.3. An atom approaching along the A axis of benzene and forming a complex. The principal axes remain unaffected but the center of mass changes. Darker lines are for the complex.

Is there a way to get the C rotational constant of C_6H_6 from an experimentally determined microwave spectrum? There appears to be no way. If C_6H_6 is made asymmetric, for example, by substituting an isotope, it would be possible. If a complex is formed with C_6H_5D or $^{13}CC_5H_6$ with an atom approaching it along the C_6 axis of C_6H_6, the complex would be an asymmetric top and the A rotational constant for the complex would be the C rotational constant for the C_6H_5D or $^{13}CC_5H_6$ isotopologue. This is evident from the work of Gutowsky, Emilsson and Arunan who investigated the microwave spectrum of C_6H_6•••H_2O complex. They noted that the C_6H_5D•••H_2O and C_6H_5D•••D_2O were asymmetric tops and had identical A rotational constants (2765.5 MHz) within experimental uncertainty.[7] A rigid structure for the complex would have resulted in A rotational constants that differ by 10 MHz between the isotopologues having H_2O and D_2O. Free internal rotation in the complex ensured that H_2O/D_2O did not contribute to the moments of inertia along the A principle axis for the complex.[2,8] However, this was different from the experimentally determined C rotational constant of C_6H_5D, 2749.676(6) MHz.[9] Bauder could record the rotational spectrum of C_6H_5D as it has a small dipole moment due to the difference in C-H and C-D vibrations. However, pure rotational spectrum of $^{13}CC_5H_6$ has not been recorded yet. A reasonable estimate of C rotational constant for $^{13}CC_5H_6$ was not provided,[7] due to the assignment problems in the $^{13}CC_5H_6$•••H_2O spectrum. This was corrected by Ram Prasad, Krishnan and Arunan later and they have reported a value of 2832(3) MHz for the same.[8] Moreover, the same authors have reported that the combined fit of m =0 and 1 (m is the internal rotor angular momentum) lead to an A value of 2787(1)

MHz, which is significantly smaller. It was felt that such determinations on C_6H_6•••Ar would give a more realistic estimate for the monomer rotational constants. Bauder's group has in fact studied this complex.[10] However, both $^{13}CC_5H_6$ and C_6H_5D isotopologues were not investigated. In this chapter, the rotational spectrum of these two isotopologues are reported and compared with the parent isotopologue. Results from these complexes are unlikely to give any new information about the complex. However, our main motivation was the direct determination of C rotational constant of asymmetric benzene isotopologues.

The centrifugal distortion constants of C_6H_6•••Rg (Rg = Ar/Kr) have been analyzed in detail to extract the intermolecular potential and also some information about intermolecular vibrations.[11] There have been several such attempts to use the centrifugal distortion constants to extract information about intermolecular potentials and vibrations.[11-15] These depended on models and programmes developed in-house. Recently, such vibrational-rotational calculations have been incorporated in several packages, such as Gaussian09,[16] which makes it easy for every-one. Such electronic structure theory calculations have become standard for calculating short amplitude high frequency vibrations. Scaling factors are well established for these modes which improve the accuracy of theoretical predictions.[17-19] However, such scaling factors do not work for large amplitude low frequency vibrations. Moreover, experimental data on these modes are scarce. Development of terahertz spectroscopy does offer some hope in this direction.[20] The question we address here is the following: Can we use the centrifugal distortion constants to determine which of the methods and basis sets work better for predicting the low frequency vibrations? The C_6H_6•••Ar data is used here for this exploratory study as well.

VI.2. Experimental and theoretical methods

Spectral transitions for C_6H_5D•••Ar and $^{13}CC_5H_6$•••Ar were predicted based on the known structure of C_6H_6•••Ar and readily observed. Benzene and C_6H_5D (99.9 % D) were procured from Aldrich and $^{13}CC_5H_6$ was observed in natural abundance. Argon (99.999%) was obtained from Bhuruka Gases Ltd and it was flown through silica gel and charcoal traps to remove any residual H_2O/hydrocarbons. MW pulse of 3 μs duration was used. All the theoretical calculations were performed using the commercial Gaussian09 suite of programs.

VI.3. Results and discussion

VI.3.a. Observed transitions and determined rotational constants

The observed transitions for both isotopologues C_6H_5D•••Ar and $^{13}CC_5H_6$•••Ar are given in *Tables VI.1 and VI.2*. These transitions could be fitted to a Watson S-reduction Hamiltonian and the rotational and centrifugal distortion constants are given in *Table VI.3*. Not surprisingly, the distortion constants are very close to those determined for the parent isotopologue, C_6H_6•••Ar. The RMS deviations for both these asymmetric complexes were close to 10 kHz compared to less than 2 kHz for the parent symmetric top. More importantly, the *A* rotational constants for the C_6H_5D•••Ar and $^{13}CC_5H_6$•••Ar complexes were determined to be 2760.3(17) and 2810(22) MHz, respectively. For the C_6H_5D•••Ar complex, this value can be compared to the *C* rotational constant for the C_6H_5D. As mentioned earlier, the direct measurement reported by Bauder[9] yields 2749.674(6) MHz, which differs by about 10 MHz. For the C_6H_5D•••H_2O/D_2O complexes, the *A* rotational constant was determined to be 2765.5(3) MHz.[7] For $^{13}CC_5H_6$, there has been no previous experimental measurement of *A* rotational constant and based on comparisons with the C_6H_5D, our measurement of 2810(22) MHz should be reasonably good. This may be compared with the value of 2832(3) MHz determined from $^{13}CC_5H_6$•••H_2O complex spectrum. The uncertainty in $^{13}CC_5H_6$ constant is significantly more than that for the C_6H_5D which is possibly due to the lower signal to noise. These numbers could be improved if more transitions from higher J/K are measured. However, the calculated rotational constant for the $^{13}CC_5H_6$ isotopologue, based on the experimental structure[21] of C_6H_6 is 2812.884 MHz, is very close to the *C* rotational constant determined for the $^{13}CC_5H_6$•••Ar complex. Clearly Ar as an electrophore has resulted in a more accurate determination of the *C* rotational constants for C_6H_5D and $^{13}CC_5H_6$. Still, these constants are somewhat different from the respective monomer values and the possible reasons are discussed next.

The principle coordinates for the complex are only slightly different from that of the monomer and hence, this difference cannot be attributed to this. The center of mass of C_6H_6 gets shifted closer to the D in C_6H_5D, but only by 0.003 Å. As the electronic structure of the monomer does not alter much, the location of Ar atom in these two complexes would not change. Though the *a*-axis for the C_6H_5D•••Ar complex would be slightly tilted from the *c*-axis of C_6H_5D, this change also cannot account for the

change of 10 MHz. Assuming these two axes as parallel shifted by 0.003 Å, parallel axis theorem shows that the change in the rotational constant will be of the order 0.1 MHz. Thus, this change must have its origin in the large amplitude vibrations, particularly the degenerate bending modes. For C_6H_6•••Ar, there has been an estimate of these vibrational frequencies based on the analysis of centrifugal distortion constants. Here, we use the standard Gaussian 09 software to calculate the vibration-rotational interaction constants and these results are discussed in the next section.

Table VI.1. Observed transitions for the Ar•••C_6H_5D complex. Residues from the fit are also given.

$J'\ K_{-1}'\ K_{+1}'$	$J\ K_{-1}\ K_{+1}$	*Frequency (MHz)*	*Residue(kHz)*
2 0 2	1 0 1	4676.3410	-0.0013
3 1 3	2 1 2	6989.3680	-0.0109
3 0 3	2 0 2	7013.9980	0.0000
3 1 2	2 1 1	7039.2970	0.0104
4 1 4	3 1 3	9318.6640	-0.0036
4 0 4	3 0 3	9351.0300	-0.0052
4 2 3	3 2 2	9351.6800	0.0048
4 2 2	3 2 1	9352.9750	-0.0045
4 1 3	3 1 2	9385.2150	0.0069
5 0 5	4 0 4	11687.2550	0.0063
5 1 5	4 1 4	11647.5100	-0.0158
5 2 3	4 2 2	11691.4660	-0.0042
5 3 3	4 3 2	11688.7210	0.0059
5 1 4	4 1 3	11730.6980	0.0051
6 0 6	5 0 5	14022.4480	0.0133
6 1 6	5 1 5	13975.8460	-0.0024
6 2 5	5 2 4	14025.5710	0.0085
6 2 4	5 2 3	14030.1070	-0.0148
6 1 5	5 1 4	14075.6250	-0.0042
7 1 7	6 1 6	16303.5500	0.0186
7 0 7	6 0 6	16356.3740	-0.0190
7 2 6	6 2 5	16361.6900	0.0128
7 3 4	6 3 3	16362.5783	-0.0087
7 2 5	6 2 4	16368.9677	0.0063
7 1 6	6 1 5	16419.8937	-0.0098

Table VI.2. Observed transitions for the Ar•••$^{13}CC_5H_6$ complex. Residues from the fit are also given.

J' K_{-1}' K_{+1}'	J K_{-1} K_{+1}	Frequency(MHz)	Residue(MHz)
3 1 3	2 1 2	7039.9600	-0.0085
3 0 3	2 0 2	7048.0170	0.0014
3 1 2	2 1 1	7055.9620	0.0114
4 1 4	3 1 3	9386.2520	0.0028
4 3 2	3 3 1	9395.8950	0.0092
4 0 4	3 0 3	9396.9410	0.0074
4 2 3	3 2 2	9396.5000	-0.0186
4 2 2	3 2 1	9396.6350	-0.0137
4 1 3	3 1 2	9407.5520	-0.0067
5 1 5	4 1 4	11732.2200	0.0117
5 3 3	4 3 2	11744.3000	0.0155
5 2 4	4 2 3	11745.0400	-0.0108
5 0 5	4 0 4	11745.4900	-0.0011
5 2 3	4 2 2	11745.3000	-0.0111
5 1 4	4 1 3	11758.8500	0.0052
6 1 6	5 1 5	14077.7650	-0.0003
6 5 2	5 5 1	14089.0200	-0.0011
6 2 5	5 2 4	14093.1750	-0.0097
6 0 6	5 0 5	14093.6100	0.012
6 2 4	5 2 3	14093.6500	0.0097
6 1 5	5 1 4	14109.7300	0.0015
7 0 7	6 0 6	16441.1565	-0.0077

Table VI.3. Rotational and Centrifugal Distortion Constants for the Ar•••C_6H_6 isotopologues

	Ar---C_6H_5D	*Ar---$^{13}CC_5H_6$*	*Ar---C_6H_6*	*Ar---C_6D_6*
A(MHz)	2760.3(17)	2810(22)	---	
B(MHz)	1177.46150(91)	1177.3994(12)	1181.25953(14)	1112.4412(6)
C(MHz)	1160.82539(91)	1172.0720(12)	---	
D_J(KHz)	3.1566(83)	3.212(14)	3.2577(17)	2.673(6)
D_{JK}(KHz)	17.589(93)	16.59(25)	17.8011(76)	14.53(4)
H_{JK}(KHz)	---	-0.0040(36)		
σ^a (KHz)	10.72	11.08		
#transitions	25	22		
Reference	This work	This work	Reference 10	Reference 10

VI.3.b. Ab initio calculations of distortion constants and large amplitude vibrations

The C_6H_6•••Ar complex was fully optimized at both MP2 and DFT level calculations with various triple zeta basis sets. At the DFT level calculations, the full optimization resulted in lower symmetry. Normal mode frequency calculations indicated that the optimized structures were true minima. These calculations were extended to determine the anharmonic vibration-rotation coupling via perturbation theory as implemented in Gaussian09. These resulted in zero-point vibrationally averaged rotational constants and centrifugal distortion constants that can be directly compared to the experimental results. We focus our discussion here on these constants and the frequencies of the three large amplitude vibrations for the complex. Our main emphasis here is to see which levels of calculations do better for the large amplitude vibrations. All these data are presented in *Table VI.4*.

The data are presented for C_6H_6•••Ar, C_6H_5D•••Ar, 1,3,5-$C_6H_3D_3$•••Ar, C_6D_6•••Ar and $^{13}CC_5H_6$•••Ar. These complexes were chosen as experimental results are available for all. As mentioned above, the DFT calculations with B3LYP functional and 6-311++G(2d,2p) and 6-311++G(3df,2p) basis sets resulted in a slightly asymmetric geometry and the rotational constants *B* and *C* differ by 0.2 MHz. This has also led to the removal of the degeneracy in the bending modes and these frequencies differ by a few cm^{-1}. MP2/6-311+(2d,2p) level calculations led to the experimentally found symmetric structure with a doubly degenerate bending mode. However, both these level of calculations led to rotational constants differing by – 70 MHz for DFT and +54 MHz for MP2 for C_6H_6•••Ar. The three large amplitude vibrational modes were predicted at 33.1 cm^{-1} (doubly degenerate intermolecular bending) and 39.6 cm^{-1} (intermolecular stretching) based on the analysis of centrifugal distortion constants for C_6H_6•••Ar.[11] MP2 calculations overestimate these vibrational frequencies by 6 cm^{-1} for the degenerate bending and 10 cm^{-1} for the stretching modes. Not surprisingly, the centrifugal distortion constants calculated at this level are D_J = 2.66 kHz and D_{JK} = 13.76 kHz compared to the experimental values of 3.258(1) kHz and 17.801(8) kHz. The DFT (B3LYP) calculations do a better job here. With 6-311++(3df,2p) basis set, the D_J is calculated to be 3.34 kHz which is very close to the experimental value. Not surprisingly, the intermolecular stretching mode which contributes significantly to D_J is calculated to be 40.3 cm^{-1} at this level in close agreement with the earlier determination. The B3LYP/6-311++G(2d,2p) level calculations give the best agreement for D_{JK}, 16.03 kHz. Hence, the frequency of degenerate bending modes,

33.9 cm^{-1} (averaged), at this level agrees very well with the earlier determination of 33.1 cm^{-1}. Our attempt here is not to evaluate these methods rigorously. Rather, in a pragmatic way, it can be seen that the methods that reproduce experimental D_J give an accurate estimate of intermolecular stretching frequency and the methods that reproduce D_{JK} can predict the intermolecular bending modes accurately. As centrifugal distortion constants are available for a larger number of complexes than for which large amplitude vibrational frequencies are known, it is suggested that ab initio predictions of these frequencies can be corroborated by comparison of experimental centrifugal distortion constants. It must be mentioned that the description of these modes as stretching and bending are reasonable approximations only.

Table VI.4. Rotational, centrifugal distortion constants, and low frequency vibrations of Ar••• C_6H_6 isotopologues.

Ar•••C_6H_6						
Level of theory	*A(MHz)*	*B(MHz)*	*C(MHz)*	D_J	D_{JK}	*Low frequency modes(cm^{-1})*
B3LYP/ 6-311++G(2d,2p)	2865.55	1110.88	1110.65	2.9	16.03	31.3, 36.4, 42.4
B3LYP/ 6-311++(3df,2p)	2867.28	1111	1110.77	3.34	12.38	33.5, 38.1, 40.3
MP2/ 6-311+G(2d,2p)	2848.24	1235.42	1235.42	2.66	13.76	39.9, 39.9, 49.7
Experimental[10]	---	1181.25953 (14)	----	3.2577(17)	17.8011(76)	33.1, 33.1, 39.6
Ar•••C_6H_5D						
B3LYP/ 6-311++G(2d,2p)	2770.48	1106.77	1092.11	2.8	15.53	31.3, 36.4, 42.4
B3LYP/ 6-311++(3df,2p)	2772.08	1106.89	1110.77	3.23	12.04	33.5, 36.8, 40.3
MP2/ 6-311+G(2d,2p)	2753.81	1231.12	1213.14	2.57	13.32	38.8, 39.9, 49.7
Experimental	2760(2)	1177.4615(9)	1160.8254 (9)	3.157(8)	17.59(9)	----
Ar•••1,3,5-$C_6H_3D_3$[11]						
B3LYP/ 6-311++G(2d,2p)	2594.12	1077.93	1077.68	2.64	14.84	30.0, 34.7, 42.0
B3LYP/ 6-311++(3df,2p)	2595.49	1078.03	1077.8	3.03	11.59	32.1, 36.3, 39.7
MP2/ 6-311+G(2d,2p)	2579.02	1196.36	1136.36	2.4	12.41	38.3, 38.3, 49.4
Experimental	---	1145.58441 (77)	---	2.9384(94)	16.038(67)	31.9, 31.9, 39.3
Ar•••C_6D_6[11]						
B3LYP/ 6-311++G(2d,2p)	2369.67	1047.37	1047.11	2.41	13.78	28.8, 33.1, 41.7
B3LYP/ 6-311++(3df,2p)	2370.77	1047.47	1047.21	2.78	10.86	30.8, 34.6, 39.2
MP2/ 6-311+G(2d,2p)	2356.29	1160.22	1160.22	2.17	11.25	37.0, 37.0, 49.1
Experimental	---	1112.4412(6)	----	2.673(6)	14.53(4)	30.9, 30.9, 39.1

Table VI.4 (continued)

			Ar•••$^{13}CC_5H_6$			
B3LYP/ 6-311++G(2d,2p)	2835.28	1106.47	1102.13	2.87	15.87	31.2, 36.1, 42.4
B3LYP/ 6-311++ (3df,2p)	2836.99	1106.59	1102.25	3.3	12.19	33.2, 38.0, 40.3
MP2/ 6-311+G (2d,2p)	2817.65	1232.4	1226.64	2.6	13.49	39.7, 40.0, 49.9
Experimental	2822(32)	1177.400(2)	1172.073(2)	3.23(2)	16.79(5)	----

As evident from all the data presented in *Table VI.3 and VI.4*, all levels of calculations can reproduce the effect of isotopic substitution on centrifugal distortion constants of these complexes. For example, the experimental D_J decreases in the order C_6H_6 > $^{13}CC_5H_6$ > C_6H_5D > $C_6H_3D_3$ > C_6D_6 and all levels of theory predict the difference nearly quantitatively.

VI.3.c. Is the concept of electrophore useful?

One natural question that arises is that why should any one go through the trouble of determining the rotational constants of a molecule that does not have a dipole moment through microwave spectroscopy. Rotationally resolved vibrational[22] and electronic spectroscopy[23] can often help. However, none of the other techniques can match microwave spectroscopy in resolution and the structures determined by microwave spectroscopy are accurate. The determination of Si=C double bond length by microwave spectroscopy resolved a long standing controversy.[24] Preliminary work on C_6H_6•••C_2H_4 complex indicates that the *A* rotational constant for the complex is very close to the *A* rotational constant of C_6H_6.[25] Hence, for benzene both rotational constants can now be determined by microwave spectroscopy. We present one example of a complex, which appears to be of enormous interest with no experimental data available as on date: parallel displaced benzene dimer.[26]

The benzene dimer has attracted enormous interest. There have been numerous publications on this dimer. Theoretical calculations have shown that both T-shaped and parallel-displaced structures are possible.[26] Obtaining the microwave spectrum of this dimer was a big challenge and in 1993 Arunan and Gutowsky reported some important microwave transitions which provided positive confirmation of the T-shaped geometry.[27] Several more transitions of this important dimer remain unassigned. The spectrum is not yet completely solved and detailed molecular symmetry group analysis was presented recently.[28] For the parallel-displaced structure

as of now there is no experimental data though theoretical calculations show it to be a minimum. The interaction in this structure could be characterized as π–π interactions as opposed to the T-shaped structure which has a C-H•••π interaction. The π–π interaction is very important in biological chemistry and the structure of DNA is influenced by this and hydrogen bonding.[29] However, in biological systems, the aromatic rings contain a heteroatom and such interactions have been seen both experimentally[30] and theoretically.[31] Does the π stacked structure exist only for heteroaromatics and not for simple benzene, as there is no experimental evidence? Absence of evidence is not evidence for absence. If parallel-displaced benzene dimer exists, it should be able to form a complex with Argon as shown in *Figure VI.4*. Now this structure will have a dipole moment. While, the complex rotational constants may or may not be related to the benzene dimer rotational constants, the distance between the two benzene planes can be accurately determined. However, the rotational constants for this trimer are predicted to be of the order of 100s of MHz only. The recent technological advances[32,33] indicate that a spectrometer that can work below 1 GHz should become available. If microwave evidence for a parallel-displaced benzene dimer could be obtained, it will be worth all the efforts in building such a spectrometer. The concept of electrophore would have become important. Whether it will become as important as the concept of a chromophore in electronic spectroscopy is not clear now.

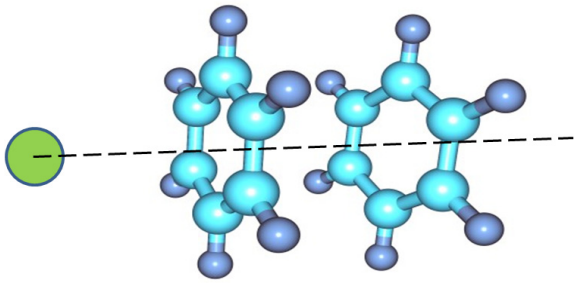

Figure VI.4. Structure of Ar•••C_6H_6•••C_6H_6 complex. Argon atom can induce a dipole moment by forming a complex with parallel displaced benzene dimer. Microwave spectrum can give structural information about the benzene dimer.

VI.4. Conclusions

In this chapter, the rotational spectra of C_6H_5D•••Ar and $^{13}CC_5H_6$•••Ar isotopologues have been presented. It has been shown that the experimental *A* rotational constants for these complexes are very close to the *C* rotational constants of the benzene

isotopologue and these have been determined using microwave spectroscopy for the molecules without dipole moment. The argon atom assumes the role of an electrophore giving a dipole moment to benzene. Anharmonic vibration-rotation interaction calculations have been performed on C_6H_6•••Ar complex to show that experimental centrifugal distortion constants can be used for validating the predictions of large amplitude/low frequency vibrational modes. Scaling factors do not work for these modes and this approach could be used to test various models. Finally, the concept of electrophore could become important if it can lead to structural information of important complexes, for example parallel-displaced benzene dimer.

VI.5. References

1. Schawlow, A.; Townes, C. H. *Microwave spectroscopy*; Dover, **1975**.

2. Gordy, W.; Cook, R. L. *Microwave Molecular Spectra*; Wiley: New York, **1984**.

3. Balle, T. J.; Flygare, W. H. *Rev. Sci. Instrum.* **1981**, *52*, 33-45.

4. Arunan, E.; Dev, S.; Mandal, P. K. *Applied Spectroscopy Reviews* **2007**, *39*, 131-181.

5. Brown, G. G.; Dian, B. C.; Douglass, K. O.; Geyer, S. M.; Shipman, S. T.; Pate, B. H. *Rev. Sci. Instrum.* **2008**, *79*, -.

6. Brown, G. G.; Dian, B. C.; Douglass, K. O.; Geyer, S. M.; Pate, B. H. *J. Mol. Spectrosc.* **2006**, *238*, 200-212.

7. Gutowsky, H. S.; Emilsson, T.; Arunan, E. *J.Chem.Phys.* **1993**, *99*, 4883-4893.

8. Prasad, B. R.; Krishnan, M. S.; Arunan, E. *J. Mol. Spectrosc.* **2005**, *232*, 308-314.

9. Oldani, M.; Ha, T. K.; Bauder, A. *Chem. Phys. Lett.* **1985**, *115*, 317-320.

10. Brupbacher, T.; Bauder, A. *Chem. Phys. Lett.* **1990**, *173*, 435-438.

11. Brupbacher, T.; Makarewicz, J.; Bauder, A. *J. Chem. Phys.* **1994**, *101*, 9736-9746.

12. Gutowsky, H. S.; Klots, T. D.; Chuang, C.; Schmuttenmaer, C. A.; Emilsson, T. *J.Chem.Phys.* **1987**, *86*, 569-576.

13. Cooke, S. A.; Cotti, G.; Evans, C. M.; Holloway, J. H.; Kisiel, Z.; Legon, A. C.; Thumwood, J. M. A. *Chemistry – A European Journal* **2001**, *7*, 2295-2305.

14. Mandal, P. K.; Ramdass, D. J.; Arunan, E. *Phys. Chem. Chem. Phys.* **2005**, *7*, 2740-2746.

15. Legon, A. C.; Lister, D. G. *Chem. Phys. Lett.* **1995**, *238*, 156-162.

16. Frisch, M. J.; Trucks, G. W.; Schlegel, H. B.; Scuseria, G. E.; Robb, M. A.; Cheeseman, J. R.; Scalmani, G.; Barone, V.; Mennucci, B.; Petersson, G. A.;

Nakatsuji, H.; Caricato, M.; Li, X.; Hratchian, H. P.; Izmaylov, A. F.; Bloino, J.; Zheng, G.; Sonnenberg, J. L.; Hada, M.; Ehara, M.; Toyota, K.; Fukuda, R.; Hasegawa, J.; Ishida, M.; Nakajima, T.; Honda, Y.; Kitao, O.; Nakai, H.; Vreven, T.; Montgomery, J. A.; Peralta, J. E.; Ogliaro, F.; Bearpark, M.; Heyd, J. J.; Brothers, E.; Kudin, K. N.; Staroverov, V. N.; Kobayashi, R.; Normand, J.; Raghavachari, K.; Rendell, A.; Burant, J. C.; Iyengar, S. S.; Tomasi, J.; Cossi, M.; Rega, N.; Millam, J. M.; Klene, M.; Knox, J. E.; Cross, J. B.; Bakken, V.; Adamo, C.; Jaramillo, J.; Gomperts, R.; Stratmann, R. E.; Yazyev, O.; Austin, A. J.; Cammi, R.; Pomelli, C.; Ochterski, J. W.; Martin, R. L.; Morokuma, K.; Zakrzewski, V. G.; Voth, G. A.; Salvador, P.; Dannenberg, J. J.; Dapprich, S.; Daniels, A. D.; Farkas; Foresman, J. B.; Ortiz, J. V.; Cioslowski, J.; Fox, D. J. Wallingford CT, 2009.

17. Pulay, P.; Fogarasi, G.; Pang, F.; Boggs, J. E. *J. Am. Chem. Soc.* **1979**, *101*, 2550-2560.

18. Andersson, M. P.; Uvdal, P. *The Journal of Physical Chemistry A* **2005**, *109*, 2937-2941.

19. Chakraborty, D.; Ambashta, R.; Manogaran, S. *The Journal of Physical Chemistry* **1996**, *100*, 13963-13970.

20. Lin, W.; Han, J.-X.; Takahashi, L. K.; Harker, H. A.; Keutsch, F. N.; Saykally, R. J. *J.Chem.Phys.* **2008**, *128*, -.

21. Herzberg, G. *New York: Van Nostrand, Reinhold, 1966* **1966**, *1*.

22. Stiles, P. L.; Moore, D. T.; Miller, R. E. *J.Chem.Phys.* **2004**, *121*, 3130-3142.

23. Morgan, P. J.; Alvarez-Valtierra, L.; Pratt, D. W. *Phys. Chem. Chem. Phys.* **2010**, *12*, 8323-8328.

24. Gutowsky, H. S.; Chen, J.; Hajduk, P. J.; Keen, J. D.; Chuang, C.; Emilsson, T. *J. Am. Chem. Soc.* **1991**, *113*, 4747-4751.

25. Aiswaryalakshmi, P.; Arunan, E. *To be published*.

26. Řezáč, J.; Hobza, P. *Journal of Chemical Theory and Computation* **2008**, *4*, 1835-1840.

27. Arunan, E.; Gutowsky, H. S. *J.Chem.Phys.* **1993**, *98*, 4294-4296.

28. van der Avoird, A.; Podeszwa, R.; Szalewicz, K.; Leforestier, C.; van Harrevelt, R.; Bunker, P. R.; Schnell, M.; von Helden, G.; Meijer, G. *Phys. Chem. Chem. Phys.* **2010**, *12*, 8219-8240.

29. Riley, K. E.; Pitoňák, M.; Černý, J. i.; Hobza, P. *Journal of Chemical Theory and Computation* **2009**, *6*, 66-80.

30. Goly, T.; Spoerel, U.; Stahl, W. *Chem. Phys.* **2002**, *283*, 289-296.

31. Mishra, B. K.; Arey, J. S.; Sathyamurthy, N. *The Journal of Physical Chemistry A* **2010**, *114*, 9606-9616.

32. Etchison, K. C.; Dewberry, C. T.; Kerr, K. E.; Shoup, D. W.; Cooke, S. A. *J. Mol. Spectrosc.* **2007**, *242*, 39-45.

33. Storm, V.; Dreizler, H.; Consalvo, D.; Grabow, J. U.; Merke, I. *Rev. Sci. Instrum.* **1996**, *67*, 2714-2719.

Appendix I.

Fe as Hydrogen/Halogen Bond Acceptor in The Trigonal Bipyramidal-$Fe(CO)_5$: A DFT and Atoms in Molecules Study of $Fe(CO)_5$●●●HF/HCl/HBr/ClF Complexes.

A.I.1. Introduction

Transition metal complexes acting as hydrogen bond acceptors have been studied by Alkorta *et al*.[1] They studied the complexes of $(CO)_4Ni$ and $(CO)_4Co^-$ with different hydrogen bond donors like HF, HCN, HNC and $HNMe_3$. The complexes with $(CO)_4Co^-$ were found to be more stable than the $(CO)_4Ni$ complexes. This extra stabilization could be attributed to the charge present in the $(CO)_4Co^-$ which leads to more electrostatic interactions in these complexes.

$Fe(CO)_5$ is a fluxional molecule. In the gas phase it exists in a trigonal bipyramidal geometry (TBP, D_{3h}-point group). Square pyramidal geometry (SP, C_{4v}-group) of the molecule, is a saddle point on the potential energy hypersurface and is the transition state for the Berry pseudo rotation.[2] We have recently studied hydrogen bonded complexes formed with square pyramidal $Fe(CO)_5$.[3] The study was inspired by the work of Rose-Petruck *et al*.[4,5] They studied the solvation properties of $Fe(CO)_5$ in different organic solvents using FTIR spectroscopy. $Fe(CO)_5$ has five CO stretching modes. In the TBP and SP geometries two of these modes are degenerate. In the TBP geometries three of the modes are IR-active (including the two degenerate modes) and the other two modes are IR-inactive. In the SP geometry one of the higher frequency modes (ν_1) becomes IR active and thus, in this geometry $Fe(CO)_5$ has a total of four IR-active (including the two degenerate modes) and only one IR-inactive mode. In the geometries in which symmetry is lowered (C_{2v}-geometries) the degeneracy of the modes is lifted. The ν_1 mode has much less IR-intensity than the other three IR-active CO stretching modes in the SP geometry. However, this mode showed strong solvent dependence and was thus, chosen for monitoring structural changes due to the solvation in the different solvents. It was found that this vibrational mode appears in the IR spectra taken in the aromatic solvents like benzene and pentafluorobenzene. Therefore, it was concluded that the TBP-$Fe(CO)_5$ gets distorted in these solvents. Using the IR experimental data and theoretical analysis it was concluded that about 60-90% of the molecules have ~C_{4v} geometry in these solvents. This observation was attributed to the formation of $Fe(CO)_5$•••C_6H_6 complex in which the benzene is located trans to the axial CO ligand of $Fe(CO)_5$ (which was concluded to be present in a ~ C_{4v} geometry in the complex) and one of the hydrogens of benzene points towards Fe (C-H•••Fe interaction). In a different work from the same group[6], solvation of $Fe(CO)_5$ by alcohols was studied. In this case also, the ν_1-mode appeared in the IR-

spectra. However, this time the reason given for the appearance of this mode was different from the reason given in case of solvation with the aromatic solvents. It was suggested that alcohol molecules interact with $Fe(CO)_5$ through interaction between the lone-pair electrons of oxygen of the hydroxyl group with $Fe(CO)_5$ and due to this interaction the electron density is transferred to $Fe(CO)_5$. The electron density transfer to different ligands takes place in different proportions and this results in the development of a dipole moment in the TBP-$Fe(CO)_5$ geometry. It was concluded that the structure of $Fe(CO)_5$ does not change much in alcohols and the gain of IR-activity by the ν_1-band is due to the development of this dipole moment in the TBP-$Fe(CO)_5$ unit. Surprisingly, the hydrogen bonding interactions between alcohols and $Fe(CO)_5$ unit were not considered even when alcohols are known to be stronger hydrogen bond donors than benzene.

The SP-$Fe(CO)_5$ has a net dipole moment which points towards the sixth coordination site and facilitates the formation of X-H•••Fe hydrogen bonds with molecules like HF, HCl and HBr.[3] As expected the halogen bonded complex with ClF was also found to be a stable minima.[3] On the contrary, the more stable TBP-$Fe(CO)_5$ (D_{3h}) has no dipole moment. Objective of the current study was twofold : (i) Can $Fe(CO)_5$ form hydrogen bonded complexes in the TBP geometry, which has zero dipole moment and (ii) can the observed IR-spectra be explained on the basis of hydrogen bonded geometries with TBP-$Fe(CO)_5$? We have tried to answer these questions using DFT methods, AIM studies and NBO analysis in the upcoming sections.

A.I.2. Theoretical methods

Full optimization was done for all the complexes. The optimization and frequency calculations were performed using Gaussian 09 suite of programs.[7] Functionals like B3LYP and wB97xD functional with basis sets 6-311+G(d,p) and Aug-cc-pVTZ were used for the calculations. The wB97xD has been found to be suitable for recovering the dispersion contribution.[8] The Atoms in Molecules (AIM) calculations were performed using AIM 2000 and AIMALL software.[9,10] The Natural bond orbital analysis was performed using NBO 6.0 software.[11,12] Interaction energies were calculated as the difference between energy of the complex and sum of energies of the constituting monomers optimized at the same level. The interaction energies were further corrected for the BSSE using counterpoise method,[13] and the zero-point errors.

A.I.3. Results and discussions

A.I.3.a. Geometry optimization

As mentioned earlier the SP-$Fe(CO)_5$ complex has a net dipole moment. ESP calculations also show the presence of high electron density along the sixth coordination site in this molecule, *Figure A.I.1*. ESP surface for the TBP-$Fe(CO)_5$ is also shown in the same figure. At the Fe atom along the C-Fe bond the ESP value is locally more negative, shown in yellow. Having this electronegative region can Fe act as hydrogen bond acceptor in the TBP-$Fe(CO)_5$?

Complexes of $Fe(CO)_5$ with hydrogen bond donors HF, HCl, HBr and halogen bond donor ClF were taken into consideration. The geometry optimizations were started with initial geometries in which $Fe(CO)_5$ was taken in the TBP geometry and the hydrogen/halogen bond donor moiety approaches from the other side of the one of the equatorial CO groups facing the electronegative centre. Since we were interested in exploring interactions with Fe, the hydrogen bonding interactions with oxygen of CO, which are expected to be much stronger, were not considered. Full optimization was performed for all the complexes and frequency calculations were also performed to confirm if the optimized geometry is a minimum. The calculations were performed at the B3LYP/6-311+G(d,p), B3LYP/Aug-cc-pVTZ, wB97xD/6-311+G(d,p) and wB97xD/Aug-cc-pVTZ levels of theory. At different levels of theory the BSSE corrected *(ΔE_{BSSE})* and BSSE + zero-point corrected *($\Delta E_{BSSE+ZPC}$)* interaction energies for the optimized complexes, are given in *Table A.I.1*. The structural parameters as well as HX/ClF frequency shifts on complex formation are given in *Table A.I.2*. The negative values of the interaction energies imply stabilization on complexation and the positive values imply destabilization. It can be noted that at the B3LYP/6-311+G(d,p) and B3LYP/Aug-cc-pVTZ levels, there is destabilization on complexation with HCl and HBr. However, other parameters like increase in bond length (Δr) , red-shift in frequency ($\Delta \nu$) of HX/ClF stretching mode on complexation suggest an interaction between the two monomers, see *Table A.I.2*. All the complexes at the B3LYP/6-311+G(d,p) level, are minima as confirmed by the presence of all real frequencies for the normal mode of vibrations. At the B3LYP/Aug-cc-pVTZ level, all the complexes except $Fe(CO)_5$•••HBr complex, are minima. The $Fe(CO)_5$•••HBr complex at this level has one low (~$10cm^{-1}$) imaginary frequency. At the wB97xD/6-311+G(d,p) level, complex formation with all the four donor molecules leads to

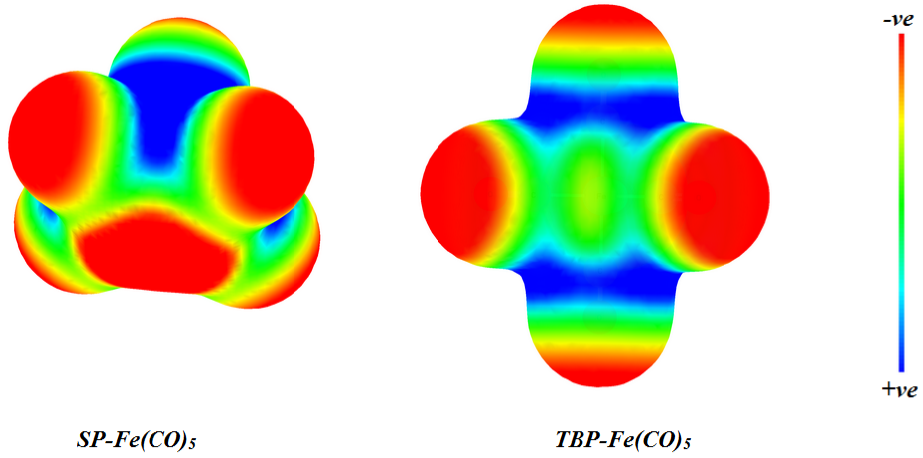

Figure A.I.1. Electrostatic potential surfaces for the square pyramidal (SP)-$Fe(CO)_5$ and trigonal bipyramidal (TBP)-$Fe(CO)_5$ at the wB97xD/6-311+G(d,p) level. The color code bar is also given. The surfaces were plotted using GaussView software.

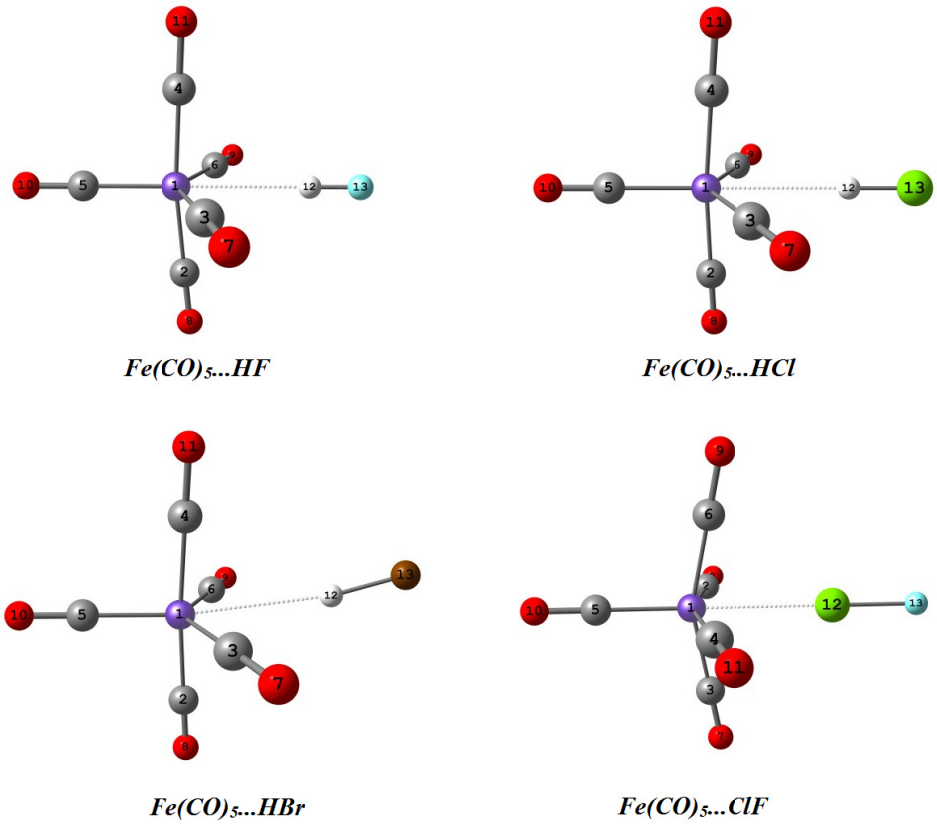

Figure A.I.2. Optimized geometries for the $Fe(CO)_5$●●●HF, $Fe(CO)_5$●●●HCl, $Fe(CO)_5$●●●HBr and $Fe(CO)_5$●●●ClF complexes the wB97xD/6-311+G(d,p) level.

stabilization as suggested by the negative interaction energies, *Table A.I.1*. The calculated interaction energy at this level, increases in the order $Fe(CO)_5$•••HCl < $Fe(CO)_5$•••HBr < $Fe(CO)_5$•••HF < $Fe(CO)_5$•••ClF. It should be noted that the complex with HBr is more stable than the complex with HCl. At the wB97xD/Aug-cc-pVTZ level the complex formation with HBr results in huge destabilization (ΔE_{BSSE}=+566.1 kJ/mol). This completely different result for the complex with HBr, as compared to the complexes with HF/HCl/ClF, may either be due to its very different geometry or inefficiency of this level of theory for this complex. However, other parameters given in *Table A.I.2* again suggest interaction between the $Fe(CO)_5$ and HBr moieties. With the wB97xD functional, all the complexes, except the $Fe(CO)_5$•••HCl complex, are found to be minima with both the basis sets at the potential energy hypersurface. The $Fe(CO)_5$•••HCl complex has a low imaginary frequency of magnitude 10.5 and 12.9cm^{-1} at the wB97xD/6-311+G(d,p) and the wB97xD/Aug-cc-pVTZ levels respectively. Optimized geometries at the wB97xD/6-311+G(d,p) level are given in *Figure A.I.2*. It should be noted that similar complexes with SP-$Fe(CO)_5$ were much stronger.[3]

A.I.3.b. Atoms in molecules theoretical analysis

From the above discussion it is clear that among the four levels considered for the calculations, wB97xD/6-311+G(d,p) level works the best for these complexes. Therefore, the optimized geometries at this level were considered for further analysis. Wave functions used for the AIM analysis were those of the optimized geometries at the wB97xD/6-311+G(d,p) level. Electron density topologies resulting from these calculations are shown in the *Figure A.I.3*. As shown in the figure, an intermolecular bond critical point (BCP) exists between the $Fe(CO)_5$ and HX/ClF moiety. A bond path also exists which connects the BCP to the Fe atom and the H/Cl atom. The electron density, $\rho(r)$, and Laplacian of electron density, $\nabla^2\rho(r)$, values at the intermolecular BCP are given in the *Table A.I.3*. Positive values of the Laplacian imply that these intermolecular interactions are closed shell interaction. Mutual penetration between the interacting atoms is also given in the *Table*. For each of the complexes, the mutual penetration is significantly high which confirms the bonding interaction between the two interacting atoms.

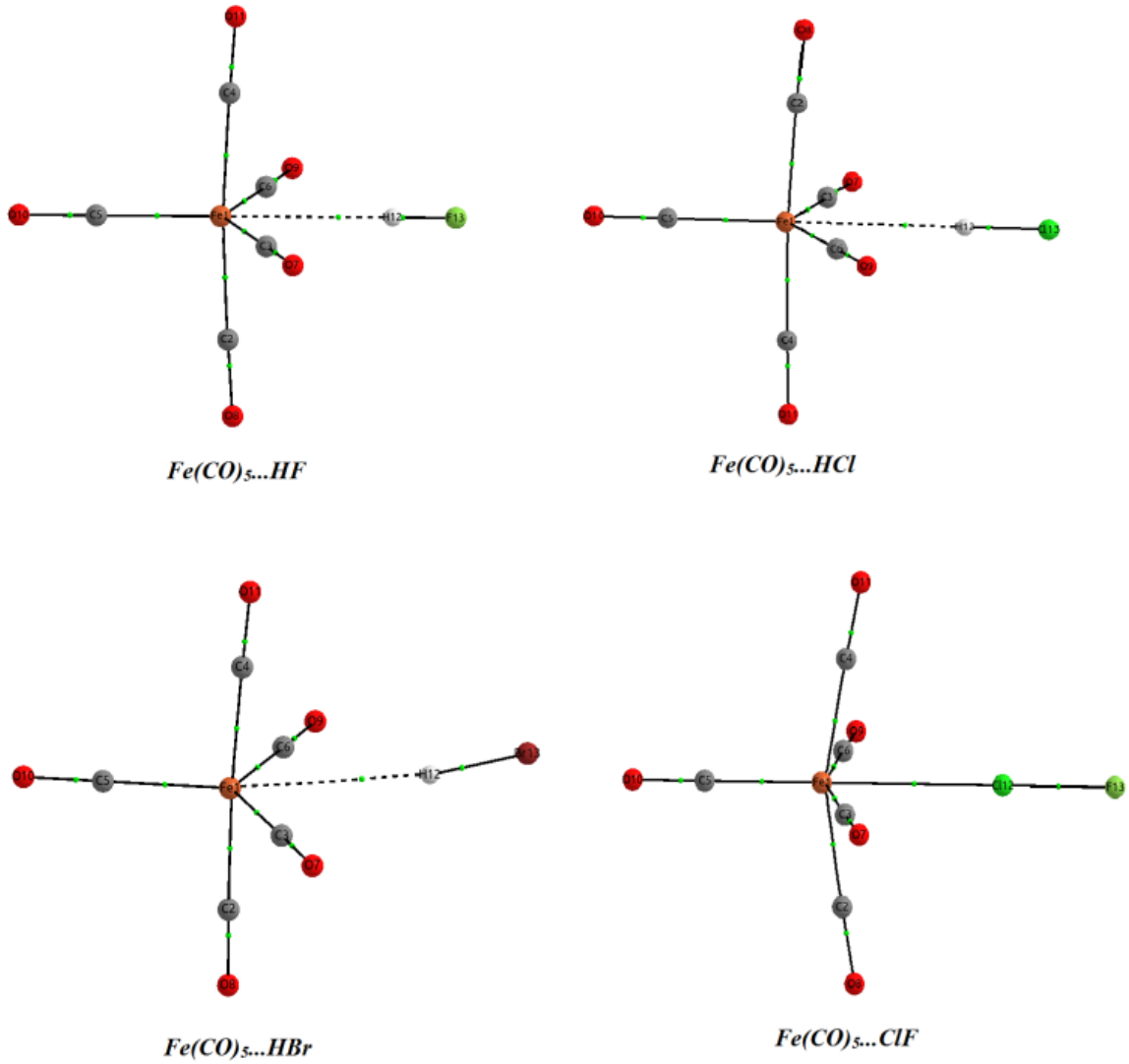

Figure A.I.3. AIM topologies of $Fe(CO)_5$●●●HF, $Fe(CO)_5$●●●HCl, $Fe(CO)_5$●●●HBr and $Fe(CO)_5$●●●ClF complexes.

Table A.I.1. Interaction energies for different complexes of $Fe(CO)_5$ at different levels of theory. The negative value of interaction energy implies stabilization and positive value implies destabilization on complex formation.

Complex	*ΔE_{BSSE} (in kJ/mol)*	*$\Delta E_{BSSE+ZPC}$ (in kJ/mol)*	*ΔE_{BSSE} (in kJ/mol)*	*$\Delta E_{BSSE+ZPC}$ (in kJ/mol)*
	At B3LYP/6-311+G(d,p)		*At B3LYP/Aug-cc-pVTZ*	
$Fe(CO)_5$•••HF	-4.7	0.0	-4.4	0.5
$Fe(CO)_5$•••HCl	1.6	5.0	1.3	4.2
$Fe(CO)_5$•••HBr	2.1	4.0	0.0	3.0
$Fe(CO)_5$…ClF	-31.5	-29.5	-20.9	-19.1
	At wB97xD/6-311+G(d,p)		*At wB97xD/Aug-cc-pVTZ*	
$Fe(CO)_5$•••HF	-12.3	-7.5	-12.5	-7.4
$Fe(CO)_5$•••HCl	-8.5	-4.7	-8.2	-4.9
$Fe(CO)_5$•••HBr	-8.6	-5.8	566.1	568.9
$Fe(CO)_5$•••ClF	-24.5	-22.5	-17.3	-15.8

Table A.I.2. Structural parameters for the intermolecular interactions in $Fe(CO)_5$ complexes at different levels of theory. Shifts in the HX/ClF stretching frequency are also given.

Complex	*$R_{Fe-H/Cl}$ (Å)*	*$\angle X(H/Cl)Fe$*	*Δr* (Å)*	*$\Delta \nu$* (cm^{-1})*	*$R_{Fe-H/Cl}$ (Å)*	*$\angle X(H/Cl)Fe$*	*Δr* (Å)*	*$\Delta \nu$* (cm^{-1})*
	B3LYP/6-311+G(d,p)				*B3LYP/Aug-cc-pVTZ*			
$Fe(CO)_5$···HF	2.5895	180.0^0	0.0115	-282.3	2.5892	180.0^0	0.0115	-284.8
$Fe(CO)_5$···HCl	3.0047	180.0^0	0.0075	-121.0	3.1156	180.0^0	0.0058	-97.1
$Fe(CO)_5$···HBr	3.2134	180.0^0	0.0050	-78.7	3.3576	180.0^0	0.0040	-60.5
$Fe(CO)_5$···ClF	2.7503	180.0^0	0.1764	-98.1	2.8398	180.0^0	0.1257	-137.4
	wB97xD/6-311+G(d,p)				*wB97xD/Aug-cc-pVTZ*			
$Fe(CO)_5$···HF	2.5174	180.0^0	0.0132	-320.6	2.5158	180.0^0	0.0130	-316.9
$Fe(CO)_5$···HCl	2.7547	180.0^0	0.0126	-145.2	2.8002	180.0^0	0.0110	-130.5
$Fe(CO)_5$···HBr	2.8615	171.2^0	0.0096	-133.3	2.8929	170.9^0	0.0092	-123.0
$Fe(CO)_5$···ClF	2.8351	180.0^0	0.1074	-108.0	2.9893	180.0^0	0.0620	-140.8

**Δr=r(HX/ClF in complex)-r(HF/ClF in monomer)*

$\Delta \nu$=ν(HX/ClF in complex)-ν(HF/ClF in monomer)

Table A.I.3. Electron density, $\rho(r)$ and Laplacian of electron density, $\nabla^2\rho(r)$, at the intermolecular bond critical point and mutual penetration between the interacting Fe and H/Cl atoms.

Complex	*$\rho(r)$(a.u.)*	*$\nabla^2\rho(r)$(a.u.)*	*Mutual penetration (Å)*
$Fe(CO)_5$•••HF	0.0170	0.0302	1.11
$Fe(CO)_5$•••HCl	0.0127	0.0220	1.05
$Fe(CO)_5$•••HBr	0.0112	0.0191	0.99
$Fe(CO)_5$•••ClF	0.0302	0.0405	1.49

Plot between electron density at the intermolecular BCPs and interaction energy is given in the *Figure A.I.4*. It is clear that the interaction energy and electron density are almost linearly dependent, correlation coefficient=0.992, for these complexes.

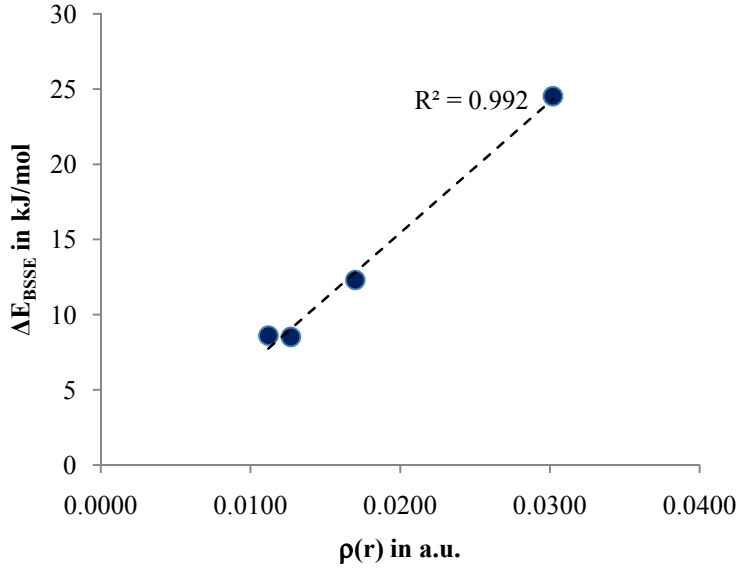

Figure A.I.4. Correlation between electron density at intermolecular BCPs and interaction energy for the $Fe(CO)_5$ complexes.

A.I.3.c. Natural bond orbital (NBO) analysis

The results obtained from the NBO analysis are given in the *Table A.I.4* and *Table A.I.5*. The *Table A.I.4* gives charge transfer from $Fe(CO)_5$ moiety to the HX/ClF moiety upon complex formation. The charge transfer is significantly high for the complex with ClF. Note that the interaction energies for these complexes increases in the order $Fe(CO)_5$•••HCl < $Fe(CO)_5$•••HBr < $Fe(CO)_5$•••HF < $Fe(CO)_5$•••ClF, *Table A.I.1*, while NBO charge transfer increases in the order $Fe(CO)_5$•••HBr < $Fe(CO)_5$•••HCl < $Fe(CO)_5$•••HF < $Fe(CO)_5$•••ClF, *Table A.I.4*. It is clear that in general interaction energy increases as the charge transfer increases, except for going from $Fe(CO)_5$•••HBr to $Fe(CO)_5$•••HCl complex. This might be because the hydrogen bond parameters of $Fe(CO)_5$•••HBr complex are different from the other three complexes, *Figure A.I.2, Table A.I.2*. Overall correlation between the charge transfer and interaction energies is given in the *Figure A.I.5*. The correlation coefficient is 0.954. On leaving out the ClF data, correlation becomes very poor (correlation coefficient=0.363).

Table A.I.4. Charge transfer from $Fe(CO)_5$ unit to HX/ClF unit in different complexes calculated from NBO analysis.

Complex	*Charge transfer (ΔQ, e)*
$Fe(CO)_5\cdots HF$	0.015
$Fe(CO)_5\cdots HCl$	0.011
$Fe(CO)_5\cdots HBr$	0.007
$Fe(CO)_5\cdots ClF$	0.274

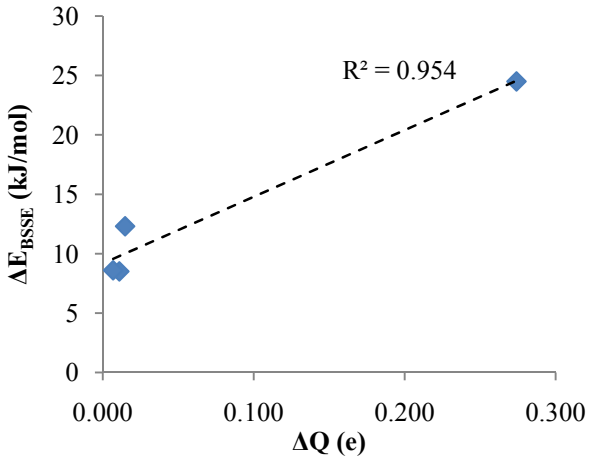

Figure A.I.5. Correlation between NBO charge transfer (ΔQ) and interaction energy (ΔE) for the $Fe(CO)_5$ complexes.

Results from the second order perturbation analysis in NBO basis are given in the *Table A.I.5*. In case of complexes with HX molecules, interaction is between d-orbital lone pair of Fe and antibonding (HX) orbital as well as between bonding (Fe-C) orbitals and the antibonding (HX) orbital. In case of the ClF complex, the interaction is between Fe-C orbitals (bonding as well as antibonding) and antibonding Cl-F orbital. The major contribution in this case comes from the interaction between antibonding Fe-C orbital and antibonding Cl-F orbital. Note that the antibonding Fe-C orbitals in the TBP-$Fe(CO)_5$ are occupied. The occupancy calculated from NBO analysis is, 0.04 e for the two axial Fe-C antibonding orbitals and 0.03 e for the three equatorial Fe-C antibonding orbitals. The atom labelling used in *Table A.I.5* is adopted from the *Figure A.I.2*.

Table A.I.5. Results from the second order perturbation analysis for the $Fe(CO)_5$ complexes. The orbitals which contribute significantly in the charge transfer and the $E^{(2)}$ energy corresponding to the charge transfer, are given.

Complex	*Donor orbital*	*Acceptor orbital*	*$E^{(2)}$ (donor--->acceptor) in kJ/mol*
$Fe(CO)_5$•••HF	LP Fe1	BD*(1) H12- F13	5.5
	BD Fe1- C2	BD*(1) H12- F13	4.4
	BD Fe1- C6	BD*(1) H12- F13	10.8
$Fe(CO)_5$•••HCl	LPFe1	BD*(1) H12-Cl13	3.7
	BD Fe1- C2	BD*(1) H12-Cl13	3.5
	BD Fe1- C6	BD*(1) H12-Cl13	9.5
$Fe(CO)_5$•••HBr	LP Fe1	BD*(1) H12-Br13	2.9
	BD Fe1- C3	BD*(1) H12-Br13	8.2
	BD Fe1- C4	BD*(1) H12-Br13	3.2
$Fe(CO)_5$•••ClF	BD Fe1- C2	BD*(1)Cl12- F13	7.5
	BD Fe1- C3	BD*(1)Cl12- F13	7.5
	BD* Fe1- C5	BD*(1)Cl12- F13	388.5

A.I.3.d. Shifts in the CO stretching frequencies on complex formation

The CO stretching frequencies and their IR-intensities for these molecules and complexes, are given in the *Table A.I.6*. For the frequency calculations of TBP-$Fe(CO)_5$ its geometry was restricted to be in the TBP shape. The unrestricted structural optimization leads to removal of the degeneracy of the normal modes of vibration. This happens because of the slight loss of symmetry on the unrestricted optimization. Results from the unrestricted (full) optimization are also given in the *Additional Information* section. On complex formation there is blue-shifts in the CO stretching frequencies. This is due to the loss of electrons from the CO antibonding orbitals on complex formation. This loss of electrons strengthens the CO bonds and therefore, results in the blue shifts of stretching frequencies. The band at 2227.1 cm^{-1} is IR-inactive in the TBP-$Fe(CO)_5$ and it becomes IR-active in the SP-$Fe(CO)_5$. On complexation of the TBP-$Fe(CO)_5$ with HF, HCl, HBr and ClF the band gains IR-activity and should be observed in these complexes as well. The intensity of this band is largest for the $Fe(CO)_5$•••ClF complex which is because of strong halogen bonding in this complex which leads to the significant structural deformation.

It is clear that the hydrogen/halogen bonding interactions with the TBP-$Fe(CO)_5$ are

strong enough to deform the TBP structure of $Fe(CO)_5$. This deformation provides IR-activity to one of the originally IR-inactive band of the TBP-$Fe(CO)_5$. This band has been used to predict the change in the structure of $Fe(CO)_5$ on solvation in different solvents.[4,6] However, our calculations show that the $Fe(CO)_5$ geometry is not 'near C_{4v}' on complex formation with molecules like HF/HCl/HBr and it is still closer to the D_{3h} TBP geometry though little distorted. Only in case of bonding with ClF the structure distorts to near square planar (C_{4v}) geometry.

Table A.I.6. Stretching frequencies for the CO ligand in different complexes calculated at the wB97xD/6-311+G(d,p) level of theory.

TBP-Fe(CO)$_5$		*SP-Fe(CO)$_5$*		*TBP-Fe(CO)$_5$●●●HF*	
ν/cm^{-1}	IR intensity	ν/cm^{-1}	IR intensity	ν/cm^{-1}	IR intensity
2120.0	1468.9	2122.5	1921.3	2133.0	1605.3
2120.0	1467.9	2122.5	1921.4	2142.2	953.3
2147.1	0.0	2130.8	0.0	2161.2	153.4
2148.8	1658.4	2132.3	723.7	2161.4	1563.3
2227.1	0.0	2216.7	34.8	2236.3	13.7
TBP-Fe(CO)$_5$●●●HCl		*TBP-Fe(CO)$_5$●●●HBr*		*TBP-Fe(CO)$_5$●●●ClF*	
ν/cm^{-1}	IR intensity	ν/cm^{-1}	IR intensity	ν/cm^{-1}	IR intensity
2126.1	1535.6	2122.5	1488.7	2165.5	1447.4
2136.0	1030.5	2131.6	1127.4	2165.5	1447.4
2157.2	138.2	2154.2	420.4	2168.7	775.3
2157.7	1554.1	2156.9	1222.0	2172.1	0.0
2231.6	29.2	2229.2	33.5	2237.0	231.4

A.I.4. Conclusions

Interactions of TBP-$Fe(CO)_5$ with HX/ClF molecules have been analysed using DFT/DFT-d methods as well as AIM and NBO methods. The structural changes, frequency shifts on complex formation and AIM analysis suggest a strong intermolecular interaction in the complexes. NBO analysis suggest that there is a significant charge transfer from the $Fe(CO)_5$ moiety to the HX/ClF moiety. It is clear that the TBP geometry of $Fe(CO)_5$ which has no dipole moment, can also form Fe●●●H/Cl hydrogen/halogen bonded complexes similar to the square pyramidal geometry which has a net dipole moment.

A.I.5. Supplementary Information

Coordinates for the optimized geometries at different levels of theory and frequencies for the normal modes of vibration are given in the *Supplementary Information*.

A.I.6. References

1. Alkorta, I.; Rozas, I.; Elguero, J. *Journal of Molecular Structure: THEOCHEM* **2001**, *537*, 139-150.

2. Berry, R. S. *J.Chem.Phys.* **1960**, *32*, 933-938.

3. Aiswaryalakshmi, P.; Mani, D.; Arunan, E. *Inorg. Chem.* **2013**, *52*, 9153-9161.

4. Jiang, Y.; Lee, T.; Rose-Petruck, C. G. *The Journal of Physical Chemistry A* **2003**, *107*, 7524-7538.

5. Lee, T.; Benesch, F.; Jiang, Y.; Rose-Petruck, C. G. *Chem. Phys.* **2004**, *299*, 233-245.

6. Lessing, J.; Li, X.; Lee, T.; Rose-Petruck, C. G. *The Journal of Physical Chemistry A* **2008**, *112*, 2282-2292.

7. Frisch, M. J.; Trucks, G. W.; Schlegel, H. B.; Scuseria, G. E.; Robb, M. A.; Cheeseman, J. R.; Scalmani, G.; Barone, V.; Mennucci, B.; Petersson, G. A.; Nakatsuji, H.; Caricato, M.; Li, X.; Hratchian, H. P.; Izmaylov, A. F.; Bloino, J.; Zheng, G.; Sonnenberg, J. L.; Hada, M.; Ehara, M.; Toyota, K.; Fukuda, R.; Hasegawa, J.; Ishida, M.; Nakajima, T.; Honda, Y.; Kitao, O.; Nakai, H.; Vreven, T.; Montgomery, J. A.; Peralta, J. E.; Ogliaro, F.; Bearpark, M.; Heyd, J. J.; Brothers, E.; Kudin, K. N.; Staroverov, V. N.; Kobayashi, R.; Normand, J.; Raghavachari, K.; Rendell, A.; Burant, J. C.; Iyengar, S. S.; Tomasi, J.; Cossi, M.; Rega, N.; Millam, J. M.; Klene, M.; Knox, J. E.; Cross, J. B.; Bakken, V.; Adamo, C.; Jaramillo, J.; Gomperts, R.; Stratmann, R. E.; Yazyev, O.; Austin, A. J.; Cammi, R.; Pomelli, C.; Ochterski, J. W.; Martin, R. L.; Morokuma, K.; Zakrzewski, V. G.; Voth, G. A.; Salvador, P.; Dannenberg, J. J.; Dapprich, S.; Daniels, A. D.; Farkas; Foresman, J. B.; Ortiz, J. V.; Cioslowski, J.; Fox, D. J. Wallingford CT, 2009.

8. Johnson, E. R.; Salamone, M.; Bietti, M.; DiLabio, G. A. *The Journal of Physical Chemistry A* **2013**, *117*, 947-952.

9. Biegler-König, F.; Schönbohm, J. *J. Comput. Chem.* **2002**, *23*, 1489-1494.

10. AIMAll (Version 13.02.26), K., Todd A.; TK Gristmill Software, : Overland Park KS, USA, 2012 (aim.tkgristmill.com).

11. Glendening, E.; Badenhoop, J.; Reed, A.; Carpenter, J.; Bohmann, J.; Morales, C.; Landis, C.; Weinhold, F. In *(Theoretical Chemistry Institute, University of Wisconsin, Madison, WI, 2013); http://nbo6.chem.wisc.edu/*.

12. Glendening, E. D.; Badenhoop, J. K.; Reed, A. E.; Carpenter, J. E.; Bohmann, J. A.; Morales, C. M.; Landis, C. R.; Weinhold, F. 2013.

13. Boys, S. F.; Bernardi, F. *Mol. Phys.* **1970**, *19*, 553.

Supplementary Information

Table A.I.S.1. Coordinates for the optimized geometries of $Fe(CO)_5$ at different levels of theory.

B3LYP/6-311+G(d,p)				*B3LYP/Aug-cc-pVTZ*			
Atom	x (Å)	y (Å)	z (Å)	Atom	x (Å)	y (Å)	z (Å)
Fe	0.0000	0.0000	0.0000	Fe	0.0000	0.0000	0.0001
C	1.8287	-0.0003	0.0001	C	1.8263	0.0004	0.0002
C	0.0000	-1.6804	0.7029	C	0.0001	-1.6303	-0.8101
C	-1.8286	-0.0002	0.0002	C	-1.8263	0.0002	-0.0003
C	0.0000	0.2313	-1.8068	C	0.0000	1.5169	-1.0063
C	0.0001	1.4491	1.1036	C	-0.0003	0.1133	1.8171
O	-0.0002	-2.7349	1.1442	O	0.0004	-2.6520	-1.3181
O	2.9677	0.0000	0.0001	O	2.9635	-0.0001	-0.0004
O	0.0001	2.3586	1.7961	O	-0.0003	0.1843	2.9559
O	-0.0002	0.3765	-2.9406	O	0.0002	2.4677	-1.6372
O	-2.9677	0.0002	0.0003	O	-2.9635	-0.0003	-0.0010
wB97xD/6-311+G(d,p)				*wB97xD/Aug-cc-pVTZ*			
Atom	x (Å)	y (Å)	z (Å)	Atom	x (Å)	y (Å)	z (Å)
Fe	0.0001	0.0001	0.0003	Fe	0.0000	0.0000	0.0002
C	1.8199	-0.0001	-0.0003	C	1.8162	0.0003	0.0002
C	0.0002	-1.5636	-0.9176	C	0.0001	-1.1523	1.3964
C	-1.8198	-0.0003	-0.0003	C	-1.8162	0.0001	0.0002
C	0.0000	1.5770	-0.8950	C	0.0000	-0.6332	-1.6969
C	0.0000	-0.0129	1.8127	C	-0.0001	1.7858	0.2999
O	0.0000	-2.5460	-1.4939	O	0.0002	-1.8765	2.2726
O	2.9548	-0.0003	-0.0005	O	2.9492	0.0001	0.0006
O	-0.0002	-0.0211	2.9517	O	-0.0001	2.9069	0.4874
O	-0.0003	2.5675	-1.4572	O	0.0000	-1.0308	-2.7618
O	-2.9547	-0.0006	-0.0007	O	-2.9492	-0.0001	0.0007

Table A.I.S.2. Coordinates for the optimized geometries of HF at different levels of theory.

B3LYP/6-311+G(d,p)				*B3LYP/Aug-cc-pVTZ*			
Atom	x (Å)	y (Å)	z (Å)	Atom	x (Å)	y (Å)	z (Å)
H	0.0000	0.0000	-0.8301	H	0.0000	0.0000	-0.8317
F	0.0000	0.0000	0.0922	F	0.0000	0.0000	0.0924
wB97xD/6-311+G(d,p)				*wB97xD/Aug-cc-pVTZ*			
Atom	x (Å)	y (Å)	z (Å)	Atom	x (Å)	y (Å)	z (Å)
H	0	0	-0.82513	H	0.0000	0.0000	-0.8265
F	0	0	0.091681	F	0.0000	0.0000	0.0918

Table A.I.S.3. Coordinates for the optimized geometries of HCl at different levels of theory.

B3LYP/6-311+G(d,p)				B3LYP/Aug-cc-pVTZ			
Atom	x (Å)	y (Å)	z (Å)	Atom	x (Å)	y (Å)	z (Å)
H	0.0000	0.0000	-1.2153	H	0.0000	0.0000	-1.2124
Cl	0.0000	0.0000	0.0715	Cl	0.0000	0.0000	0.0713
wB97xD/6-311+G(d,p)				wB97xD/Aug-cc-pVTZ			
Atom	x (Å)	y (Å)	z (Å)	Atom	x (Å)	y (Å)	z (Å)
H	0.0000	0.0000	-1.2115	H	0.0000	0.0000	-1.2094
Cl	0.0000	0.0000	0.0713	Cl	0.0000	0.0000	0.0711

Table A.I.S.4. Coordinates for the optimized geometries of HBr at different levels of theory.

B3LYP/6-311+G(d,p)				*B3LYP/Aug-cc-pVTZ*			
Atom	x (Å)	y (Å)	z (Å)	Atom	x (Å)	y (Å)	z (Å)
H	0.0000	0.0000	-1.3873	H	0.0000	0.0000	-1.3844
Br	0.0000	0.0000	0.0396	Br	0.0000	0.0000	0.0396
wB97xD/6-311+G(d,p)				*wB97xD/Aug-cc-pVTZ*			
Atom	x (Å)	y (Å)	z (Å)	Atom	x (Å)	y (Å)	z (Å)
H	0.0000	0.0000	-1.3805	H	0.0000	0.0000	-1.3787
Br	0.0000	0.0000	0.0394	Br	0.0000	0.0000	0.0394

Table A.I.S.5. Coordinates for the optimized geometries of ClF at different levels of theory.

B3LYP/6-311+G(d,p)				B3LYP/Aug-cc-pVTZ			
Atom	x (Å)	y (Å)	z (Å)	Atom	x (Å)	y (Å)	z (Å)
F	0.0000	0.0000	-1.0977	F	0.0000	0.0000	-1.0780
Cl	0.0000	0.0000	0.5811	Cl	0.0000	0.0000	0.5707
wB97xD/6-311+G(d,p)				wB97xD/Aug-cc-pVTZ			
Atom	x (Å)	y (Å)	z (Å)	Atom	x (Å)	y (Å)	z (Å)
F	0.0000	0.0000	-1.0837	F	0.0000	0.0000	-1.0649
Cl	0.0000	0.0000	0.5737	Cl	0.0000	0.0000	0.5638

Table A.I.S.6. Coordinatse for the optimized geometries of $Fe(CO)_5$●●●HF complex at different levels of theory.

B3LYP/6-311+G(d,p)				*B3LYP/Aug-cc-pVTZ*			
Atom	x (Å)	y (Å)	z (Å)	Atom	x (Å)	y (Å)	z (Å)
Fe	-0.2704	0.0000	0.0000	Fe	0.2705	0.0000	0.0000
C	-0.1787	1.8314	0.0000	C	0.1803	1.8294	0.0000
C	0.4205	0.0000	-1.6918	C	-0.4207	0.0000	1.6903
C	-0.1787	-1.8314	0.0000	C	0.1803	-1.8294	0.0000
C	-2.0967	0.0000	0.0000	C	2.0958	0.0000	0.0000
C	0.4205	0.0000	1.6918	C	-0.4208	0.0000	-1.6903
O	0.8122	0.0000	-2.7640	O	-0.8125	0.0000	2.7603
O	-0.1242	2.9675	0.0001	O	0.1258	2.9635	0.0000
O	0.8124	0.0000	2.7639	O	-0.8126	0.0000	-2.7602
O	-3.2370	0.0000	0.0000	O	3.2340	0.0000	0.0000
O	-0.1242	-2.9675	0.0001	O	0.1259	-2.9635	-0.0001
H	2.3191	0.0000	0.0000	H	-2.3187	0.0000	0.0000
F	3.2529	0.0000	-0.0002	F	-3.2543	0.0000	0.0002
wB97xD/6-311+G(d,p)				*wB97xD/Aug-cc-pVTZ*			
Atom	x (Å)	y (Å)	z (Å)	Atom	x (Å)	y (Å)	z (Å)
Fe	-0.2685	0.0000	0.0000	Fe	-0.2687	0.0000	0.0000
C	-0.1488	1.8207	0.0001	C	-0.1501	-1.8175	-0.0001
C	0.3996	0.0000	-1.6903	C	0.3992	0.0000	1.6877
C	-0.1488	-1.8207	0.0000	C	-0.1501	1.8175	0.0000
C	-2.0882	0.0000	0.0000	C	-2.0861	0.0000	0.0000
C	0.3998	0.0000	1.6903	C	0.3993	0.0000	-1.6877
O	0.7860	0.0001	-2.7600	O	0.7856	-0.0001	2.7552
O	-0.0715	2.9514	0.0001	O	-0.0720	-2.9462	-0.0001
O	0.7863	0.0000	2.7599	O	0.7858	0.0000	-2.7551
O	-3.2243	0.0000	0.0000	O	-3.2200	0.0000	-0.0001
O	-0.0715	-2.9514	0.0000	O	-0.0719	2.9462	0.0000
H	2.2489	0.0000	-0.0001	H	2.2471	0.0000	0.0001
F	3.1789	0.0000	-0.0002	F	3.1784	0.0000	0.0002

Table A.I.S.7. Coordinates for the optimized geometries of $Fe(CO)_5$●●●HCl complex at different levels of theory.

B3LYP/6-311+G(d,p)				*B3LYP/Aug-cc-pVTZ*			
Atom	x (Å)	y (Å)	z (Å)	Atom	x (Å)	y (Å)	z (Å)
Fe	-0.6326	0.0000	0.0000	Fe	-0.6530	-0.0001	0.0001
C	-0.5731	1.8307	-0.0001	C	-0.6110	1.8287	-0.0002
C	0.1289	0.0001	-1.6585	C	0.1331	0.0005	-1.6451
C	-0.5732	-1.8306	-0.0002	C	-0.6086	-1.8288	-0.0001
C	-2.4557	0.0001	-0.0002	C	-2.4751	-0.0012	0.0007
C	0.1285	-0.0001	1.6585	C	0.1343	0.0005	1.6448
O	0.5732	0.0001	-2.7108	O	0.5969	0.0008	-2.6870
O	-0.5359	2.9680	0.0002	O	-0.5864	2.9646	-0.0003
O	0.5726	-0.0001	2.7109	O	0.5987	0.0009	2.6864
O	-3.5970	0.0001	-0.0003	O	-3.6145	-0.0021	0.0012
O	-0.5363	-2.9680	0.0000	O	-0.5825	-2.9646	-0.0002
H	2.3721	-0.0001	0.0003	H	2.4625	-0.0004	0.0001
Cl	3.6664	-0.0001	0.0003	Cl	3.7520	0.0005	-0.0001
wB97xD/6-311+G(d,p)				*wB97xD/Aug-cc-pVTZ*			
Atom	x (Å)	y (Å)	z (Å)	Atom	x (Å)	y (Å)	z (Å)
Fe	-0.5928	0.0000	0.0000	Fe	-0.6026	0.0003	0.0001
C	-0.4952	1.8208	-0.0002	C	-0.5223	1.8185	-0.0005
C	0.1213	-0.0002	-1.6696	C	0.1385	-0.0013	-1.6548
C	-0.4954	-1.8207	0.0005	C	-0.5283	-1.8182	0.0001
C	-2.4107	0.0002	-0.0001	C	-2.4173	0.0031	0.0002
C	0.1214	0.0004	1.6697	C	0.1384	-0.0006	1.6551
O	0.5427	-0.0006	-2.7268	O	0.5803	-0.0022	-2.7013
O	-0.4297	2.9526	-0.0002	O	-0.4678	2.9490	-0.0010
O	0.5429	0.0004	2.7268	O	0.5801	-0.0013	2.7017
O	-3.5473	0.0000	-0.0003	O	-3.5521	0.0049	0.0003
O	-0.4301	-2.9526	0.0007	O	-0.4779	-2.9489	0.0000
H	2.1619	-0.0001	0.0000	H	2.1976	-0.0008	0.0000
Cl	3.4573	-0.0001	-0.0002	Cl	3.4892	-0.0016	-0.0001

Table A.I.S.8. Coordinates for the optimized geometries of $Fe(CO)_5$●●●HBr complex at different levels of theory.

B3LYP/6-311+G(d,p)				*B3LYP/Aug-cc-pVTZ*			
Atom	x (Å)	y (Å)	z (Å)	Atom	x (Å)	y (Å)	z (Å)
Fe	-1.2322	0.0000	0.0000	Fe	1.2743	0.0001	0.0001
C	-1.1888	1.8306	-0.0001	C	1.2456	-1.8281	0.0000
C	-0.4356	0.0000	-1.6412	C	0.4546	-0.0006	-1.6277
C	-1.1887	-1.8306	0.0001	C	1.2428	1.8283	-0.0001
C	-3.0549	-0.0001	-0.0001	C	3.0957	0.0015	0.0008
C	-0.4357	0.0001	1.6412	C	0.4533	-0.0006	1.6272
O	0.0366	-0.0001	-2.6817	O	-0.0372	-0.0011	-2.6570
O	-1.1619	2.9685	-0.0001	O	1.2287	-2.9644	-0.0001
O	0.0365	0.0002	2.6818	O	-0.0393	-0.0010	2.6561
O	-4.1966	-0.0001	-0.0001	O	4.2355	0.0024	0.0012
O	-1.1617	-2.9685	0.0001	O	1.2241	2.9645	-0.0002
H	1.9812	0.0000	0.0001	H	-2.0833	0.0004	0.0001
Br	3.4131	0.0000	0.0000	Br	-3.5113	-0.0002	-0.0001
wB97xD/6-311+G(d,p)				*wB97xD/Aug-cc-pVTZ*			
Atom	x (Å)	y (Å)	z (Å)	Atom	x (Å)	y (Å)	z (Å)
Fe	-1.1308	0.0235	0.0003	Fe	-1.1400	0.0218	0.0001
C	-1.4179	-1.7758	-0.0007	C	-1.4204	-1.7752	-0.0005
C	-0.3965	-0.1329	1.6537	C	-0.3894	-0.1283	1.6441
C	-0.6935	1.7941	0.0015	C	-0.7341	1.7963	0.0007
C	-2.9111	0.3861	-0.0010	C	-2.9212	0.3648	-0.0014
C	-0.3955	-0.1309	-1.6529	C	-0.3869	-0.1275	-1.6429
O	0.0408	-0.2307	2.7001	O	0.0607	-0.2221	2.6831
O	-1.5911	-2.8966	-0.0014	O	-1.5908	-2.8944	-0.0010
O	0.0423	-0.2270	-2.6992	O	0.0648	-0.2205	-2.6813
O	-4.0255	0.6125	-0.0020	O	-4.0359	0.5787	-0.0024
O	-0.4183	2.8939	0.0025	O	-0.4801	2.8992	0.0012
H	1.7230	-0.1854	0.0024	H	1.7453	-0.1878	0.0025
Br	3.1480	-0.0710	-0.0004	Br	3.1673	-0.0653	0.0000

Table A.I.S.9. Coordinates for the optimized geometries of $Fe(CO)_5$●●●ClF complex at different levels of theory.

B3LYP/6-311+G(d,p)				*B3LYP/Aug-cc-pVTZ*			
Atom	x (Å)	y (Å)	z (Å)	Atom	x (Å)	y (Å)	z (Å)
Fe	-0.6373	0.0000	0.0001	Fe	-0.6643	0.0001	-0.0002
C	-0.3105	1.8139	-0.1062	C	-0.3201	-1.8052	-0.0665
C	-0.3124	-0.1064	-1.8141	C	-0.3169	-0.0668	1.8045
C	-0.3126	-1.8143	0.1062	C	-0.3183	1.8050	0.0671
C	-2.4725	0.0012	0.0009	C	-2.4973	0.0009	-0.0004
C	-0.3102	0.1060	1.8139	C	-0.3166	0.0669	-1.8048
O	-0.1229	-0.1715	-2.9313	O	-0.1102	-0.1083	2.9191
O	-0.1197	2.9309	-0.1715	O	-0.1155	-2.9202	-0.1072
O	-0.1193	0.1712	2.9308	O	-0.1099	0.1078	-2.9194
O	-3.6095	0.0020	0.0015	O	-3.6330	0.0016	-0.0004
O	-0.1231	-2.9315	0.1711	O	-0.1122	2.9197	0.1089
Cl	2.1130	-0.0004	-0.0001	Cl	2.1755	-0.0004	-0.0001
F	3.9683	-0.0006	-0.0012	F	3.9499	-0.0006	-0.0003
wB97xD/6-311+G(d,p)				*wB97xD/Aug-cc-pVTZ*			
Atom	x (Å)	y (Å)	z (Å)	Atom	x (Å)	y (Å)	z (Å)
Fe	-0.6667	-0.0001	-0.0001	Fe	0.7124	-0.0001	0.0000
C	-0.3165	-0.9353	1.5338	C	0.3377	1.7752	0.1659
C	-0.3175	1.5338	0.9355	C	0.3340	-0.1657	1.7745
C	-0.3160	0.9355	-1.5337	C	0.3366	-1.7752	-0.1657
C	-2.4914	-0.0009	-0.0009	C	2.5339	-0.0007	-0.0001
C	-0.3151	-1.5337	-0.9353	C	0.3340	0.1658	-1.7745
O	-0.1079	2.4842	1.5152	O	0.1008	-0.2678	2.8777
O	-0.1062	-1.5148	2.4842	O	0.1065	2.8788	0.2683
O	-0.1039	-2.4839	-1.5147	O	0.1008	0.2689	-2.8776
O	-3.6251	-0.0013	-0.0014	O	3.6663	-0.0010	-0.0002
O	-0.1053	1.5151	-2.4838	O	0.1047	-2.8786	-0.2681
Cl	2.1684	0.0004	0.0003	Cl	-2.2769	0.0002	0.0000
F	3.9332	0.0006	0.0006	F	-3.9676	0.0001	0.0000

Table A.I.S.10. Frequencies for the normal modes of vibration of $Fe(CO)_5$ at different levels of theory.

B3LYP /6-311+G(d,p)		*B3LYP /Aug-cc-pVTZ*		*wB97xD /6-311+G(d,p)*		*wB97xD /Aug-cc-pVTZ*	
Frequency (cm^{-1})	IR intensities	Frequency (cm^{-1})	IR intensities	Frequency (cm^{-1})	IR intensities	Frequency (cm^{-1})	IR intensities
53.2	0.0	52.2	0.0	53.6	0.0	52.2	0.0
53.5	0.0	52.7	0.0	54.3	0.0	52.6	0.1
96.6	0.0	95.5	0.0	96.6	0.0	93.9	0.0
96.9	0.0	95.6	0.0	96.7	0.0	95.0	0.0
104.2	0.4	104.7	0.4	103.9	0.3	104.2	0.3
104.3	0.4	104.8	0.4	104.1	0.3	104.6	0.3
107.3	1.0	106.3	1.0	108.3	1.1	105.4	1.0
366.2	0.0	368.6	0.0	371.6	0.0	377.7	0.0
366.6	0.0	372.2	0.0	372.3	0.0	379.5	0.0
366.9	0.0	372.3	0.0	377.9	0.0	380.4	0.0
409.4	0.0	410.0	0.0	420.6	0.0	425.1	0.0
432.8	0.0	433.7	0.0	444.3	12.8	450.1	15.7
435.6	14.5	437.9	17.4	446.9	12.2	451.2	14.1
436.0	14.6	438.2	17.4	451.7	0.3	456.2	0.4
467.4	9.7	469.7	10.1	477.0	11.1	481.9	11.0
479.4	2.3	480.1	2.3	502.1	2.4	508.0	2.6
479.5	2.3	480.4	2.2	504.2	2.2	508.8	2.6
565.4	0.0	566.6	0.0	574.5	0.0	575.9	0.0
565.9	0.0	566.8	0.0	574.7	0.0	576.9	0.0
615.2	131.4	618.8	127.2	631.3	147.3	637.9	141.5
655.1	136.9	660.6	128.8	668.8	154.0	677.8	144.0
655.3	136.7	660.6	128.8	670.3	154.2	679.5	144.2
2069.3	1361.2	2068.7	1296.7	2119.9	1468.9	2121.6	1384.0
2069.5	1361.1	2068.9	1296.4	2120.3	1467.9	2122.0	1386.3
2094.8	0.0	2094.2	0.0	2147.1	0.0	2148.1	1554.0
2099.1	1562.0	2097.4	1478.1	2148.8	1658.4	2148.4	0.1
2175.8	0.0	2173.3	0.0	2227.2	0.0	2225.8	0.0

Table A.I.S.11. Stretching frequencies for HF, HCl, HBr and ClF at different levels of theory.

	B3LYP /6-311+G(d,p)		B3LYP /Aug-cc-pVTZ		wB97xD /6-311+G(d,p)		wB97xD /Aug-cc-pVTZ	
Molecule	Frequency (cm^{-1})	IR intensities	Frequency (cm^{-1})	IR intensities	Frequency (cm^{-1})	IR intensities	Frequency (cm^{-1})	IR intensities
HF	4094.4	130.2	4070.2	111.4	4173.8	141.6	4148.7	111.9
HCl	2927.2	32.3	2935.0	40.8	2967.1	39.4	2973.3	45.3
HBr	2595.9	6.2	2624.6	11.9	2672.1	8.3	2688.5	12.9
ClF	739.7	21.3	787.0	28.7	774.1	23.6	818.9	31.7

Table A.I.S.12. Frequencies for the normal modes of vibration of $Fe(CO)_5$●●●HF complex at different levels of theory.

B3LYP/6-311+G(d,p)		*B3LYP/Aug-cc-pVTZ*		*wB97xD/6-311+G(d,p)*		*wB97xD/Aug-cc-pVTZ*	
Frequency (cm^{-1})	IR intensities	Frequency (cm^{-1})	IR intensities	Frequency (cm^{-1})	IR intensities	Frequency (cm^{-1})	IR intensities
21.2	1.8	20.0	1.6	21.4	1.9	20.0	1.6
42.8	0.1	41.4	0.1	41.7	0.0	40.1	0.1
51.2	1.6	50.9	1.2	53.6	1.5	54.9	1.0
71.0	0.6	69.4	0.5	73.6	0.8	72.1	0.7
92.8	0.1	91.4	0.0	91.4	0.1	90.1	0.0
97.9	0.3	95.9	0.3	98.9	0.0	97.7	0.0
99.1	0.0	98.0	0.0	105.1	0.2	102.8	0.2
105.4	0.8	105.2	0.8	105.7	0.8	105.4	1.5
107.7	1.8	106.5	1.6	107.2	1.7	105.4	0.7
113.9	0.0	113.6	0.0	120.9	0.1	119.6	0.1
362.4	2.5	368.9	0.3	366.7	2.9	376.3	0.0
366.8	0.0	371.4	0.0	370.0	0.0	376.9	0.1
369.0	0.0	372.1	0.1	379.5	0.0	384.1	0.2
399.6	5.4	402.0	6.3	404.3	3.7	408.9	4.9
406.7	0.2	407.5	0.8	416.3	36.1	420.0	0.0
414.2	39.7	428.5	0.3	418.1	0.1	450.0	0.1
420.0	3.5	429.9	0.0	448.3	2.3	466.6	2.8
427.7	0.2	450.3	13.6	448.5	0.0	470.5	1.1
463.2	17.1	466.4	26.7	473.9	17.7	483.2	35.1
464.4	37.8	468.3	6.6	483.9	33.8	495.0	6.6
468.2	6.5	469.0	37.7	493.7	5.8	495.3	30.9
496.5	0.1	496.8	0.3	518.8	0.0	519.3	0.4
559.5	3.8	560.1	4.1	566.6	4.7	568.4	5.3
564.2	0.0	564.7	0.0	573.5	0.0	575.1	0.0
618.6	135.9	622.9	130.7	634.8	149.3	642.8	143.3
650.8	135.2	656.1	125.7	666.5	151.0	674.1	139.9
655.1	152.6	658.3	144.6	671.9	169.4	675.8	160.0
2080.6	1476.7	2079.5	1393.7	2133.0	1605.3	2131.7	1500.1
2088.4	945.6	2087.7	901.3	2142.2	953.3	2141.8	898.9
2108.3	103.9	2107.6	100.3	2161.2	153.4	2160.4	1457.4
2111.8	1473.0	2110.3	1389.1	2161.4	1563.3	2161.3	149.2
2184.1	11.8	2181.7	12.0	2236.3	13.7	2233.8	14.0
3812.1	852.3	3785.4	805.1	3853.2	941.6	3830.9	873.0

Table A.I.S.13. Frequencies for the normal modes of vibration of $Fe(CO)_5$●●●HCl complex at different levels of theory.

B3LYP/6-311+G(d,p)		*B3LYP/Aug-cc-pVTZ*		*wB97xD/6-311+G(d,p)*		*wB97xD/Aug-cc-pVTZ*	
Frequency (cm-1)	IR intensities	Frequency (cm-1)	IR intensities	Frequency (cm-1)	IR intensities	Frequency (cm-1)	IR intensities
13.8	0.3	12.3	0.2	-10.5	0.4	-12.9	0.3
33.5	0.5	28.0	0.5	39.0	0.3	34.9	0.2
35.4	0.3	30.9	0.2	39.6	0.3	41.4	0.3
56.3	0.1	53.3	0.0	68.9	0.1	65.6	0.1
64.6	0.1	61.4	0.0	75.2	0.6	74.4	0.5
94.1	0.0	93.4	0.0	92.2	0.0	91.5	0.0
98.2	0.0	96.9	0.0	98.4	0.0	96.8	0.0
104.8	0.6	104.9	0.6	105.2	0.6	104.9	1.3
106.0	0.0	105.6	0.0	106.8	1.4	105.4	0.5
107.1	1.3	106.2	1.3	107.9	0.0	107.5	0.0
283.6	9.2	238.2	6.0	290.9	6.1	254.0	3.3
298.8	2.5	242.3	1.7	331.8	0.6	293.9	0.2
366.4	0.0	369.0	0.0	370.5	0.0	376.9	0.0
367.5	0.1	371.4	0.0	376.0	1.3	382.0	0.6
369.0	0.8	373.1	0.3	383.8	0.4	384.9	0.1
406.6	1.9	407.5	0.7	411.9	5.8	420.8	2.9
412.2	7.0	418.9	11.6	418.8	0.1	422.6	6.1
429.8	0.2	430.9	0.6	449.5	0.0	451.7	0.1
454.0	23.9	452.6	25.0	473.8	11.8	475.3	25.9
464.3	10.7	466.4	10.9	474.8	23.6	477.9	11.9
471.7	4.8	472.9	4.3	496.0	4.8	499.7	4.9
489.2	0.0	487.6	0.0	514.7	0.1	513.2	0.0
562.4	2.8	564.2	1.8	568.3	5.3	571.6	3.8
563.9	0.0	564.8	0.0	573.2	0.0	574.9	0.0
615.8	125.5	618.6	120.3	633.1	137.3	638.6	130.5
651.1	127.5	657.2	119.8	665.4	140.0	673.9	131.3
655.3	159.8	658.7	149.6	672.2	184.1	676.1	173.5
2074.1	1405.5	2071.4	1295.2	2126.1	1535.6	2124.3	1397.2
2081.2	1072.3	2078.7	1076.1	2136.0	1030.5	2134.3	1050.0
2103.3	66.7	2101.4	49.8	2157.2	138.2	2156.6	1443.4
2107.4	1476.4	2104.8	1391.8	2157.7	1554.1	2156.8	96.4
2179.7	18.7	2176.6	15.6	2231.6	29.2	2229.1	25.4
2806.2	404.1	2838.0	346.5	2821.9	628.4	2842.8	576.3

Table A.I.S.14. Frequencies for the normal modes of vibration of $Fe(CO)_5$●●●HBr complex at different levels of theory.

B3LYP/6-311+G(d,p)		*B3LYP/Aug-cc-pVTZ*		*wB97xD/6-311+G(d,p)*		*wB97xD/Aug-cc-pVTZ*	
Frequency (cm-1)	IR intensities	Frequency (cm-1)	IR intensities	Frequency (cm-1)	IR intensities	Frequency (cm-1)	IR intensities
0.5	0.1	-10.3	0.1	10.3	0.1	10.0	0.1
17.8	0.3	11.6	0.1	19.7	0.1	14.9	0.0
24.4	0.1	13.0	0.2	34.5	0.5	37.0	0.5
52.5	0.0	51.9	0.0	59.1	0.1	60.1	0.1
61.8	0.0	58.5	0.0	64.0	0.1	60.9	0.0
94.7	0.0	93.5	0.2	93.4	0.0	91.8	0.0
97.9	0.0	96.5	0.0	97.4	0.0	95.3	0.0
104.6	0.6	103.7	2.4	102.5	0.5	102.0	0.4
104.6	0.0	104.4	0.0	106.8	0.0	105.1	0.9
106.8	1.4	104.5	0.7	107.7	1.1	106.7	0.2
166.5	3.8	117.2	0.9	233.0	0.0	227.7	0.0
189.1	0.9	117.4	0.4	286.7	8.2	296.7	5.8
366.3	0.0	368.1	0.0	369.7	0.0	375.8	0.0
366.5	0.0	371.5	0.0	373.7	0.5	380.0	0.3
367.0	0.2	372.4	0.1	380.7	0.2	382.9	0.1
407.0	0.9	408.1	0.5	418.2	2.3	421.9	0.5
417.6	9.9	424.3	13.9	419.5	5.8	426.7	10.3
430.3	0.3	431.7	0.8	447.8	0.1	452.1	0.1
449.9	21.6	449.1	22.7	467.9	21.9	470.4	23.6
464.7	10.3	467.3	10.5	474.9	11.3	479.0	11.3
472.9	3.9	474.8	3.5	495.1	4.9	501.1	4.3
485.9	0.1	485.0	0.2	508.4	0.0	511.0	0.1
563.4	2.0	565.2	0.0	570.2	4.0	572.4	3.0
564.0	0.0	565.3	1.1	572.2	0.0	573.8	0.0
614.8	124.5	618.3	119.7	632.1	135.9	638.1	129.3
651.5	127.0	658.0	119.6	663.8	140.2	673.6	129.9
654.1	160.4	659.0	150.0	669.9	187.4	675.5	177.0
2071.3	1363.9	2069.8	1255.6	2122.5	1488.7	2122.7	1353.6
2077.8	1144.6	2075.8	1154.8	2131.6	1127.4	2131.8	1114.0
2100.9	49.4	2099.4	30.4	2154.2	420.4	2154.1	733.6
2105.4	1477.1	2103.0	1393.1	2156.9	1222.0	2156.2	775.7
2177.8	18.9	2175.3	12.9	2229.2	33.5	2227.4	29.5
2517.2	190.6	2564.0	145.9	2538.8	396.6	2565.5	363.3

Table A.I.S.15. Frequencies for the normal modes of vibration of $Fe(CO)_5$●●●ClF complex at different levels of theory.

B3LYP/6-311+G(d,p)		*B3LYP/Aug-cc-pVTZ*		*wB97xD/6-311+G(d,p)*		*wB97xD/Aug-cc-pVTZ*	
Frequency (cm-1)	IR intensities	Frequency (cm-1)	IR intensities	Frequency (cm-1)	IR intensities	Frequency (cm-1)	IR intensities
47.5	0.0	37.9	0.0	38.6	0.0	10.1	0.0
53.9	1.8	49.5	1.2	53.3	0.9	44.8	0.5
53.9	1.8	49.7	1.2	53.3	0.9	45.1	0.5
86.9	0.0	84.8	0.0	86.0	0.0	82.5	0.0
86.9	0.0	84.8	0.0	86.0	0.0	82.6	0.0
101.9	0.0	101.2	0.0	101.4	0.0	86.3	13.3
107.8	1.3	102.5	9.3	102.3	18.5	100.4	0.0
107.9	1.3	106.8	1.1	107.5	1.1	105.5	0.9
111.7	0.6	106.8	1.1	107.5	1.1	105.5	0.9
139.3	37.1	124.9	25.1	121.6	30.8	118.1	9.8
156.9	0.4	165.3	0.7	161.2	0.4	161.0	0.6
156.9	0.4	165.3	0.7	161.2	0.4	161.1	0.6
363.9	0.0	370.6	0.0	368.6	0.0	372.4	0.0
372.2	1.5	375.6	1.5	382.6	0.0	376.2	0.0
372.3	1.5	375.6	1.5	383.4	2.1	384.9	2.0
379.5	178.5	380.8	0.0	383.4	2.1	385.0	2.0
388.2	0.0	391.2	62.0	402.0	45.0	412.1	13.6
410.1	0.0	416.0	0.0	431.3	0.0	439.0	0.0
434.4	428.6	455.8	13.2	469.4	13.7	478.5	13.4
449.1	13.6	455.9	13.2	469.4	13.7	478.6	13.4
449.2	13.6	457.4	1.7	482.7	2.5	486.9	7.0
454.9	47.1	487.7	684.5	521.7	768.1	537.6	16.8
522.9	10.3	525.5	13.0	537.2	11.9	538.0	16.8
523.0	10.3	525.8	13.0	537.2	11.9	575.5	0.0
559.8	0.0	563.2	0.0	570.9	0.0	611.4	755.8
627.7	101.5	635.7	96.4	645.4	117.9	656.0	109.8
627.7	101.5	635.8	96.4	645.4	117.9	656.2	109.8
641.6	151.0	649.6	112.3	666.2	106.5	678.1	20.1
2122.4	728.9	2115.1	719.7	2165.5	1447.4	2152.4	1398.9
2129.8	1283.5	2118.0	1246.9	2165.5	1447.4	2152.6	1398.6
2129.8	1283.6	2118.2	1246.9	2168.7	775.3	2159.6	8.7
2136.0	0.0	2124.6	0.0	2172.1	0.0	2160.3	784.1
2194.5	209.6	2186.4	177.5	2237.0	231.4	2229.5	164.8

Appendix II.

Towards A New Low Frequency Broadband Spectrometer.

(This work has been published in Indian J Phys 2012, 86, 225-235.)

A.II.I. Introduction

The PNFTMW spectrometers provide very high resolution and sensitivity, simultaneously and have enjoyed wide range of application. However, these Cavity spectrometers have two very serious limitations: (i) very low bandwidth which makes searching for unknown transitions long and tedious and (ii) low frequency cut off near about 4 GHz for most of the spectrometers. Though it is now possible to do gas phase spectroscopy on larger molecules and complexes, the moments of inertia for these are much larger and the rotational constants are smaller. It would be desirable to have a spectrometer with similar sensitivity and resolution down to 1 GHz or less.

Today microwave spectroscopists are trying to target heavier molecules and larger complexes. With increase in molecular mass, the rotational constants decrease and most of the low J transitions which are usually the most informative, lie in the low frequency region. As an example, consider a T-shaped structure of phenylacetylene—benzene complex, in which acetylenic hydrogen is interacting with the π cloud of benzene, *Figure A.II.1*.

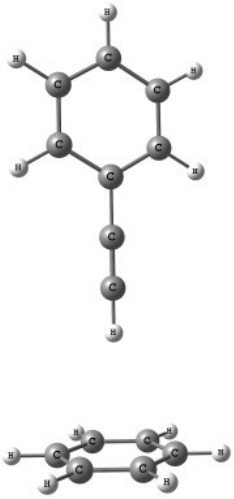

Figure A.II.1. T-shaped geometry of the Phenylacetylene●●●benzene complex. The complex was optimized at B3LYP/6-311++G(2d,2p) level of theory.

The calculated rotational constants for this structure are A = 1907.45 MHz, B = 189.17 MHz and C = 183.13 MHz at B3LYP/6-311++G(2d,2p) level. The $0_{0,0}$-$1_{0,1}$ transition for this complex is expected at 372.3 MHz. All the frequencies corresponding to $J = 2$ to 3 transitions for this complex range from 725 MHz to 1130MHz. These transitions are not accessible with the typical Fabry-Perot PN-FTMW spectrometers. More interestingly, one can consider the benzene dimer which

is also expected to have a minimum having both benzene molecules parallel to each other, slightly displaced[1]. As this would not have a dipole moment, microwave spectroscopy cannot be used to investigate such a structure. If C_6H_6•••C_6H_6•••Ar trimer could be formed in which the two benzene molecules have parallel-displaced geometry, microwave spectroscopy can given unambiguous evidence for the same. However, the rotational transitions for such a complex are also expected below 1 GHz.

These limitations show the need for a new spectrometer which can work in low frequency range (below 2GHz) and can perform data collection over a broad frequency range in a short time. Pate and co-workers came up with a novel design, which has given the most significant fillip to microwave spectroscopy[2,3].

Our initial attempts in building a new broadband spectrometer which can work in low frequency ranges also, are summarized in the next few sections.

AII.2. Initial attempts to produce a chirped pulse of 1 GHz

We are planning to build a spectrometer which works in 1-12GHz frequency range and uses the chirp pulse technique. Considering the reliability of *ab initio* calculations in geometry optimization and thus in predicting rotational constants, we focused on generation of a chirp pulse of 1 GHz bandwidth and 1μs time duration. We used Agilent N8241A Arbitrary waveform generator (AWG) and E8267D PSG vector signal generator (VSG) for the chirp pulse generation.

The N8241A is a dual channel AWG which has two options: option 125 and option 062. Under option 125 each channels can simultaneously deliver 1.25GS/s with 15 bits of vertical resolution, and 500MHz of instantaneous analog bandwidth while under option 062 each channel delivers 250 MHz of bandwidth at sampling rate 625MS/s with 15 bits of vertical resolution. The E8267D PSG vector signal generator can deliver frequency ranging from 250 KHz to 44GHz with 0.001Hz resolution. It has a built in wideband I/Q modulator that delivers up to 2GHz RF modulation bandwidth and thus can be used as a I/Q up-convertor also. Using E8267D in compliment to N8241A AWG as I/Q up-convertor one can get modulation bandwidth of 1GHZ (at 1.25GS/s) or 500MHz (at 625MS/s) at MW frequencies. We used option 125 of AWG to generate a chirp of 1GHz after up-conversion by VSG. The setup for the chirp generation is shown in *Figure A.II.2*.

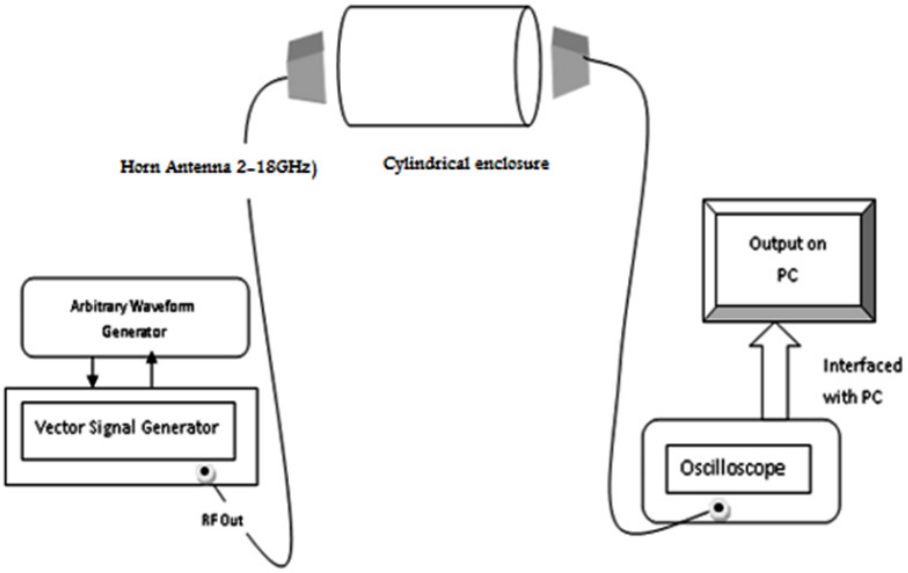

Figure A.II.2. Setup for chirp generation and measurements

The start, end and center frequencies and the time duration of the chirp can be set by the VSG. As a very first test, the chirp output (with 5 GHz center frequency,1 GHz span and 1μs time duration) from VSG was directly fed to the Spectrum analyzer (Agilent, E4407B ESA-E Spectrum Analyzer 100 Hz to 26.5GHz) which displays the generated chirp. After this direct measurement, two wideband horn antennae (2-18GHz) were introduced between the VSG and the spectrum analyzer. One was connected to VSG and was used as emitter of chirp pulse and the other was connected to the spectrum analyzer and was used as receiver of chirp pulse. The two horn antennae were placed close to each other and the chirp was recorded in spectrum analyzer. In *Figure A.II.3*, the frequency spectra shown at the top, is the result of measurement when VSG output was directly connected to the spectrum analyzer while the low intensity spectra shown in the figure is obtained when horn antennae were used as emitter and receiver. It is clear that the spectra are similar in both the cases but the amplitude decreases on using horn antennae as expected.

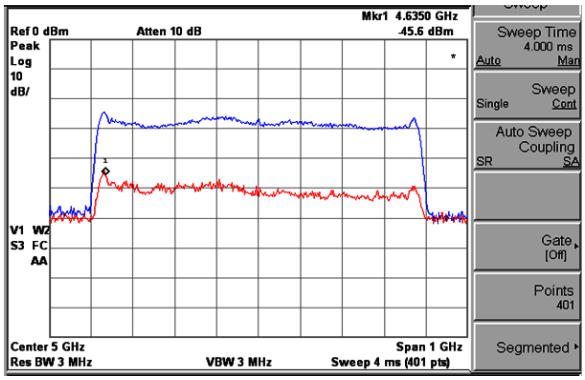

Figure A.II.3. Chirp output measured by Spectrum analyzer, for description see text.

To measure the linearity of the chirp and phase variation with time we fed the chirp output to a wide band oscilloscope (DSA 1304A infiniium high performance oscilloscope with 13GHz bandwidth) and interfaced the oscilloscope with a PC as shown in *Figure A.II.4*. The PC runs a software called 'Vector signal analyzer' developed by Agilent, which shows the frequency and time domain chirp signal, frequency and phase variation of chirp with time. *Figure A.II.4* shows the result of direct measurement (without using horn antennae) using this software. In this figure, the user interface of VSA software is shown. The two graphs in first column of the figure shows frequency and time domain chirp pulse respectively while in the second column, the top graph shows variation of chirp frequency with time and the bottom graph shows variation of phase of the chirp with time for 1μs time duration. The chirp range is same as before (4.5-5.5 GHz). It is clear from this measurement that the frequency of generated chirp varies linearly with time.

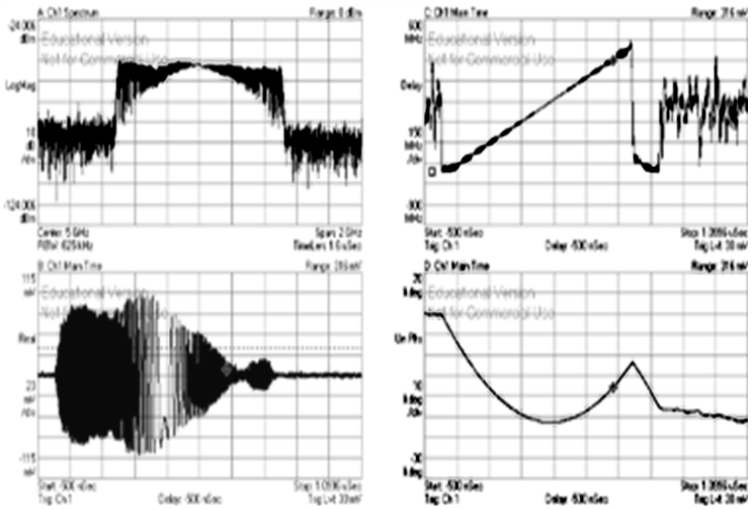

Figure A.II.4. Result of direct measurement of chirp obtained using VSA software.

The horn antennae have to be introduced into a vacuum chamber in our experiment. Hence, it was decided to test how the reflections from a metal chamber would affect the chirp. Moreover, the horn antennae will be separated by a finite distance in the spectrometer, and it would be useful to see the effect of varying distances between the antennae on the chirp. For these tests, a temporary arrangement was made using an aluminium sheet, folded to give the shape of a cylindrical cavity. The two horn antennae were mounted on two circular aluminium sheets. The diameter of one circular sheet was taken more than that of cylinder while diameter of other circular sheet was taken slightly less than cylinder. One horn antenna (mounted on bigger circular sheet) was kept static on one side of the cylinder while the other one was moved inside the cylindrical cavity to vary the distance between two antennae. This arrangement is shown in *Figure A.II.5*.

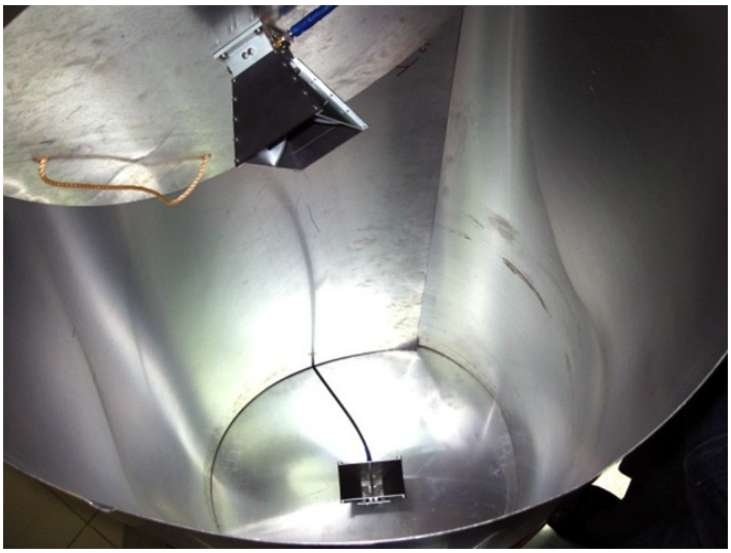

Figure A.II.5. The temporary arrangement for testing chirp performance inside the metal cavity.

By moving the antenna inside the cylindrical cavity, we did measurements at several distances. *Figure A.II.6(a) and A.II.6(b)* show the measurement results at 50 cm and 100 cm distances, respectively, between the two antennae. The chirp shows minor distortion possibly due to reflections of radiations from cylindrical cavity. However, the most important result is that at both the distances 50 cm and 100 cm, the linearity of the chirp with time is maintained inside the cavity. Moreover, for both the distances the phase variation is same as for the direct measurement result shown in the *Figure A.II.4*.

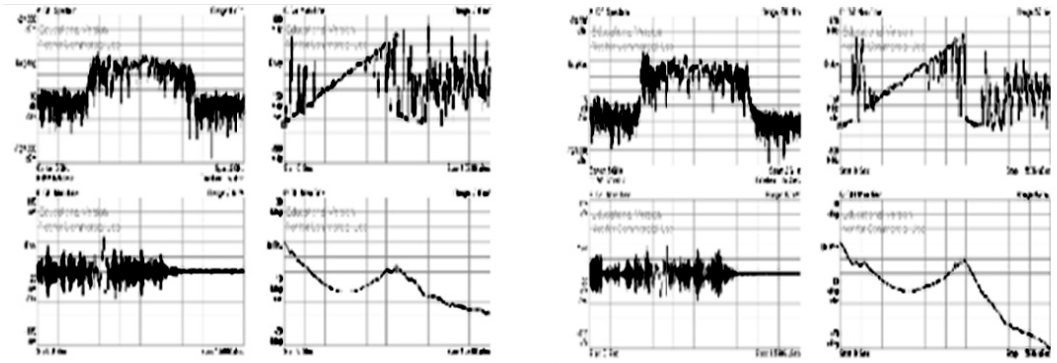

(a) Distance between the two antennae = 50 cm *(b) Distance between the two antennae = 100cm*

Figure A.II.6. Effect of putting horn antennae inside the metal cavity at different distances

A.II.3. Conclusions

We have summarized our initial attempts to build a broadband spectrometer which can work in low frequency range. A microwave chirp pulse of 1 μs time duration and 1 GHz band width could be generated. The chirp behaves well in the metal chamber also and the measurements show that the linearity of the chirp is maintained at different separation between the horn antennae.

A.II.4. References

1. Řezáč, J.; Hobza, P. *Journal of Chemical Theory and Computation* **2008**, *4*, 1835-1840.

2. Brown, G. G.; Dian, B. C.; Douglass, K. O.; Geyer, S. M.; Pate, B. H. *J. Mol. Spectrosc.* **2006**, *238*, 200-212.

3. Brown, G. G.; Dian, B. C.; Douglass, K. O.; Geyer, S. M.; Shipman, S. T.; Pate, B. H. *Rev. Sci. Instrum.* **2008**, *79*, -.

Appendix III.

Preliminary Investigations on

Propargyl Alcohol•••Water Complex.

A.III.1. Introduction

As in the case of PA-dimer, many different possibilities exist for the PA•••H_2O complex as well. Both of the molecules, PA and H_2O, can act as hydrogen bond acceptors as well as hydrogen bond donors. Moreover, multifunctional nature of PA molecule offers additional possibilities for the intermolecular interactions. What is the most stable structure of the PA•••H_2O complex ? Is it PA which acts as hydrogen bond donor or it is H_2O ? Does the complex has cyclic structure as has been observed for the other PA complexes, Ar•••PA complex and PA-dimer ? These questions can be answered by microwave spectroscopy which is very sensitive towards the geometry of system under study.

A.III.2. Ab initio and AIM analysis

The PA•••H_2O complex was optimized starting with different initial geometries. The calculations were performed using Gaussian 09 software suite. MP2 theory with 6-311++G(d,p) basis set was used to perform the optimization and frequency calculations. The optimized geometries are shown in the *Figure A.III.1*. Each of these geometry was found to be a minima on potential energy hypersurface as confirmed by the presence of all real normal modes of vibration for each of them. Further AIM analysis was performed on each of the optimized structure and the resulting electron density topologies are shown in the *Figure A.III.2*. In the *Structure 1*, propargyl alcohol acts as O-H•••O hydrogen bond donor. The AIM analysis shows presence of bond critical point corresponding to the O-H•••O hydrogen bond as well as presence of the bond critical point corresponding to O-H•••π interaction. In the *Structure 2 and 3* H_2O acts as O-H•••O hydrogen bond donor. The *Structure 4* is bound with C-H•••O interaction in which water acts as the hydrogen bond acceptor. Geometrical parameters for the hydrogen bonds present in these structures are given in the *Table A.III.1* and BSSE corrected and BSSE+ zero-point corrected interaction energies are given in the *Table VI.2*. Values of electron density ρ(r), and Laplacian of electron density at the intermolecular BCPs resulting from the AIM analysis are given in the *Table A.III.3*.

Table A.III.1. Structural parameters for the hydrogen bonds present in different structures of the PA●●●water complex.

	r[(O-)H●●●O] in Å	*∠(O-H●●●O) in degree*	*r[(O-)H●●●π] in Å*	*∠(O-H●●●π) in degree*	*r[(C-)H●●●O] in Å*	*∠(C-H●●●O) in degree*
Structure 1	1.9463	156.1	2.5145	129.1	-	-
Structure 2	1.9514	152.2	-		-	-
Structure 3	1.9259	157.5				
Structure 4	-	-	-	-	2.1944	179.5

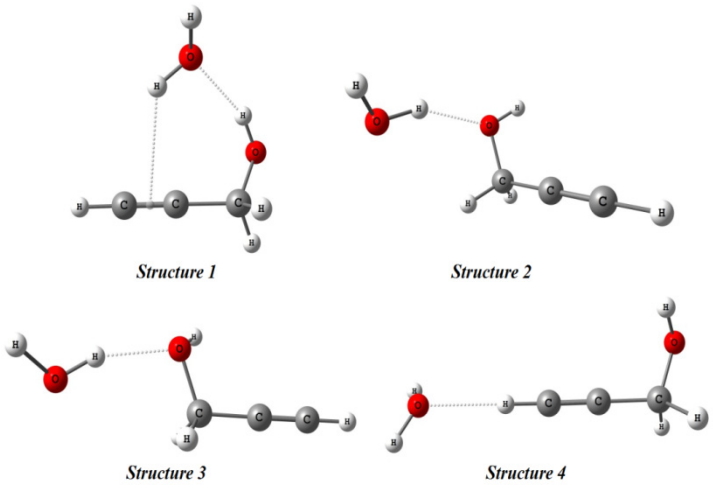

Figure A.III.1. Optimized structures for PA●●●water complex at MP2/6-311+G(d,p) level.

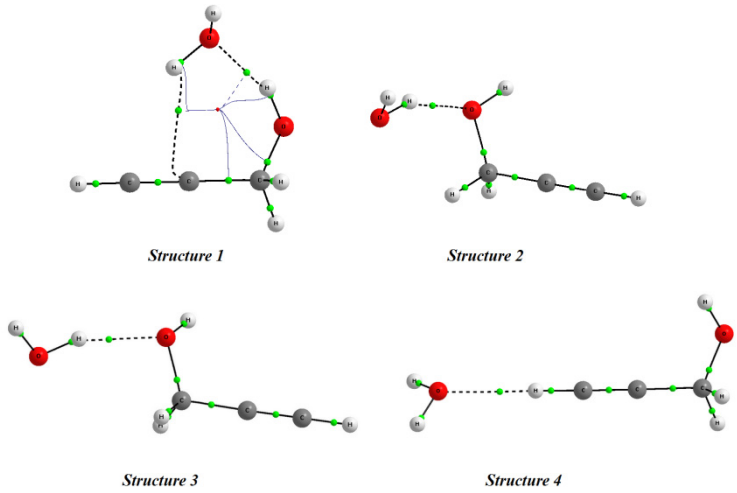

Figure A.III.2. AIM topologies for the different structures of the PA●●●water complex. BCPs are shown in green and RCPs in red

Table A.III.2. BSSE corrected ΔE_{BSSE}, and BSSE+ZPC corrected $\Delta E_{(BSSE+ZPC)}$, interaction energies for different structures of the PA•••water complex.

	ΔE_{BSSE} *in kJ/mol*	$\Delta E_{(BSSE+ZPC)}$ *in kJ/mol*
Structure 1	22.7	14.7
Structure 2	18.5	11.1
Structure 3	18.9	11.6
Structure 4	10.6	3.8

Table A.III.3. Electron density $\rho(r)$, and Laplacian of electron density $\nabla^2\rho(r)$ at the intermolecular BCPs of different structures of the PA•••water complex. The wave function used for these calculations were extracted from the ab initio calculations at MP2/6-311++G(d,p) level.

	At (O-)H•••O BCP		*At (O-)H•••π BCP*		*At (C-)H•••O BCP*	
	$\rho(r)$ *in a.u.*	$\nabla^2\rho(r)$ *in a.u.*	$\rho(r)$ *in a.u.*	$\nabla^2\rho(r)$ *in a.u.*	$\rho(r)$ *in a.u.*	$\nabla^2\rho(r)$ *in a.u.*
Structure 1	0.0223	0.0972	0.0103	0.0351		
Structure 2	0.0213	0.0982	-	-	-	-
Structure 3	0.0236	0.1038	-	-	-	-
Structure 4	-	-	-	-	0.0131	0.0544

It is clear from the interaction energies given in the *Table A.III.2* that the *Structure 1* which is stabilized by O-H•••O and C-H•••π hydrogen bonds, is the most stable structure.

The calculated rotational constants and dipole moment components along the principal axes for all the four structures of the PA•••water complex are given in the *Table A.III.4*. The rotational constants for these structures are very different from each other and these can easily be distinguished by microwave spectroscopy.

Table A.III.4. Rotational constants and dipole moment components along the principle axes for different structures of PA•••water complex calculated at MP2/6-311++G(d,p) level.

	A/MHz	*B/MHz*	*C/MHz*	$\lvert\mu_a\rvert$/D	$\lvert\mu_b\rvert$/D	$\lvert\mu_c\rvert$/D
Structure 1	4577.8	3862.0	2252.7	0.2	2.9	2.5
Structure 2	8296.5	1987.0	1760.1	0.0	2.0	2.6
Structure 3	22592.5	1554.9	1475.5	1.8	1.3	0.0
Structure 4	23387.3	1055.9	1020.3	3.6	0.8	0.1

Rotational spectra was predicted for the four structures using *ab initio* calculated rotational constants given in the *Table A.III.4*.

A.III.3. Search for the Rotational spectra

Search was first started using argon as the carrier gas which led to detection of many signals which correspond to the Ar•••PA complex. Therefore, the carrier gas was changed to helium to avoid the formation of complexes with Ar. Equal proportion of the carrier gas was bubbled through PA and water samples contained in two different bubblers. While using Ar as the carrier, the gas mixture was expanded from a stagnation pressure of 0.5 bar into the vacuum chamber and while using He as the carrier gas the stagnation pressure was increased to 1.5 bar. Microwave pulse of 1 μs time duration was used during the search.

A total of 18 signals which depend on both the PA and water concentration, have been observed. All the signals were observed while using helium as the carrier gas. The signals are reported in the *Table A.III.5*.However, these signals could not be assigned as of now. Total searched regions till date are given in the *Table A.III.6*.

Table A.III.5. Observed but unassigned signals which depend on PA as well as water's concentration. All these signals were observed while using He as carrier gas.

Frequency	Intensity
7001.8000	weak
8503.4000	very strong
8603.8600	very strong
8692.1600	medium
8756.5800	strong
8788.1200	medium
8864.9582	weak
8911.1316	strong
9073.5000	very--weak
9086.8100	very weak
9191.3620	weak
9195.9660	strong
9278.7800	very weak
9282.1000	weak
9309.1400	weak
9317.4750	medium
11348.1410	medium
11348.1898	medium

Table A.III.6. Searched regions with Ar and He as carrier gas. The gas was bubbled through the PA and water samples.

using Ar as carrier gas	using He as carrier gas
3247.0-3361.5 MHz	4490.0-4510.0 MHz
4677.0-5050.0 MHz	6748.0-7002.0 MHz
6100.0-6255.5 MHz	8381.0-8428.0 MHz
6558.0-6592.0 MHz	8489.0-8510.5 MHz
7983.0-8010.0 MHz	8600.0-8605.0 MHz
8133.5-8614.5 MHz	8675.0-8679.0 MHz
8659.0-8681.0 MHz	8692.0-8786.5 MHz
9750.5-9881.0 MHz	8838.5-8940.0 MHz
	8935.0-9365.0 MHz
	10000.0-10150.0 MHz
	11331.0-11339.0 MHz
	11348.5-11412.0 MHz
	11445.0-11495.5 MHz
	11622.5-11769.0 MHz

A.III.4. Conclusions

Ab initio and AIM analysis show that the Propargyl alcohol•••H_2O complex is bound with strong hydrogen bonding interactions. A total of 18 signals which depend on the concentration of both PA as well as water, have been observed. However, these signals could not be fit to any of the structures as of now. More experimental data is required to fit the observed signals. Work is under progress.

List of Publications

1. "Measuring Rotational Constant of a Molecule without Dipole Moment and Confirming Low Frequency Vibrations Using Microwave Spectroscopy: $^{13}CC_5H_6$/ C_6H_5D•••Ar Complex", **Devendra Mani**, Aiswaryalakshmi P. , E. Arunan, *Asian J Spectrosc. Special issue* **31** (2010).

2. "Towards a broadband chirped pulse Fourier transform microwave spectrometer", **Devendra Mani**, Vijayashree T. Bhat, K.J. Vinoy and E.Arunan, *Ind. J. Phy.* **86,** 225 (2012).

3. "Microwave Spectroscopic and Atoms in Molecules Theoretical Investigations on the Ar···Propargyl Alcohol Complex: Ar···H-O, Ar···π, and Ar···C Interactions ", **Devendra Mani** and E. Arunan, *ChemPhysChem* **14**, 754 (2013).

4. "Fe as hydrogen/halogen bond acceptor in square pyramidal $Fe(CO)_5$", Aiswaryalakshmi P., **Devendra Mani** and E. Arunan, *Inorg. Chem.,* **52**, 9153-9161 (2013).

5. "The X-C···Y (X = O/F, Y = O, S, F, Cl, Br, N, P,) Carbon bond and hydrophobic interactions",
Devendra Mani and E. Arunan, *Phys. Chem. Chem. Phys.* **15,** 14377-14383 (2013).
(This work was selected under "Hot article" category by the journal and was also selected for the cover page of the issue.)

6. **"**Rotational Spectroscopic Studies on Propargyl alcohol dimer: A system bound by OH···O, OH···π and CH···π interactions ", **Devendra Mani** and E. Arunan. *(Manuscript under preparation)*

7. **"**Hydrogen Bonding as a Prototype for All Intermolecular Bonds ",
Devendra Mani, Abhishek Shahi and E. Arunan. *(Manuscript under preparation)*

8. Hydrogen Bond vs. Carbon Bond.
Devendra Mani and E. Arunan. *(Manuscript under preparation)*